NASA CONTRACTOR REPORT

NASA CR-111909

PROPERTIES OF ABLATION AND INSULATION MATERIALS

VOLUME III:

THERMAL AND MECHANICAL PROPERTIES OF LOW-DENSITY PHENOLIC-NYLON AND SILICONE-PHENOLIC ABLATORS

by E. D. Smyly, W. F. Swoger and C. D. Pears

CASE FILE COPY

Prepared by
SOUTHERN RESEARCH INSTITUTE
Birmingham, Alabama
for Langley Research Center

NATIONAL AERONAUTICS AND SPACE ADMINISTRATION   June 1971

PROPERTIES OF ABLATION AND INSULATION MATERIALS

Volume III

Thermal and Mechanical Properties of Low-Density Phenolic-Nylon
and Silicone-Phenolic Ablators

by E. D. Smyly, W. F. Swoger and C. D. Pears

ABSTRACT

Thermal and mechanical property measurements were made on a low-density silicone-phenolic (MG-1), a low-density silicone-phenolic in a phenolic-glass honeycomb (MG-45) and a low-density phenolic-nylon in a phenolic-glass honeycomb (MG-58). Mechanical property measurements were made only on the virgin materials and thermal properties were measured on the virgin and charred materials.

The thermal properties were measured on the virgin materials from 150 K to 500 K. The properties measured included thermal conductivity, enthalpy (heat capacity), thermal expansion, permeability, bulk density, true density and pore size and volume fraction measurements. For the chars of the honeycombed materials (MG-45 and MG-58), which were prepared in an arc-jet, thermal conductivity, enthalpy, bulk density, true density and pore size and volume fraction measurements were made. For the chars of the silicone-phenolic (MG-1), which were prepared in a laboratory furnace, thermal conductivity, enthalpy, permeability, emittance, bulk density, true density and pore size and volume fraction measurements were made. Thermal conductivity and enthalpy measurements on the chars were made to 3000 K and 2000 K respectively, for the MG-45 and MG-58 and to about 1500 K for the MG-1.

Strength, Young's modulus and axial strain-to-failure were determined in tension and compression on the virgin materials. Properties were determined from 150 K to 500 K in one direction on the silicone-phenolic and at room temperature, parallel and perpendicular to the honeycomb reinforcement, on the honeycombed materials. Specimen configurations for evaluating honeycomb reinforced, low-density ablation materials were evaluated. Moisture effects on the mechanical properties of the phenolic-nylon, honeycomb reinforced material were studied.

TABLE OF CONTENTS

LIST OF TABLES

vi

viii

LIST OF TABLES - CONCLUDED

LIST OF ILLUSTRATIONS

LIST OF ILLUSTRATIONS - CONTINUED

LIST OF ILLUSTRATIONS - CONTINUED

LIST OF ILLUSTRATIONS - CONTINUED

LIST OF ILLUSTRATIONS - CONTINUED

xviii

LIST OF ILLUSTRATIONS - CONCLUDED

PROPERTIES OF ABLATION AND INSULATION MATERIALS

Volume III

Thermal and Mechanical Properties of Low-Density Phenolic-Nylon and Silicone-Phenolic Ablators

By E. D. Smyly, W. F. Swoger and C. D. Pears
Southern Research Institute

INTRODUCTION

This is the final report to the National Aeronautics and Space Administration, Langley Research Center, for the work on virgin and charred ablative materials under Subtasks B and C of Contract NAS1-7732-1. This work involved the measurement of physical, thermal and mechanical properties of three low-density phenolic-nylon and silicone-phenolic ablators.

The materials evaluated are listed below:

    MG-1:   Silicone-phenolic
    MG-45: Silicone-phenolic in phenolic-glass honeycomb
    MG-58: Phenolic-nylon in phenolic-glass honeycomb

The thermal and physical properties measured on the virgin materials are summarized below:

1. Thermal conductivity in thickness or "c" direction[1] from 150 to 500 K

2. Enthalpy (heat capacity) from 150 to 500 K

3. Thermal expansion from 150 to 500 K (MG-1 only)

4. Bulk density, "true" density (apparent density on pulverized samples), and pore size distribution

---

[1] Superscripts denote references cited. Directions are defined in Reference 1.

5. Permeability in the thickness or "c" direction

The thermal and physical properties measured on the charred materials were:

1. Thermal conductivity from 500 to 3000 K in the thickness or "c" direction (to 1500 K on MG-1)

2. Enthalpy (heat capacity) from 300 to 1920 K (to 1644 K on MG-1)

3. Bulk density, "true" density, and pore size distribution

4. Permeability (MG-1 only)

Tensile and compressive evaluations were performed on each material. The MG-45 and MG-58 materials were evaluated in two orthogonal directions ("a" and "b") at room temperature only, while the MG-1 was evaluated in one direction at eight temperatures between 150 K and 500 K. A stress rate of 172 N/m^2/sec was used for the tensile and compressive evaluations of the three materials. Additionally, bulk density was determined for each specimen and sonic velocity was measured on the MG-1 specimens.

The scope of the mechanical property program was expanded to include a limited specimen configuration study of the honeycomb reinforced materials. Since no standard specimen configuration exists for this type of material, the study was performed to assure a specimen design which would best represent the bulk material. The configuration study was conducted using the MG-58 material. Square gage sections having areas of 3.63 cm^2, 6.45 cm^2 and 10.09 cm^2 for the tensile specimens and areas of 1.61 cm^2, 3.63 cm^2 and 6.45 cm^2 for the compressive specimens were evaluated. One tensile and one compressive configuration were then selected for evaluation of the MG-45 material. Also investigated were the effects of moisture on the mechanical properties of the MG-58 material.

All virgin materials were supplied by the NASA Langley Research Center. In addition, char discs for the MG-45 and MG-58 were prepared in the arc-jet facility at the NASA Langley Research Center. The MG-1 char was prepared at Southern Research Insitute.

2

SPECIMEN MATERIAL

The three materials supplied were a silicone-phenolic (MG-1), a silicone-phenolic in a phenolic-glass honeycomb (MG-45) and a phenolic-nylon in a phenolic-glass honeycomb (MG-58). The compositions of the three materials are given in Table 1 and pictures of the materials are shown in Figure 1.

The virgin materials were supplied by the NASA Langley Research Center in bulk form. The MG-45 and MG-58 were received as discs 38 cm diameter by 3.2 cm thick with the thickness direction corresponding to the "c" direction of the honeycomb.[1] Two billets of virgin MG-1 were received. One billet was 20.4 cm diameter by 10.2 cm thick and the other (MG-1B) was 38.1 cm diameter by 8.25 cm thick.

The nominal bulk densities of the virgin MG-1, MG-45 and MG-58 materials were 0.60 gm/cm^3, 0.23 gm/cm^3, and 0.23 gm/cm^3, respectively.

Chars of the MG-45 and MG-58 were prepared in the arc-jet facility at the NASA Langley Research Center. These chars were supplied in the form of discs about 7.6 cm diameter which were charred to depths ranging from 0.64 cm to 2.54 cm. The MG-1 char was prepared in a high temperature furnace at SRI.

The nominal bulk densities of the charred MG-1, MG-45 and MG-58 were about 0.19 gm/cm^3, 0.17 gm/cm^3 and 0.14 gm/cm^3, respectively.

More detailed material discussions are given in sections under Parts I and II, "Thermal Properties" and "Mechanical Properties", respectively. In these other sections, specific utilization of billets and detailed information concerning observations are given. Also, information pertinent to the materials is given under specific headings such as "Quantitative Microscopy (Pore Size Distribution)".

---

[1] Directions are defined in Reference 1.

3

PART I

THERMAL PROPERTIES

Summary

Thermal property measurements were made on three ablative
materials in the virgin and charred conditions. The materials
evaluated were a silicone-phenolic (MG-1), a silicone-phenolic
in a phenolic-glass honeycomb (MG-45), and a phenolic-nylon
in a phenolic-glass honeycomb (MG-58). Properties determined
included (1) thermal conductivity, (2) heat capacity, (3) thermal
expansion, (4) bulk and "true" density, (5) pore size and volume
fraction, (6) permeability and (7) emittance.

The MG-1 was the most dense of the three virgin materials
with a value of about 0.60 gm/cm^3. The densities of the MG-45
and MG-58 virgin materials were about 0.23 gm/cm^3. The MG-1
was also the most dense of the charred materials with a value
of about 0.19 gm/cm^3 as compared to 0.17 and 0.14 gm/cm^3 for the
MG-45 and MG-58 charred materials. All chars exhibited varia-
bility in density value.

The chars of the MG-45 and MG-58 were prepared in the arc-
jet at NASA Langley Research Center. The MG-1 was furnace charred
at SRI. The MG-45 and MG-58 both remained structurally sound to
temperatures of 3000 K. The MG-1 exhibited total degradation
to a powder above about 1700 K.

The MG-1 had the highest thermal conductivity of the three
virgin materials. The value for the MG-1 at 300 K was about
0.115 W/m-K as compared to values of about 0.055 and 0.050 W/m-K
for the MG-45 and MG-58, respectively.

For the charred materials, the MG-58 had the highest value
of thermal conductivity. At 1400 K, the thermal conductivities
of the MG-1, MG-45 and MG-58 chars were about 0.3 W/m-K, 0.9 W/m-K
and 1.2 W/m-K, respectively. At 3000 K, the thermal conductivity
values for the MG-45 and MG-58 were 4.1 W/m-K and 6.1 W/m-K,
respectively.

The virgin MG-1 had the highest value for heat capacity at
200 K and the lowest value at 500 K. The heat capacities of the
MG-1, MG-45 and MG-58 virgin materials at 200 K were 1100, 950
and 900 J/Kg-K, respectively. At 500 K, the heat capacities of
the MG-1, MG-45 and MG-58 were 1600, 1800 and 2100 J/Kg-K,
respectively.

4

For the charred materials, the heat capacities at 500 K were about 1100, 600 and 550 J/Kg-K for the MG-1, MG-45 and MG-58, respectively. At 1600 K, the heat capacities of the charred MG-1, MG-45 and MG-58 were about 1850, 2750 and 2700 J/Kg-K, respectively.

The virgin MG-1 exhibited a shrinkage of about -15×10^{-3} cm/cm at 150 K and expansion ranging from 10×10^{-3} to 16×10^{-3} cm/cm at 500 K when data were obtained by stablizing at discrete temperature levels. When the MG-1 was heated continuously at 10 K/min the expansion peaked at 78×10^{-3} cm/cm at 670 K and then shrank to a value of -150×10^{-3} cm/cm (15 percent) at 1200K. For the steady-state expansion measurements, the MG-1 exhibited more expansion in the X direction than in the Y direction (directions are defined in Figure 10).

The porosities of the MG-1, MG-45 and MG-58 virgin materials were about 48, 83 and 82 percent, respectively. For the charred materials, the porosity was in the vicinity of 90 percent for all materials. The pore and microballoon sizes ranged from about 4 to 85 microns with some variation between materials and between virgin and char of the same material.

The total normal emittance of the charred MG-1 decreased from about 0.81 at 800 K to 0.56 at 1900 K. It was believed that the decrease was a result of the behavior of the silica in the char.

The virgin MG-1 had the most resistance to gas flow as it was found to be impervious at pressure differentials up to about 270×10^{3} N/m^{2}. The virgin MG-58 had less resistance to gas flow than the virgin MG-45. The permeabilities of the charred MG-45 and MG-58 were not measured. However, for these materials there were large gaps between the honeycomb and filler which would offer little resistance to flow. The charred MG-1 had more inertial resistance than either the MG-45 or MG-58 virgin materials. However, the viscous resistance of the charred MG-1 was less than that of the virgin MG-58 and greater than that of the MG-45.

From the measurements and the concept of "boxing" the properties of ablative materials, estimates were made of the properties of the three materials over the complete temperature range. The bulk density of the MG-1 and the thermal conductivities and heat capacities of all materials were estimated throughout the temperature range from virgin to char.

Specimen Materials and Specimen Preparation

The compositions of the virgin MG-1, MG-45 and MG-58 are given in Table 1. Pictures of the virgin materials are shown in Figure 1.

Photomicrographs of the virgin MG-45 and MG-58 are presented in Figures 2 and 3, respectively. For these photomicrographs, the materials were vacuum impregnated and polished. Suitable quality photomicrographs were not obtained for the MG-1 because it would not impregnate and could not be polished as it was. In Figure 2, the gray area in the MG-45 is the impregnant. This material contained 18 weight percent elastomer and it was hard to discern the elastomer from the photomicrograph. Most of what can be seen in Figure 2 is the impregnant and the phenolic microballoons.

In Figure 3, the darker gray area in the virgin MG-58 is the impregnant. The lighter areas surrounding the microballoons and connecting them is the phenolic. The large region of phenolic in the left hand portion of the photomicrograph is the phenolic-glass honeycomb. In the lower portion of the photomicrograph, slightly to the right of center, is what appears to be a nylon particle. Note that with 30 weight percent powdered phenolic, the phenolic does not begin to fill all of the void spaces.

The MG-1 was charred at SRI. The schedule used to char the material was to heat at 10 K/min until the desired temperature was reached, hold at temperature for 30 minutes, and cool at 10 K/min. Attempts were also made to prepare specimens by immersing blanks of MG-1 in the furnace after it was preheated to 1561 and 3033 K. In both cases, the material was found decomposed into a grayish powder upon removal from the furnace. A helium purge was employed during charring. The high temperature furnaces described in Reference 2 were used. Pictures of the MG-1 before and after charring are presented in Figure 4. It was found that chars could be prepared to a maximum temperature of 1644 K. Above that temperature, there was a breakdown of the material into a powder. These observations are supported by the pictures of the chars of MG-1 shown in Figure 4. Expansion measurements showed that the degradation to a powder began at about 1700 K. Hence studies on the charred MG-1 were limited by the material behavior to 1644 K and below.

For the char specimens used for the ASTM C177 guarded hot plate, discs for use in charring were cut from the MG-1 to 8.25 cm diameter by 1.27 cm thick with the thickness direction aligned with the thickness direction of the billet. To obtain char specimens for the measurements with the radial inflow apparatus, blocks were cut 5.08 cm by 8.75 cm by 1.9 cm thick

6

with the thickness direction parallel to the thickness direction
of the virgin billet. These discs and blocks were then charred
and specimens were removed such that the measurements were made
in the thickness direction.

The weight losses observed during preparation of the chars
of the MG-1 are presented in Table 2. The weight losses ranged
from 70 percent for the chars prepared at 811 K to 76-78 percent
for the chars prepared at 1644 K.

Photomicrographs of the charred MG-1 are presented in Figure
5. The samples were vacuum impregnated to facilitate polishing.
From the photomicrographs, it appears that about all that remains
after charring is microquartz fibers and the carbon from the
degradation of the phenolic. The photomicrograph shown in Figure
5-b is of a sample prepared by immersing the virgin blank in a
furnace preheated to 1561 K.

The chars of the MG-45 and MG-58 were prepared in the arc-
jet at the NASA Langley Research Center. Discs about 7.6 cm
diameter were charred to a depth suitable for property measure-
ments. Information on the char discs which were supplied by the
NASA Langley Research Center is summarized in Table 3. The
table gives the exposure time for the various discs and the use
to which the discs were put at SRI.

A section through a char disc of the MG-58 is shown in
Figure 6. This disc was charred for 125 seconds. A quite thick
char layer was obtained. The char layer for the MG-45 was
thinner and less structurally sound. Other char discs of the
MG-58 are shown in Figure 7.

Photomicrographs of the charred MG-45 and MG-58 are presented
in Figures 2 and 3, respectively. Again, the specimens were
vacuum impregnated. About all that can be observed in the
photomicrographs is the charred phenolic microballoons and the
impregnant.

Photographs of the charred MG-58 taken at various magnifica-
tions with a scanning electron microscope, are presented in
Figure 8. These photographs were made at the NASA Langley
Research Center. The structure of the char is much more clearly
defined by these pictures than by the one shown in Figure 3-b.
It should be pointed out that the sample of which the pictures
with the scanning electron microscope were taken had been im-
pregnated with polyalphamethylstyrene, machined and then the

impregnant baked out. That probably accounts for the large number of open microballoons. From the pictures shown in Figure 8 one can observe charred microballoons held together with fillets of charred phenolic at contact points. There are significant amounts of void space between microballoons.

As-received, the arc-jet char discs of the MG-45 and MG-58 were too friable to allow direct machining of specimens. The char discs were vacuum impregnated with polyalphamethylstyrene to provide rigidity so that they could be machined. Polyalphamethylstyrene is made from 38 weight percent Amaco Resin 18 and 62 percent Toluene. This material provides a rigid resin which, after curing, degrades to a monomer and leaves no residue upon heating to about 644 K. Pictures of impregnated char discs are shown in Figure 9. Strip specimens for thermal conductivity measurements with the radial inflow apparatus were machined from the impregnated discs with the measurement direction parallel to the honeycomb cell walls. The impregnant was baked out in the furnace prior to the thermal conductivity evaluation.

Cutting plans to obtain thermal property specimens for measurements on the virgin materials are given in Figures 10 and 11. Shown in Figure 10 is the cutting plan for the virgin MG-1 and shown in Figure 11 is the cutting plan used for the virgin MG-45 and MG-58.

Apparatuses and Procedures

Thermal Conductivity – ASTM C177 Guarded Hot Plate. – This apparatus is described in Volume I. The 3 inch apparatus was used for all measurements reported in this volume. The specimen configuration for these measurements was 7.62 cm diameter by 0.635 cm thick. All measurements were made in an air environment.

Thermal Conductivity – Radial Inflow Apparatus. – A radial inflow apparatus was used for thermal conductivity measurements above 811 K. For the MG-1, a standard cylindrical specimen configuration and a strip specimen configuration were employed.

The standard cylindrical specimen configuration is described in Reference 2. One modification had to be made for the measurements on the MG-1. The material was friable and a graphite support cylinder (thin walled) was placed around the specimen to prevent the specimen from cracking when the center annulus between the calorimeter and specimen was packed with graphite granules.

8

The strip specimen configuration employed with the radial inflow apparatus for the measurements on the charred MG-1 is described in Volume II. The specimen strips (4 required for one run) for these measurements were 2.26 cm wide by 6.35 cm long by 0.254 cm thick. These measurements were made in the environmental furnace described in Volume II.

Most of the measurements on the MG-1 were made in a nitrogen environment. Some data were obtained in helium and argon.

For the MG-45 and MG-58, the strip specimen configuration described in Reference 2 was employed. The strip configuration is shown in Figure 12. The specimens were made from char discs which had been vacuum impregnated with polyalphamethylstyrene. The cutting plan used to obtain specimens from an impregnated disc is shown in Figure 13. Note that the bottom of the drilled hole (see Figure 12) was placed in the center of a honeycomb cell so that it would not see radiation through the gaps between the honeycomb and the filler.

The impregnated specimens of MG-45 and MG-58 were placed in the buildup as shown in Figure 12. After being installed in the furnace, the specimen was taken to about 644 K and held for a time sufficient to allow the impregnant to leave the specimen. Then, the measurement was continued. The measurements on the MG-45 and MG-58 were made in a helium environment.

Enthalpy (Heat Capacity) - Adiabatic Calorimeter. - Enthalpy measurements were made on the virgin materials and on the charred MG-1 in a drop-type adiabatic calorimeter. This apparatus is described in Volume I.

For the MG-45 and MG-58, bulk material was used for the measurements. However, for the charred MG-1, the material was pulverized and placed in a holder to increase the sample weight and provide containment for the material which was friable. Aluminum foil was used as a sample holder. The foil used for these measurements was calibrated so that the signal due to the foil could be subtracted from the total signal. The enthalpy values measured on the aluminum foil are plotted in Figure 14 and a curve from the literature is shown in the figure. Agreement between measured and literature values was rather good so the literature

values were used in correcting the data. The correction was made from the following equation:

$$(t_2 - t_1)_{SH} = \frac{h_{SH}W_{SH}}{K} \tag{1}$$

where

$(t_2 - t_1)_{SH}$ = temperature change in drop cup due to the aluminum foil
h_{SH} = enthalpy of aluminum foil
W_{SH} = weight of aluminum foil
K = calorimeter constant = 503.7 J/K

The temperature rise calculated from Equation 1 was subtracted from the total change in cup temperature to obtain the change in cup temperature due to the specimen. Generally, the correction for the aluminum foil was about 10 percent of the total signal.

Enthalpy (Heat Capacity) - Ice Calorimeter. - A drop-type ice calorimeter was used for enthalpy measurements on the charred materials. For these measurements, the apparatus and procedures described in Volume II were employed. The specimens were powdered and were placed in thin-walled C. S. graphite drop cups for the measurements.

Tungsten wire was used to hold the lid on the drop cup for the measurements on one of the specimens of charred MG-1 (1000-10-3#1). Enthalpy values for tungsten which were taken from Reference 3 are plotted in Figure 15. These values were used to calculate the volume of ice which would be melted per gram of tungsten wire used. Since the tungsten wire weighed 0.120 gram, the maximum signal (cm^3 of ice melted) would be about 0.01 cm^3 at 1750 K. The specimen signal at about this temperature level was 1.94 cm^3, hence, the tungsten wire introduced less than 1 percent uncertainty in the measurements and was neglected in the calculations.

Heat Capacity Calculations from Enthalpy Measurements. - Heat capacity was calculated from the enthalpy data by the procedure described in Volume I. The analytical equation which was fit to

the data by the method of least squares was

$$h_{273} = aT + bT^2 + \frac{c}{T} + d \tag{2}$$

where

h_{273} = enthalpy above 273 K reference
T = absolute temperature

Heat capacity is determined from the derivative of Equation 2

$$HC = a + 2bT - c*T^{-2} \tag{3}$$

In Equation 3, the constant $c*$ is obtained by forcing the heat capacity through a graphically calculated value at some predetermined temperature level.

The heat capacity was also determined graphically from the slope of the enthalpy versus temperature curves. A judgement was made in drawing the best curve through the analytically and graphically determined values of heat capacity.

Thermal Expansion. - Thermal expansion measurements were made from 150 K to 500 K on the virgin MG-1 with the quartz dilatometer described in Volume I. Measurements were made in both the X and Y directions of the billet (see Figure 10). In addition, the expansion of one sample of virgin MG-1 was measured from 300 K to 1800 K (above degradation temperature) in the graphite dilatometer described in Volume II. For the run in the graphite dilatometer, the sample was heated continuously at 10 K/min. Normally, the samples are brought to equilbrium at some temperature and held there for 10 to 15 minutes before readings are obtained.

Quantitative Microscopy (Pore Size Distribution). - The geometric arrangements of the MG-45 and MG-58 virgin materials and all chars were studied using techniques of quantitative microscopy. The samples were vacuum impregnated using Bakelite ERL 2795 and Hysol H2-3404 hardener. The epoxy filled the void structure and it appeared that no reaction took place between epoxy and virgin or char material. The virgin MG-1 could not be impregnated and sectioned well enough to provide a sample for measurements.

Measurements of dimensions (as viewed on a plane section through the 3-dimensional structures) and the areal fractions of the various parts of the complex structure were made. The dimensions were measured with a filar eyepiece, sampling along a random line arbitrarily imposed into the field of view of a reflection type microscope. The structure was sampled using bright field illuminations. Histograms of the number of entities of a given size (2-D plane) within an arbitrarily chosen range of 5 filar units versus the size of entity were plotted. Microscopy sampling was limited to the filler (solid) structure within the honeycomb and the cracks between the filler and honeycomb were not included.

For the MG-45 and MG-58 virgin and charred materials, the microballoon diameters on a plane were measured. The void areas were highly irregular and it would be difficult to define the proper dimensions. However, for the MG-1, dimensional measurements were made of components other than the microballoons. These measurements give some idea of the sizes of components other than the microballoons but can not be called diameters.

A point counting method (P_p) was used for sampling the areal fractions of the various structural parts within the ablative material. This method involved applying a fixed grid of points at random within the field of view of the microscope (points applied). The number of points occupied by any specific structural part were counted (points occupied). The ratio of the points occupied to the points applied gives the point fraction (P_p) or areal fraction of the structural part. The volume fraction (V_v) is equivalent to the point fraction (P_p).

The requirements for making areal fraction measurements are that the grid be applied at random and that sufficient points are applied that the point fraction (P_p) becomes a mildly fluctuating average value with an increasing number of points applied. Some problems were encountered related to the procedures for random sampling; e.g., irregular trends for some of the average volume fractions with increasing sample volume rather than a settling to a mildly fluctuating value. This indicated that the structure the sampling procedures , or both, were not random. Analysis showed that the structure was not random (there were clusters of microballoons) and this condition affected the average because of sampling with an ordered array of points. The translation screws on the microscope (orthogonal axes) were used for positioning the specimens for most of the point counts. Although rotation of the stage was also included with the translation of the sample, this procedure provides an ordered array for sampling. For a statistically accurate analysis, it is necessary that a completely random procedure (within the limits of optical magnification and resolution) be used.

12

The sum of the volume fraction of all parts (if none are neglected) should total to 1. The graphical data are expressed in a percentage and the sum of the average volume fractions total approximately 100 percent for each material. This indicates that the sampling is fairly representative, but for the reasons discussed in the paragraph above it still remains statistically unacceptable.

On the MG-45 and MG-58 virgin and charred materials, the following measurements were made:

1. Microballons diameter distribution - filled (impregnated) and unfilled microballoons

2. Areal fraction measurements
   a. hollow unimpregnated microballoons
   b. impregnated microballoons
   c. larger microballoons containing other microballoons and impregnant
   d. areas other than the microballoons which were filled with impregnant
   e. phenolic material (walls of microballoons and small broken pieces of microballoon walls in the virgin and charred conditions)
   f. nylon particles - MG-58 virgin only

For the charred MG-1 the following structural parts were sampled and measured for both size and areal fraction:

1. hollow (unfilled or unimpregnated) microballoons

2. filled (impregnated) microballoons

3. open porosity (impregnated void areas)

4. fibers

5. solid particles not considered walls of microballoons

6. microballoons walls - areal fraction only

Emittance. - The emittance of the charred MG-1 was determined by comparing the energy received by a radiometer from the sample to that received from a blackbody cavity maintained at the same temperature. A complete description of the apparatus is given in Appendix A.

For these runs the specimens were heated by placing them on a tungsten heating disc situated in the field of a flat concentrator induction coil. The surface temperature of the specimen was monitored with a thermocouple up to about 1100 K and with an optical pyrometer above 1100 K. The calibration of the radiometer was checked with a small blackbody cavity and the calibration curve shown in Appendix A was confirmed. The millivolt response of the radiometer remained unchanged for blackbody temperatures above 950 K; however, below 950 K the response increased about 5 percent from the original curve.

The specimens evaluated were extremely friable and porous precluding the precise measurement of temperature. The surface thermocouple was pressed against the surface underneath a stack of two small pads of fiberfrax and zirconia. This assembly was loaded with a tungsten cantilever spring. Due to the surface roughness and the softness of these specimens intimate contact of the thermocouple with the emitting surface was questionable. With insufficient pressure, poor surface contact and erroneously low readings will result, and too much pressure will cause the thermocouple to sink below the surface and monitor erroneously high readings.

Accurate measurement of the surface temperature with the optical pyrometer was also difficult. Due to the low thermal conductivity of this material, a significant temperature gradient existed causing a high level or radiation from the subsurface. Due to the rough appearance of the surface, filament disappearance was impossible and the measurement of an average temperature was merely by operator judgement.

These above difficulties created larger than normal uncertainties in both temperature and emittance, since the calculation of emittance is dependent on the measured temperature.

Permeability. - Permeability was measured at about 300 K with the apparatus described in Appendix G of Reference 2.

For the measurements on the virgin MG-45 and MG-58, a specimen about 2.54 cm diameter by 1.27 cm thick was used in the high temperature apparatus. For the measurements on the virgin MG-1, a specimen 2.54 cm diameter by about 0.635 cm thick was used in the apparatus for low permeability materials. For the measurements on the charred MG-1, a specimen about 1.59 cm diameter by about 1.7 cm thick was employed in the high temperature apparatus. The high temperature apparatus was used for two of the virgin materials and the char because it measures total pressure head and is probably better for relatively high flow rates.

14

Silicone rubber (Dow Corning RTV-731 Silastic) was used as the sealant for all measurements except the evaluation of the virgin MG-1. For the virgin MG-1, epoxy was used because the silicone rubber did not seal the interface adequately for this low permeability material.

In reducing the data, a viscous-inertial flow correlation equation was used. The analysis used has been called a Cornell and Katz data correlation (see Appendix G of Reference 2) and may be written

$$\frac{MP_m \Delta P}{LRT\mu G} = \alpha + \beta \ (G/\mu) \tag{4}$$

where

P_m = absolute mean specimen pressure
M = molecular weight of permeating gas
ΔP = absolute pressure difference across specimen
L = specimen thickness
R = universal gas constant
T = absolute temperature
μ = absolute viscosity

$$G = \frac{Q_{stp}\rho_{stp}}{A}$$

Q_{stp} = volumetric flow rate at standard conditions
ρ_{stp} = gas density at standard conditions
A = total cross-sectional area of porous media normal to flow
α = viscous flow coefficient (reciprocal of Darcy's Constant, K)
β = inertial flow coefficient

A plot of Equation 4 with the left hand side plotted as a function of (G/μ) yields a straight line. The slope is β and the intercept is α. This is known as a Cornell and Katz plot.

Experimental data were obtained in helium and nitrogen. The data were then calculated into a form suitable for use in Equation 4. The constants used in the equation and simplified expressions are given in Table 4. A plot of $(MP_m \Delta P/LRT\mu G)$ versus (G/μ) was made and the coefficients were determined from the slope and intercept.

15

Inspection of Equation 4 reveals the following: The higher the coefficients α and β, the more resistance there is to flow. On the other hand, the higher the value of Darcy's constant (reciprocal of α), the less resistance to flow.

Density. - Bulk and "true" density were measured on all virgin and charred materials. Bulk density was determined from measurements of weight and dimensions on specimens machined to a known geometry. Weight was measured to the nearest 0.0001 gram and dimensions were measured to the nearest 0.002 cm.

Bulk density of the MG-45 and MG-58 chars was measured as follows: (1) the char was impregnated with polyalphamethylstyrene, (2) the impregnated char was machined to a known geometry and dimensions were measured and (3) the impregnant was baked out of the char and the weight was obtained. In addition to the gross bulk density values of the MG-45 and MG-58 chars, the bulk density of the charred filler in the MG-58 was measured separately. This was done by removing the filler from the honeycomb. The filler columns were weighted and then coated with a thin coat of wax (pictures of filler columns are shown in Figure 16). The volume of the wax-coated filler columns was then measured in the apparatus shown in Figure 17.

What has been referred to as "true" density was also measured on the materials. In reality, the property measured was apparent density because all materials contain enclosed porosity which can never be completely removed. The materials were pulverized for the measurements and as the particle sizes get smaller and smaller the density values measured approach the true density. Hence, even though the property measured has been called "true" density, it is truly a measure of the apparent density of a prepared sample which can approximate the real true density. Apparent density measured on bulk material has been called apparent density.

"True" density was measured with both a liquid pycnometer and a helium pycnometer. With the liquid pycnometer, the procedure outlined in ASTM C135-66 was used and both water and ethanol were used as pycnometer fluids. Prior to performing the measurements, the samples were pulverized to as fine a particle size as was possible with a mortar and pestle. Prior experience has shown that for charred materials, about 75 percent of the particles are below 2 microns after the pulverization. However, for the virgin materials, some entrained porosity may remain after pulverization.

16

Pulverization with a mortar and pestle in liquid nitrogen was also performed on a sample of virgin material. Higher "true" density values were measured on this sample which indicates more complete pulverization.

When water and ethanol were used as the fluids for the pycnometer, a wetting agent was used. The wetting agent employed was Tergitol TNN, a nonionic detergent, which is a product of Union Carbide. The wetting agent reduces surface tension effects. Nevertheless, a small amount of flotation occurred which lent inaccuracy to the measurements.

In addition to the "true" density measurements, apparent density was measured. This was done by removing the filler from the honeycomb and performing measurements with the helium pycnometer. The samples were not pulverized prior to the measurements and any closed porosity was included in the measurement of sample volume.

For the honeycombed materials, "true" density measurements were made on the filler which was removed from the honeycomb. For the chars of MG-45 and MG-58, the filler and the honeycomb were separated and measured separately.

True densities of the materials were calculated from the densities of the components. The equation used for the calculations was:

$$\rho_t = \frac{1}{\dfrac{A}{\rho_a} + \dfrac{B}{\rho_b} + \dfrac{C}{\rho_c} + \ .. \ + \dfrac{i}{\rho_i}} \tag{5}$$

where

$$\rho_t = \text{true density of composity}$$
$$A, \ B, \ C, \ i = \text{weight percentages of components A, B. C,} \ \cdots i$$
$$\rho_a, \rho_b, \rho_c, \rho_i = \text{densities of components A, B, C,} \ \cdots i$$

Data and Results

Thermal Conductivity - Virgin Materials.

MG-1: The thermal conductivity data for the virgin MG-1 are
presented in Tables 5 and 6 and in Figure 18. The thermal con-
ductivity increased from about 0.10 W/m-K at 150 K to 0.115 W/m-K
at 300 K and then decreased slightly to about 0.11 W/m-K at 500 K.

MG-45: The thermal conductivity data for the virgin MG-45
are presented in Tables 7 through 10 and in Figure 19. There was
a significant amount of data scatter between the four specimens
evaluated. After the large difference in thermal conductivity
between Specimens 1 and 2 was noted (see Figure 19), two additional
specimens were evaluated. These data fell in with the higher thermal
conductivity values. The thermal conductivity increased from about
0.036 W/m-K at 170 K to about 0.062 W/m-K at 500 K.

The filler began to shrink at about 340 K. This probably
contributed to the scatter in the data above this temperature.
Pictures which show the shrinkage are presented in Figure 20.
Note in the figure that the shrinkage was severe.

MG-58: The thermal conductivity data for the virgin MG-58
are presented in Tables 11 and 12 and in Figure 21. The thermal
conductivity increased from about 0.036 W/m-K at 150 K to 0.054
W/m-K at 500 K. The disagreement between the two specimens
above 450 K was probably related to the shrinkage of the material.
Pictures of a specimen which show the shrinkage are presented in
Figure 22.

Thermal Conductivity - Charred Materials.

MG-1: The thermal conductivity data for the charred MG-1
are presented in Tables 13 through 26 and in Figures 23 and 24.
The materials were charred by heating at 10 K/min to a given temper-
ature level and holding at temperature for 30 minutes. Measure-
ments were limited to a hot face temperature of 1644 K because
the material turned to a powder above this temperature.

Shown in Figure 23 are the thermal conductivity data for chars
of MG-1 prepared at 811 and 1000 K. Most of the measurements were
in nitrogen. The data identified as "in helium" were obtained
with a helium purge; however, the furnace was not evacuated and
backfilled with helium. The data point identified as "in argon"
was taken on the sample by simply changing the purge gas to
argon. Hence, even through the environment was not rigidly con-
trolled, it appears that the specimen tended to be filled with the
purge gas.

18

In nitrogen, the thermal conductivity of the char prepared at 811 and 1000 K increased from 0.08 W/m-K at 400 K to about 0.33 W/m-K at 1500 K.

The data for the thermal conductivity of chars of the MG-1 prepared at 1500 and 1644 K are presented in Figure 24. There was a great deal of scatter in these data, probably because the charring temperature was near the temperature at which total degradation occurs and the material varied. In drawing the curve, the data for Specimen 1644-10-6 were ignored since the agreement with the guarded hot plate was poor. Emphasis was placed on the data for Specimen 1644-10-5 because of the agreement with the guarded hot plate and the smooth lineup of data points.

MG-45: The thermal conductivity data for the MG-45 charred in the arc-jet are presented in Tables 27 and 28 and in Figure 25. There was good agreement between the two specimens evaluated. The thermal conductivity increased from about 0.6 W/m-K at 1000 K to 4.1 W/m-K at 3000 K. A helium purge was used for the measurements.

MG-58: The thermal conductivity data for the MG-58 charred in the arc-jet are presented in Tables 29 through 32 and in Figure 26. There was some disagreement between the first runs on the two samples. Specimen 2, which had the lower thermal conductivity on the first run was rerun and the thermal conductivity values were higher and had a different character. Further, at 2900 K the data for the second run on Specimen 2 fell in with the data for Specimen 1. Hence, it appears that the difference between the two specimens may have been related to differences in thermal exposure prior to the evaluations.

The thermal conductivity of the charred MG-58 increased from about 0.1 W/m-K at 500 K (see guarded hot plate data in Figure 26) to a range from 3.4 to 4.9 W/m-K at 2600 K and was about 6.2 W/m-K at 3000 K. The data were obtained in a helium purge.

Enthalpy - Virgin Materials.

MG-1: The enthalpy data for the virgin MG-1 are presented in Table 33 and in Figure 27. The enthalpy increased smoothly from -1.5×10^5 J/Kg at 150 K to 3.4×10^5 J/Kg at 500 K.

The derived values of heat capacity for the virgin MG-1 are presented in the upper portion of Figure 27. There was good agreement between the graphical and analytical values of heat capacity. The heat capacity increased from 1100 J/Kg-K at 150 K to 1600 J/KG-K at 500 K.

MG-45: The enthalpy data for the virgin MG-45 are presented in Table 34 and in Figure 28. The enthalpy increased smoothly from -1.35×10^5 J/Kg at 150 K to 3.5×10^5 J/Kg at 500 K.

The heat capacity of the virgin MG-45 is presented in the upper portion of Figure 28. There was some disagreement between the graphical and analytical values of heat capacity. In particular, the analytical value appears low at 200 K and the graphical value appears high at 500 K. From the best curve through the analytical and graphical values, the heat capacity increases from about 800 J/Kg-K at 160 K to 1750 J/Kg-K at 500 K.

MG-58: The enthalpy data for the virgin MG-58 are presented in Table 35 and in Figure 29. The enthalpy increased smoothly from -1.2×10^5 J/Kg at 150 K to 3.5×10^5 J/Kg at 500 K.

The heat capacity of the virgin MG-58 is presented in the upper portion of Figure 29. The graphical and analytical values of heat capacity agreed well. The heat capacity increased from about 850 J/Kg-K at 150 K to 2100 J/Kg-K at 500 K.

Enthalpy - Charred Materials.

MG-1: The enthalpy data for the charred MG-1 are presented in Tables 36 and 37 and in Figure 30. The material used for these measurements had been charred at 1000 K. The enthalpy increased smoothly from the reference point to a value of 19×10^5 J/Kg at 1600 K.

The derived values of heat capacity are presented in the upper portion of Figure 30. There was some disagreement between the graphical and analytical values of heat capacity, especially at the higher temperatures. Hence, a best curve was drawn through both sets of values. The heat capacity increased from about 1050 J/Kg-K at 500 K to 1800 J/Kg-K at 1600 K.

MG-45: The enthalpy data for the MG-45 charred in the arc-jet are presented in Table 38 and Figure 31. The enthalpy increased smoothly from the reference point to a value of 3.4 $\times 10^6$ J/Kg at 2000 K.

The derived values of heat capacity are presented in the upper portion of Figure 31. The graphical and analytical solutions for heat capacity were in reasonable agreement. The heat capacity increased from a value of about 600 J/Kg-K at 500 K to about 3400 J/Kg-K at 2000 K.

20

MG-58: The enthalpy data for the MG-58 charred in the arc-jet are presented in Table 39 and in Figure 32. The enthalpy increased smoothly from the reference point to a value of 3.3×10^6 J/Kg at 2000 K.

The derived values of heat capacity are presented in the upper portion of Figure 32. The graphical and analytical solutions were in reasonable agreement. The heat capacity increased from a value of about 600 J/Kg-K at 500 K to about 3400 J/Kg-K at 2000 K.

Thermal Expansion - Virgin MG-1. - The thermal expansion data for the virgin MG-1 are presented in Tables 40 through 43 and in Figures 33 and 34. These data were obtained by holding the specimens at thermal equilibrium at successively higher temperature levels.

Shown in Figure 33 are the data for the thermal expansion in the X direction (see Figure 10 for definition of directions). The shrinkage at 150 K (from a 300 K reference) was about -15 $\times 10^{-3}$ cm/cm. Above 300 K, the virgin MG-1 expanded to a value between 8×10^{-3} and 13×10^{-3} cm/cm at 430 K, then showed a slight decrease in expansion between 430 and 470 K. The expansion increased between 470 and 500 K to maximum values ranging from about 10×10^{-3} to 17×10^{-3} cm/cm. A permanent shrinkage of about -13×10^{-3} cm/cm was observed upon cooling from 500 K to 300 K.

The thermal expansion in the Y direction is shown in Figure 34. The expansion in the Y direction was lower than that in the X direction. Also, the two specimens evaluated behaved differently. Specimen W-1 reached a maximum value of expansion of about 8×10^{-3} cm/cm at 500 K. Specimen W-2 exhibited a shrinkage of -8.5×10^{-3} cm/cm at 150 K and a maximum expansion of about 1.3×10^{-3} cm/cm throughout the range from 400 to 500 K. Both specimens exhibited permanent shrinkages of about -14.5×10^{-3} cm/cm after cooling from 500 K to 300 K.

One thermal expansion measurement was made on the virgin MG-1 in the graphite dilatometer at a constant temperature rise rate of 10 K/min. These data are presented in Table 44 and in Figure 35. The expansion peaked at a value of 78×10^{-3} cm/cm at 670 K at which point it began to outgas and shrink. The outgassing subsided at a temperature of about 770 K. However, the material continued to shrink until a plateau was reached at about 1200 K with a value of -150×10^{-3} cm/cm (15 percent). The shrinkage remained fairly constant from 1200 to 1700 K. Above 1700 K, the material became powdery with a subsequent indication of severe shrinkage.

Quantitative Microscopy (Pore Size Distribution). - Measurements
of microballoon diameters and areal fractions of the various struc-
tural components were made on the charred MG-1 and the virgin and
charred MG-45 and MG-58 materials. The virgin MG-1 could not be
polished to a degree sufficient to provide a sample for microscopy.
All materials were vacuum impregnated and polished to provide
samples for microscopy.

In general, microballoons were classified as being either
filled or unfilled. The filled microballoons were those which were
open such that they could communicate with the outside and become
filled with impregnant. The unfilled microballoons were those
which did not communicate with the outside and might be considered
as closed porosity.

MG-1: A partial view of the sample of the charred MG-1 is shown
in the photomicrograph in Figure 5-a. Histograms of the number of
entities within a given range versus the size are presented in
Figures 36 through 40. Shown in Figure 36 is the histogram for
the unfilled microballoons (closed porosity). Most of these micro-
balloons were grouped in the size range from 12 to 95 microns.
Shown in Figure 37 is the histogram of the filled microballoons
(one component of open porosity). Again, most of these microballoons
grouped in the range of 12 to 95 microns. Shown in Figure 38 is the
histogram for the open porosity (does not include filled micro-
balloons). Most of the open porosity grouped within the size
range of from about 6 to 70 microns. The histogram for the fiber
diameters is shown in Figure 39. Most of the fibers had a diameter
of about 7.7 microns with almost all of them being in the range
from 5.9 to 11.8 microns. Figure 40 gives the histogram from
small solid particles which were not considered as part of the
walls of the microballoons.

Shown in Figure 41 are the results of areal fraction (volume
fraction) measurements of the various structural components
in the charred MG-1. Note that after about 600 points applied the
fractions started to fluctuate about relatively constant values.
The areal fraction analysis indicates about 62.5 percent open
porosity (open porosity and filled microballoons) and about 84.5
percent total porosity (open and closed porosity). The solids,
excluding fibers, accounted for about 11.5 percent of the volume
and the fibers accounted for about 4 percent.

22

MG-45: Partial views of the samples used for the microscopy measurements on the virgin and charred MG-45 are shown in the photomicrographs in Figure 2. Histograms of the microballoon diameters for the virgin and charred MG-45 are presented in Figures 42 and 43, respectively. For the virgin MG-45, the unfilled and filled microballoons had similar size distributions with most of the diameters lying in the range from 4 to 47 microns (see Figure 42). For the charred MG-45, the unfilled and filled microballoons have similar size distributions with most of the diameters lying in the range of 4 to 34 microns.

Shown in Figure 44 are the volume fractions of the various structural parts for the virgin MG-45. The open porosity was about 31.5 percent (open porosity and filled microballoons) and the closed porosity was about 63.5 percent. Hence, the total porosity was about 95 percent. Observe that few of the microballoons were open to the outside, only about 2 percent.

The volume fractions of the structural components of the char prepared in the arc-jet from the MG-45 are shown in Figure 45. The open porosity was about 50 percent (open porosity and filled microballoons) and the closed porosity was about 40 percent. This yields a total porosity of 90 percent.

In general, the microballoon diameters for the virgin MG-45 were larger than for the charred MG-45. Further, the measurements indicated more total porosity for the virgin MG-45 than for the charred MG-45.

MG-58: Partial views of the samples used for the microscopy measurements on the virgin and charred MG-58 are shown in Figure 3. Histograms of the microballoon diameters for the virgin and charred MG-58 are presented in Figures 46 and 47. For the virgin MG-58, most of the microballoon diameters fell within the range of 2 to 51 microns. The filled and unfilled microballoons had about the same distribution. For the charred MG-58, most of the microballoon diameters were within the range of 4 to 30 microns. There were some differences in the distributions of the filled and unfilled microballoons. The peak for the unfilled microballoons occurred at about 12 microns and for the filled microballoons occurred at about 14 microns.

23

The volume fractions of the various structural parts for the virgin MG-58 are shown in Figure 48. The open porosity (open porosity and filled microballoons) was about 36 percent. The closed porosity (unfilled microballoons) was about 44 percent. Hence, the total porosity was about 80 percent. The phenolic (microballoons plus phenolic binder) occupied about 15.5 percent of the volume.

The volume fractions of the structural components in the MG-58 char prepared in the arc-jet are shown in Figure 49. The open porosity (open porosity plus filled microballoons) was about 54.5 percent. The closed porosity (unfilled microballoons) was about 30 percent. Hence, the total porosity was about 84.5 percent. The solid material in the char occupied about 15 percent of the total volume.

There was a great deal of similarity between the microballoon diameter distributions for the virgin and charred MG-58. The total porosity was slightly higher for the charred MG-58 than for the virgin MG-58. Both the virgin and charred material showed about the same volume fraction of solid.

Emittance - MG-1 Char. - The data for the total normal emittance of the MG-1 charred at 811 K are presented in Table 45 and in Figure 50. The wide scatter in values was due to the uncertainties in temperature measurement as discussed under "Apparatuses and Procedures". The mean value of emittance (from a linear fit of the data by the method of least squares) decreased from 0.81 at 800 K to 0.56 at 1900 K. The band of values around the mean represents ±0.10 (one standard deviation about regression).

Shown in Figure 51 are photographs of the emittance specimens after the runs were completed. Note the porous and cracked surface condition. This illustrates the obvious difficulty in monitoring temperature with a thermocouple or an optical pyrometer, particularly with the high temperature gradient through the thickness of the specimen (decreasing temperature from back to exposed face).

Permeability.

Virgin MG-1: The virgin MG-1 was impervious to the flow of helium within the limits of our ability to measure the flow rate. Two samples 2.54 cm diameter by about 0.64 cm thick were used in an attempt to measure permeability. A bubble flowmeter was used to measure flow rate. This device can easily measure volu-

24

metric flow rates as low as 0.1 cm^3/sec. Using epoxy as the sealing compound, the two specimens were exposed to a differential pressure of about 275 x 10^3 N/m^2 (40 psi) with no evidence of helium flow through the samples. One specimen failed by shearing around the edges at the restraining lip of the specimen holder.

Virgin MG-45: The data for the permeability of the virgin MG-45 parallel to the honeycomb cell walls are presented in Table 46 and in Figures 52 and 53. The viscous and inertial flow coefficients reduced from the Cornell and Katz plots in Figures 52 and 53 are summarized in Table 47. The inertial flow coefficient, β, averaged about 3600 cm^{-1} and the viscous flow coefficient, α, averaged about 20.3 x 10^6 cm^{-2}. The average value of Darcy's constant was 5.0 x 10^{-8} cm^2.

Virgin MG-58: The data for the permeability of the virgin MG-58 parallel to the honeycomb cell walls are presented in Table 48 and in Figures 54 and 55. The viscous and inertial flow coefficients reduced from the Cornell and Katz plots in Figures 54 and 55 are summarized in Table 47. The average inertial flow coefficient, β, was 2200 cm^{-1} and the average viscous flow coefficient, α, was 11.2 x 10^6 cm^{-2}. The average value of Darcy's constant was 9.0 x 10^{-8} cm^2.

Charred MG-1: Permeability measurements were made on MG-1 charred at 811 K. The permeability data are presented in Tables 49 and 50 and in Figures 56 and 57. The viscous and inertial coefficients were reduced from the Cornell and Katz plots shown in Figures 56 and 57 and are given in the figures. The inertial flow coefficients, β, reduced from the data were 4700 and 5350 cm^{-1} with an average value of 5025 cm^{-1}. The viscous flow coefficients, α, were 14.2 x 10^6 and 14.5 x 10^6 cm^{-2} with an average value of 14.4 x 10^6 cm^{-2}. The average value of Darcy's constant was 7.0 x 10^{-8} cm^2.

Charred MG-45 and MG-58: Permeability measurements were not made on the arc-jet chars of the MG-45 and MG-58. The filler in the MG-45 char was powdery and after impregnating, machining and baking out the specimen, the filler material was too loose to provide a suitable sample.

The filler in the MG-58 was sufficiently strong to withstand specimen preparation. However, there were large gaps between the filler and the honeycomb. Through discussions with the technical monitor it was decided that the permeability measurements on the charred MG-58 would be meaningless since all that would be measured would be the flow through the gaps. A picture of a permeability sample of the charred MG-58 is shown in Figure 58.

Density.

Bulk Density of Virgin Materials: The results of bulk density measurements on the MG-1, MG-45 and MG-58 virgin materials are presented in Tables 51, 52 and 53, respectively. The bulk density of the virgin MG-1 ranged from 0.584 to 0.608 gm/cm^3 for the six samples evaluated. The bulk density of the virgin MG-45 ranged from 0.206 to 0.244 gm/cm^3 for the ten samples evaluated. The bulk density of the virgin MG-58 ranged from 0.224 to 0.239 gm/cm^3 for the six samples evaluated.

Bulk Density of Charred Materials: The results of bulk density measurements on the chars of MG-1, MG-45 and MG-58 are presented in Tables 54 and 55, respectively. As shown in Table 54, the bulk density of the MG-1 ranged from a low of 0.156 gm/cm^3 for a char prepared at 811 K to a high of 0.206 gm/cm^3 for a char prepared at 1500 K. Average values were calculated for the chars prepared at different temperature levels. The average was 0.162 gm/cm^3 for the char prepared at 811 K and increased to about 0.192 gm/cm^3 for the chars prepared at 1000 and 1500 K. The average dropped slightly to a value of 0.173 gm/cm^3 for the char prepared at 1644 K.

Results of bulk density measurements made on the chars of MG-45 and MG-58 are presented in Table 55. For the charred MG-45, the measured bulk density ranged from 0.145 to 0.196 gm/cm^3. For the charred MG-58, the measured bulk density ranged from 0.138 to 0.146 gm/cm^3. Bulk density was also measured on the charred filler of the MG-58 (honeycomb removed). There was a large difference in density between the fillers from char discs Q3 and T4. The bulk density of the filler from char Disc Q3 was 0.160 gm/cm^3 while that from Disc T4 was 0.354 gm/cm^3. This may reflect differences in composition of the virgin.

True Density of Virgin Materials. - The results of "true" density measurements on the MG-1, MG-45 and MG-58 virgin materials are presented in Table 56. Recall that the property measured is actually the apparent density of pulverized samples but has been called "true" density. Calculated values of "true" density are also shown in Table 56. The true densities were calculated from the nominal compositions of the materials. The property values used for the true density calculations and the calculations themselves are presented in Table 57.

26

For the virgin MG-1, the calculated and measured values of "true" density disagreed at most, 9 percent from the calculated values. This seems to be reasonable agreement.

For the MG-45 and MG-58 virgin materials, the measured values of true density fell about 25 percent below the calculated values when standard pulverization techniques were used. Since these two materials contained significant amounts of phenolic microballoons it appears that perhaps some entrained porosity remained in the true density sample due to incomplete pulverization of all of the microballoons. One would certainly expect the calculated value to be accurate to less than 25 percent uncertainty unless the composition varied significantly from the nominal values given.

One sample of virgin MG-58 was pulverized in liquid nitrogen. Using this technique, a "true" density value of 1.20 gm/cm^3 was measured which is about 5 percent lower than the calculated value of 1.26 gm/cm^3. This tends to confirm that the standard techniques result in incomplete pulverization of virgin phenolic microballoons.

The calculated porosities of the virgin materials are given in Table 57. The porosity was calculated from the calculated true density and the measured bulk density. The virgin MG-1 had the lowest values for porosity of 47-49 percent. The porosities of the MG-45 and MG-58 virgin materials were 80-85 percent and 81-82 percent, respectively. In Table 57, these values for the MG-45 and MG-58 are compared with the total porosity values obtained from quantitative microscopy. There was reasonable agreement between the calculated porosity and the value from quantitative microscopy for the MG-58. However, for the MG-45, the value of total porosity obtained from quantitative microscopy (97 percent) appears too high.

True Density of Charred Materials. - The results of "true" density measurements for the MG-1, MG-45 and MG-58 charred materials are presented in Table 58. For the charred MG-1, the true density ranged from 2.07 gm/cm^3 for the 1000 K char to 1.63 for the 1644 K char. The average value was 1.85 gm/cm^3. A true density value was calculated under the assumptions that the silicone-elastomer and dimethyl oil were completely lost during charring and that the phenolic lost 50 percent of its weight. This gave a weight loss of 74.5 percent which agrees rather well with the observed weight loss. Under these assumptions, the char consisted of 62.7 weight percent silica and 37.3 percent carbon. This is a simplified analysis and it should be realized that the material could contain compounds of silica and carbon or silica and oxygen. If it is further

assumed that the density of the silica is 2.08 gm/cm^3 and the density of the carbon is 1.6 gm/cm^3, the true density of the char is calculated to be 1.87 gm/cm^3. This calculated value is within the range of the measured values. The total porosity of the charred MG-1 as calculated from the average measured "true" density and the bulk density is 90 percent. The total porosity from quantitative microscopy was 85 percent.

Shown in Table 58 are the measured values of "true" density for the charred filler and honeycomb materials of the MG-45 and MG-58. The average values of "true" density for the fillers of the charred MG-45 and MG-58 were 1.51 and 1.47 gm/cm^3, respectively. The average values of "true" density for the honeycomb of the charred MG-45 and MG-58 were 2.21 and 1.86 gm/cm^3, respectively. Why these values for the honeycomb are different is not known.

Apparent density measurements were also made on the filler of the charred MG-45 and MG-58. These values were obtained on unpulverized samples and are presented in Table 58. The values obtained were 0.76 and 0.60 gm/cm^3 for the MG-45 and MG-58, respectively. Using the measured values of apparent and true density, closed porosity values of 50 percent and 59 percent are obtained for the MG-45 and MG-58, respectively. For comparison, the closed porosity values obtained from quantitative microscopy were 40 percent and 30 percent for the MG-45 and MG-58 chars, respectively.

Discussion

General. - The MG-45 and MG-58 both performed to 3000 K without collapse of the char. However, the MG-58 did appear to provide a more structurally sound char layer than the MG-45. The char layer for the MG-45 appeared "looser" and maybe even somewhat powdery. The MG-1 would not perform to 3000 K. Above 1700 K, the charred MG-1 turned into a powder with total loss of structural integrity.

28

Thermal Conductivity - Virgin Materials. - The MG-1 had the highest thermal conductivity of the three virgin materials. Its maximum value was 0.115 W/m-K as compared to maximum values of 0.06 and 0.053 W/m-K for the MG-45 and MG-58, respectively. The higher thermal conductivity value for the MG-1 probably reflects the higher density (lower porosity) of this material insofar as more conduction area was available for heat transfer.

Thermal Conductivity - Charred Materials. - The MG-58 had the highest thermal conductivity of the three chars. At 1500 K, the thermal conductivities of the charred MG-45 and MG-58 were about the same at 1 W/m-K, whereas the charred MG-1 had a much lower thermal conductivity value of 0.32 W/m-K. At 3000 K, the thermal conductivity of the charred MG-45 was about 4.1 W/m-K as compared to a value of about 6 W/m-K for the charred MG-58.

Heat Capacity - Virgin Materials. - The heat capacities of the three virgin materials at 150 K were about 800 J/Kg-K, 800 J/Kg-K and 1100 J/Kg-K for the MG-45, MG-58 and MG-1, respectively. At 500 K, the values were 1600 J/Kg-K, 1800 J/Kg-K and 2100 J/Kg-K for the MG-1, MG-45 and MG-58, respectively. These values of heat capacity were slightly lower than the values of heat capacity given in Reference 4 for low-density phenolic-nylon (see Figure 29). For the virgin MG-45 and MG-58, the heat capacity values were about the same and the MG-1 had a heat capacity about 18 percent lower at 500 K.

Heat Capacity - Charred Materials. - The charred MG-1 had the highest heat capacity at 500 K (1125 J/Kg-K as compared to 500-600 J/Kg-K for the charred MG-45 and MG-58). However, at 1600 K, the charred MG-1 had the lowest heat capacity (about 1800 J/Kg-K as compared to about 2750 J/Kg-K for the charred MG-45 and MG-58).

The heat capacities of the charred MG-45 and MG-58 were lower than previous values for low-density phenolic-nylon to about 1250 K and were significantly higher above 1250 K (see Reference 4 and Figure 32). The values were even higher than values for graphite. This was primarily caused by the enthalpies of the charred MG-45 and MG-58 being lower than the enthalpy of the low-density phenolic-nylon at 1500 K but about the same at 2000 K. Thus, the slope of the curves and hence, the heat capacities, were higher for the charred MG-45 and MG-58. This behavior may be related to the fact that there was glass in the honeycomb of the charred MG-45 and MG-58 materials. Perhaps there was some new phase formed which altered the enthalpy curve and changed the "apparent" heat capacity. The data for the MG-45 and MG-58 chars should be used with caution.

29

Thermal Expansion - Virgin MG-1. - The expansion of the MG-1 was high up to 500 K. It was higher than the expansions of the virgin ablators for which data are reported in Volume I. The expansion of the MG-1 was also quite variable above 300 K. This is typical for elastomers above the curing temperature. In general, the expansion of the MG-1 was higher in the X direction than in the Y direction (see Figure 34). Permanent shrinkages on the order of 15 x 10^{-3} cm/cm were observed in both directions.

The expansion of the virgin MG-1 was much higher under a constant temperature rise rate than it was when allowing the material to equilibrate at successively higher temperature levels. These results are shown in Figure 35. Note that this behavior occurred at a relatively low temperature rise rate, 10 K/min.

Of interest to the ablation analyst is the large shrinkage of the material as it is charred. As can be seen in Figure 35, a shrinkage of -150 x 10^{-3} cm/cm (15 percent) was observed after charring to 1200 K. This should be investigated in more detail; however, it is apparent that shrinkages of this magnitude would show up as apparent surface recession in experimental ablation measurements and should be accounted for in ablation analysis. Similar behaviors would be expected for other ablative materials.

Quantitative Microscopy (Pore Distribution), Density and Porosity. - Most of the microballoon diameters for the MG-1, MG-45 and MG-58 fell in the range of 4 to 90 microns. The range for most of the microballoon diameters for the MG-45 and MG-58 virgin materials was about 4 to 43 microns. For the MG-45 and MG-58 charred materials, the range for most of the microballoon diameters was 4 to 30-34 microns. Hence, the microballoons diameters were slightly smaller for the charred materials, probably as a result of shrinkage.

The charred MG-1 had the most uniform microballoon diameter distribution and also the broadest range. The distribution of the open porosity (not including fractured microballoons) for the charred MG-1 was similar to the microballoon diameter distribution.

Calculated values of porosity are compared with the porosity determined by quantitative microscopy in Table 59. The porosity values from quantitative microscopy were in generally good agreement with the calculated values of porosity with the exception of the values for the virgin MG-45. The calculated value for the MG-45 is probably more meaningful. The virgin MG-1 had the lowest

30

porosity, 47-49 percent. The porosity of the MG-45 and MG-58 virgin materials were in the range of 80-85 percent. The charred materials all had porosities of about 90 percent.

As can be seen in Table 54, the MG-1 char prepared at 811 K had the lowest bulk density and the density increased as the char temperature was raised. This is probably a result of the shrinkage of the material during charring as shown in Figure 35. Between 811 and 1200 K the material must shrink faster than it loses weight; hence, the bulk density increases. This suggests that the bulk density of ablators during degradation might be best defined by calculation from TGA and expansion data obtained at heating rates close to those anticipated in use.

The measured values of bulk density on different samples exhibited considerable scatter (see Tables 54 and 55). This could be a result of local concentration gradients in the materials. Hence, one must consider the range of values until sufficient data are obtained to get meaningful averages.

Emittance - Charred MG-1. - The total normal emittance of the charred MG-1 decreased from about 0.81 at 800 K to 0.56 at 1900 K (see Figure 50). The reasons for the decrease in emittance are not well understood. However, recall that calculations indicated that the charred material consisted of about 63 weight percent silica and 37 percent carbon. The large quantity of silica in the material may have affected the emittance. As reported in Reference 5, the total normal emittance of fused silica decreases from about0.68 at 700 K to about 0.4 at 1200 K. Hence, the silica may have been controlling the character of the emittance curve for the carbon-silica composite.

Permeability. - The permeability coefficients for the MG-45 and MG-58 virgin materials are compared in Table 47. The virgin MG-45 offered more resistance to flow as can be noted from the table by the higher values of the viscous and inertial flow coefficients. The charred MG-1 offered more inertial flow resistance than either the MG-45 or MG-58 virgin materials but the viscous flow resistance of the charred MG-1 was within the range of the MG-45 and MG-58 virgin materials.

The virgin MG-1 was impervious to flow at pressures up to 270×10^3 N/m^2. Measurements were not made on the charred MG-45 and MG-58; however, an inspection of these materials indicated that they would offer little resistance to flow because of the large gaps between the honeycomb and the filler (see Figure 58).

31

Best Estimate of Density of MG-1 During Degradation. - An estimate of the bulk density of MG-1 during degradation is presented as a function of temperature in Figure 59. This estimate was prepared by plotting the bulk density values measured at room temperature as a function of charring temperature. Most of the decrease in density was assumed to occur within the temperature range at which outgassing occurred during the expansion measurement reported in Table 44 and Figure 35. A curve was then faired through the data to correspond with these observations. This seems a realistic approach to use until more detailed studies are made.

Best Estimate of Thermal Conductivity During Degradation.

MG-1: An estimated curve of thermal conductivity for the MG-1 as a function of temperature during degradation is shown in Figure 60. The "boxing" approach of Pears described in References 6 and 7, was used. Boxed values of thermal conductivity were obtained at 1000 and 1644 K from values measured at these temperatures on chars prepared at these temperatures (see Figures 23 and 24). The curve was drawn through the data for the virgin material to 500 K and was faired to the values for the 1000 K char at about 600 K. Then, the curve was drawn through the "boxed" values at 1000 and 1644 K. This is believed to provide a reasonably realistic definition of thermal conductivity.

MG-45: The best estimate of the thermal conductivity for the MG-45 as a function of temperature is shown in Figure 61. Prior experience was used in developing the curve. From the boxing data on phenolic-nylon char which were reported in Reference 2, it was known that the char thermal conductivity is very low at low charring temperatures. Hence, in drawing the curve, the thermal conductivity of the initial char was assumed to be the same as the virgin material at low temperatures and the same as that measured on the char at 3000 K. Then, a smooth curve was drawn in between these points. Our prior experience with phenolic-nylon char was used to estimate the character. Note that the measured values of char conductivity at 1000 K were ignored. This was done because the arc-jet char had been exposed to a temperature above 1000 K during degradation. Hence, from prior experience, it was known that the values at 1000 K were probably higher than the values which the char would have for the first exposure to 1000 K. Boxing data would be helpful in better defining the curve.

32

Preliminary values for the conductivity of charred MG-35 which have been used at NASA Langely to provide a reasonable correlation between observed and calculated responses during ablation, are presented in Figure 61. The MG-35 was similar in composition to the filler of the MG-45. The MG-35 contained 33 weight percent Sylgard 182 and 63 percent microballoons as compared to 18 and 78 percent, respectively, for the MG-45. The values obtained from NASA for the MG-35, in general, are about the same as the estimate made for the MG-45.

MG-58: The best estimate of thermal conductivity of the MG-58 as a function of temperature during degradation, is presented in Figure 62. This curve was developed in the same fashion as described for the MG-45. Again, boxing data would be helpful to better define the curve. Note that values which have been used by NASA Langley in analytical-experimental correlations of ablation data for high-density phenolic-nylon, are presented in Figure 61. There is a great deal of similarity between the estimated curve and the values used by NASA Langley.

Best Estimates of Heat Capacity During Degradation. - The best estimates of the heat capacities of MG-1, MG-45 and MG-58 as a function of temperature during degradation are presented in Figures 63, 64 and 65, respectively. The curves were developed by fitting them through the data for the virgin materials to 500 K and then fairing the curves into the data for the chars. The transition portion of the curve from virgin to char is, of course, somewhat uncertain. However, it is believed to be more representative than an abrupt change from virgin values to char values. The shape of the enthalpy curve during degradation (transition) is similar to that developed by Pears and Shoffner (Reference 6) from boxing data on phenolic-nylon. Boxing data on the materials in this program would provide a better definition of the heat capacity.

Preliminary values used by the NASA Langley Research Center in experimental-analytical correlations on MG-35 are shown in Figure 64 along with the estimates for the MG-45. These values are somewhat different than the estimated curve, especially in the transition from virgin to char. The MG-35 contained 33 weight percent Sylgard 182 and 63 percent microballoons which was a somewhat different composition than the MG-45.

33

Concluding Remarks

Several thermal properties of MG-1, MG-45 and MG-58 in the virgin and charred states were measured. Properties determined included: (1) thermal conductivity, (2) heat capacity, (3) thermal expansion, (4) permeability, (5) pore size and volume fractions of structural parts, (6) emittance, (7) bulk density and (8) true density. Thermal conductivity was defined from 150 K to 3000 K for the MG-45 and MG-58 and to only 1600 K for the MG-1. Heat capacity was determined from 200 K to 2000 K on the MG-45 and MG-58 and to 1600 K on the MG-1. Permeability, bulk density and true density were measured on all materials. Thermal expansion was measured on the virgin MG-1, and emittance was measured on the charred MG-1.

The MG-45 and MG-58 both performed to 3000 K with the MG-58 seemingly providing a more sound char layer. The charred filler in the MG-45 was "looser" and could be considered somewhat powdery. The MG-1 would perform only to about 1700 K. Above this temperature, there was total degradation of the MG-1 into a grayish powder.

Best estimates were made of the thermal conductivities and heat capacities of the material throughout the entire temperature range, including the degradation zone. The "boxing" concept [6,7] was utilized in making these estimates. When thinking along these lines, one begins to see why thermal conductivity values measured at low temperatures on arc-jet chars may be higher than the values obtained upon initial degradation to that temperature. The arc-jet char has generally been predegraded at temperatures above the initial charring temperature and studies have demonstrated that the thermal conductivity of a charring ablator is dependent upon the precharring temperature level.[2] These effects were considered in making the best estimates of thermal conductivity.

The high values of heat capacity for the chars of MG-45 and MG-58 above about 1250 K were somewhat surprising. The heat capacity was higher than that of previous phenolic-nylon chars and graphite. Exactly what caused this cannot be ascertained from the data, since only a limited amount of data were obtained (three temperature levels). However, it is possible that the glass in the honeycomb may have reacted with the carbon in such a fashion as to result in an increased heat capacity. This warrants more study to resolve the reasons for the high heat capacity.

34

Material variability was evidenced in some degree in most all measurements but was most pronounced in the bulk density measurements on the chars. The source of the variability may have been variations in composition and/or molding pressure.

The true density measurements on the virgin materials were suspect. Whereas the true density values on the virgin MG-1 were in reasonable agreement with calculated values and values supplied by NASA Langley, the values for the virgin MG-45 and MG-58 appeared low. The latter two materials contained significant fractions of phenolic microballoons and it is believed that these microballoons were not completely broken up by the standard pulverization techniques used. However, calculated values of true density for the virgin materials, are throught to be realistic.

The thermal expansion of the virgin MG-1 was dependent upon the manner in which data were taken. The values obtained by heating slowly to a given temperature level and then allowing the specimen to equilibrate were significantly lower than values obtained while heating continuously at a rate of 10 K/min. Also, of particular interest, is the fact that the MG-1 exhibited a shrinkage of about -150×10^{-3} cm/cm (15 percent) at 1200 K when heating continuously at 10 K/min. Such gross shrinkage is of importance in ablation analysis. Future expansion data should be obtained under controlled heating rates to define such effects.

PART II

MECHANICAL PROPERTIES

Summary

Tensile and compressive strength, initial elastic modulus, and axial strain-to-failure measurements were made on three virgin, low-density, ablation materials. A silicone-phenolic, MG-1, and two phenolic-glass honeycomb reinforced materials, one with phenolic-nylon filler, MG-58, and one with a silicone-phenolic filler, MG-45, were evaluated. For the MG-1, the mechanical properties were measured at eight temperatures from 150 K to 500 K along one orientation. For the MG-45 and MG-58, the measurements were made at room temperature along two orthogonal orientations, one parallel to the reinforcement ribbon and one perpendicular to the ribbon. Three rectangular tensile and compressive specimen configurations were studied using the phenolic-nylon, honeycomb reinforced, MG-58 material to define a suitable specimen for evaluating the reinforced materials. Also, the effects of the moisture content of the MG-58 material were studied.

The tensile strength of the MG-1 silicone-phenolic decreased dramatically from 7.91×10^6 N/m^2 at 150 K to 0.224×10^6 N/m^2 at 300 K, but decreased only slightly to 0.190×10^6 N/m^2 at 500 K. The room temperature tensile strengths in the "a" (parallel to the reinforcement ribbon) direction for the reinforced materials were 0.444×10^6 N/m^2 for the MG-45 and 0.594×10^6 N/m^2 for the MG-58. The "b" (perpendicular to the reinforcement ribbon) direction strengths of 0.100 and 0.281×10^6 N/m^2 for the MG-45 and MG-58 respectively, were significantly less than the "a" direction strength. The tensile initial elastic modulus for the MG-1 decreased from a high of $1,219 \times 10^6$ N/m^2 at 150 K to 51.5×10^6 N/m^2 at 300 K to 10.9×10^6 N/m^2 at 500 K. However, at room temperature, the reinforced phenolic-nylon MG-58 "a" direction modulus of 103×10^6 N/m^2 was about 2.5 times that of the reinforced silicone-phenolic MG-45 modulus of 41.9×10^6 N/m^2. The "b" direction tensile moduli were 40.0 and 13.8×10^6 N/m^2, for the MG-58 and MG-45, respectively. Tensile strain-to-failure for the MG-1 remained constant between 8 and 9×10^{-3} cm/cm from 150 to 300 K, but increased to 25.1×10^{-3} cm/cm at 500 K. At room temperature, the "b" direction strain-to-failure for both the MG-45 and MG-58 and also the "a" direction strain for the MG-58 were all about 7×10^{-3} cm/cm. However, the "a" direction strain of 18.4×10^{-3} cm/cm measured for the MG-45 is significantly higher than previously noted strain values for the reinforced materials.

The compressive strength of the silicone-phenolic MG-1 varied with temperature similar to the tensile strength. The strength decreased dramatically from 35.2 x 10^6 N/m^2 at 150 K to 0.615 x 10^6 N/m^2 at 300 K and only slightly to 0.560 x 10^6 N/m^2 at 500 K. At room temperature, the reinforced MG-45 "a" direction compressive strength of 0.280 x 10^6 N/m^2 was significantly less than the MG-58 strength of 0.902 x 10^6 N/m^2. In the "b" direction the 0.05% compressive yield strengths were 0.104 and 0.378 x 10^6 N/m^2 for the MG-45 and MG-58 respectively. The compressive initial elastic modulus for the MG-1 decreased from a high of 1.300 x 10^9 N/m^2 at 150 K to 0.0309 x 10^9 N/m^2 at 300 K to the lowest value of 0.0162 x 10^9 N/m^2 at 500 K. The reinforced phenolic-nylon MG-58 had compressive moduli of 119 and 88 x 10^6 N/m^2 in the "a" and "b" directions respectively, while the corresponding moduli measured for the reinforced silicone-phenolic MG-45, were 47.6 and 12.4 x 10^6 N/m^2. The compressive strain-to-failure for the MG-1 increased from 38.9 x 10^{-3} cm/cm at 150 K to 60.9 x 10^{-3} cm/cm at 500 K. The "a" and "b" direction strains measured for the MG-45 were 68.9 and 154.0 x 10^{-3} cm/cm respectively, while the "a" direction strain for the MG-58 was 9.7 x 10^{-3} cm/cm. No "b" direction strain-to-failure was measured for the MG-58.

To insure an optimum specimen design for evaluation of the reinforced MG-45 and MG-58, three square tensile specimen configurations having gage section areas of 3.63, 6.45 and 10.09 cm^2 and three square compressive specimen configurations having gage section areas of 1.61, 3.63 and 6.45 cm^2 were evaluated. The configuration study was conducted on the MG-58 only and then one tensile and compressive configuration was selected for evaluation of the MG-45. The configuration study showed no apparent strength-gage area relation for the configurations evaluated. There was bending on some occasions in compression. From these observations we conclude that the aspect ratio might have been a little high but that the cross-sectional dimensions were adequate for the cell sizes involved, except for problems related to material heterogeneity.

In the moisture effects study of the reinforced phenolic-nylon MG-58, moisture content was determined to be about 5 percent by weight. Tensile and compressive evaluations using dried and undried specimens, indicated that moisture content affected the mechanical properties of the MG-58 material. Since it was not the intent of this program to study moisture effects in detail, all specimens were dried, sealed in a bag and then run under normal laboratory conditions.

Specimen Materials and Preparation

The following materials provided by NASA Langley, were evaluated:

MG-1 - a low-density silicone-phenolic. Two cylindrical billets about 38 cm in diameter were provided (designated by NASA as Billets 1A and 1B). Billet 1A was about 7 cm thick while Billet 1B was about 8 cm thick.

MG-45 - a low-density silicone-phenolic with a phenolic-glass honeycomb reinforcement. Four cylindrical billets (designated by NASA as Billets 2, 3, 4 and 5), each about 38 cm in diameter x 3.8 cm thick, were provided.

MG-58 - a low-density phenolic-nylon with a phenolic-glass honeycomb reinforcement. Four cylindrical billets (designated by NASA as cakes (billets) 2, 3, 4 and 5) were provided. Each was about 38 cm diameter x 3.8 cm thick.

On examination of the MG-58 billets it was noted that delaminations existed between the filler material and the honeycomb reinforcement. The delaminations occurred in about 5 to 15 percent of the area of all MG-58 billets, with Billet 2 having the highest frequency. Location of the delminations was generally in the outer 5 to 8 cm of the billet. Delaminations up to about 0.05 cm wide and 2 cm deep were noted. Figure 66a is a photograph of the surface of Billet 2 showing the most severely delaminated area noted. Also Figure 66c, a photograph of specimen MG-58-3-T35b3, shows the depth of typical delaminations. Photograph b of Figure 66 illustrates another problem encountered with the MG-58 material-misalignment of the honeycomb ribbon. The "a" direction was carefully determined by a line parallel to the predominance of the honeycomb ribbons. However, the ribbons were not parallel throughout any billet and in small areas misalignment existed. On Figure 66c, the sides of the specimen are parallel to the "a" direction.

Also, during initial inspection of the MG-45 material, honeycomb misalignment was noted. However, the misalignment was not as widespread as previously noted in the MG-58 material. Photographs of Specimens C2a2 and C12b2 in Figure 67 give an indication of honeycomb misalignment in the MG-45. Delaminations, as seen on the surface of the MG-58 billets, were not visible on the surface of this material.

After inspection of the materials, the billets were laid out and cutting plans were drawn. These are shown in Figures 68 through 72. Each specimen was assigned an identification number which designated the material, billet, determinations, specimen number, loading direction and configuration. For example, MG-45-2-C5a2 designates:

MG-45 - material; others are MG-1 and MG-58
   2 - specimen was from Billet 2
   C - compressive loading; T - tensile loading
   5 - specimen number
   a - "a" direction; for MG-45 and 58 materials this direction is parallel to the honeycomb ribbon; for MG-1 this direction was selected to correlate with thermal specimen orientations
   b - "b" direction; for MG-45 and 58 materials this direction is perpendicular to the honeycomb ribbon; for MG-1 this direction is perpendicular to the "a" direction in plane of the billet
   c - "c" direction - billet thickness for all three materials
   2 - type two compressive specimen configuration

After initial inspection, the billets were sent to the machine shop to be machined into specimen blanks. While cutting the MG-1 billet a black rubber-like inclusion was noted. The inclusion was cylindrically shaped (about 0.25 cm diameter and 1.2 cm long). The location is shown in Figure 71 and was about 4 cm from the top of the billet. No other inclusions were found in the MG-1. However, in the machining of the MG-58 material, hard "slag" inclusions were encountered in some of the specimens. These inclusions appeared to be irregular shaped concentrations of phenolic resin that had not been completely mixed with the filler material and were about 0.08 to 0.5 centimeter in diameter. The inclusions were noted in each of the four billets from which specimens were machined, however, the greatest concentration occurred in Billet 2. Also, the inclusions appeared to be more heavily concentrated near the top and bottom surfaces of the billets as the majority were found while machining the blank specimens and relatively few were encountered in the machining of the final configuration. The grinding process caused these inclusions to be torn from the filler material leaving surface voids, however careful grinding minimized the surface effects. Surface voids caused by the inclusions occurred in the gage section of only four specimens and failure did not occur at the voids in any of the specimens.

40

The MG-45 material presented considerable difficulty during specimen fabrication. The most severe problem was the extremely low bonding strength between the silicone-phenolic filler and the honeycomb ribbon in some billets. Also, the bonding strengths varied randomly within and between billets. As in the preparation of the MG-58 specimens, the grinding process was used to machine the MG-45 specimens. Very light cuts were made to keep tool pressure to a minimum. Yet it was difficult to produce a finished MG-45 specimen without loss of filler materials from one or more of the partial "cells" along the specimen edges parallel to either the "ac" or "bc" planes.

To provide a rough quantitive evaluation of the filler-ribbon bond in the various billets, a simple fixture was used to apply a dead weight load on a single cell in the "c" direction. Weights were added until the filler material was "pushed" out. Four replications were made at random locations on each billet. The average load values for each of the billets were:

Billet 2 - 5000 grams
Billet 3 - 3400 grams
Billet 4 - 1000 grams
Billet 5 - 5300 grams

Variations of 30-50 percent were noted within Billets 2, 3 and 5, with the lower values occuring in the center portion of the billets. In Billet 4 extremely low values (200-300 grams) were noted for most of the billet (indicated by shaded area in Figure 69). Higher values (1500-1800 grams) were noted for the remainder of the billet. The extremely poor filler-ribbon bonding noted in Billet 4 necessitated machining several blanks before two (C5a2 and T12b1) usuable specimens were obtained.

A possible explanation for the poor filler-ribbon bonding may be the extremely large number of voids or delaminations noted between the filler and ribbon in Billet 4. As mentioned previously, no delaminations were visible at the surface of the MG-45 billets, however, during machining, delaminations were found below the billet surface. Figure 73, which is a photograph of several cells from each billet, gives an indication of the extent of the filler-ribbon delaminations in the MG-45 material. The delaminations were found in all billets, with the fewest being found in Billets 2 and 5. Delaminations of up to 0.5 cm diameter were noted, however most were on the order of 0.1 to 0.2 cm across. The photograph of Specimen C2a2 in Figure 67 shows typical delaminations found, while the

41

photographs of Specimen C12b2 shows the most severe delaminations found in these specimens. Another interesting fact is the location of the delaminations within the MG-45 billets. An inspection of the specimens indicated that the delaminations generally occurred within a 25 cm diameter circle. This could account for the lower filler-ribbon bond previously noted for the core areas. Also, this contrasts with the general location of the delaminations in the MG-58 material, which was the outer 5 to 8 cm of the billet.

All specimens were first finish machined, using a 46 grit silicon-carbide wheel, to a known geometry for accurate measurement of bulk density. The grinding process was used to machine both the blank specimens and the final test specimens. This process was selected over other machining processes, such as milling, to reduce the surface effects on the specimen and for ease of machining.

After the specimens had been blanked to a known size, bulk density measurements were made. Dimensions were measured with micrometers accurate to 0.0013 cm and weights were determined on an analytical balance sensitive to 0.001 gram. It was noted after the density measurements of the MG-1 were completed that a density gradient existed in the panel thickness ("c") direction. The bulk density values are shown in Table 60. Note that in the "c" direction the density, with two exceptions, increases from the top to a maximum in the middle of the billet and then decreases to a value at the bottom which is less than the density at the top.

It was noted during the weighing of the MG-58 specimens that the weight was increasing at a rate of 0.01 gram every 2-5 minutes. The cause of this phenomenum was considered to be an apparent difference in environmental conditions between the specimen storage area and the laboratory area and the known affinity of phenolic-nylon for moisture. Apparently the phenolic-nylon was abosrbing moisture to reach a stable state consistent with the environmental conditions of the laboratory. The specimens were allowed to stabilize, and the density measurements were then made.

To obtain bulk density values for the MG-58 material, unaffected by the relative humidity, the specimens were dried for 24 hours at 377 K in a thermostatically controlled oven. Bulk density measurements were made immediately after removal from the oven. The results of the two bulk density determinations are shown in

42

Table 63 for the tensile specimens and Table 66 for the compressive specimens. After the bulk density measurements were completed, the specimens were returned to the shop for machining to final test configuration.

To provide an indication of the environmental effects on the MG-58 material over a prolonged period of time, a test to monitor the moisture absorption rate and moisture content variations was conducted. This evaluation consisted of machining a specimen to a known geometry and then accurately measuring and weighing the specimen to determine bulk density. The specimen was then placed in a thermostatically controlled oven and dried at a constant temperature of 377 K for 24 hours. After removal from the oven, the specimen was immediately sealed in a moisture proof, plastic bag and allowed to cool to room temperature. Measurements to determine bulk density were then made. The specimen was then exposed to the laboratory atmosphere and bulk density measurements were made at regular intervals for 30 days. No attempt was made to control the laboratory environment during this period. The specimen was taken from Billet 5 (see Figure 68). The specimen configuration was a rectangular parallelepiped about 3.2 cm square x 6.4 cm long. The results of the moisture absorption evaluation are shown in Figure 74. As Figure 74 shows, the drying process resulted in about 4.3 percent decrease in bulk density. Moisture content was 4.96 percent by weight. Four hours after removal from the oven the specimen had regained about 50 percent of the loss in density and 20 hours after removal the bulk density was about the same as it was prior to drying. Over the next month the bulk density showed minor fluctuations of about 0.5 percent but remained essentially constant at about 0.2300 gm/cm^3. It is noted that variations in moisture content probably exist between the various material billets, however, this test served to provide a general indication of moisture content for the MG-58 material.

Sonic velocity measurements were also made on the MG-1 material. The velocity measurements for the MG-1 are shown in Tables 61 and 64. Note that the velocity measurements on the tensile specimens were in the "b" direction while the velocity measurements on the compressive specimens were in the "a" direction. Due to the nature of the MG-1 material, sonic velocity measurements could not be made in the "a" direction on the tensile specimens. The difference between the two velocities indicates possible anisotropy in the a-b plane. Due to the nature of the MG-45 and MG-58 materials, sonic velocity measurements could not be made on these materials.

43

For the evaluation of the MG-58 and MG-45 materials, much thought was given to the design of a specimen configuration which would best represent the bulk material. No standard specimen configuration exists for these type of materials and past experience has shown a strength/configuration dependence. Although the project goal was not to determine the effects of specimen configuration on properties, we felt justified in assuring ourselves that quality data were being obtained.

It appeared that the specimen strength would be influenced by the bonding strength between the phenolic-nylon filler and the glass honeycomb ribbon and also the bonding strength at the honeycomb ribbon joints. These two factors, particularly the latter, indicated that possibly the number of honeycomb cells within the gage section would influence the material strength. To include as many honeycomb cells as possible within the gage section, specimen configurations having rather large cross-sectional areas were evaluated. For the tensile determination, specimens having a gage section area of 3.63, 6.45 and 10.09 cm^2 were evaluated. Specimens having a gage section area of 1.61, 3.63 and 6.45 cm^2 were evaluated in the compressive determinations. Figure 76 shows the specimen configurations evaluated. A square configuration was selected for the gage section due to the material geometry and for ease of machining. To preclude introduction of another variable into the evaluation, a constant length/width (l/d) ratio was maintained for the gage section (for the tensile specimens the l/d ration was 4:1, for the compressive specimens the l/d ratio was 2.4:1).

The configuration study was conducted using only the MG-58 material. Since the MG-45 and MG-58 are similar, it was felt that the specimen configurations that properly defined the mechanical properties of one material would also be suitable for the evaluation of the other. Accordingly, tensile specimen configuration T-1 and compressive configuration C-2 used in the evaluation of the MG-58 material were selected for the MG-45 material determinations. However, in the evaluation of the MG-45 material, these configurations provided to be less than optimum. Specifically, most tensile failures occurred outside the gage section and the compressive specimens tended to bend. Physical characteristics of the MG-45 material probably have influenced the specimen failure. This will be discussed in greater detail later in this report.

44

Apparatuses and Procedures

Tensile. - The tensile evaluations of the three materials were made on a Tinius-Olsen universal testing machined which uses a screw loading mechanism as the basic apparatus. Light weight grips and chain completed the loading train (see Figure 75). The output from the Tinius-Olsen provided the input to the ordinate of a Moseley recorder. Calibration was accomplished by dead weight loading and was checked regularly during the evaluation to insure accurate calibration.

Strain measurement was accomplished by using clip-on extensometers (see Figure 75). An extensometer was clipped on each side of the specimen. Steatite ceramic was used as the rigid contact arms which translated the elongation within the gage length into flexure of the springs. Strain gages were mounted on both sides of the springs and electrically connected into a bridge circuit. Since two gages were in tension and two in compression, the four strain gages acted as strain measuring and temperature compensating elements. The output of the bridge circuit provided a signal that was proportional to the strain on the edge of the specimen. The extensometers were attached to yokes mounted on the specimen at a known distance apart.

The distance between the ends of the ceramic rods was about 10 percent greater than the gage length. Thus, the ends of the rods had to be depressed slightly for attachment to the yokes. The restoring forces were small yet sufficient to permit the extensometers to be supported between the yokes and follow the elongation of the specimen. The output of the bridge circuit provided the input to the abscissa of the X-Y recorder. Thus, a complete stress-strain plot to failure was obtained. The extensometers were calibrated using a shunt resistor calibration circuit and a micrometer accurate to 0.00025 cm.

Previous experience with pehnolic-nylon indicated that variations in moisture content could affect the mechanical properties of the MG-58 material. The experience previously noted during the bulk density determinations indicated that, unless environmental conditions were stringently controlled in the laboratory area, variations in moisture content would occur and introduce an additional variable in the evaluations. To insure that the moisture content was uniform for all specimens at the time of evaluation, the specimens were dried again after machining at 377 K for 24 hours. After the drying process, the specimens were sealed in moisture proof, plastic bags for storage. Evaluation of each specimen was made within about five minutes after removal from the storage bag. Undried specimens were also evaluated as a control measure.

The evaluations of the MG-45 and MG-58 materials were conducted at room temperature while the MG-1 material was evaluated at 150, 200, 250, room temperature, 350, 400, 450 and 500 K. Three tensile specimen configurations, designated T-1, T-2 and T-3 were used in the configuration study conducted with the MG-58 material. These configurations are defined in Figure 76. Tensile specimen configuration T-1, developed from the evaluations of the MG-58 materials, was used for the MG-45 and the undried MG-58 material determinations. The specimen configuration shown in Figure 77, designated Configuration T-4, was used for evaluation of the MG-1 material.

For the higher temperature determinations of the MG-1, two five element quartz infrared lamps located 7.5 centimeters from the opposite sides of the test specimen were used for heating. The lamps were controlled by a Powerstat to provide variable heating rates. Temperature gradients and heating rates were determined from heat runs made with specimens instrumented with six thermocouples (Chromel/Alumel). All thermocouples were located within the gage section - four surface thermocouples and two interior thermocouples (installed at the bottom of holes drilled to the center of the specimen). See Figure 78 for thermocouple locations along the gage length. Powerstat settings required to induce the proper heating rate and the final, stable test temperature were determined by time versus temperature runs made with the instrumented specimen. For actual test runs, these Powerstat settings versus time were used to heat and maintain the test temperature of the specimens.

Typical heating curves for the MG-1 tensile specimens to 350, 400, 450, and 500 K are shown in Figures 79 through 82, respectively. A heating rate of 55 K/min was used for all evaluations. As shown on the heating curves, heating continued until a uniform temperature was reached throughout the gage section (a gradient of <10 K was achieved). This condition was achieved in about 10-15 minutes, depending upon the temperature desired. Loading was initiated at the times indicated on the heating curves.

During the heating of most of the MG-1 specimens to the elevated temperatures, the thermal expansion was monitored. This was done by recording the strain indicated on the X-Y recorder from the initiation of heating until about one minute prior to loading when the recorder was zeroed for the tensile run. The expansion values are recorded in Table 61 and represent the total expansion of the 5.08 cm gage length.

46

For the low temperature evaluations of the MG-1 material, the specimen was cooled with vapors from liquid nitrogen. An insulated, cylindrical shell was placed around the specimen and the nitrogen vapors were blown into it. Again, temperature gradients were determined from runs made with a specimen instrumented with six thermocouples (Chromel/Alumel). See Figure 78 for thermocouple locations. One of the four surface thermocouples was taped to the outside surface while the other three were installed similarly to those used in the high temperature evaluations. All four surface thermocouples indicated equivalent temperatures. Thus, each specimen tested for cold temperature effects was monitored by a thermocouple taped to the gage section surface. The specimens were cooled slowly to the test temperature and then allowed to stabilize prior to conducting the run. The time required to achieve a uniform (<5 K gradient) temperature throughout the gage section after the monitor (surface) thermocouple (No. 2, Figure 78) reached the test temperature was 25, 15 and 15 minutes for 150, 200 and 250 K respectively.

During one run each at 150 K and 200 K, two thermocouples were used to monitor the specimen. One was taped to the gage section (as previously described) and one was mounted in the gripped section of the specimen (indicated as Thermocouple 7 in Figure 78). By using the second thermocouple an indication of the temperature gradient between the upper end of the specimen and the gage section was obtained. At 150 K the gradient was 13 K while at 200 K a gradient of 20 K existed. Failures still occurred in the gage section.

All tensile specimens were evaluated at a stress rate of 172×10^3 N/m^2/sec. This stress rate was selected because it satisfied the requirement for evaluation at threshold rates. Also, higher compressive rates proved impractical (see discussion of compressive data) thus, determining the stress rate for both the tensile and compressive evalutions.

Compression. - The compressive evaluations of the three materials were performed using a Tinius-Olsen universal testing machine. Calibration was accomplished by deadweight loading and was checked regularly during the evaluation to ensure accuracy. Clip-on extensometers (described in the previous section) were used for measuring axial strain.

As in the tensile evaluations of the MG-58 material, the test specimens were dried at 377 K for 24 hours after finish machining to preclude the introduction of possible anomalies caused by variations in moisture content. Additional undried specimens were also evaluated for comparison.

Initial compressive runs on the MG-58 material were made at a stress rate of 668 x 10^3 N/m^2/sec. However, at this rate, the duration of the run was too short to permit reaction to changing stress rates. Slower stresses were tried and a rate of 172 x 10^3 N/m^2/sec was found to be satisfactory. Thus, the compressive evaluations of the three materials, except those MG-58 specimens noted in Table 66, were made at a stress rate of 172 x 10^3 N/m^2/sec. The MG-45 and MG-58 materials were evaluated at room temperature while evaluations of the MG-1 were made at eight temperatures (intervals of 50 K) from 150 K to 500 K.

For the high temperature evaluations of the MG-1 material, the five element quartz lamps were again used. For the cold temperature evaluations, the specimen was again cooled with liquid nitrogen vapors. This equipment and the test procedures associated with it were discussed in the previous section. Figure 84 illustrates the placement of the six thermocouples on the instrumented compressive specimens utilized in the heating rate and cooling evaluations. Shown in Figures 85 through 88 are typical heating curves for the MG-1 compressive specimens. Again, a heating rate of 55 K/min was used for all evaluations. Heating continued until a uniform temperature was achieved throughout the gage section. This occurred after about 10 minutes of heating for all elevated temperatures except 500 K, for which 15 minutes was required. Uniform temperatures were achieved after 20 minutes, 15 minutes and 15 minutes for the 150 K, 200 K and 250 K runs respectively.

Three compressive specimen configurations, designated C-1, C-2 and C-3 were evaluated in the configuration study conducted with the MG-58 material. These configurations are defined in Figure 76. Compressive specimen Configuration C-2 was used for the evaluation of the MG-45 and undried MG-58 materials. Shown in Figure 83 is the compressive specimen configuration used previously on similar materials. This configuration is designated C-4 and was used for the MG-1 material evaluations.

48

Ultrasonics. - Ultrasonic measurements for velocity are made using a Sperry UM721 reflectoscope. Acoustic velocity is determined by the through-transmission, elapsed-time method. The Sperry UM721 is used as the pulser, and a Tektronix 564 oscilloscope complete with a 3B3 time base (precision of 1 precent)and a 3A3 vertical amplifier are used as signal measuring devices. Ultrasonic inspection is performed on specimens having machined, flat surfaces normal to the direction of measurement.

In using the through-transmission, elapsed-time technique for measuring acoustic velocity, a short pulse of longitudinal-mode sound is transmitted through the specimen. An electrical pulse originates in a pulse generator and is applied to a ceramic piezoelectric crystal (SFZ). The pulse generated by this crystal is transmitted through a short delay line and inserted into the specimen. The time of insertion of the leading edge of this sound beam is the reference point on the time base of the oscilloscope which is used as a high-speed stopwatch. When the leading edge of this pulse of energy reaches the other end of the specimen, it is displayed on the oscilloscope. The difference between the entrance and exit times is used with the specimen length in calculating ultrasonic velocity. A short lucite delay line is used to allow time isolation of the sound wave from electrostatic coupling and to facilitate clear presentation of the leading edge of the entrant wave resulting in a more accurate "zero" for time. Transducers having resonance frequencies of 1MHz and a 1.27 cm diameter cross-section are used. Alcohol is used as the couplant to reduce errors incurred by solid couplants.

Tensile Data and Results

MG-1 Material. - The results of the MG-1 material tensile evaluations are tabulated in Table 61. These results, depicting the effect of temperature on the tensile properties, are plotted in Figures 89 through 91. Photographs of typical failed tensile specimens are shown in Figure 92. Typical stress-strain curves are shown in Figures 93 through 100.

The tensile strength (see Figure 89) decreased somewhat from an average of 0.249×10^6 N/m^2 at 250 K to 0.130×10^6 N/m^2 at 450 K. At 500 K, there is a slight increase in strength to an average of 0.190×10^6 N/m^2, which is almost equal to the room temperature strength of 0.224×10^6 N/m^2. At temperatures below 250 K, the tensile strength increased dramatically to an average of 7.910×10^6 N/m^2 at 150 K.

49

The variation of the tensile elastic modulus with temperature, was similar to that of the tensile strength; a dramatic increase in modulus values at temperatures below 250 K and a decrease in values at temperatures greater than 250 K (refer to Figure 90). The modulus showed an increase from an average of 0.0711×10^9 N/m^2 at 250 K to 1.219×10^9 N/m^2 at 150 K. At temperatures above 250 K, the average value for initial modulus decreased to about 0.01×10^9 N/m^2 at 400 K and remained at approxiamtely that value to 500 K.

The average axial strain-to-failure for the MG-1 material generally increased with temperature (see Figure 91). The average strain-to-failure increased from 8.2×10^{-3} cm/cm at 150 K to 25.1×10^{-3} cm/cm at 500 K.

Scatter of the tensile data for the MG-1 material generally was somewhat greater than that of the compressive evaluations. The approximate data scatter (range/2) about the mean values of tensile strength and initial elastic modulus were:

±Percent Data Scatter About Mean

Temp K	Strength	Initial Elastic Modulus
500	2	10
450	15	23
400	9	16
350	20	5
300	17	21
250	13	19
200	7	4
150	20	21

The tensile strength values have been corrected to account for the loading imposed upon the specimen by the clip-on extensometer springs. Calibrations determined that the extensometers imposed a stress of 0.018×10^6 N/m^2 on the specimen. This value was added to the ultimate strength recorded during evaluation to give the true tensile strength. The typical stress-strain curves (Figures 93 through 100) are uncorrected.

Generally, the tensile specimens were allowed to stabilize at the proper temperature before any loading was applied. However, during the evaluations at 150 K, loading caused the load train to rotate which resulted in the clip-on extensometers rubbing against the insulated cylinder and producing erratic strain signals. This

occurred on two specimens (T20a4 and T37a4). In each case, loading was stopped, and after adjustments, the specimen was reloaded. It was thought that a small preload might solve the problem. Accordingly, a small preload was applied to two specimens (<2.2 kgm to Specimen T31a4 and <4.5 kgm to Specimen T33a4) when each specimen had been cooled to 200 K. The preload (about 10 percent of the ultimate load at 200 K) solved the rotation problem. But, apparently as a result of the small preload, the two specimens failed at low strength values, had lower strain values and had higher modulus values than Specimens T20a4 and T37a4.

As shown in Figure 92, the normal failure mode was a tensile failure similar to that of brittle materials. In most cases the fracture plane is normal to the specimen axis and is mostly flat.

MG-45 Material. - The results of the tensile evaluations of the MG-45 material are shown in Table 62. The effects of bulk density on the tensile strength, initial elastic modulus and strain-to-failure are shown in Figures 101 through 103. Photographs of typical failed specimens are shown in Figure 104. The typical stress-strain curves shown in Figures 105 and 106 are uncorrected for clip-on induced stress.

As Figures 101 through 103 show, there is no apparent correlation between the tensile properties, in either the "a" or "b" direction, and bulk density. The tensile properties measured in the "a" direction are all greater than the corresponding "b" direction property. The tensile strength was about 4.5 times greater in the "a" direction than in the "b" direction (0.444 versus 0.100 x 10^6 N/m^2), while the "a" direction values for modulus and strain-to-failure were about three times greater than the "b" direction values (41.9 and 13.8 x 10^6 N/m^2 for modulus; 18.4 and 6.5 x 10^{-3} cm/cm for strain, respectively).

Note in Table 62, that the tensile properties measured for Specimen T13b1 are significantly higher than the values measured for the other three "b" direction specimens. Note also the photographs of the failed "b" direction tensile specimens (Specimens T11b1 and T13b1) in Figure 104. The typical "b" direction tensile failure is characterized by the separation of the filler material from the honeycomb ribbon as shown in the photograph of Specimen T11b1. Specimen T13b1 was the only "b" direction tensile specimen in which fracture of the filler material within the honeycomb cell occurred and in which the filler material remained bonded to the ribbon. Recall also the previous discussion of the filler-

ribbon bonding strength in which it was noted that Panel 5 appeared to have the highest bonding strength. Thus, the "b" direction tensile strength is directly influenced by the filler-ribbon bonding strength as indicated by the higher strength of Specimen T13b1.

All "a" direction specimens failed in an area in which some degree of honeycomb misalignment existed. Initial fracture occurred with the separation of the filler material from the honeycomb reinforcement, generally beginning with the incomplete cells along the outer edges. Concurrently with the separation of the filler, failure of the bond between honeycomb ribbons occurred. Initial fracture in the "a" direction generally occurred at a tangent point at the end of the gage section. To provide stress relief at that area, the radius at the ends of the gage section of Specimen T1a1 was increased to 12.2 cm. This did not change the fracture location; however, it is felt that the rather severe honeycomb misalignment noted in the fracture area for this specimen determined the failure location.

As mentioned earlier in this report, the tensile specimen configuration design may be marginal since failure generally occurred outside the gage section (see Table 62). However, as shown above, material characteristics affect the failure location. Thus, the honeycomb alignment and the filler-ribbon bond appear to have influenced the failure location to a greater extent than the specimen design.

MG-58 Material. - The results of the tensile evaluation of the MG-58 material are shown in Table 63. As shown in Figure 107, there is apparently no tensile strength-area relationship in either the "a" or "b" directions for the specimen configurations evaluated. The average "a" direction tensile strength was 594×10^3 N/m^2 while the average "b" direction strength was 281×10^3 N/m^2. Initial tensile elastic modulus also shows little area dependence (see Figure 108). Average modulus values for the "a" and "b" directions were 107 and 40×10^6 N/m^2 respectively.

Scatter of the tensile data for the MG-58 material was generally somewhat less than that of the MG-1 tensile evaluations. The approximate data scatter (range/2) about the mean values of tensile strength and initial modulus were:

52

±Percent Data Scatter About Mean

Configuration	a Direction		b Direction	
	Strength	Modulus	Strength	Modulus
T-1	13	8	24	9
T-2	24	7	42	5
T-3	7	40	3	2

There were however, two "a" direction specimens (T3a2 and T4a2) that showed significantly higher than average strength (see Figure 107). The factor influencing this behavior appears to be bulk density. Note in Table 64, that the bulk density of these two specimens is noticeably higher than that of most of the "a" direction specimens indicating a possible strength-density relationship. Figures 109 and 110, which are plots of bulk density versus tensile strength and modulus respectively, show that for the "a" direction, there is probably a relationship between strength and material density. Note, however, that one type 3 specimen (T6a3) has high values for density and modulus but only about average strength. This behavior indicates that possibly another factor is influencing the "a" direction mechanical properties. An examination of the fracture areas indicated that honeycomb alignment could be that factor.

In the "a" direction evaluation, it was noted that all specimens, except T1a1, failed in an area in which some degree of misalignment of the honeycomb ribbon existed. In Specimen T1a1 there was no noticeable honeycomb misalignment. It was also noted that those specimens having the lower strengths tended to have the greatest ribbon misalignment either in the number of honeycomb ribbons in the failure area not aligned or in the degree of misalignment of the ribbons. (Specimen T6a3 had a high degree of honeycomb mis-alignment whereas Specimens T3a2 and T4a2 had only slight mis-alignment at the fracture areas.) Thus, the "a" direction tensile strength of the MG-58 material, appears to be influenced by bulk density and honeycomb alignment.

Figure 111 shows photographs of typical tensile fracture areas. Initial fracture of specimens subjected to a tensile loading in the "a" direction occurred with the separation of the filler material from the honeycomb reinforcement, generally beginning with the incomplete cells along the outer edges. Also, concurrently with the separation of the filler, failure of the bond between honeycomb ribbons occurred. Continued loading after initial failure resulted in fracture of the honeycomb ribbon - usually along the line at one end of the bonding area between adjacent ribbons. Failure of the specimens subjected to a "b" direction

tensile loading usually occured by separation of the filler from the honeycomb and failure of the bond between honeycomb ribbons as shown in Figure 111c. On a few "b" direction specimens the bond between the filler and the honeycomb was greater than the tensile strength of the filler material and some filler materials remained attached to the honeycomb. However, Specimen T34b1, shown in Figure 111d was the only "b" direction specimen in which complete fracture of the cell material occurred. This specimen also had a very high strain-to-failure. Typical tensile stress-strain plots are shown in Figures 112 and 113.

In the previous evaluations of the MG-58 material, moisture effects on the material were controlled. Two additional tensile specimens (one each in the "a" and "b" directions) were evaluated in which no attempt was made to control the moisture content of the specimens. Tensile specimen configuration T-1 was used.

The results of these evaluations are shown in Table 63. Note that the strength values for the undried specimens have been corrected for the stress induced by the clip-on extensometers. It is not considered necessary to correct the previously determined values for the dried MG-58 specimens. Different extensometers, unavailable for use in these determinations, that exerted significantly less load on the specimens were used for the earlier evaluations. The stress induced by the extensometers was less than 0.009×10^6 N/m^2, and is not considerd significant in view of the ultimate strength of the MG-58 material.

Note that in the "a" direction the dried specimens showed higher values, while in the "b" direction, except for strain, the undried specimen had slightly higher values. For the "a" direction determinations the ultimate strength and strain-to-failure for the undried specimen were significantly less (about 33 percent and 40 percent respectively) than the averages for the dried specimens. The initial modulus was only slightly (9 percent) less than the average modulus determined for the dried specimens. In the "b" direction the strength values were identical (0.292 $\times 10^6$ N/m^2 for the undried and 0.281 $\times 10^6$ N/m^2 for the dried) while significant differences were noted in the values of modulus (35 percent) and strain-to-failure (22 percent). These evaluations were too limited to draw firm conclusions but they do indicate that moisture content does affect the mechanical properties of the MG-58 material.

54

Compressive Data and Results

MG-1 Material. - Shown in Table 64 are the results of the compressive evaluations of the MG-1 material. The relationship between temperature and ultimate strength, Young's modulus and strain-to-failure are shown in Figures 114 through 116, respectively. Photographs of typical failed specimens are shown in Figure 117 while Figures 118 through 125 show typical stress-strain curves.

At elevated temperatures the compressive strength decreased with increasing temperature up to 400 K(0.615 x 10^6 N/m^2 at 300 K to 0.391 x 10^6 N/m^2 at 400 K). The strength increased to 0.560 x 10^6 N/m^2 at 500 K which is slightly below the room temperature strength. As the temperature was decreased below room temperature, the strength increased slightly to 0.910 x 10^6 N/m^2 at 250 K but increased to about 60 times the room temperature strength at 150 K.

The initial compressive elastic modulus constantly decreased with increasing temperature from 150 K to 500 K. A very sharp decrease in modulus occurred from 150 K to 250 K (1.30 to 0.0649 x 10^9 N/m^2). Above 250 K, the initial elastic modulus decreased only moderately to 0.0162 x 10^9 N/m^2 at 500 K.

As expected, the axial "a" direction strain-to-failure generally increased with temperature. From 300 K to 400 K the average strain-to-failure remained fairly constant at about 49 x 10^{-3} cm/cm. Above 400 K, the average strain increased to about 61 x 10^{-3} cm/cm at 500 K. At temperatures below 250 K the average strain decreased to about 34 x 10^{-3} cm/cm at 200 K and about 39 x 10^{-3} cm/cm at 150 K. At 250 K abnormally high strain-to-failure was noted. A possible reason for the high strain values at 250 K may be found by examining the failure mode. As shown by the photograph of Specimens C29a4, in Figure 117, specimens at 250 K tended to fail in a double fracture of a compound nature, while the general failure mode at other temperatures was a single shear fracture. We have no explanation for this behavior.

The compressive data for the MG-1 material generally showed good agreement. The approximate data scatter (range/2) about the mean value of the compressive strength and initial elastic modulus was:

±Percent Data Scatter About Mean

Temp K	Strength	Initial Elastic Modulus
500	7	16
450	3	15
400	10	8
350	6	27[1]
300	3	4
250	0	11
200	9	6
150	10	8

[1] Low value dropped

During the evaluation of the cold temperature specimens at 200 K, failure was noted to be occuring in the foot rather than in the gage section. This was thought to be caused by a temperature gradient between the specimen gage section and foot. Accordingly, to investigate the existance of a temperature gradient, additional thermocouples were installed in the center of each foot of one of the previously instrumented specimens. (see Figure 84 for locations) Because of equipment limitations, two of the thermocouples installed in the gage section (Numbers 3 and 4) were disconnected. Thus, six thermocouples were used to monitor temperature throughout the specimen. The instrumented specimen was cooled and thermocouple readings were monitored as previously described. Results showed that a temperature gradient did exist between the gage section and the specimen foot with the foot being greater than 16 K warmer at 200 K. Adjustments were made to the nitrogen vapor discharge nozzles which reduced the gradient to 10 K. One specimen (C28a4) was evaluated having a 10 K gradient but it also failed in the foot. Further adjustments, which included flowing the nitrogen vapors through tubing around the push rods prior to discharge into the shell, resulted in reducing the thermal gradient to about 2 K at 200 K. Evaluations performed with this gradient resulted in the proper failure mode. Prior to evaluations at 150 K and 250 K, the instrumented specimen was cooled to the proper test temperature and allowed to stabilize. The thermocouple readings indicated a uniform temperature throughout the specimen. The photograph of Specimen C28a4 in Figure 117, shows a typical failure resulting for the temperature gradient.

Generally, the compressive specimens failed in shear as shown in the photographs of Specimens C10a4 and C19a4 in Figure 117. The failure plane, except at 250 K, was approximately perpendicular to the a-c plane and inclined at about 45° to the a-b plane. This indicates possible anisotropy and lower strength in the "c" direction. A somewhat different failure occurred at 150 K. The failure mode was still a shear failure with the failure plane oriented as previously noted. However, a complete fracture did not occur. The fracture appeared as a crack with noticeable bonding strength remaining between the specimen halves. In Figure 117 the photograph of Specimen C30a4 shows a typical fracture at 150 K.

MG-45 Material. - The results of the compressive evaluations of the MG-45 material are shown in Table 65. Note that the maximum strength shown is not the failure strength. By observation of the specimens during the runs, it was determined that failure actually occurred at an indeterminate point on the stress-strain curve between the yield and maximum strengths. However, due to the material properties and failure mechanism the point of failure was obscured on the stress-strain curve. Initial failure occurred through separation of the filler from the honeycomb ribbon, generally at the incomplete cells along the specimen edge. In the "a" direction, failure of the filler-ribbon bond would result in a loss of support for the ribbon causing a sharp change in the stress-strain curve. Thus, it is indicated that in the "a" direction failure probably occurred near the yield point. Continued loading resulted in compaction of the filler material accompanied by a gradual increase in load. It was also noted that the "a" direction specimens (except C5a2) failed along about a 45° shear plane. See the photograph of Specimen C6a2 in Figure 130. A typical "a" direction compressive stress-strain curve is shown in Figure 131. In the "b" direction, loading produced no discernable yield point as occurred in the "a" direction. Refer to Figure 132. This is expected since very little of the load is supported by the honeycomb ribbon in the "b" direction. The stress-strain curve then approximates that of the filler material. Continued "b" direction loading resulted in crushing of the filler material accompanied by a gradual indication of higher strengths. Thus, the "b" direction true ultimate strength was not determined.

The maximum "a" and "b" direction compressive strengths are about the same. However, the average 0.2 percent yeild strength measured in the "a" direction was about 1.5 times greater than in the "b" direction (0.204×10^6 N/m^2 versus 0.132×10^6 N/m^2).

This is as expected considering the different loading of the honeycomb ribbon in the two directions. Also, as expected the average initial elastic modulus for the "a" direction was greater than for the "b" direction (24.7 x 10^6 N/m^2 in the "a" direction and 9.42 x 10^6 N/m^2 in the "b" direction). As with the MG-45 tensile evaluations, no apparent correlation exists between bulk density and 0.2 percent compressive yield strength, initial elastic modulus or strain. (See Figures 126 through 128 respectively)

Examination of the failed MG-45 compressive specimens indicated bending had occurred on most of the specimens. However, it was not known whether bending occurred during the initial portion of the stress-strain curve or commenced at some point after yield. The high strain values further indicate the possibility of bending. To determine the possible influence of bending on the compressive evaluations, special compressive blocks (3.17 cm square x 6.35 cm long) were tested. Two blocks were run for both "a" and "b" directions. All blocks were machined from Billet 2 (Figure 69) to reduce the influence of material variability between billets. The results of these tests are also shown in Table 65. For the "a" direction, both the maximum and 0.2 percent yield strength for the specimen and blocks showed very good agreement (disregarding the values for Specimens C2a2 and C5a2 and comparing only the specimens from Billet 2 with the blocks to minimize material variability effects). The modulus for the blocks (47.6 x 10^6 N/m^2) is significantly greater than that for the two specimens from Billet 2 (31.4 x 10^6 N/m^2). The expected relationship between compressive initial elastic modulus and l/r ratio is shown in Figure 129. The values for these evaluations apparently fall at one extreme of the curve resulting in the differences in values noted.

In the "b" direction determinations, no maximum value was obtained for the blocks and loading was stopped after noticeable specimen failure, but prior to reaching a maximum stress value. The average 0.2 percent yield strength for the compressive blocks of 0.247 x 10^6 N/m^2 is about twice that observed for the specimens (0.132 x 10^6 N/m^2). In reviewing these values, remember that for compressive blocks friction restraint from the heads of the testing machine tend to change the apparent strength relations under test and provide values higher than the actual true value. This could account for some of the difference in yield strength values, however, it appears that specimen bending must have occurred prior to yield to account for the lower specimen strengths. Non-symetric nature of the specimens, having more or less of the cells at one edge, can cause the bending. The relation between the initial elastic modulus determined in the "b" direction for the specimens and compr sive blocks is similar to that noted for the respective moduli in the "a" direction.

A well designed compressive specimen should not buckle or barrel during loading. However, there are several factors inherent in the MG-45 material that could contribute to specimen bending. The first factor is honeycomb alignment which can introduce undesirable stresses that could cause bending and affect the material strength. As previously noted under Material and Specimen Preparation, honeycomb misalignment occurred randomly throughout each of the billets. This factor is considered to have a more pronounced effect in the "a" direction determinations than in the "b" direction. All of the "b" direction specimens failed in an area having some degree of ribbon misalignment except Specimen C11b2 in which no misalignment was noted. Note the significantly greater yield strength for this specimen as compared to that of Specimens C10b2 and C12b2. (Refer to Table 65) In the "a" direction determinations, all specimens failed where ribbon misalignment was present. Specimen C2a2 had noticeably greater ribbon misalignment in the failure area than did Specimens C1a2 and C6a2. Note in Table 65 that the strength of Specimen C2a2 is also lower. A second property noted in the MG-45 material is believed to be the primary cause of the very low 0.2 percent yield strength shown in Specimen C5a2. That factor is the filler ribbon bonding strength. Recall from previous discussion that this bonding strength varied widely within and between billets and that Billet 4 showed very low bonding strength compared to the other billets. This would account for the low yield strength for Specimen C5a2. A third factor affecting strength could be density variations within and between billets, however, the overriding effects of the first two factors preclude determining density effects. A fourth factor, though not inherent in the material, could also influence specimen bending. This factor is the relative size of the incomplete cells along two opposite sides of the specimen. On machining the specimens, no attempt was made to equalize the opposing cells. The ribbon misalignments would have made such an attempt nearly impossible. Under loadings, it is probable that the smaller of opposing cells would fail first, causing a shift in the neutral axis which would introduce bending loads.

The correlation between the compressive data for the MG-45 material is poor. Such data scatter is to be expected when one considers that honeycomb ribbon misalignments exist to varying degrees throughout the billets, and that the filler-ribbon strength varies greatly within and between billets. The effects of these two factors should produce large variations within the data.

MG-58 Material. - The results of the compressive evaluation of the MG-58 material are shown in Table 66. The relationships between gage section, cross-sectional area, 0.05 percent compressive yield strength and compressive initial elastic modulus are shown in Figures 133 and 134, respectively. Initial inspection of these figures indicates a correlation between specimen configuration and material strength and modulus. However, the possible influence of bulk density should also be considered. Note in Table 66 that for the "a" direction determination there is a decreasing trend in bulk density as specimen size increased. However, for the "b" direction determination the opposite trend is noted. These trends indicate a possible dependence of compressive strength and modulus upon material density in both the "a" and "b" directions rather than the specimen size. Figures 135 and 136, which are plots of bulk density versus 0.05 percent compressive yield strength and initial elastic modulus, respectively, indicate such a density-strength modulus relationship.

The compressive evaluation of the MG-58 material showed that the average "a" direction ultimate compressive strength was 0.902 x 10^6 N/m^2. The average 0.05 percent yield strength was 0.663 x 10^6 N/m^2 while the average initial elastic modulus was 119 x 10^6 N/m^2. In the "b" direction, the average values for 0.05 percent compressive yield strength and initial elastic modulus were 0.378 x 10^6 N/m^2 and 41.9 x 10^6 N/m^2 respectively.

Considerable data scatter is noted in the results of the "a" direction Type 2 specimen configuration evaluation. The most probable factor affecting this behavior is bulk density. Note in Table 66, that there is a rather large variation in bulk density between the specimens (from 0.2014 - 0.2454 gm/cm^3). The previously noted density-strength-modulus relationship would indicate a rather large scatter in the strength and modulus values for the wide range of density values noted for these specimens. A rather large range of strength-modulus values would be expected in a test matrix for a material which exhibited a strength-density relationship associated with varying densities. Another factor possibly affecting the data scatter and also the strength of the "a" direction specimens is honeycomb alignment. As occurred in the tensile determination, failure of the "a" direction compressive specimens occurred in regions of honeycomb misalignment. The extent to which the honeycomb is skewed in any one area probably is a strength determining factor. Since the occurence of the honeycomb misalignment was random in nature, the reinforcement material orientation could affect data scatter and material strength.

60

Ultimate strength was not obtained for the "b" direction compressive evaluations. Application of a compressive load in the "b" direction merely caused continuous compaction of the specimen until the loading was terminated. Considerable lateral expansion and failure (powdering) of the filler material was noted. Also, large amounts of specimen bending usually occurred after the initial stages of loading. The bending could be indicative of possible density variations within the specimen and also precluded the obtaining of the "b" direction strain values. Typical failed "b" direction compressive specimens are shown in Figure 137. The flat areas on the gage section were caused by the attachment yokes for the clip-on extensometers.

Figure 137 also shows typical failed "a" direction compressive specimens. The difference in the appearance of the two specimens resulted from the continued loading of Specimen C3a2 for a longer time after ultimate strength was reached. For the "a" direction compressive determinations, failure occurred when the filler material separated from the honeycomb reinforcement as shown in Figure 137a. Continued loading caused degradation of the filler material and failure of the honeycomb ribbon along the line at the end of bonding area of two ribbons. Note that in specimen C4a2 the honeycomb has fewer areas of honeycomb misalignment than Specimen C3a3. Also note that failure occurred in those areas of honeycomb misalignment.

Typical compressive stress-strain plots are shown in Figures 138 and 139.

Two undried compressive specimens (one each in the "a" and "b" directions) were also evaluated to provide an indication of the effects of moisture on the compressive properties. No attempt was made to control the moisture content of these specimens. Compressive specimen configuration C-2 was used.

The results of these evaluations are also shown in Table 66. Moisture appears to affect the compressive properties of the MG-58 material differently in the "a" and "b" directions. Note that in the "a" direction the strength of the undried specimen is about 15 percent less than the average strength of dried specimens, but in the "b" direction the undried specimen 0.05 percent yield strength is about 2.2 times that of the dried specimens. However, in both the "a" and "b" directions, the initial elastic modulus of the undried specimen is greater than the dried specimen.

61

Discussion of Results

In view of the different characteristics between the MG-1 material and the MG-45 and MG-58 materials the MG-1 will be discussed separately from the other two materials.

MG-1 Material. - Composite plots of the effects of temperature on strength, initial elastic modulus, and strain-to-failure for the MG-1 material are indicated in Figures 140 through 142, respectively.

As Figure 140 shows, the compressive strength is about 2.5 - 3 times greater than the tensile strength at temperatures from 300 K to 500 K. Below 300 K, the compressive strength is 3.9, 2.4 and 4.5 times greater than the tensile strength at 250, 200 and 150 K, respectively. Both the tensile and compressive strengths indicate a marked increase at low temperatures as would be expected. Also, both tensile and compressive strengths show a slight increase from 450 K to 500 K. A possible explanation for this strength increase above 450 K could be the absence of volatile materials (water, resin) which would affect the material characteristics. It was noted during the 450 K and 500 K determinations that the specimens began emitting a gray-white smoke at about 430 K. Also an inflection point on the thermal expansion curve for the MG-1 occurs at about 430 K, which further indicates that a change in the material characteristics occurs at that temperature. Also, inspection of the failed specimens evaluted at elevated temperatures indicated a darkening or "charring" effect which increased with temperature. (See Figures 92 and 117)

The compressive and tensile initial elastic moduli indicated very good agreement (see Figure 141). The difference between the averages of the two moduli was less than 0.05×10^9 N/m^2 at all temperatures except 300 K where the difference was 0.081×10^9 N/m^2.

The compressive strain-to-failure, as expected, was much greater than the tensile strain at all temperatures (see Figure 142). From 400 K to 500 K the compressive strain was about 2.5 times greater than the tensile strain. However, at lower temperatures the compressive strain was generally more than 4 times as much as the tensile strain. This indicates that temperature has a greater elastic effect on the MG-1 material in tension than compression. This is further illustrated by a comparison of the compressive and tensile strain values with temperature. The maximum compressive strain of 60.9×10^{-3} cm/cm at 500 K is less than twice that of the strain of 38.9×10^{-3} cm/cm at 150 K. But the tensile strain indicates a more than threefold increase from 8.2×10^{-3} cm/cm at 150 K to 25.1×10^{-3} cm/cm at 500 K.

62

MG-45. - Composite plots of tensile and compressive 0.2 percent yield strength and initial elastic modulus versus bulk density are shown in Figures 143 and 144. The average "a" direction 0.2 percent tensile yield strength of 0.318×10^6 N/m^2 was significantly higher than the average "a" or "b" direction 0.2 percent compressive yield strengths of 0.204 and 0.132×10^6 N/m^2 respectively. Note in Table 65 that the 0.2 percent yield strengths of Specimens Cla2 and C6a2 are only slightly less than the average 0.2 percent tensile yield strength. Recall from previous discussion that the strengths of Specimens C2a2 and C5a2 were affected by gross material defects thus, lowering the average compressive yield strength. This indicates that, if material properties (honeycomb alignment and filler-ribbon bonding) were more closely controlled during manufacture, the "a" direction tensile and compressive 0.2 percent yield strengths would probably be about the same.

As shown in Figure 144, the "a" direction tensile and compressive initial elastic moduli are about three times greater than the corresponding "b" direction moduli. The average "b" direction tensile and compressive moduli show reasonable agreement (13.8 and 9.4×10^6 N/m^2 respectively). If one considers the effect of possible bending on the "b" direction compressive modulus and considers further the modulus of the "b" direction compressive blocks (12.4×10^6 N/m^2) an even closer correlation is shown between the "b" direction tensile and compressive moduli. In the "a" direction, the average tensile modulus (41.9×10^6 N/m^2) is about 1.7 times the average compressive modulus (24.7×10^6 N/m^2). Again the moduli for Specimens C2a2 and C5a2 lowered the average. The average modulus for the remaining two "a" direction compressive "a" direction specimens (31.4×10^6 N/m^2) shows reasonable correlation with the "a" direction tensile modulus. Thus, closer control of material properties during manufacture may produce a material with tensile and compressive strengths and moduli in the "a" or "b" direction approximately equal.

MG-58 Material. - Composite plots of average tensile and compressive strength, initial elastic modulus and strain-to-failure are shown in Figures 145 through 147. The average "a" direction ultimate compressive strength of 0.902×10^5 N/m was about 1.5 and 3.2 times respectively of the "a" and "b" direction ultimate tensile strengths. Note in Table 63 that the tensile strengths of Specimens T3a2 and T4a2 were only about 10 percent lower than the average "a" direction compressive strength. Recall from earlier discussion that the honeycomb alignment influenced the tensile properties and also that Specimens T3a2 and T4a2 had only minimal honeycomb misalignment. Thus, as noted for the MG-45 material, adequate control of the honeycomb alignment during material manufacture would probably produce a material having similar "a" direction tensile and compressive strengths

As shown in Figure 146, the average "a" direction tensile and compressive initial moduli are about equal (103×10^6 N/m^2 in tension and 119×10^6 N/m^2 in compression). The different effects of the honeycomb reinforcement in the "a" direction and the "b" direction should produce higher (here about 2.5 times) "a" direction moduli. The average "a" direction compressive strain-to-failure of 9.7×10^{-3} cm/cm was about 1.3 times the average "a" direction tensile strain of 7.2×10^{-3} cm/cm and about twice the average "b" direction tensile strain of 5.1×10^{-3} cm/cm (refer to Figure 145). Note in Table 63 that Specimen T34b1 showed an abnormally high strain-to-failure. Also recall that Specimen T34b1 was the only "b" direction tensile specimen which did not fail almost exclusively along the filler-ribbon bond. Thus, it is indicated that a stronger filler-ribbon bond could result in increased "b" direction tensile strain-to-failure.

MG-45 and MG-58 Material Comparison. - Figures 148 through 150 are composite plots of bulk density versus ultimate tensile strength, initial tensile elastic modulus and strain-to-failure respectively, for the MG-45 and MG-58 materials. The average ultimate tensile strength for the MG-58 material was markedly greater than the MG-45 material. In the "a" direction the MG-58 average strength of 0.594×10^6 N/m^2 is about 40 percent greater than the MG-45 average strength of 0.426×10^6 N/m^2. In the "b" direction, the average tensile strength of the MG-58 material (0.281×10^6 N/m^2) is about 3.4 times greater than the average MG-45 tensile strength (0.082×10^6 N/m^2). The initial tensile elastic moduli for the MG-58 material in the "a" and "b" directions (107 and 40×10^6 N/m^2 respectively) are about 2.6 and 2.9 times greater than the corresponding moduli for the MG-45 material (42 and 14×10^6 N/m^2 for the "a" and "b" directions respectively). As expected, the MG-45 material showed significantly (2.5 times greater strain-to-failure than the MG-58 material in the "a" direction (18.4 versus 7.2×10^{-3} cm/cm). In the "b" direction the average strain-to-failure for both materials was about equal (6.5×10^{-3} cm/cm for MG-45 and 6.3×10^{-3} cm/cm for MG-58).

Composite plots of 0.05 percent compressive yield strength and compressive initial elastic modulus versus bulk denisty for the MG-45 and MG-58 materials are shown in Figures 151 and 152, respectively. As expected the MG-58 material exhibited significantly (about 3.5 times) higher strength in both the "a" and "b" directions. In the "a" direction, MG-58 material showed an average 0.05 percent yield strength of 0.663×10^6 N/m^2 compared to 0.192×10^6 N/m^2 for the MG-45 material. In the "b" direction the 0.05 percent yield strength values for the MG-58 and MG-45 materials were

64

0.378 and 0.104 x 10^6 N/m^2 respectively. The initial compressive elastic modulus for the MG-58 was, in both directions, higher than shown by the MG-45 material. For the "a" direction, the average moduli were 119 and 24.7 x 10^6 N/m^2 while "b" direction moduli of 41.9 and 9.4 x 10^6 N/m^2 were noted for the MG-58 and MG-45 materials.

The MG-45 and MG-58 materials are similar in that both have phenolic-glass honeycomb reinforcement, but differ in the filler material used (phenolic-nylon for MG-58 and silicone-phenolic for MG-45). However, the mechanical properties of these materials are noticeably different. The difference in properties of these composites can be attributed to the difference in the properties of the two filler materials. Table 67 provides a comparison of mechanical properties for the filler materials at room temperature. As shown in Table 67, the tensile and compressive strengths of the phenolic-nylon are about 40 times higher than the corresponding strengths of the silicone-phenolic. Thus, we would expect the MG-58 (phenolic-nylon filler) material to exhibit higher strength than the MG-45 (silicone-phenolic filler) material. However, since the strength of the MG-45 and MG-58 materials is affected by other factors (honeycomb influence, filler-honeycomb bending, voids) the difference in the strength of these materials (as shown above) is not as great as of the filler materials considered separately. Table 67 also shows that the tensile and compressive moduli of the phenolic-nylon is more than 20 times greater than the corresponding moduli of the silicone-phenolic. As shown above, the MG-58 material exhibited higher tensile and compressive moduli than the MG-45 material. Thus, the mechanical properties of the different filler materials affect the properties of the composite materials.

Concluding Remarks

Tensile and compressive properties were evaluated from 150 K to 500 K for the silicone-phenolic, MG-1. Tensile and compressive strengths of the MG-1 both decreased rapidly from 150 to 300 K. However, both strengths decreased only modestly from 300 to 450 K. From 450 to 500 K a slight increase in both strengths was observed, which is attributed to a loss of volatile materials between 450 and 500 K. The compressive strength was more than 2.4 times the tensile strength at all temperatures. The tensile and compressive moduli agreed closely from 150 to 500 K. Both moduli decreased rapidly from 150 to 300 K, but decreased only modestly from 300 to 500 K. Strain-to-failure in tension and compression increased from 150 to 500 K, with the compressive strain over 2.5 times greater than the tensile strain.

Tensile and compressive properties were evaluated at room temperature in two orthogonal directions for the phenolic-glass honeycomb reinforced materials - one silicone-phenolic filled, MG-45 and the other phenolic-nylon filled, MG-58. The filler material of the MG-45 and MG-58 affected the mechanical properties with the phenolic-nylon filled MG-58 having significantly higher tensile and compressive strengths; both parallel to and perpendicular to the honeycomb reinforcement ribbon, than the silicone-phenolic filled MG-45. The "a" (parallel to the honeycomb ribbon) direction and the "b" (perpendicular to the ribbon) direction compressive strengths of the MG-58 more materially greater than the corresponding tensile strengths. The "a" direction tensile or compressive strengths were notably higher than the corresponding "b" direction strengths. However, for the MG-45, the "a" direction tensile strength was higher than either compressive strength while the "b" direction tensile strength was lower and both the "a" and "b" direction compressive strengths were about the same. The tensile and compressive initial elastic moduli measured for the phenolic-nylon filled MG-58 were significantly higher than the corresponding moduli measured for the silicone-phenolic filled MG-45. However, for the MG-58, the "a" direction tensile and compressive moduli were approximately the same and also the "b" direction tensile and compressive moduli were about equal. A similar relation was noted for the moduli measured for the MG-45. The "a" direction tensile strain-to-failure for the MG-45 was more than twice the strain for the MG-58. However, in the "b" direction, the tensile strain-to-failure for both materials was the same. The compressive strain for the MG-45 was dramatically greater than the strain measured for the MG-58.

Material defects significantly affected the mechanical properties of the phenolic-glass honeycomb reinforced MG-45 and MG-58. Poor filler-honeycomb bond acted to reduce material strength. The location of the areas having the weak bond within a billet varied between the MG-45 and MG-58. For the MG-45 the area having the low bond strength was the inner portion of the billet while for the MG-58 the low bond strength area was found in the outer portion of the billet. Misalignment of the honeycomb ribbon also acted to reduce material strength. Areas of honeycomb misalignment were located randomly throughout the billets of both materials. Closer control of the manufacturing process to eliminate the above defects could result in stronger materials.

For the three tensile and three compressive specimen configurations evaluated using the reinforced phenolic-nylon, MG-58, the mechanical properties were not affected by the variations in gage volume. The moisture content of the MG-58 was about five percent by weight. The mechanical properties of the MG-58 appear to be affected by moisture content, however, due to the limited replications, firm conclusions cannot be made.

Southern Research Institute
Birmingham, Alabama
December, 1970

APPENDIX A

TOTAL NORMAL EMITTANCE TO 5000°F

General

Emittance is measured by comparing the energy received by a radiometer from the sample to that received from a blackbody cavity maintained at the same temperature. The specimen usually is 1/2" diameter by about 1/8" thick. Diameters up to 1 inch have been accommodated.

The equipment may be divided into three main parts: the induction heating furnace, the radiometer, and the temperature measurement equipment. Figure 1 shows a picture of the complete equipment.

Description of Apparatus

A cross-section of the apparatus is shown in Figure 2. The specimen (1) is supported in the center of the flat concentrator induction coil (2) by a zirconia cylinder filled with fine zirconia grog and tungsten wires(3). The zirconia cylinder rests on a crucible filled with coarse zirconia grog(4). The radiometer (5) views the specimen from directly above through a water-cooled tube(6). A water-cooled optical valve (7) is used to blank off the specimen from the radiometer. Optical-temperature readings are taken through a mirror (9) from directly above. When radiometer readings are being taken, the main port is pulled out and away from the line of sight of the radiometer. Auxiliary port (10) is used to view the specimen directly as a check for the main port. Both viewing ports contain sapphire windows. The portion of the furnace above the specimen (11) is water-cooled to eliminate any possibility of energy being reflected back onto the specimen surface. The emittance furnace is built of steel and sealed with "O" rings so that a vacuum may be attained.

The radiometer, see Figure 3, was constructed according to Snyder[1] and Geir[2] with some modifications. The receiver element consists of approximately 160 turns of No. 40 AWG bare-constantan

---

[1] Snyder, N.W.; Gier, J.T.; and Dunkle, R.V. "Total Normal Emissivity Measurements of Aircraft Materials Between 100 and 1000 F", Trans the A. S. M. E., Vol. 77, 1944, p. 1011

[2] Gier, J.T.; and Boelter, L. M. K.; "The Silver-Constantan Plated Thermopile," Temperature - Its Measurement and Control in Science and Industry, American Institute of Physics, 1941, p.1284.

68

wire (104 turns per inch) wound around a plastic insulator strip about 2" long by 1-5/8" wide by 5/16" thick. Silver was electroplated in several stages onto the constantan coil so that two 1/8" wide lines of silver-constantan junctions, 1/2" apart, were formed on the same side of the coil and across all of the wire turns. The remainder of the entire coil was silver plated. Each of the two lines of junctions was covered with a thin, narrow strip of black paper. One of these junction lines is designated as the active or "hot" junction and is placed to receive energy from the sample. The other is shielded and termed the passive or "cold" junction.

In order to shield the element from extraneous radiation, a cylindrical housing is placed immediately around the thermopile. The front of the housing contains a rectangular opening 1/4" by 1-1/2" to allow the element to "see" the specimen. The actual limiting of the receiver field is accomplished by this rectangular slit and the 1/4" round stop (12) just above the specimen. Additional stops in the water-cooled tube were installed as an added insurance to further minimize spurious reflections. The radiometer views the specimen directly. This eliminates the possibility of dirty lenses affecting the reading and, also, eliminates the spectral selectivity of the different types of materials used as windows.

The voltage generated by the receiver is measured with a Type K-3 Leeds and Northrup potentiometer in conjunction with an L and N Type 2430 DC galvanometer of 0.43 microvolts per millimeter deflection sensitivity. Temperatures are measured with a Leeds and Northrup portable potentiometer.

The receiver element was calibrated against a carbon-filament lamp of known radiation[3] and demonstrated a sensitivity of 8.66 Btu/hr/sq ft/millivolt.

The radiometer was checked, also, against an Eppley thermopile with 12 bismuth-silver junctions and a 1-mm quartz window and agreed within 10% scatter of data points. By factory calibration the sensitivity of the Eppley thermopile is 0.048 microvolts/microwatt/sq cm.

The optical pyrometers used are L and N catalog type 8622 calibrated in accordance with the International Critical Table of 1948 for an emittance of unity.

---

[3]Lamp No. C584, calibration by the National Bureau of Standards and reported in NBS Report 132737 A, July 1, 1952.

Calibration Procedure

To calibrate the radiometer for blackbody radiation, a blackbody cavity with a 6 to 1 aspect ratio made from graphite was used. The blackbody cavity was insulated by zirconia grog and lamp black placed in the annulus between the blackbody and the load coil, see Figure 4.

The accurate determinations of the specimen and blackbody temperatures are essential to good data. For the cavity-type blackbody, the temperatures are determined relatively easily by (1) thermocouples placed in the bottom of the cavity, (2) thermocouples dropped into the cavity, and (3) optical pyrometer observations. Up to 3000 F, agreement to within 15 F has been obtained regularly between these three readings. Above 3000 F the agreement between tungsten-rhenium couples and the optical pyrometer has been generally within 50 F or the repeatability of this type of thermocouple. Actually, the optical readings have no error other than those of the instrument calibration and the human error, which appears to provide a readout scatter of about 20 F at 4000 F.

Radiometer output versus temperature for blackbody radiation is plotted in Figure 5. Notice that the output is essentially linear from 2500 F to 5000 F with a slight curvature below 2000 F. As in-house standards, the emittance of 304 stainless steel, tarnished tungsten, and graphite were measured, see Figure 6. The emittance of the stainless steel ranged from 0.15 at 700 F to 0.67 at 2000 F. These values are in close agreement with the literature values. The sanded CS graphite, also, checked out closely with the literature with values from 0.95 to 0.98.

Operating Procedures

The specimen is placed directly on the surface provided by the zirconia tube, grog, and tungsten wires. However, if the material of interest cannot be heated inductively, tungsten and tantalum heating discs are placed under the specimen with the specimen in contact with the tungsten disc.

The furnace is then evacuated to 15 mm of Hg and filled with high-purity, dry argon. This operation is carried out at least twice to assure an inert atmosphere. Throughout the run a slight pressure is maintained in the furnace by an argon purge, which is brought in through the radiometer enclosure and exhausted from the furnace housing, see Figure 2. In addition to maintaining an inert atmosphere, the purge flow tends to keep fumes away from the radiometer.

The temperature of the specimen is raised and maintained at the desired point by transferring energy to the specimen through the induction coil. About three hours are required to complete a single run with the temperature increasing stepwise but in uniform intervals. At each temperature level a radiometer reading is taken in conjunction with the temperature readings.

To obtain the radiometer reading, the following procedure is followed: As the specimen is heated, the blank-off valve is shut so that the thermopile can see no impulse. When the specimen temperature reaches steady state, a zero reading is obtained for the thermopile output. This reading is usually in the order of ±0.002 millivolts. The blank-off valve is then opened, and the thermopile output increases several fold in a few seconds. The reading levels off as heat is transferred down the wires to the cold junction. The radiometer output is taken at the peak reading immediately after steady state. The net reading for that temperature is then obtained as the difference between the zero and steady-state reading.

If the blank-off valve were left open, the thermopile output would decrease slowly with time. After about 10 minutes, this reading might decrease by 50%; however, if the blank-off valve were shut and a new zero reading obtained, the difference between this new ouput and zero reading would be about the same as the original readings. The variation might be about 5 to 10 percent. The shift in readings is a result of the heating of the cold junctions.

The purge to the radiometer housing has no influence on the readings within the ranges at which the purge is operated. To determine this limit, the purge rate was increased to about 10 times the normal metered reading, and a small shift in readings of less than one percent was noted.

The temperature of the specimen is monitored by (1) thermocouples mounted directly on the target surface (usually held in place by a small zirconia pad) and (2) optical pyrometer readings on the target surface. Low temperature readings were made with thermocouples; however, in the intermediate temperature range from 1500 F to 2700 F a cross check was made between the thermocouple readings and the optical readings. The high-temperature measurements are made with an optical pyrometer. A main-port optical and an auxiliary-port optical-temperature reading are taken at each temperature level. The auxiliary-port temperature is normally used only as a check; however, if conditions warrant, such as a dirty main-port window or mirror, the auxiliary-port value may be used. Usually very good agreement is maintained between the main-port and auxiliary-port optical readings.

Emittance Calculation

The optical temperature reading must first be corrected to obtain true temperatures. The main-port reading is corrected for the sapphire window and mirror while the auxiliary-port readings is corrected for the sapphire window and the angle at which the port views the specimen. The corrections are shown as curves in Figure 7.

After assuming an arbitrary-initial, emittance value, the brightness temperature is corrected for this assumed emittance, see Figure 8. The blackbody ouput is then read at this "true" temperature from Figure 5. The ratio of the observed specimen radiometer output to the blackbody output is calculated and is the emittance of the material at that temperature. If the assumed emittance is correct, the calculated value will agree with it; if not, the calculated value must be used as the former assumed value and the process repeated until the assumed emittance value agrees with the calculated value. This iterative process will converge on the correct emittance value assuming gray body distribution of most of the energy at the particular temperature. The above process was programmed for analysis by a digital computer.

Error Analysis

The above procedure for determining emittance is strictly correct only for those materials which radiate as gray bodies, since the total emittance is assumed to be equal to the spectral emittance at the wave-length of the pyrometer. This approximation was used above to convert the brightness temperature to true temperature.

The error in emittance values for non-gray materials will vary depending on the difference between the 0.665 microns spectral and the total emittance, and the distribution of radiant energy within the particular spectrum. If the deviation from gray body becomes very great at temperatures up to 2500 F, it is indicated by the thermocouple measurements. On materials of low emittance, such as tungsten, the emittance values calculated by this procedure could be in error by as much as 20 percent at the highest temperatures. However, it is believed that for most materials, the accuracy is within 10 percent. Several things indicate that the accuracy of the emittance values is good. First, the radiometer output versus temperature curves are orderly and almost linear with only normal data scatter. Second, the data obtained on two samples of the same material are in close agreement. Third, the values of emittance for the check samples agree very well with the literature, see Figure 6.

A statistical analysis of the data accuracy is of interest. Generally, the probable error in each blackbody reading is about 4 percent, and the probable error in each specimen reading is about 8 percent. If the data points are used to calculate emissivity, the maximum probable error would then be about 12 percent. The curve-fitting approach undoubtedly reduces this maximum to about five percent. As a general conclusion, the accuracy of the measuring system is well within the range of variation as is experienced by different finishes on the same material, the changing chemistry of the surface at the high temperatures, surface temperature measurements, and other variables.
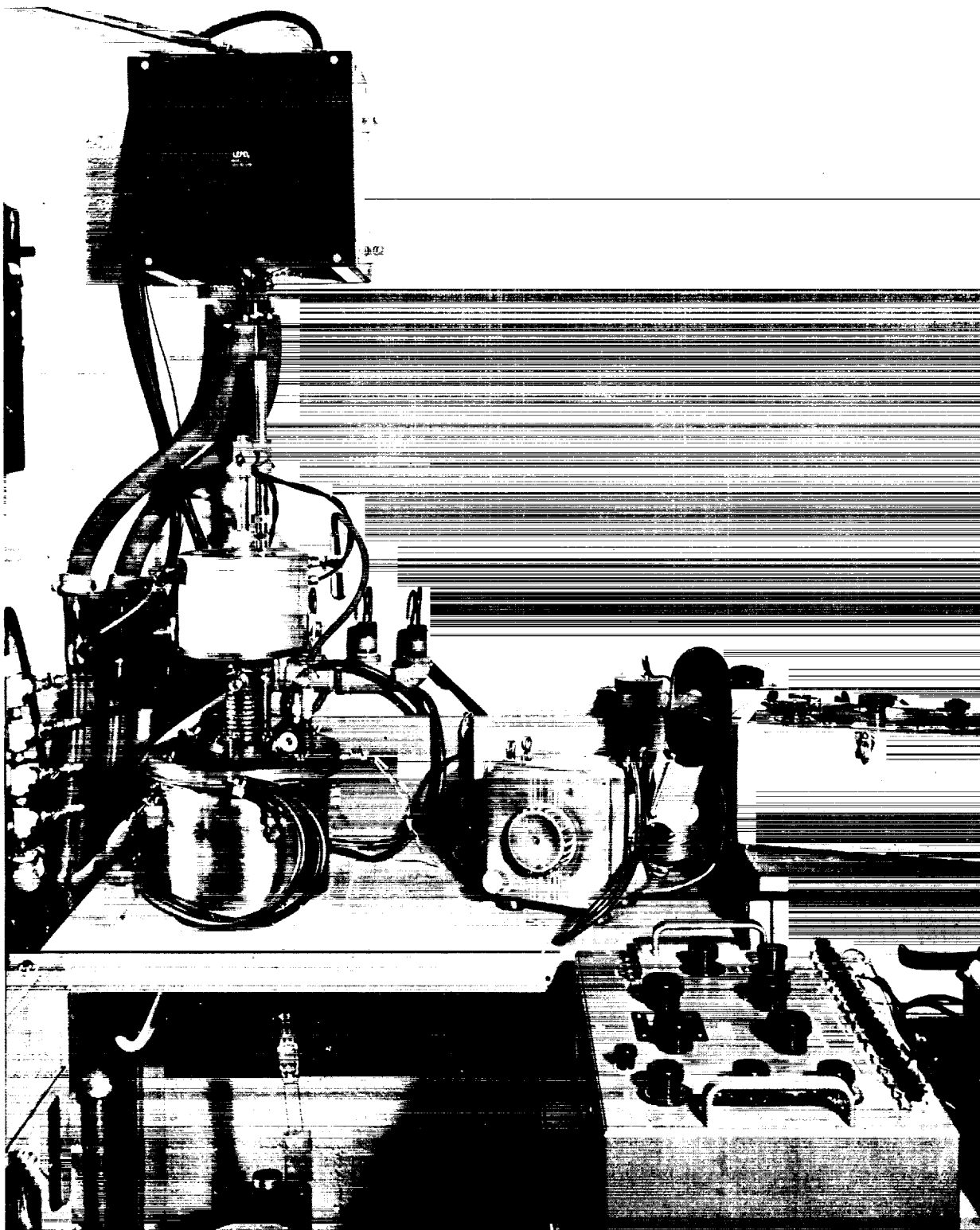
Figure A1. Picture of the apparatus for measuring total normal
emittance

74
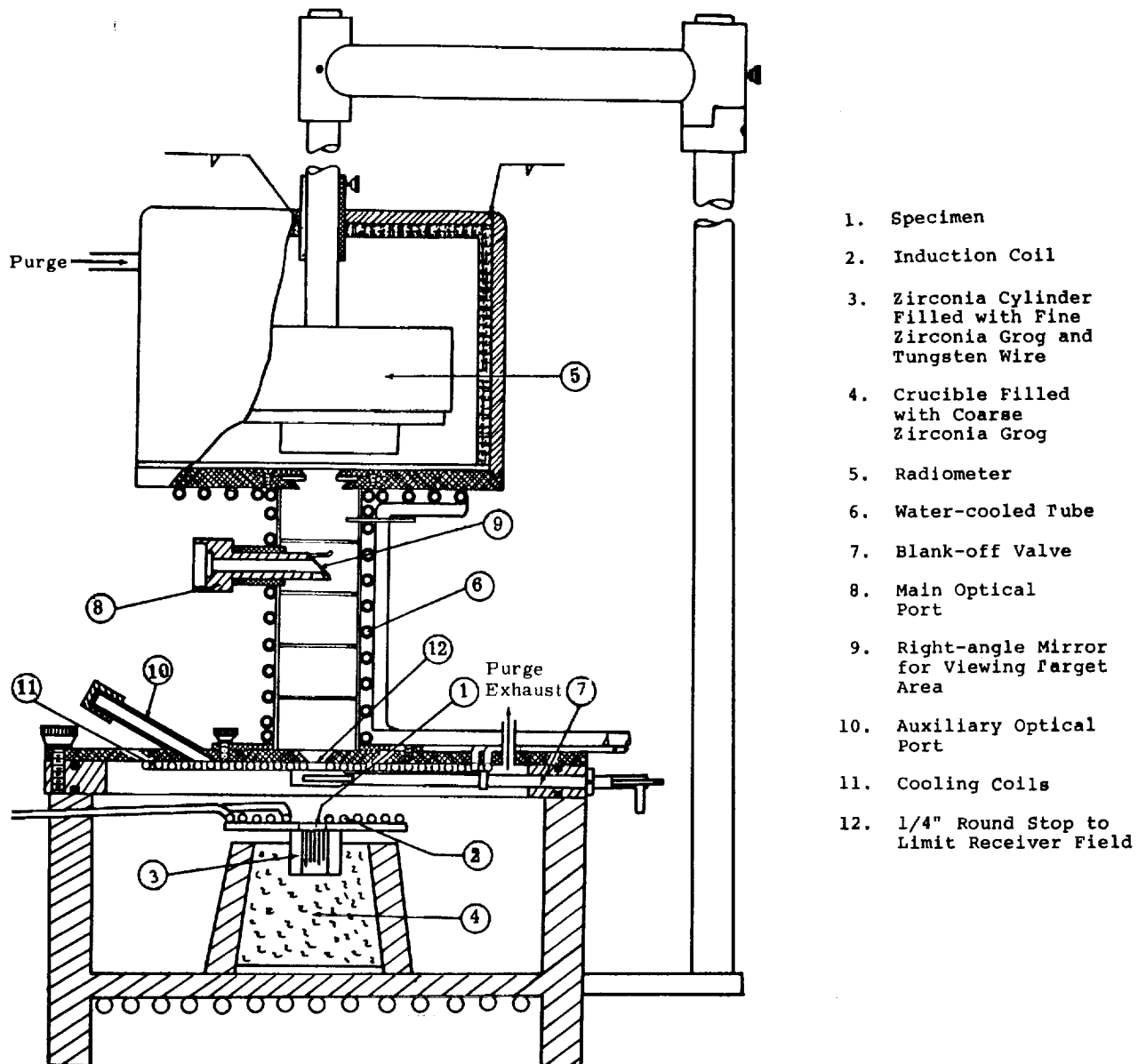
Figure A2. Cross-section of emittance apparatus with F at coil furnace

1. Specimen

2. Induction Coil

3. Zirconia Cylinder
    Filled with Fine
    Zirconia Grog and
    Tungsten Wire

4. Crucible Filled
    with Coarse
    Zirconia Grog

5. Radiometer

6. Water-cooled Tube

7. Blank-off Valve

8. Main Optical
    Port

9. Right-angle Mirror
    for Viewing Target
    Area

10. Auxiliary Optical
    Port

11. Cooling Coils

12. 1/4" Round Stop to
    Limit Receiver Field

Optical Black
Paper Absorbers

160 Cold Junctions

Plastic Frame
$1\frac{5}{8}''$ x $3''$ x $\frac{5}{16}''$

Silver-Plated
Constantan Wire

160 Hot Junctions

Thermocouple Leads

Figure A3. Schematic of 160-junction thermopile
in emittance equipment
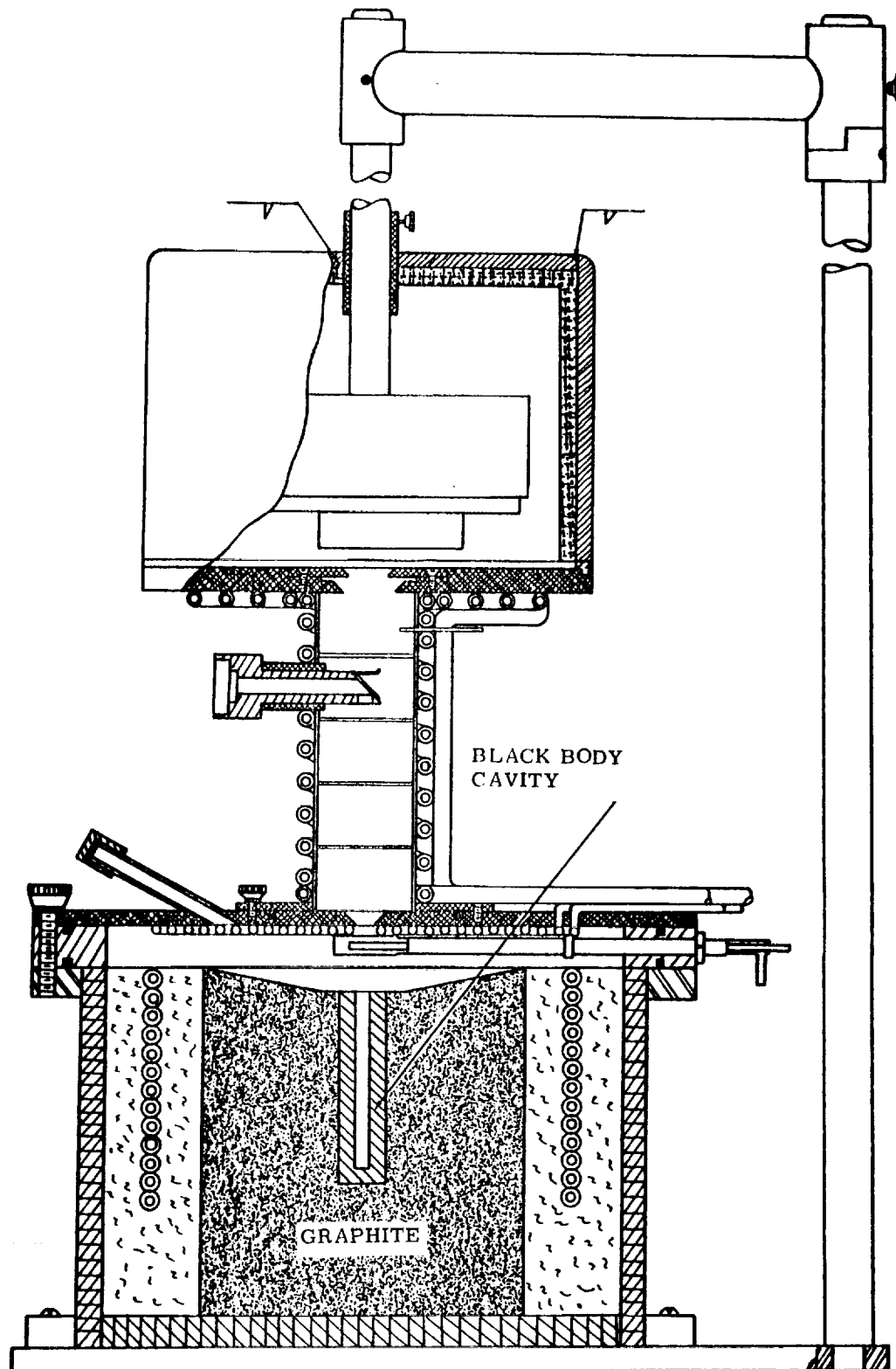
Figure A4. Cross-section of emittance apparatus
with blackbody furnace
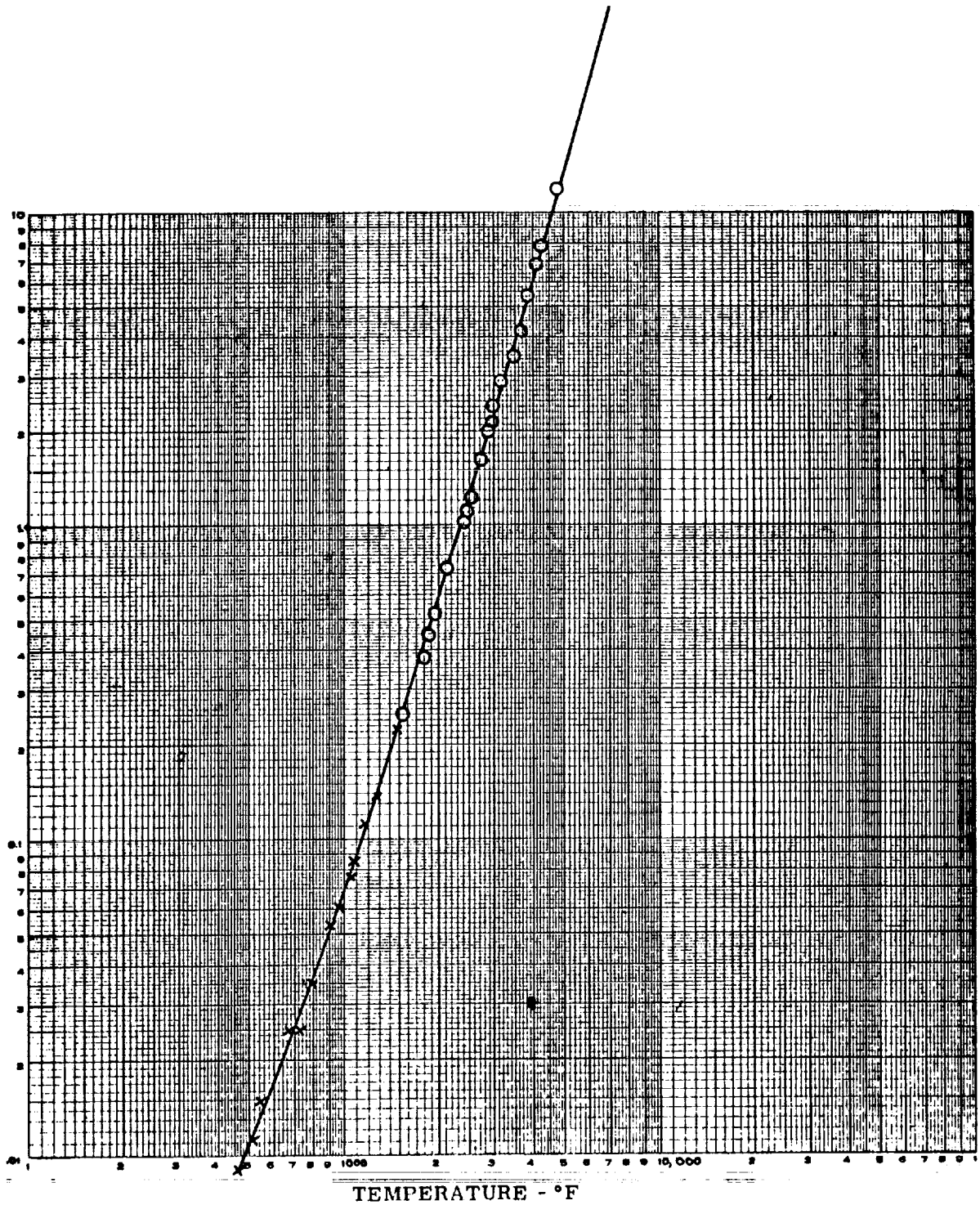
Figure A5. Radiometer output versus temperature for blackbody radiation

78
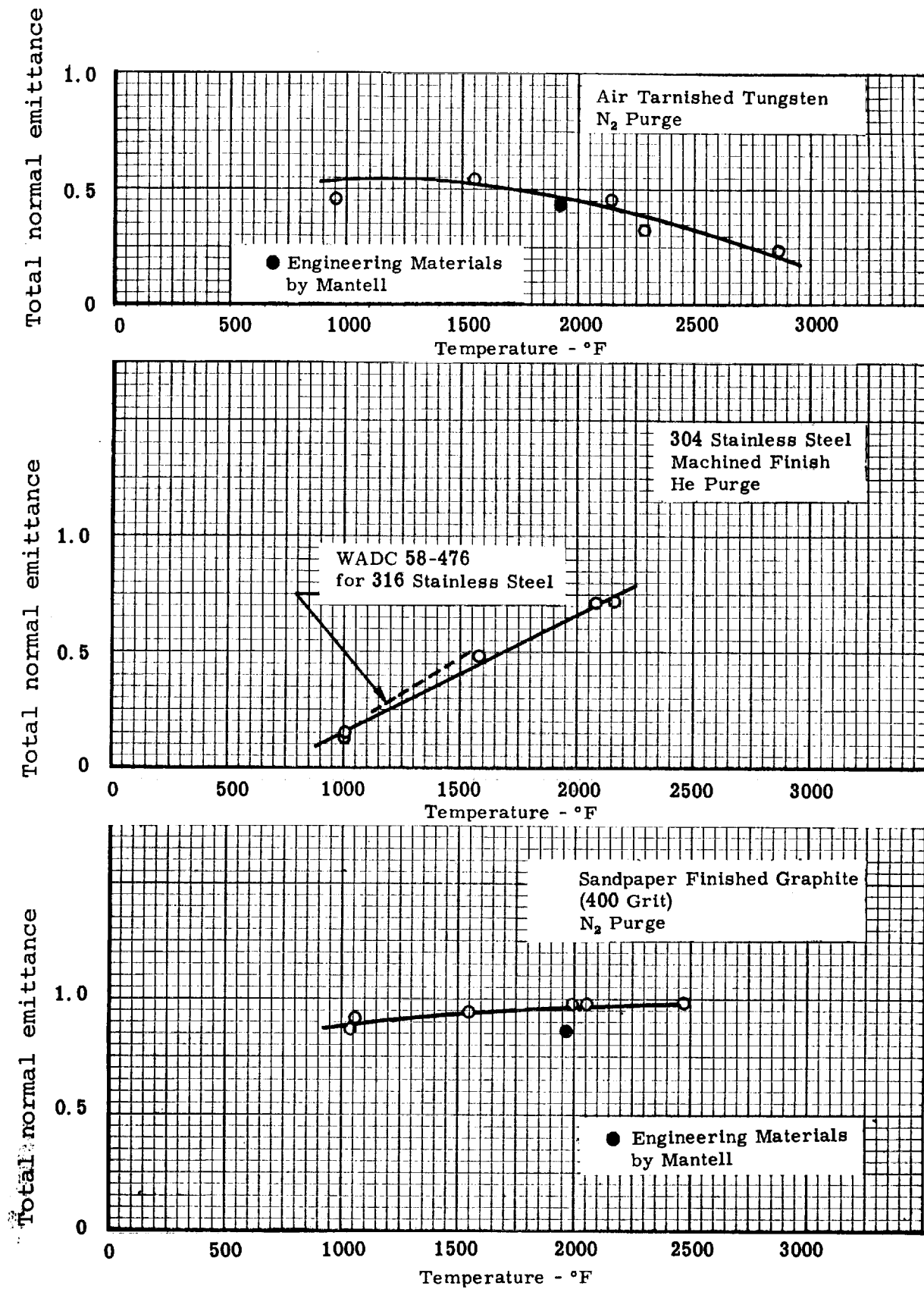
Figure A6. Calibration standards for total normal emittance
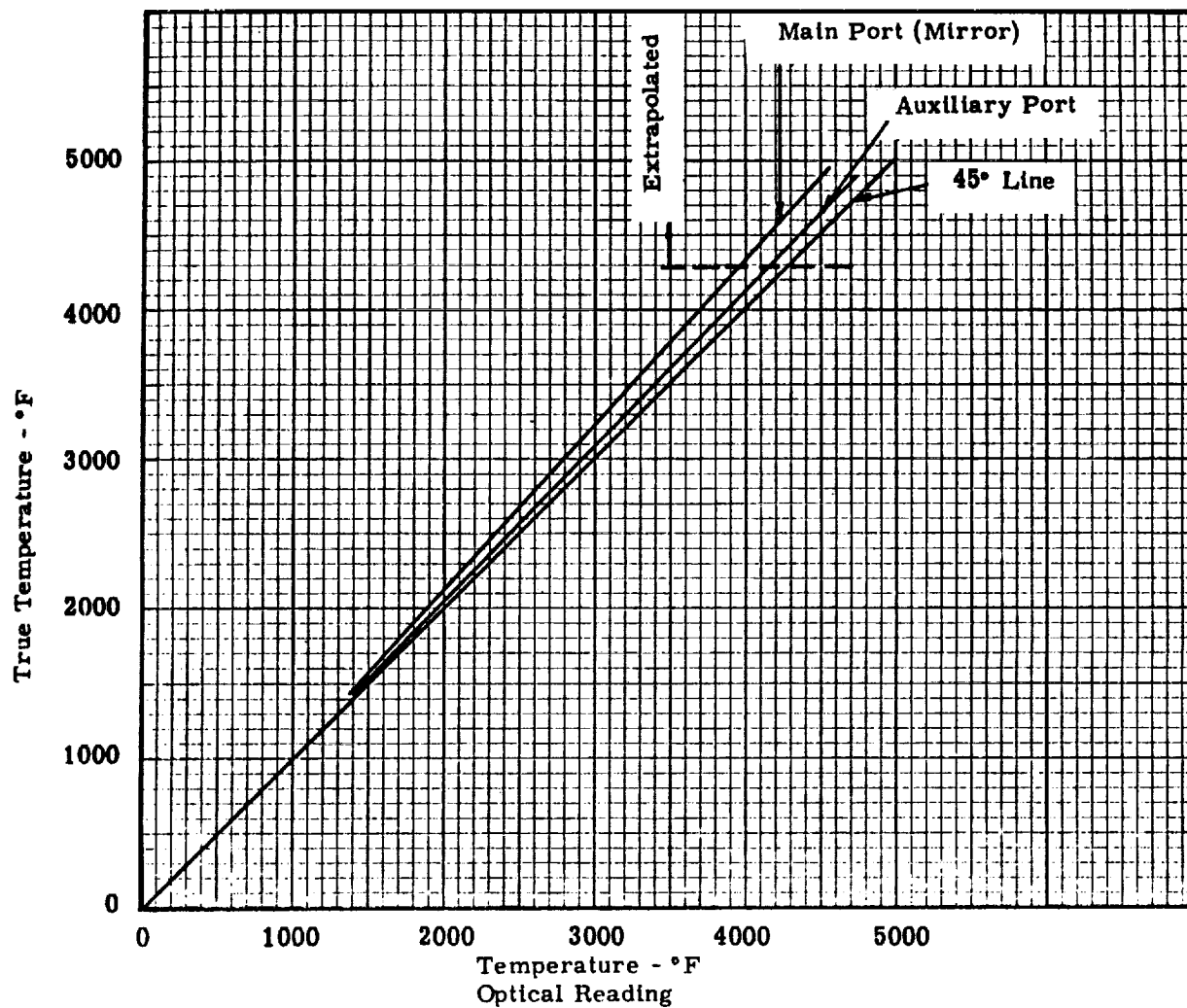
Figure A7. Correction for mirror and sapphire window in emittance apparatus
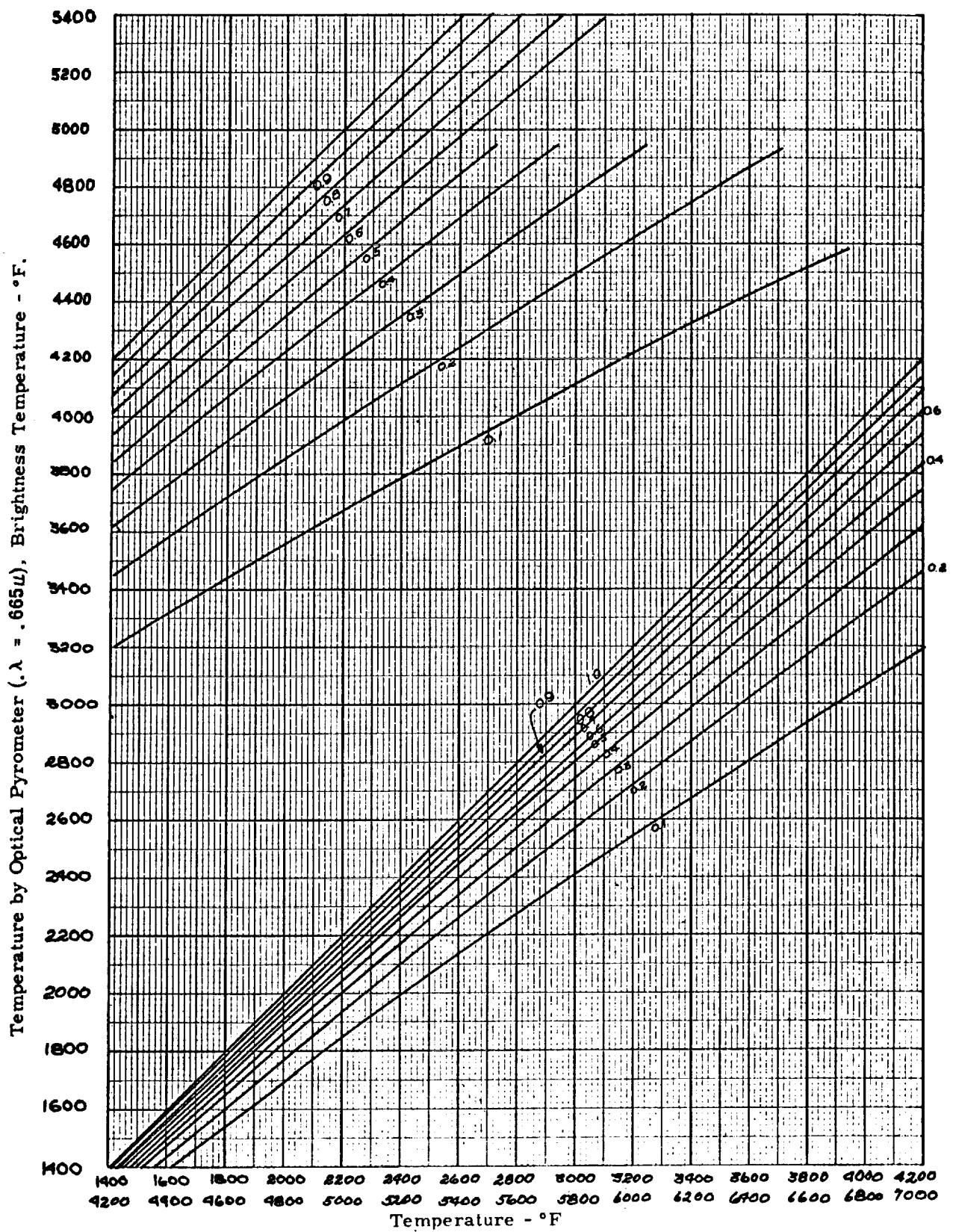
Figure A8. Correction for brightness temperature to
true temperature   81

TABLE 1

COMPOSITION OF ABLATION MATERIALS

Material	Ingredient	Commercial designation	Percent by weight
MG-1	Elastomer	General Electric RTV-602	60
	Phenolic spheres	Union Carbide BJO-0930	19
	Silica eccospheres		8
	Silica fiber	Johns-Manville Microquartz	8
	Dimethyl oil (silica oil)		5
MG-45	Elastomer	Dow Corning, Sylgard 182	18
	Phenolic spheres	Union Carbide BJO-0930	78
	Silica fiber	Johns-Manville Microquartz	4
	Honeycomb	Hexcel 3/8" HRP GF-11	(a)
MG-58	Powdered phenolic	Union Carbide BRP-5549	30
	Phenolic spheres	Union Carbide BJO-0930	60
	Powdered nylon	Polymer Corp. 66D	10
	Honeycomb	Hexcel 3/8" HRP GF-11	(a)

(a) Exact composition of honeycomb not known. Approximately 50% phenolic, 50% glass fabric (by weight). Measured 49-51% glass with burnout tests. Honeycomb density: 2.2 lb/ft³ (0.035 gm/cm³)

TABLE 2

INFORMATION ON PREPARATION OF CHARS FOR THERMAL CONDUCTIVITY SPECIMENS FROM MG-1, SILICONE-PHENOLIC

Billet No.	Billet size	Specimen number	Heating rate K/min	Held 30 minutes at K	Initial density gm/cm³	Initial weight g	Final weight g	Weight loss	Remarks
O	20.4 cm dia x 10.2 cm thick (8 in. dia x 4 in. thick)	1000-10-A3	10	1000		92.652	26.806	71	
		1000-10-A4	10	1000		92.652	26.806	71	
		1500-10-A1	10	1500		89.801	24.026	73	
		1500-10-A2	10	1500		89.801	24.026	73	
1B	38 cm dia x 8.25 cm thick (15 in. dia x 3-1/4 in. thick)	811-10-1	10	811		11.4768	3.3817	71	
		811-10-3	10	811		54.2505	15.8215	71	
		811-10-4	10	811		54.6617	16.1645	70	
		811-10-5	10	811		84.3606	24.8310	71	
		811-10-6	10	811		90.3515	26.7200	70	
		1000-10-3	10	1000		51.8343	14.7417	72	
		1000-10-6	10	1000		100.7451	28.0750	72	
		1000-10-A11	10	1000	0.58	41.140	11.915	71	
		1000-10-A12	10	1000	0.62	42.381	11.768	72	
		1500-10-A9	10	1500	0.61	38.488	10.146	74	
		1500-10-A10	10	1500	0.59	36.921	9.893	73	
		1500-10-R16	10	1500	0.60	22.2075	5.8268	74	
		1500-10-R19	10	1500	0.60	22.0588	5.8073	74	
		1644-10-5	10	1644		99.9653	23.9850	76	
		1644-10-6	10	1644		86.9426	20.4350	76	
		1644-10-A7	10	1644	0.61	37.614	9.110	76	Chalky appearance
		1644-10-A8	10	1644	0.60	37.161	9.098	76	Chalky appearance
		1644-10-A13	10	1644	0.60	41.637	9.010	78	Chalky appearance
		1644-10-A14	10	1644	0.60	42.086	9.310	78	Chalky appearance

TABLE 3

SUMMARY OF INFORMATION SUPPLIED BY NASA LANGLEY
ON ARC-JET CHARS OF MG-45 AND MG-58

| Material | Char disc No. | Exposure time sec | Thickness indication | | Disc used at SRI |
			before	after	
MG-45	Q1	150	2.814	2.525	RIA Specimen 1
	T2	110	2.810	2.610	RIA Specimen 1
	H2	150	2.815	2.580	RIA Specimen 2
	T1	125	2.816	2.650	Heat capacity - ice calorimeter
	P2	150	2.811	2.450	Heat capacity - ice calorimeter
	N2	150	2.820	2.537	Heat capacity - ice calorimeter
	G1	150	2.814	2.570	True density
	U2	110	2.811	2.595	True density
	O1	150	2.815	2.562	True density
	P1	150	2.812	2.630	Apparent density
MG-58	P2	150	2.810	2.592	ASTM Specimen 3
	Q2	150		2.595	ASTM Specimen 3
	M2	150	2.821	2.632	RIA Specimen 1
	O2	150	2.820	2.620	RIA Specimens 1,2
	P3	150	2.813	2.619	RIA Specimen 1
	Q4	150	2.795	2.592	RIA Specimen 2
	J1	300	3.576	3.116	Heat capacity - ice calorimeter
	J2	150	2.808	2.623	Heat capacity - ice calorimeter
	Q3	150	2.816	2.610	True density
	T4	150	2.820	2.590	True density
	K4	125	2.823	2.696	True density
	U2	150	2.816	2.590	Apparent density

84

TABLE 4

CONSTANTS FOR CALCULATING PERMEABILITY PARAMETERS FOR CORNELL-KATZ DATA CORRELATION

Gas	Molecular weight	Gas temperature K	Gas viscosity at 294.3 K centipoise	Gas density at 294.3 K gm/cm³	$\frac{MP_m\Delta P}{LRT\mu G}$ cm^{-2}	$\frac{G}{\mu}$ cm^{-1}
Helium	4.0026	294.3	1.98×10^{-2}	1.656×10^{-4}	$0.4988 \dfrac{P_m\Delta PA}{LQstp}$	$0.8363 \dfrac{Qstp}{A}$
Nitrogen	28.0134	294.3	1.756×10^{-2}	1.16×10^{-3}	$0.5620 \dfrac{P_m\Delta PA}{LQstp}$	$6.6059 \dfrac{Qstp}{A}$

Units: P_m, ΔP – N/m^2

A – cm^2

L – cm

$Qstp$ – cm^3/sec

$$\frac{MP_m\Delta P}{LRT\mu G} = \alpha + \beta \left(\frac{G}{\mu}\right) \quad \text{(correlation equation)}$$

α – viscous flow coefficient, cm^{-2}, $= 1/K$

β – inertial flow coefficient, cm^{-1}

K – Darcy's constant, cm^2

Note: 1 darcy = 0.987×10^{-8} cm^2

TABLE 5

THERMAL CONDUCTIVITY OF VIRGIN MG-1, SILICONE-PHENOLIC
(ASTM C177 GUARDED HOT PLATE APPARATUS)

Average specimen mean temperature K	Total heat input watts	Average specimen ΔT K	Specimen thickness[2] cm	Specimen thermal conductivity W/m-K	Time to temperature[3] hr
Specimen 1					
Bulk density: Disc 1, Top 0.5844 gm/cm³; Initial weight: 19.5017 g; Final weight: 18.3100 g					
Disc 4, Bottom 0.6016 gm/cm³; Initial weight: 19.9712 g; Final weight: 18.7838 g					
Gum Rubber Filler					
167.30	6.09	106.50	0.635	0.099	10.5
167.26	6.09	106.23	0.635	0.100	11.5
206.73	9.43	148.68	0.635	0.110	1.8
289.44	6.63	93.60	0.635	0.123	7.0
292.37	6.52	95.83	0.635	0.118	9.5
Fiberfrax Filler					
320.91	1.76	25.40	0.640	0.121	4.0
383.02	4.81	72.45	0.627	0.114	3.8
382.50	4.89	71.30	0.627	0.118	18.4
Fiberfrax filler - one set asbestos pads					
434.57	4.22	62.97	0.620	0.113	6.5
433.68	4.21	62.61	0.620	0.114	7.4
499.73	6.44	88.94	0.615	0.121	6.8
502.18	6.46	90.19	0.615	0.120	7.5

Notes:
1. Diameter of central heater = 4.826 cm (Area - 18.29 cm²).
2. Thermal conductivity values based on measured thickness at each temperature level.
3. Time to temperature implies the time elapsed between adjustment of power and obtaining data.
4. Data obtained at compaction pressure of 1.65×10^5 N/m².

TABLE 6

THERMAL CONDUCTIVITY OF VIRGIN MG-1, SILICONE-PHENOLIC
(ASTM C177 GUARDED HOT PLATE APPARATUS)

Average specimen mean temperature K	Total heat input watts	Average specimen ΔT K	Specimen thickness[2] cm	Specimen thermal conductivity W/m-K	Time to temperature[3] hr
Specimen 2					
Bulk density: Disc 2, Top 0.5984 gm/cm³; Initial weight: 20.0062 g; Final weight: 18.6352 g					
Disc 3, Bottom 0.6037 gm/cm³; Initial weight: 20.1318 g; Final weight: 20.1318 g					
Gum Rubber Filler					
138.89	3.83	67.76	0.635	0.098	2.4
139.76	3.83	68.12	0.635	0.097	3.0
192.89	7.70	125.87	0.635	0.106	2.5
193.31	7.70	125.86	0.635	0.106	3.4
256.28	3.43	52.72	0.635	0.113	6.0
284.51	5.20	81.62	0.635	0.110	7.5
282.15	5.12	80.38	0.635	0.110	9.4
281.87	5.08	79.71	0.635	0.111	10.0
Fiberfrax filler					
329.99	2.03	31.27	0.638	0.113	4.8
330.78	2.04	31.68	0.638	0.111	5.5
378.37	4.22	66.43	0.638	0.110	15.6
458.69	4.44	70.46	0.622	0.107	5.8
457.77	4.43	70.19	0.622	0.107	6.5
532.55	4.25	99.08	0.615	0.106	5.2
532.71	4.20	98.52	0.615	0.106	5.8

Notes:
1. Diameter of central heater = 4.826 cm (Area - 18.29 cm²)
2. Thermal conductivity values based on measured thickness at each temperature level.
3. Time to temperature implies the time elapsed between adjustment of power and obtaining data.
4. Data obtained at compaction pressure of 1.65 x 10⁵ N/m².

TABLE 7

THERMAL CONDUCTIVITY OF VIRGIN MG-45, SILICONE-PHENOLIC IN PHENOLIC-GLASS HONEYCOMB
(ASTM C177 GUARDED HOT PLATE APPARATUS)

Average specimen mean temperature K	Total heat input watts	Average specimen ΔT K	Specimen thickness[2] cm	Specimen thermal conductivity[4] W/m-K	Time to temperature[3] hr
Specimen 1					
Bulk Density: Disc 1, Top 0.207 gm/cm³; Initial Wt: 6.792 g ; Final Wt: 5.757 g					
Disc 2, Bottom 0.217 gm/cm³; Initial Wt: 7.171 g ; Final Wt: 6.155 g					
Gum Rubber Filler					
158	2.53	123	0.630	3.54×10^{-2}	~8.0
159	2.53	122	0.630	3.57×10^{-2}	~8.5
194	4.18	175	0.630	4.11×10^{-2}	2.25
195	4.12	177	0.630	4.01×10^{-2}	2.75
267	2.62	86.4	0.630	5.22×10^{-2}	2.25
268	2.62	88.3	0.630	5.11×10^{-2}	3.75
Fiberfrax Filler					
293	2.65	84.5	0.630	5.40×10^{-2}	5.1
364	2.78	80.0	0.630	5.98×10^{-2}	~4.0
366	2.78	81.7	0.630	5.86×10^{-2}	~5.25
414	4.48	129	0.630	5.98×10^{-2}	4.5
414	4.49	128	0.630	6.04×10^{-2}	5.75

Notes:
1. Diameter of central heater = 4.826 cm (Area = 18.29 cm²).
2. Thermal conductivity values based on measured thickness at each temperature level. Values shown are for measurements across honeycomb web. The filler exhibited shrinkage after exposure to the maximum temperature level. Final values of filler thickness were about: Disc 1 - 0.521 cm; Disc 2 - 0.554 cm.
3. Time to temperature implies the time elapsed between adjustment of power and obtaining data.
4. Data obtained at a compaction pressure of 1.65×10^5 N/m².

88

TABLE 8

THERMAL CONDUCTIVITY OF VIRGIN MG-45, SILICONE-PHENOLIC IN PHENOLIC-GLASS HONEYCOMB
(ASTM C177 GUARDED HOT PLATE APPARATUS)

Average specimen mean temperature - K	Total heat input watts	Average specimen ΔT K	Specimen thickness[2] cm	Specimen thermal conductivity[4] W/m-K	Time to temperature[3] hr
Specimen 2					
Bulk Density: Disc 3, Top 0.213 gm/cm³; Initial Wt: 7.070 gm; Final Wt: 5.807 gm					
Disc 4, Bottom 0.206 gm/cm³; Initial Wt: 6.804 g ; Final Wt: 5.944 g					
Gum Rubber Filler					
160	2.50	125	0.630	3.44×10^{-2}	~8.0
160	2.50	124	0.630	3.47×10^{-2}	~8.5
196	4.09	177	0.630	3.98×10^{-2}	2.75
280	3.05	105	0.630	5.00×10^{-2}	2.5
Fiberfrax Filler					
291	2.46	86.1	0.630	4.92×10^{-2}	5.25
292	2.50	86.7	0.630	4.97×10^{-2}	6.0
370	2.48	85.0	0.630	5.02×10^{-2}	23.25
371	2.46	86.1	0.630	4.92×10^{-2}	24.5
418	3.84	131	0.630	5.05×10^{-2}	5.5

Notes:
1. Diameter of central heater = 4.826 cm (Area = 18.29 cm²).
2. Thermal conductivity values based on measured thickness at each temperature level. Values shown are for measurements across honeycomb web. The filler exhibited shrinkage after exposure to the maximum temperature level. Final values of filler thickness were about: Disc 3 - 0.538 cm; Disc 4 - 0.533 cm.
3. Time to temperature implies the time elapsed between adjustment of power and obtaining data.
4. Data obtained at a compaction pressure of 1.56 x 10⁵ N/m².

TABLE 9

THERMAL CONDUCTIVITY OF VIRGIN MG-45, SILICONE-PHENOLIC IN PHENOLIC-GLASS HONEYCOMB
(ASTM C177 GUARDED HOT PLATE APPARATUS)

Average specimen mean temperature K	Total heat input watts	Average specimen ΔT K	Specimen thickness[2] cm	Specimen thermal conductivity W/m-K	Time to temperature[3] hr
Specimen 3 Bulk density: Disc 8, Top 0.228 gm/cm³; Initial weight: 7.5562 g; Final weight: 7.0038 g					
Disc 10, Bottom 0.244 gm/cm³; Initial weight: 8.2588 g; Final weight: 6.4538 g					
Gum Rubber Filler					
344.50	2.68	83.17	0.6322	0.0555	19.5
344.27	2.69	82.68	0.6322	0.0562	20.4
Fiberfrax Filler					
370.87	2.76	87.54	0.6322	0.0545	21.0
371.87	2.82	87.59	0.6322	0.0556	22.0
416.31	4.45	129.82	0.6322	0.0592	18.0
415.87	4.46	130.21	0.6322	0.0591	20.0
485.09	4.05	113.90	0.6322	0.0614	44.0
485.92	4.04	113.82	0.6322	0.0612	44.5
507.70	4.26	120.42	0.6322	0.0611	3.3
507.42	4.24	120.48	0.6322	0.0608	3.6

Notes:

1. Diameter of central heater = 4.826 cm (Area - 18.29 cm²)
2. Thermal conductivity values based on measured thickness at each temperature level. Values shown are for measurements across honeycomb web.
3. Time to temperature implies the time elapsed between adjustment of power and obtaining data.
4. Data obtained at a compaction pressure of 1.65×10^5 N/m².

TABLE 10

THERMAL CONDUCTIVITY OF VIRGIN MG-45, SILICONE-PHENOLIC
IN PHENOLIC-GLASS HONEYCOMB
(ASTM C177 GUARDED HOT PLATE APPARATUS)

Average specimen mean temperature K	Total heat inputs watts	Average specimen ΔT K	Specimen thickness[2] cm	Specimen thermal conductivity W/m-K	Time to temperature[3] hr
Specimen 4					
Bulk density: Disc 9, Top 0.228 gm/cm³; Initial weight: 7.6065 g; Final weight: 4.8658 g					
Disc 11, Bottom 0.218 gm/cm³; Initial weight: 7.3609 g; Final weight: 4.4237 g					
Gum Rubber Filler					
338.70	2.66	76.73	0.6304	0.0597	16.8
338.52	2.66	76.78	0.6304	0.0595	18.0
Fiberfrax Filler					
360.73	2.68	79.21	0.6304	0.0581	25.8
360.93	2.68	79.78	0.6304	0.0578	26.2
441.00	6.15	159.12	0.6304	0.0666	21.0
441.77	6.15	159.67	0.6304	0.0663	21.8
484.19	4.19	108.83	0.6304	0.0662	20.0
515.16	4.98	114.11	0.6304	0.0691	21.8
513.51	4.98	112.76	0.6304	0.0700	22.5

Notes:
1. Diameter of central heater = 4.826 cm (Area - 18.29 cm²)
2. Thermal conductivity values based on measured thickness at each temperature level. Values shown are for measurements across honeycomb web.
3. Time to temperature implies the time elapsed between adjustment of power and obtaining data.
4. Data obtained at a compaction pressure of 1.65 x 10⁵ N/m².

TABLE 11

THERMAL CONDUCTIVITY OF VIRGIN MG-58,
PHENOLIC-NYLON IN PHENOLIC-GLASS HONEYCOMB
(ASTM C177 GUARDED HOT PLATE APPARATUS)

Average specimen mean temperature - K	Total heat input watts	Average specimen ΔT K	Specimen thickness[2] cm	Specimen thermal conductivity W/m-K		Time to temperature[3] hr

Specimen 1
Bulk Density: Disc 1, Top 0.238 gm/cm³; Initial Wt: 7.777 g; Final Wt: 6.650 g
Disc 2, Bottom 0.226 gm/cm³; Initial Wt: 7.405 g; Final Wt: 6.612 g

Gum Rubber Filler						
155	2.49	113	0.632	3.81×10^{-2}	(4)	2.75
154	2.44	114	0.632	3.70×10^{-2}	(4)	3.25
195	3.41	149	0.632	3.96×10^{-2}	(4)	1.58
275	2.59	96.1	0.632	4.66×10^{-2}	(4)	6.25
276	2.60	96.7	0.632	4.65×10^{-2}	(4)	7.83
Fiberfrax Filler						
290	2.63	91.7	0.635	4.98×10^{-2}	(5)	3.17
359	2.59	88.9	0.635	5.05×10^{-2}	(5)	1.33
360	2.58	88.9	0.635	5.04×10^{-2}	(5)	2.00
362	2.51	87.8	0.635	4.96×10^{-2}	(4)	5.25
410	4.19	137	0.635	5.31×10^{-2}	(4)	4.00
411	4.23	138	0.635	5.32×10^{-2}	(4)	5.58
Fiberfrax and Asbestos Filler						
474	2.75	97.8	0.632	4.86×10^{-2}	(4)	2.17
475	2.73	98.9	0.632	4.78×10^{-2}	(4)	3.50
523	3.03	116	0.632	4.52×10^{-2}	(4)	3.00

Notes:
1. Diameter of central heater = 4.826 cm (Area = 18.29 cm²).
2. Thermal conductivity values based on measured thickness at each temperature level. Values shown are for measurements across honeycomb webs. The filler exhibited shrinkage after exposure to the maximum temperature level. Final values of filler thickness were about: Disc 1 - 0.521 cm; Disc 2 - 0.526 cm.
3. Time to temperature implies the time elapsed between adjustment of power and obtaining data.
4. Data obtained at compaction pressure of 1.65 x 10⁵ N/m².
5. Data obtained at compaction pressure of 4.95 x 10⁵ N/m².

TABLE 12

THERMAL CONDUCTIVITY OF VIRGIN MG-58,
PHENOLIC-NYLON IN PHENOLIC-GLASS HONEYCOMB
(ASTM C177 GUARDED HOT PLATE APPARATUS)

Average specimen mean temperature - K	Total heat input watts	Average specimen ΔT K	Specimen thickness[2] cm	Specimen thermal conductivity[4] W/m-K	Time to temperature[3] hr
Specimen 2					
Bulk Density: Disc 3, Top 0.224 gm/cm³; Initial Wt: 7.467 gm; Final Wt: 7.024 gm					
Disc 4, Bottom 0.239 gm/cm³; Initial Wt: 7.818 g ; Final Wt: 6.737 g					
Gum Rubber Filler					
152	2.28	108	0.630	3.64×10^{-2}	2.4
151	2.28	111	0.630	3.54×10^{-2}	3.0
186	3.47	163	0.630	3.67×10^{-2}	1.75
186	3.51	157	0.630	3.85×10^{-2}	2.5
266	2.46	86.1	0.630	4.92×10^{-2}	6.5
266	2.49	86.1	0.630	4.98×10^{-2}	7.5
Fiberfrax Filler					
290	2.50	82.5	0.638	5.28×10^{-2}	4.7
365	2.50	82.8	0.635	5.24×10^{-2}	9.75
364	2.49	82.8	0.635	5.22×10^{-2}	10.75
417	4.16	132	0.635	5.47×10^{-2}	6.2
417	4.15	131	0.635	5.50×10^{-2}	7.0
Fiberfrax and Asbestos Filler					
474	3.29	108	0.632	5.27×10^{-2}	15.2
473	3.27	108	0.632	5.24×10^{-2}	16.8
505	3.81	121	0.632	5.45×10^{-2}	5.75

Notes:
1. Diameter of central heater = 4.826 cm (Area = 18.29 cm²).
2. Thermal conductivity values based on measured thickness at each temperature level. Values shown are for measurements across honeycomb webs. The filler exhibited shrinkage after exposure to the maximum temperature level. Final values of filler thickness were about: Disc 3 - 0.564 cm; Disc 4 - 0.554 cm.
3. Time to temperature implies the time elapsed between adjustment of power and obtaining data.
4. Data obtained at a compaction pressure of 1.65×10^5 N/m².

93

TABLE 13

THERMAL CONDUCTIVITY OF MG-1, SILICONE-PHENOLIC, CHARRED AT 1000 K
MEASURED IN ASTM C177 GUARDED HOT PLATE APPARATUS

Average specimen mean temperature - K	Total heat input watts	Average specimen ΔT K	Specimen thickness[1] cm	Specimen thermal conductivity W/m-K	Time to temperature[2] hr
Specimen 1000-10-A3, A4 Bulk Density: Disc No. 1 0.198 gm/cm³ Disc No. 2 0.203 gm/cm³					
Gum Rubber					
351	2.60	41.93	0.4686	0.079	3.25
354	2.60	43.22	0.4686	0.077	.75
Fiberfrax					
356	2.46	44.83	0.4686	0.070	1
355	2.46	44.64	0.4686	0.070	.5
Fiberfrax and 2 sets asbestos pads					
548	4.71	63.28	0.4686	0.095	3
549	4.71	63.27	0.4686	0.095	.5

Central Diameter 4.826 cm (Area = 18.29 cm²)

[1]Thermal conductivity values based on measured thickness at each temperature level.

[2]Time to temperature implies the time elapsed between adjustment of power and obtaining data.

94

TABLE 14

THERMAL CONDUCTIVITY OF MG-1, SILICONE-PHENOLIC, CHARRED AT 1000 K
MEASURED IN ASTM C177 GUARDED HOT PLATE APPARATUS

Average specimen mean temperature - K	Total heat input watts	Average specimen ΔT K	Specimen thickness[1] cm	Specimen thermal conductivity W/m-K	Time to temperature[2] hr
Specimen 1000-10-A11-12					
Bulk Density: Disc No. 11 0.187 gm/cm³					
Disc No. 12 0.201 gm/cm³					
Fiberfrax					
374	2.59	53.10	0.6695	0.089	2
376	2.59	54.21	0.6695	0.087	3
563	4.12	87.40	0.6695	0.086	6
562	4.07	87.39	0.6695	0.087	.75

Central Diameter 4.826 cm (Area = 18.29 cm²)
[1]Thermal conductivity values based on measured thickness at each temperature level.

[2]Time to temperature implies the time elapsed between adjustment of power and obtaining data.

95

TABLE 15

THERMAL CONDUCTIVITY OF MG-1, SILICONE-PHENOLIC. CHARRED AT 1500 K
MEASURED IN ASTM C177 GUARDED HOT PLATE APPARATUS

Average specimen mean temperature - K	Total heat inputs watts	Average specimen ΔT K	Specimen thickness[1] cm	Specimen thermal conductivity W/m-K	Time to temperature[2] hr
Specimen 1500-10-A1, A2 Bulk Density: Disc No. 1 0.200 gm/cm^3 Disc No. 2 0.206 gm/cm^3					
Gum Rubber					
331	2.73	33.42	0.6027	0.135	5
331	2.73	33.47	0.6027	0.135	.5
Fiberfrax					
345	2.48	26.08	0.6027	0.157	3
342	2.48	24.74	0.6027	0.166	4
Fiberfrax and 2 sets Asbestos Pads					
543	5.08	42.27	0.6027	0.199	4.5
543	5.08	42.43	0.6027	0.197	.5

Central Diameter 4.826 cm (Area = 18.29 cm^2)
[1]Thermal conductivity values based on measured thickness at each temperature level.

[2]Time to temperature implies the time elapsed between adjustment of power and obtaining data.

96

TABLE 16

THERMAL CONDUCTIVITY OF MG-1, SILICONE-PHENOLIC, CHARRED AT 1500 K
MEASURED IN ASTM C177 GUARDED HOT PLATE APPARATUS

Average specimen mean temperature - K	Total heat input watts	Average specimen ΔT K	Specimen thickness[1] cm	Specimen thermal conductivity W/m-K	Time to temperature[2] hr
Specimen 1500-10-A9-10 Bulk Density: Disc No. 1 0.189 gm/cm^3 Disc No. 2 0.189 gm/cm^3					
Gum Rubber					
348	2.52	31.84	0.6307	0.136	6
348	2.52	31.82	0.6307	0.136	.5
Fiberfrax and 2 sets Asbestos Pads					
532	4.54	51.34	0.6307	0.152	2
533	4.54	51.05	0.6307	0.153	.5
533	4.53	51.46	0.6307	0.151	1

Central Diameter 4.826 cm   (Area = 18.29 cm^2)

[1]Thermal conductivity values based on measured thickness at each temperature level.

[2]Time to temperature implies the time elapsed between adjustment of power and obtaining data.

97

TABLE 17

THERMAL CONDUCTIVITY OF MG-1, SILICONE-PHENOLIC, CHARRED AT 1644 K MEASURED IN ASTM C177 GUARDED HOT PLATE APPARATUS

Average specimen mean temperature - K	Total heat input watts	Average specimen ΔT K	Specimen thickness[1] cm	Specimen thermal conductivity W/m-K	Time to temperature[2] hr
Specimen 1644-10-A7-8 Bulk Density: Disc No. 1 0.180 gm/cm³ Disc No. 2 0.180 gm/cm³					
Gum Rubber					
346	2.59	33.11	0.6363	0.136	4
346	2.59	32.99	0.6363	0.136	.5
Fiberfrax 2 sets Asbestos Pads					
541	4.88	57.57	0.6363	0.147	2
541	4.88	57.39	0.6363	0.148	.5

Central Diameter 4.826 cm   (Area = 18.29 cm²)

[1]Thermal conductivity values based on measured thickness at each temperature level.

[2]Time to temperature implies the time elapsed between adjustment of power and obtaining data.

98

TABLE 18

THERMAL CONDUCTIVITY OF MG-1, SILICONE-PHENOLIC, CHARRED AT 1644 K
MEASURED IN ASTM C177 GUARDED HOT PLATE APPARATUS

Average specimen mean temperature - K	Total heat input watts	Average specimen ΔT K	Specimen thickness[1] cm	Specimen thermal conductivity W/m-K	Time to temperature[2] hr
Specimen 1644-10-A13 and A14					
Bulk Density: Disc No. 1 0.1579 gm/cm^3					
Disc No. $\overline{2}$ 0.1669 gm/cm^8					
Fiberfrax					
345	2.68	30.30	0.6817	0.165	3
344	2.68	30.22	0.6817	0.165	.75
Fiberfrax					
2 sets					
Asbestos Pads					
536	4.66	51.10	0.6817	0.170	4
535	4.66	51.18	0.6817	0.169	4

Central Diameter   4.826 cm   (Area = 18.29 cm^2)

[1]Thermal conductivity values based on measured thickness at each temperature level.

[2]Time to temperature implies the time elapsed between adjustment of power and obtaining data.

99

TABLE 19

THERMAL CONDUCTIVITY OF MG-1, SILICONE-PHENOLIC, CHARRED AT 811 K
(RADIAL INFLOW APPARATUS - STRIP SPECIMEN)

Specimen	Time	Average hot hole temperature K	Average ΔT each strip K	Heat flow to calorimeter watts	Average mean temp. of specimen K	Average thermal conductivity of specimen W/m-K	Average specimen thickness at temp cm	Environment and Pressure
Spec RIA-4-811-10-5 Run 5294-38-A5 Average density: 0.156 gm/cm³ Average initial thickness: 0.254 cm Average final thickness: 0.188 cm	7:10	777 772 767 778	F-238 B-237 L-231 R-239	11.02 12.07 10.75 10.75 11.25 11.40				~1 ATM nitrogen purge
	Average	$\overline{774}$	$\overline{236}$	$\overline{11.19}$	$\overline{656}$	$\overline{0.102}$	$\overline{0.248}$	
	10:50	1097 1099 1094 1089	F-247 B-258 L-251 R-252	20.5 21.0 20.2 20.9 21.2 20.0				~1 ATM nitrogen purge
	Average	$\overline{1095}$	$\overline{252}$	$\overline{20.6}$	$\overline{969}$	$\overline{0.173}$	$\overline{0.243}$	
	12:35	1345 1337 1336 1341	F-237 B-243 L-240 R-237	29.0 30.4 27.8 27.8 29.4				~1 ATM nitrogen purge
	Average	$\overline{1340}$	$\overline{239}$	$\overline{28.8}$	$\overline{1221}$	$\overline{0.252}$	$\overline{0.240}$	
	2:10	1595 1590 1595 1592	F-234 B-245 L-242 R-234	38.7 39.6 39.0 37.8 39.3 39.3				~1 ATM nitrogen purge
	Average	$\overline{1593}$	$\overline{240}$	$\overline{39.0}$	$\overline{1473}$	$\overline{0.336}$	$\overline{0.237}$	

Note: Calculation of thermal conductivity

$$K = \frac{Q\Delta X}{A\Delta T}$$

where

K = thermal conductivity
ΔX = specimen thickness
Q = heat flow to 1.27 cm calorimeter gage section
A = gage area of specimen (total for 4 strips) = 11.5 cm²
ΔT = temperature drop across specimen

TABLE 20

THERMAL CONDUCTIVITY OF MG-1, SILICONE-PHENOLIC, CHARRED AT 811 K
(RADIAL INFLOW APPARATUS - STRIP SPECIMEN)

Specimen	Time	Average hot hole temperature K	Average ΔT each strip K	Heat flow to calorimeter watts	Average mean temp. of specimen K	Average thermal conductivity of specimen W/m-K	Average specimen thickness at temp cm	Environment and Pressure
Spec RIA-1-811-10-6	2:30	946	F-277	17.58				
Run 5294-13-A5		950	B-279	17.64				
Average density: 0.168 gm/cm³		962	L-272	17.05				
Average initial thickness: 0.256 cm		945	R-275	17.52				
Average final thickness: 0.211 cm				16.73				
				16.06				
				18.61				
				18.46				
	Average	946	276	17.46	808	0.137	0.248	~1 ATM nitrogen purge
	5:30	1126	F-264	22.09				
		1131	B-265	22.09				
		1123	L-260	21.92				
		1124	R-262	22.06				
				22.91				
				21.74				
				21.62				
				21.80				
				22.33				
	Average	1126	263	22.06	995	0.179	0.245	~1 ATM nitrogen purge
	7:30	1318	F-262	30.8				
		1324	B-264	30.2				
		1318	L-259	29.3				
		1316	R-260	29.0				
				29.3				
	Average	1319	261	29.9	1188	0.242	0.243	~1 ATM nitrogen purge
	9:30	1624	F-254	38.7				
		1624	B-249	39.0				
		1624	L-247	38.4				
		1624	R-252	38.7				
	Average	1624	251	38.7	1501	0.322	0.239	1 ATM nitrogen purge

Note: Calculation of thermal conductivity

$$K = \frac{Q\Delta X}{A\Delta T}$$

where

K = thermal conductivity
ΔX = specimen thickness
Q = heat flow to 1.27 cm calorimeter gage section
A = gage area of specimen (total for 4 strips) = 11.5 cm²
ΔT = temperature drop across specimen

TABLE 21

THERMAL CONDUCTIVITY OF MG-1, SILICONE-PHENOLIC, CHARRED AT 1000 K
(RADIAL INFLOW APPARATUS - CYLINDRICAL SPECIMEN)

Specimen and Run	Time	Outer face temp K	Outside hole temp K	Inside hole temp K	Specimen ΔT	Heat to Calorimeter watts	Mean temperature K	Thermal conductivity W/m-K
Spec 1000-10-R-13 Run 5294-110-A5	1:30	--- ---	F-B 793 S-S 800	556 575	236 225	6.89 7.38 7.38 6.89		
Density: 0.189 gm/cm³	Average		796	566	231	7.15	681	0.244[1]
	2:30	1197 1197	F-B 1103 S-S 1116	748 775	355 341	16.8 14.9 14.9 14.9 14.4		
	Average	1197	1110	762	348	15.2	935	0.345[1]
	4:00	1578 1586	F-B 1482 S-S 1489	1108 1103	374 386	10.05 10.05 10.58 9.79 10.58		
	Average	1582	1485	1106	380	10.20	1295	0.211[2]

Notes:

1. Measurements in helium.
2. Measurements in argon.

Calculation of thermal conductivity

$$K = \left(\frac{\ln (R_o/R_i)}{2\pi L} \right) \frac{Q}{\Delta T}$$

where

K = thermal conductivity
R_o = outside radius = 1.111 cm
R_i = inside radius = 0.592 cm
Q = heat flow to calorimeter gage section
ΔT = temperature drop from hot to cold hole on the outside and inside radius, respectively
L = gage length of calorimeter = 1.270 cm

TABLE 22

THERMAL CONDUCTIVITY OF MG-1, SILICONE-PHENOLIC, CHARRED AT 1000 K
(RADIAL INFLOW APPARATUS - STRIP SPECIMEN)

Specimen	Time	Average hot hole temperature K	Average ΔT each strip K	Heat flow to calorimeter watts	Average mean temp. of specimen K	Average thermal conductivity of specimen W/m-K	Average specimen thickness at temp cm	Environment and Pressure
Spec RIA-2-1000-10-6	11:50	785	F-248	16.91				~1 ATM nitrogen purge
Run 5294-22-A5		783	B-248	16.48				
Average density: 0.171 gm/cm³		782	L-247	15.94				
Average initial thickness: 0.254 cm		778	R-244	15.53				
				16.64				
				16.17				
Average final thickness: 0.211 cm	Average	782	247	16.29	659	0.142	0.248	
	2:50	1101	F-507	28.1				~1 ATM nitrogen purge
		1095	B-507	29.3				
		1098	L-504	28.1				
		1088	R-502	28.1				
				28.4				
				28.7				
				28.1				
	Average	1095	505	28.4	928	0.180	0.243	
	4:55	1389	F-334	40.7				~1 ATM nitrogen purge
		1386	B-328	40.4				
		1391	L-336	41.6				
		1379	R-326	39.8				
				40.7				
	Average	1386	331	41.0	1222	0.259	0.240	
	6:30	1625	F-324	48.1				~1 ATM nitrogen purge
		1625	B-316	49.5				
		1632	L-327	49.5				
		1619	R-319	48.9				
				48.6				
				48.4				
				48.1				
	Average	1625	322	48.6	1464	0.312	0.237	

Note: Calculation of thermal conductivity

$$K = \frac{Q\Delta X}{A\Delta T}$$

where

K = thermal conductivity
ΔX = specimen thickness
Q = heat flow to 1.27 cm calorimeter gage section
A = gage area of specimen (total for 4 strips) = 11.5 cm²
ΔT = temperature drop across specimen

103

TABLE 23

THERMAL CONDUCTIVITY OF MG-1, SILICONE-PHENOLIC, CHARRED AT 1500 K
(RADIAL INFLOW APPARATUS - CYLINDRICAL SPECIMEN)

Specimen and Run	Time	Outer face temp K	Outside hole temp. K	Inside hole temp K	Specimen ΔT K	Heat to calorimeter watts	Mean temperature K	Thermal conductivity W/m-K
Spec 1500-10-R-16 Run 5294-112-A5 Density: 0.180 gm/cm³	10:30	--- ---	F-B 856 S-S 860	591 594	265 267	2.80 2.80 2.80 3.31 3.31		
	Average		858	592	266	3.06	725	0.091[1]
	12:30	1265 1265	F-B 1173 S-S 1181	793 796	381 384	8.00 8.00 8.76 8.76 8.00 8.00		
	Average	1265	1177	794	383	8.26	986	0.170[1]
	2:00	1578 1583	F-B 1456 S-S 1465	994 1000	463 465	13.65 12.63 12.63 12.63 12.13 12.63		
	Average	1580	1461	996	464	12.63	1229	0.214[1]

Note: [1]Measured in nitrogen

Calculation of thermal conductivity

$$K = \left(\frac{\ln(R_o/R_i)}{2\pi L}\right) \frac{Q}{\Delta T}$$

where

K = thermal conductivity
R_o = outside radius = 1.111 cm
R_i = inside radius = 0.592 cm
Q = heat flow to calorimeter gage section
ΔT = temperature drop from hot to cold hole on the outside and inside radius, respectively
L = gage length of calorimeter = 1.270 cm

104

TABLE 24

THERMAL CONDUCTIVITY OF MG-1, SILICONE-PHENOLIC, CHARRED AT 1500 K
(RADIAL INFLOW APPARATUS - CYLINDRICAL SPECIMEN)

Specimen and Run	Time	Outer face temp K	Outside hole temp. K	Inside hole temp K	Specimen ΔT K	Heat to calorimeter watts	Mean temperature K	Thermal conductivity W/m-K
Spec 1500-10-R-19 Run 5294-114-A5 Density: 0.181 gm/cm³	10:10	----	F-B 845 S-S 843	541 539	304 304	6.62 7.91 7.91 6.62 7.15 7.15		
	Average	----	844	540	304	7.15	692	0.185[1]
	11:10	1232 1232	F-B 1141 S-S 1142	700 693	441 449	10.31 9.79 9.79 9.79 9.79 9.29		
	Average	1232	1142	696	445	9.79	919	0.173[1]
	1:10	1578 1586	F-B 1468 S-S 1469	930 932	538 537	27.6 27.6 28.4 27.1 27.6 27.1		
	Average	1582	1468	931	538	27.6	1200	0.405[1]

Note: [1]Measured in nitrogen

Note: Calculation of thermal conductivity

$$K = \left(\frac{\ln (R_o/R_i)}{2\pi L}\right) \frac{Q}{\Delta T}$$

where

K = thermal conductivity
R_o = outside radius = 1.111 cm
R_i = inside radius = 0.592 cm
Q = heat flow to calorimeter gage section
ΔT = temperature drop from hot to cold hole on the outside and inside radius, respectively
L = gage length of calorimeter = 1.270 cm

TABLE 25

THERMAL CONDUCTIVITY OF MG-1, SILICONE-PHENOLIC, CHARRED AT 1644 K
(RADIAL INFLOW APPARATUS – STRIP SPECIMEN)

Specimen	Time	Average hot hole temperature K	Average ΔT each strip K	Heat flow to calorimeter watts	Average mean temp. of specimen K	Average thermal conductivity of specimen W/m-K	Average specimen thickness at temp cm	Environment and Pressure
Spec RIA-3-1644-10-5 Run 5294-30-A5 Average density: 0.178 gm/cm³ Average initial thickness: 0.254 cm Average final thickness: 0.229 cm	10:00	779 780 781 773	F-208 B-209 L-209 R-202	15.50 15.35 16.61 16.32 15.70 15.59 15.85				~1 ATM nitrogen purge
	Average	778	207	15.85	674	0.165	0.247	
	12:00	1142 1126 1131 1115	F-319 B-311 L-314 R-300	31.1 29.9 31.1 30.8 31.1 30.8				~1 ATM nitrogen purge
	Average	1125	311	30.8	970	0.210	0.243	
	2:00	1391 1391 1396 1378	F-357 B-350 L-349 R-335	43.1 41.9 42.8 42.8 43.1 42.8				~1 ATM nitrogen purge
	Average	1389	348	42.8	1216	0.257	0.240	
	4:00	1615 1620 1624 1605	F-374 B-372 L-364 R-353	54.8 55.1 54.2 56.0 53.6 55.1 54.2 54.8				~1 ATM nitrogen purge
	Average	1616	366	54.8	1433	0.309	0.237	

Note: Calculation of thermal conductivity

$$K = \frac{Q\Delta X}{A\Delta T}$$

where

K = thermal conductivity
ΔX = specimen thickness
Q = heat flow to 1.27 cm calorimeter gage section
A = gage area of specimen (total for 4 strips) = 11.5 cm²
ΔT = temperature drop across specimen

106

TABLE 26

THERMAL CONDUCTIVITY OF MG-1, SILICONE-PHENOLIC, CHARRED AT 1644 K
(RADIAL INFLOW APPARATUS - STRIP SPECIMEN)

Specimen	Time	Average hot hole temperature K	Average ΔT each strip K	Heat flow to calorimeter watts	Average mean temp. of specimen K	Average thermal conductivity of specimen W/m-K	Average specimen thickness at temp cm	Environment and Pressure
Spec RIA-5-1644-10-6 Run 5294-46-A5 Average density 0.177 gm/cm³ Average initial thickness: 0.244 cm Average final thickness: 0.234 cm	8:45	760 765 764 762	F-172 B-174 L-172 R-173	7.48 8.35 8.53 7.53 8.23 7.85				~1 ATM nitrogen purge
	Average	763	173	8.00	677	0.096	0.237	
	10:30	1080 1083 1084 1083	F-260 B-256 L-256 R-261	15.88 15.62 16.29 16.32 17.23 16.79				~1 ATM nitrogen purge
	Average	1082	258	16.35	953	0.128	0.233	
	12:20	1348 1348 1353 1352	F-302 B-292 L-294 R-303	27.0 25.6 25.5 26.6 27.3 27.4				~1 ATM nitorgen purge
	Average	1350	298	26.6	1201	0.178	0.230	
	1:55	1605 1608 1611 1609	F-338 B-327 L-324 R-334	37.2 36.0 36.6 36.6 38.4 41.3 36.9 36.9				~1 ATM nitrogen purge
	Average	1608	331	37.5	1443	0.224	0.227	

Note: Calculation of thermal conductivity

$$K = \frac{Q\Delta X}{A\Delta T}$$

where

K = thermal conductivity
ΔX = specimen thickness
Q = heat flow to 1.27 cm calorimeter gage section
A = gage area of specimen (total for 4 strips) = 11.5 cm²
ΔT = temperature drop across specimen

TABLE 27

THE THERMAL CONDUCTIVITY OF MG-45, SILICONE-PHENOLIC IN
PHENOLIC-GLASS HONEYCOMB, CHARRED IN NASA ARC-JET,
MEASURED IN RADIAL INFLOW APPARATUS

Specimen and Run	Time	Outer face temp K	Outside hole temperature K		Inside hole temperature K		Specimen ΔT K	Heat to calorimeter watts	Mean temperature K	Thermal conductivity W/m-K
			No.1	No.2	No.1	No.2				
Spec: 1 Run:5294-1-138	10:45	1411	1313	1278	821	799		36.0		
			1314	1279	821	800		36.0		
			1314	1279	822	800		36.9		
			1335	1318	833	826		37.5		
			1337	1320	834	828		38.6		
			1325	1299	827	813	492	37.0	1066	0.66
	12:15	1894	1777	1788	1283	1255		66.2		
			1777	1794	1283	1272		65.6		
		1916	1780	1791	1286	1266		66.8		
		1905	1778	1791	1284	1264	510	66.2		1.14
								66.8	1553	
								66.2		
	1:15	2261	2099	2124	1572	1552		91.4		
			2077	2094	1588	1561		89.9		
		2278	2072	2077	1572	1533		92.8		
		2270	2083	2098	1580	1549	426	90.5		
								92.5		
								91.4	1976	1.89
	2:15	2761	2588	2599	2116	2066		131.2		
			2580	2566	2099	2099		132.1		
		2783	2566	2572	2105	2105		131.5		
			2578	2579	2107	2090		131.8		
		2783					480	130.9		
		2776						131.5	2445	2.42
	3:00	3300	2888	2894	2511	2438		183.6		
			2911	2883	2511	2444		183.6		
			2866	2866	2499	2444		177.1		
		3294	2888	2881	2505	2441	411	180.4		
		3297						181.2	3013	3.89

Note: Specimen Comprised of Strips From Following Discs: Front: Disc Q 1   Left : Disc T 2
Back : Disc Q 1   Right: Disc Q 1

Note: Calculation of thermal conductivity

$$K = \frac{Q \Delta X}{A \Delta T}$$

where

K = thermal conductivity
ΔX = distance between inside and outside temperature well = 0.427 cm
Q = heat flow to 1.27 cm calorimeter gage section
A = gage area of specimen (total for 4 strips) = 4.93 cm^2
ΔT = temperature drop from outside to inside temperature well

108

TABLE 28

THE THERMAL CONDUCTIVITY OF MG-45, SILICONE-PHENOLIC IN
PHENOLIC-GLASS HONEYCOMB, CHARRED IN NASA ARC-JET,
MEASURED IN RADIAL INFLOW APPARATUS

Specimen and Run	Time	Outer face temp K	Outside hole temperature K		Inside hole temperature K		Specimen ΔT K	Heat to calorimeter watts	Mean temperature K	Thermal conductivity W/m-K
			No.1	No.2	No.1	No.2				
Spec: 2 Run:5294-1-141	11:00	1358	1301	1292	812	821		35.7		
			1304	1294	814	822		36.0		
			1306	1296	816	824				
			1323	1306	832			38.1		
			1324	1306	832			36.9		
			1312	1297	818	822	484	36.9	1062	0.67
	12:15	1853	1694	1716	1235	1227		61.8		
			1705	1722	1233	1222		62.4		
			1688	1724	1227	1224		61.5		
		1853	1696	1721	1232	1224	480	61.8		
		1853						62.4		
								61.8	1522	1.14
	1:00	2244	2061	2074	1566	1533		83.2		
			2077	2085	1577	1538		82.9		
			2077	2077	1594	1522		83.2		
		2250	2069	2078	1579	1531	524	81.7		
		2247						83.4		
								82.9	1885	1.40
	2:15	2783	2527	2549	2138	2105		129.7		
			2555	2566	2161	2099		132.1		
			2522	2533	2152	2116		131.5		
		2789	2535	2549	2150	2107	414	132.1		
		2786						135.3		
								132.1	2500	2.81
	3:00	3294	2894	2922	2519	2483		190.6		
			2899	2899	2511	2494		194.1		
			2838	2855	2522	2499		193.8		
		3294	2877	2892	2517	2492	380	195.6		
		3294						198.5		
								194.4	3032	4.50

Note: Specimen Comprised of Strips From Following Discs: Front: Disc H 2 Left : Disc H 2
Back : Disc H 2 Right: Disc H 2

Note: Calculation of thermal conductivity

$$K = \frac{Q\Delta X}{A\Delta T}$$

where

K = thermal conductivity
ΔX = distance between inside and outside temperature well = 0.427 cm
Q = heat flow to 1.27 cm calorimeter gage section
A = gage area of specimen (total for 4 strips) = 4.93 cm^2
ΔT = temperature drop from outside to inside temperature well

TABLE 29

THE EFFECTIVE THERMAL CONDUCTIVITY OF MG-58, PHENOLIC-NYLON IN
PHENOLIC-GLASS HONEYCOMB, CHARRED IN NASA ARC-JET
MEASURED IN ASTM C177 GUARDED HOT PLATE APPARATUS

Average specimen mean temperature -K	Total heat input watts	Average specimen ΔT K	Specimen thermal conductivity W/m-K	Time to temperature[2] hr
Specimen 3[4]	Thickness:	Top Disc = 1.019 cm Bottom Disc = 1.041 cm		
Gum Rubber Filler				
339	2.32	56.7	0.115	19.5
339	2.32	55.6	0.117	21.0
Fiberfrax Filler				
350	2.39	50.0	0.135	19.3
351	2.39	50.6	0.133	19.8
513	6.07	103.0	0.166	6.2
512	6.06	103.0	0.166	6.7
671	5.64	82.2	0.193	6.5
668	5.62	80.6	0.196	7.0

Notes:

1. Diameter of central heater = 4.826 cm (Area = 18.29 cm^2)
2. Time to temperature implies the time elapsed between adjustment of power and obtaining data.
3. Data obtained at compaction pressure of 1.95 x 10^5 N/m^2
4. Specimen was comprised of the following two char discs:
   Top: P2
   Bottom: Q2

110

TABLE 30

THE THERMAL CONDUCTIVITY OF MG-58, PHENOLIC-NYLON IN
PHENOLIC-GLASS HONEYCOMB, CHARRED IN NASA ARC-JET,
MEASURED IN RADIAL INFLOW APPARATUS

Specimen and Run	Time	Outer face temp K	Outside hole temperature K		Inside hole temperature K		Specimen ΔT K	Heat to calorimeter watts	Mean temperature K	Thermal conductivity W/m-K
			No.1	No.2	No.1	No.2				
Spec: 1 Run:5294-1-130	11:30	1405	1302	1308	853	822		38.9		
			1304	1310	854	824		38.6		
			1307	1312	856	825		38.6		
			1313	1313	844	809		38.1		
			1315	1315	845	810	472	36.9		
			1308	1312	850	818		38.1	1072	0.71
	1:15	1822	1591	1561	1183	1172		63.2		
			1599	1594	1177	1169		62.9		
		1822	1602	1572	1177	1155	414	63.8		
		1822	1597	1576	1180	1165		64.4		
								65.6		
								64.1	1381	1.36
	2:15	2411	1999	1961	1636	1605		113.0		
			1988	1963	1622	1605		113.9		
		2411	1999	1966	1616	1599	365	111.0		
		2411	1993	1963	1625	1602		114.8		
								115.4		
								113.6	2022	2.76
	3:15	2955	2488	2466	2211	2172		163.4		
		2966	2483	2483	2199	2172		165.1		
			2485	2477	2194	2172	294	164.0		
		2966	2485	2475	2201	2172		167.5		
		2962						167.8		
								165.4	2649	4.95
	4:00	3194	2833	2833	2544	2522		205.8		
			2838	2836	2533	2511		203.2		
		3200	2833	2838	2538	2513		205.8		
		3197	2835	2836	2538	2515	309	204.4		
								206.7		
								205.0	2868	5.85

Note: Specimen Comprised of Strips From Following Discs: Front: Disc P 3   Left : Disc M 2
Back : Disc P 3   Right: Disc O 2

Note: Calculation of thermal conductivity

$$K = \frac{Q \Delta X}{A \Delta T}$$

where

K = thermal conductivity
ΔX = distance between inside and outside temperature well = 0.427 cm
Q = heat flow to 1.27 cm calorimeter gage section
A = gage area of specimen (total for 4 strips) = 4.93 cm^2
ΔT = temperature drop from outside to inside temperature well

TABLE 31

THE THERMAL CONDUCTIVITY OF MG-58, PHENOLIC-NYLON IN PHENOLIC-GLASS HONEYCOMB, CHARRED IN NASA ARC-JET, MEASURED IN RADIAL INFLOW APPARATUS

Specimen and Run	Time	Outer face temp K	Outer face temperature K No.1	Outer face temperature K No.2	Inside hole temperature K No.1	Inside hole temperature K No.2	Specimen ΔT K	Heat to calorimeter watts	Mean temperature K	Thermal conductivity W/m-K
Spec: 2 Run: 5294-2-136	11:00	1855 __1872__ 1864	1738 1718 __1716__ 1724	1722 1711 __1699__ 1711	1488 1469 __1449__ 1469	1491 1491 __1466__ 1478	244	115.9 115.4 115.1 115.1 __115.4__ 115.4	1604	4.16
Rerun after Initial Exposure to 3340 K on Face of Specimen	1:00	2661 __2661__ 2661	2422 2405 __2411__ 2413	2399 2366 __2394__ 2386	2116 2099 __2094__ 2103	2144 2122 __2155__ 2140	278	166.0 164.0 166.0 164.3 __166.0__ 165.0	2365	5.23
	1:30	3253 3255 __3254__	2944 2913 2927 2894 2888 __2894__ 2910	2949 2922 2899 2888 2894 __2894__ 2910	2588 2611 2588 2588 2588 __2577__ 2592	2588 2588 2611 2616 2622 __2633__ 2614	307	217.6 214.9 214.6 __217.6__ 216.2	2927	6.20

Note: Calculation of thermal conductivity

$$K = \frac{Q\Delta X}{A\Delta T}$$

where

K = thermal conductivity

ΔX = distance between inside and outside temperature well = 0.427 cm

Q = heat flow to 1.27 cm calorimeter gage section

A = gage area of specimen (total for 4 strips) = 4.93 cm^2

ΔT = temperature drop from outside to inside temperature well

TABLE 32

THE THERMAL CONDUCTIVITY OF MG-58, PHENOLIC-NYLON IN PHENOLIC-GLASS HONEYCOMB, CHARRED IN NASA ARC-JET, MEASURED IN RADIAL INFLOW APPARATUS

Specimen and Run	Time	Outer face temp K	Outside hole temperature K No.1	No.2	Inside hole temperature K No.1	No.2	Specimen ΔT K	Heat to calorimeter watts	Mean temperature K	Thermal conductivity W/m-K
Spec: 2 Run:5294-1-133	11:30	1416	1274	1284	812	810		36.0		
			1276	1286	816	814		36.6		
			1275	1285	818	810		35.7		
			1276	1286	819	811		35.7		
		1416	1276	1287	820	811		35.7		
		1416	1275	1286	817	811	467	35.9	1047	0.68
	12:30	2011	1711	1749	1288	1338		65.6		
		2022	1711	1744	1283	1333		65.9		
			1713	1747	1285	1333		65.9		
		2022	1712	1747	1285	1335	479	64.1		
		2018						65.3		
								65.3	1508	1.20
	1:45	2500	2188	2227	1811	1844		98.4		
			2199	2216	1844	1855		99.0		
		2511	2191	2219	1833	1838		99.3		
		2506	2193	2221	1829	1846	372	99.6		
								100.7		
								99.3	2110	2.35
	2:45	2939	2688	2683	2355	2377		122.7		
			2688	2677	2366	2383		122.4		
		2955	2705	2691	2355	2394		121.8		
		2947	2696	2684	2360	2385	318	122.1		
								122.4		
								122.1	2608	3.38

Heater Tube Failed Before Readings Could be Obtained. Face of Specimen was at 3340 K When Run Terminated

Note: Specimen Comprised of Strips From Following Discs: Front: Disc O 2   Left : Disc Q 4

Back : Disc Q 4   Right: Disc Q 4

Note: Calculation of thermal conductivity

$$K = \frac{Q \Delta X}{A \Delta T}$$

where

K = thermal conductivity
ΔX = distance between inside and outside temperature well = 0.427 cm
Q = heat flow to 1.27 cm calorimeter gage section
A = gage area of specimen (total for 4 strips) = 4.93 cm^2
ΔT = temperature drop from outside to inside temperature well

113

TABLE 33

ENTHALPY OF VIRGIN MG-1 SILICONE-PHENOLIC
(ADIABATIC CALORIMETER)

Specimen	Run	Initial cup temp K	Final cup temp K	Change in cup temp K	Initial sample temp - K Inside specimen	Initial sample temp - K Surface of specimen	Initial sample temp - K Average	Initial wt of sample g	Wt of final sample g	Enthalpy $h = \frac{K}{W_s}(t_2 - t_1)$ Joules/kg	Enthalpy Joules/kg Above 303 K	Enthalpy Joules/kg Above 273 K
1	1	298.13	293.68	-4.45	155	144	150	12.312	12.316	-18.2×10^4	-19.4×10^4	-15.2×10^4
1	2	291.80	288.07	-3.73	169	173	171	12.316	12.311	-15.3×10^4	-17.2×10^4	-13.0×10^4
1	3	295.85	292.90	-2.95	197	197	197	12.311	12.280	-12.1×10^4	-13.4×10^4	-9.2×10^4
1	4	290.17	288.63	-1.54	232	225	229	12.280	12.282	-6.3×10^4	-7.8×10^4	-3.6×10^4
1	5	299.54	297.11	-2.43	226	230	228	12.282	12.279	-10.0×10^4	-10.8×10^4	-6.6×10^4
1	6	302.52	300.69	-1.83	250	247	249	12.279	12.261	-7.5×10^4	-7.9×10^4	-3.7×10^4
2	1	293.66	289.55	-4.11	154	154	154	12.268	12.184	-17.0×10^4	-18.7×10^4	-14.5×10^4
2	2	291.43	287.74	-3.69	169	169	169	12.184	12.183	-15.3×10^4	-17.2×10^4	-13.0×10^4
2	3	292.92	290.14	-2.78	198	198	198	12.183	12.161	-11.5×10^4	-13.1×10^4	-8.9×10^4
2	4	288.63	286.79	-1.84	223	223	223	12.161	12.159	-7.6×10^4	-9.6×10^4	-5.4×10^4
2	5	300.69	299.21	-1.48	254	254	254	12.159	12.129	-6.2×10^4	-6.7×10^4	-2.5×10^4
3	1	298.10	300.62	+2.52			353	15.044	14.974	$+8.5 \times 10^4$	$+8.1 \times 10^4$	$+12.3 \times 10^4$
3A	2	297.40	300.01	+2.61			402	8.213	8.064	$+16.3 \times 10^4$	$+15.8 \times 10^4$	$+20.0 \times 10^4$
3A	3	302.62	305.95	+3.33			449	8.064	7.930	$+21.2 \times 10^4$	$+21.6 \times 10^4$	$+25.8 \times 10^4$
3A	4	301.91	306.29	+4.38			495	7.930	7.739	$+28.5 \times 10^4$	$+29.0 \times 10^4$	$+33.2 \times 10^4$
4	1	300.54	303.29	+2.75			365	16.164	16.086	$+8.6 \times 10^4$	$+8.7 \times 10^4$	$+12.9 \times 10^4$
4A	2	299.87	302.81	+2.94			422	8.511	8.309	$+17.8 \times 10^4$	$+17.8 \times 10^4$	$+22.0 \times 10^4$
4A	3	298.28	302.23	+3.95			476	8.309	8.140	$+24.4 \times 10^4$	$+24.3 \times 10^4$	$+28.5 \times 10^4$
4A	4	302.67	307.38	+4.71			505	8.140	8.031	$+29.5 \times 10^4$	$+30.2 \times 10^4$	$+34.4 \times 10^4$

Notes: 1. K = Calorimeter Constant = 503.7 Joules/K
         2. Specimens 3A and 4A were obtained from Specimens 3 and 4, respectively, by halving those specimens

114

TABLE 34

ENTHALPY OF VIRGIN MG-45, SILICONE-PHENOLIC IN PHENOLIC-GLASS HONEYCOMB
(ADIABATIC CALORIMETER)

Specimen	Run	Initial cup temp K	Final cup temp K	Change in cup temp K	Initial sample temp K	Initial wt of sample g	W_s, final wt of sample g	Enthalpy $h = \frac{K}{W_s}(t_2-t_1)$ Joules/kg	Enthalpy Joules/kg Above 303 K	Above 273 K
1	4	295.64	296.76	1.12	397	4.738	4.665	12.12×10^4	11.4×10^4	15.2×10^4
2	4	294.96	296.12	1.16	399	4.858	4.812	12.15×10^4	11.4×10^4	15.2×10^4
3	1	296.86	296.09	-0.77	227	4.885	4.844	-8.0×10^4	-8.7×10^4	-4.9×10^4
3	3	294.79	296.76	1.97	458	4.677	4.584	21.67×10^4	20.9×10^4	24.7×10^4
3	4	295.13	298.12	2.99	507	4.584	4.466	33.77×10^4	33.1×10^4	36.9×10^4
4	1	296.53	295.82	-0.71	227	4.220	4.209	-8.4×10^4	-9.3×10^4	-5.5×10^4
4	3	294.79	296.84	2.05	455	4.092	3.979	25.94×10^4	25.0×10^4	28.8×10^4
4	4	294.74	297.11	2.37	517	3.979	3.820	31.29×10^4	30.5×10^4	34.3×10^4
5	3	295.13	293.80	-1.33	189	4.944	4.968	-13.52×10^4	-14.6×10^4	-10.8×10^4
5	4	295.03	293.47	-1.56	139	4.968	4.968	-15.77×10^4	-16.7×10^4	-12.9×10^4
5	8	297.23	295.65	-1.58	152	4.927	4.813	-16.57×10^4	-17.4×10^4	-13.6×10^4
5	9	291.80	294.64	2.84	461	4.813	4.623	30.93×10^4	29.4×10^4	33.2×10^4
6	3	295.57	294.51	-1.06	202	4.127	4.125	-12.96×10^4	-14.1×10^4	-10.3×10^4
6	4	296.76	295.30	-1.46	129	4.125	4.092	-17.98×10^4	-18.8×10^4	-15.0×10^4
6	7	298.07	299.12	1.05	392	3.986	3.966	13.27×10^4	12.8×10^4	16.6×10^4
7	1	300.39	302.28	1.89	450	4.216	4.000	23.81×10^4	23.7×10^4	27.5×10^4
8	1	297.71	298.08	0.37	341	3.328	3.255	5.73×10^4	5.1×10^4	8.9×10^4

1. K (Calorimeter Constant) = 503.7 Joules/K

TABLE 35

ENTHALPY OF VIRGIN MG-58, PHENOLIC-NYLON IN PHENOLIC-GLASS HONEYCOMB (ADIABATIC CALORIMETER)

Specimen	Run	Initial cup temp K	Final cup temp K	Change in cup temp K	Initial sample temp K	Initial wt of sample g	W_s, final wt of sample g	Enthalpy $h = \frac{K}{W_s}(t_2 - t_1)$ Joules/kg	Enthalpy Joules/kg Above 303 K	Above 273 K
1	1	294.96	294.29	-0.67	227.6	5.319	5.319	-6.4×10^4	-7.2×10^4	-3.7×10^4
1	2	295.13	295.87	0.74	352.6	5.319	5.220	7.2×10^4	6.3×10^4	9.8×10^4
1	3	296.68	297.86	1.18	394.8	5.220	5.177	11.5×10^4	10.9×10^4	14.4×10^4
1	5	295.37	298.92	3.55	504.8	5.110	5.050	35.4×10^4	34.8×10^4	38.3×10^4
2	1	295.85	295.10	-0.75	226.5	4.469	4.462	-8.4×10^4	-9.3×10^4	-5.8×10^4
2	2	296.05	296.96	0.91	372.0	4.462	4.368	10.5×10^4	9.7×10^4	13.2×10^4
2	3	206.59	297.59	1.01	392.6	4.368	4.323	11.8×10^4	11.2×10^4	14.7×10^4
2	4	296.56	298.72	2.16	450.9	4.323	4.360	25.0×10^4	24.3×10^4	27.8×10^4
2	5	295.95	298.72	2.77	513.1	4.360	4.320	32.4×10^4	31.8×10^4	35.3×10^4
3	1	297.16	296.12	-1.04	164.3	4.312	4.316	12.1×10^4	-12.7×10^4	-9.2×10^4
3	2	297.69	296.39	-1.30	144.3	4.316	4.304	-15.2×10^4	-15.8×10^4	-12.3×10^4
3	3	293.97	295.70	1.73	443.7	4.304	4.152	21.0×10^4	20.0×10^4	23.5×10^4
4	1	296.36	295.32	-1.04	169.3	4.057	4.057	12.9×10^4	-13.6×10^4	-10.1×10^4
4	2	296.56	295.27	-1.29	135.9	4.057	4.050	16.0×10^4	-16.7×10^4	-13.2×10^4

1. K (Calorimeter Constant) = 503.9 Joules/K

TABLE 36

ENTHALPY OF MG-1, SILICONE-PHENOLIC, CHARRED AT 1000 K
(ADIABATIC CALORIMETER)

Specimen	Run	Initial cup temp K	Final cup temp K	Change in cup temp K	Initial temp of sample and holder K	Weight of aluminum sample holder (g)	Enthalpy of aluminum sample holder (Joules/Kg)	Temp change of cup due to aluminum sample holder (t_2-t_1) SH $= \frac{h_{SH} W_{SH} SH}{K}$ K	Temp change of cup due to sample (K)	Initial wt of sample g	Final wt of sample K	Enthalpy $h = \frac{K}{W_S}(t_2-t_1)$ Joules/kg	Enthalpy Joules/Kg Above 303 K	Above 273 K
MG-1 #1	1	297.47	300.63	3.16	540	0.6480	2.3×10^5	0.30	2.86	5.9629	5.7693	2.50×10^5	2.47×10^5	2.69×10^5
	2	296.77	304.34	7.57	825	0.6480	5.43×10^5	0.70	6.87	5.7693	5.5736	6.21×10^5	6.22×10^5	6.44×10^5
	3	297.68	302.68	5.00	669	0.6480	3.64×10^5	0.47	4.53	5.5736	5.5401	4.12×10^5	4.12×10^5	4.34×10^5
MG-1 #2	1	302.17	305.60	3.43	568	0.7963	2.58×10^5	0.41	3.02	6.0292	5.7945	2.63×10^5	2.66×10^5	2.88×10^5
	2	304.18	311.18	7.00	810	0.7963	5.22×10^5	0.83	6.17	5.7945	5.5743	5.58×10^5	5.67×10^5	5.89×10^5

Notes:
1. K (calorimeter constant) = 503.7 Joules/K
2. Specimens obtained from ASTM Specimens 1000-10-A2, 1000-10-A11 and 1000-10-A12

TABLE 37

ENTHALPY OF MG-1, SILICONE-PHENOLIC, CHARRED AT 1000 K
(ICE CALORIMETER)

Spec. and Run No.	Spec. temp K	Soak time at temp min	Initial wt. of C.S. graphite drop cup g	Initial wt. of spec g	Final wt. of spec. and cup g	Final wt. of spec g	Specimen wt. loss %	Total mercury displacement cm³	Mercury displacement due to cup cm³	Mercury displacement due to spec cm³	Enthalpy above 273K reference Joules/kg
MG-1 #1											
1	827.61	30	3.215	1.7223	4.7944	1.5794	8.3	1.10	0.74	0.36	8.4×10^5
2	801.49	30	3.215	1.6639	4.8475	1.6325	1.9	1.00	0.70	0.30	6.8×10^5
3	979.83	30	3.215	1.6325	4.8318	1.6168	1.0	1.32	0.96	0.36	8.1×10^5
4	1143.16	30	3.215	1.6168	4.8085	1.5935	1.4	1.70	1.18	0.52	12.0×10^5
5	1344.27	30	3.215	1.5935	4.7089	1.4939	6.3	2.17	1.47	0.70	17.2×10^5
6	1522.05	30	3.215	1.4939	4.6213	1.4063	5.9	2.37	1.72	0.64	17.0×10^5
7	1655.38	30	3.215	1.4063	4.5393	1.3243	5.8	2.65	1.90	0.75	20.8×10^5
MG-1 #2											
1	816.49	30	3.215	1.5858	4.7560	1.5410	2.8	0.95	0.73	0.22	5.3×10^5
2	993.72	30	3.215	1.5410	4.7355	1.5205	1.3	1.31	0.97	0.34	8.3×10^5
3	1147.05	30	3.215	1.5205	4.7000	1.4850	2.3	1.74	1.19	0.55	13.6×10^5
4	1360.93	30	3.215	1.4850	4.7114	1.4964	-0.8	2.06	1.50	0.56	13.8×10^5
5	1505.38	30	3.215	1.4964	4.5588	1.3438	10.2	2.27	1.69	0.58	15.8×10^5
6	1683.16	30	3.215	1.3438	4.4500	1.2350	8.1	2.65	1.94	0.71	21.1×10^5
1000-10-3 #1											
1	1147	40	3.3356[3]	2.4072	5.6513	2.3157	3.8	1.84	1.19	0.65	10.3×10^5
2	1380	40	3.3356[3]	2.3157	5.5697	2.2341	3.5	2.51	1.52	0.99	16.3×10^5
3	1683	40	3.3356[3]	2.3249[6]	5.3441	2.0085	13.6	3.06	1.94	1.12	20.5×10^5
4	1155	40	3.2370[4]	2.0085	5.2357	1.9987	0.5	1.80	1.20	0.60	11.0×10^5
1000-10-3 #2											
1	1191	40	3.214[5]	2.7906	5.9000	2.6861	3.7	2.19	1.24	0.95	13.0×10^5
2	1444	40	3.214[5]	2.6861	5.8040	2.5901	3.6	2.82	1.60	1.22	17.3×10^5
3	1636	40	3.214[5]	2.7085[6]	5.6712	2.4573	9.3	3.09	1.88	1.21	18.1×10^5
4	1405	40	3.214[5]	2.4573	5.6620	2.4481	0.4	2.56	1.55	1.01	15.2×10^5

Notes:

1. Enthalpy calculations based on value of 3.680×10^3 Joules/cm³ of ice melted
   Final weight used for calculation of enthalpy
2. Specimens.Nos. 1 and 2 obtained from ASTM Specimens 1000-10-A2, 1000-10-All and 1000-10-Al2
3. Cup weight = 3.216 gm; weight of tungsten wire = 0.120 gm
4. Tungsten wire came off before this run; weight changed by 0.0986 gm
5. Final cup weight after all runs = 3.191 gm
6. Final cup weight after all runs = 3.185 gm
7. Gained weight overnight

118

TABLE 38

ENTHALPY OF MG-45, SILICONE-PHENOLIC IN PHENOLIC-GLASS HONEYCOMB
CHARRED IN NASA ARC-JET
(ICE CALORIMETER)

Specimen and Run Number	Specimen temperature K	Soak time at temperature min	Initial wt of C.S. Graphite drop cup g	Initial wt of specimen g	Final wt of cup and specimen g	Final wt of specimen g	Specimen weight loss %	Total mercury displacement cm³	Mercury displacement due to cup cm³	Mercury displacement due to specimen cm³	Enthalpy above 273 K reference Joules/kg
T1-1 - Run 1	814	10	3.215	2.371	5.399	2.184	7.9	0.87	0.73	0.14	2.4×10^6
Run 2	1405	10	3.215	2.184	5.348	2.133	2.3	2.23	1.55	0.68	11.7×10^6
Run 3	1943	20	3.215	2.133	4.606	1.391	34.8	3.39	2.32	1.07	28.3×10^5
P2-1 - Run 1	805	20	3.215	2.534	5.614	2.399	5.3	1.00	0.70	0.30	4.6×10^6
Run 2	1383	30	3.215	2.399	5.544	2.329	2.9	2.37	1.53	0.84	13.3×10^5
Run 3	1983	20	3.215	2.329	4.283[a]	1.071[a,3]	54.0	3.29	2.38	0.91	31.2×10^5
T1, P2, N2-1 Run 1	815	20	3.215	1.969	5.013	1.798[a]	8.7	0.94	0.73	0.21	4.3×10^6
Run 2	1393	20	3.215	1.789	4.980	1.765	1.3	2.33	1.53	0.80	16.7×10^6
Run 3	1979	20	3.215	1.765	4.718	1.503	14.8	3.63	2.37	1.26	30.8×10^6

Notes: 1. Enthalpy calculations based on value of 3.680×10^3 Joules per cm³ of ice melted. Final weight used for calculation of enthalpy.

2. Weighed cup and specimen separately for following results: Cup - 3.212 g ; Specimen - 1.071 g.

3. Some spillage of powder into calorimeter. Spillage was collected for weight measurement.

TABLE 39

ENTHALPY OF MG-58, PHENOLIC-NYLON IN PHENOLIC-GLASS HONEYCOMB
CHARRED IN NASA ARC-JET
(ICE CALORIMETER)

Specimen and Run No.	Specimen temperature K	Soak Time at temperature min	Initial wt. of C.S. graphite drop cup g	Initial wt. of spec g	Final wt. of cup and spec g	Final wt. of specimen g	Specimen weight loss %	Total mercury displacement cm³	Mercury displacement due to cup cm³	Mercury displacement due to spec cm³	Enthalpy above 273K reference Joules/kg
J1-1 - Run 1	822	20	3.215	2.616	5.646	2.431	7.1	1.01	0.73	0.28	4.2×10^5
Run 2	1406	20	3.215	2.431	5.606	2.391	1.6	2.43	1.55	0.88	13.5×10^5
Run 3	1950	20	3.215	2.391	5.188	1.973	18.8	3.95	2.32	1.63	30.4×10^5
J2-2 - Run 1	809	20	3.215	2.741	5.763	2.548	7.0	1.00	0.71	0.29	4.2×10^5
Run 2	1408	20	3.215	2.548	5.711	2.496	2.0	2.63	1.56	1.07	15.8×10^5
Run 3	1955	20	3.215	2.496	5.363	2.148	13.9	4.05	2.33	1.72	29.4×10^5

Note: Enthalpy calculations based on value of 3.680×10^3 Joules per cm³ of ice melted. Final weight used for calculation of enthalpy.

TABLE 40

THERMAL EXPANSION OF VIRGIN MG-1, SILICONE-PHENOLIC IN THE X DIRECTION MEASURED IN QUARTZ DILATOMETER

Specimen 5
Run 1
Density 0.608 gm/cm³
Log 5317-81

Initial weight: 5.676 g Final weight: 5.529 g
Initial length: 7.609 cm Final length: 7.548 cm

Time	Top of specimen temperature No. 1, K	Middle of specimen temperature No. 2, K	Bottom of specimen temperature No. 3, K	Average temperature, K	Observed total elongation, cm	Observed unit elongation, cm/cm	Unit elongation correction for dilatometer motion, cm/cm	Corrected specimen unit elongation, cm/cm
1:20 pm	296	296	296	296	0	0	0	0
2:30	132	129	128	130	-132.3 x 10⁻³	-17.39 x 10⁻³	+0.03 x 10⁻³	-17.4 x 10⁻³
3:15	191	191	191	191	-90.9 x 10⁻³	-11.95 x 10⁻³	-0.01 x 10⁻³	-12.0 x 10⁻³
4:00	243	238	240	240	-34.5 x 10⁻³	-4.53 x 10⁻³	-0.02 x 10⁻³	-4.6 x 10⁻³
4:15	273	273	273	273	-11.2 x 10⁻³	-1.47 x 10⁻³	-0.01 x 10⁻³	-1.5 x 10⁻³
5:50	296	296	296	296	+8.2 x 10⁻³	+1.08 x 10⁻³	0	+1.1 x 10⁻³
7:20	336	338	338	337	+35.1 x 10⁻³	+4.61 x 10⁻³	+0.01 x 10⁻³	+4.6 x 10⁻³
8:35	383	386	385	385	+73.5 x 10⁻³	+9.66 x 10⁻³	+0.03 x 10⁻³	+9.7 x 10⁻³
9:22	419	422	420	420	+96.6 x 10⁻³	+12.70 x 10⁻³	+0.04 x 10⁻³	+12.7 x 10⁻³
10:16	464	468	466	466	+101.0 x 10⁻³	+13.27 x 10⁻³	+0.07 x 10⁻³	+13.3 x 10⁻³
10:55	511	517	514	514	+131.9 x 10⁻³	+17.33 x 10⁻³	+0.09 x 10⁻³	+17.4 x 10⁻³
10:15 am	296	296	296	296	-89.0 x 10⁻³	-11.70 x 10⁻³	0	-11.7 x 10⁻³
	299	299	299	299	-78.9 x 10⁻³	-10.37 x 10⁻³	0	-10.4 x 10⁻³
					-61.0 x 10⁻³	-8.02 x 10⁻³	0	-8.0 x 10⁻³

From micrometer measurements

TABLE 41

THERMAL EXPANSION OF VIRGIN MG-1, SILICONE-PHENOLIC IN THE X DIRECTION MEASURED IN QUARTZ DILATOMETER

Specimen No. / Time	Top of specimen temperature No. 1 K	Middle of specimen temperature No. 2 K	Bottom of specimen temperature No. 3 K	Average temperature K	Observed total elongation cm	Observed unit elongation cm/cm	Unit elongation correction for dilatometer motion cm/cm	Corrected specimen unit elongation cm/cm
Specimen 6 Run 1 Density 0.600 gm/cm^3 Log 5317-80	Initial length: 7.630 cm Final length: 7.548 cm		Initial length: 7.630 cm Final length: 7.548 cm		Initial weight: 5.616 g Final weight: 5.475 g			
2:55 pm	293	293	293	293	0	0	0	0
3:40	112	106	96	105	-124.0×10^{-3}	-16.25×10^{-3}	$+0.05 \times 10^{-3}$	-16.2×10^{-3}
4:15	185	184	175	181	-84.0×10^{-3}	-11.01×10^{-3}	$+0.01 \times 10^{-3}$	-11.0×10^{-3}
4:30	214	205	211	210	-56.9×10^{-3}	-7.46×10^{-3}	-0.01×10^{-3}	-7.5×10^{-3}
4:35	244	235	242	240	-28.1×10^{-3}	-3.68×10^{-3}	-0.01×10^{-3}	-3.7×10^{-3}
5:00	273	273	273	273	-10.0×10^{-3}	-1.31×10^{-3}	-0.01×10^{-3}	-1.3×10^{-3}
5:50	296	296	296	296	$+5.2 \times 10^{-3}$	$+0.68 \times 10^{-3}$	0	$+0.7 \times 10^{-3}$
7:40	342	345	346	344	$+32.0 \times 10^{-3}$	$+4.19 \times 10^{-3}$	$+0.01 \times 10^{-3}$	$+4.2 \times 10^{-3}$
8:42	384	387	388	386	$+54.5 \times 10^{-3}$	$+7.14 \times 10^{-3}$	$+0.03 \times 10^{-3}$	$+7.2 \times 10^{-3}$
9:25	425	429	431	428	$+62.0 \times 10^{-3}$	$+8.13 \times 10^{-3}$	$+0.05 \times 10^{-3}$	$+8.2 \times 10^{-3}$
10:15	459	464	464	462	$+48.5 \times 10^{-3}$	$+6.36 \times 10^{-3}$	$+0.07 \times 10^{-3}$	$+6.4 \times 10^{-3}$
11:15	504	511	511	509	$+77.4 \times 10^{-3}$	$+10.14 \times 10^{-3}$	$+0.09 \times 10^{-3}$	$+10.2 \times 10^{-3}$
10:10 am	296	296	296	296	-112.4×10^{-3}	-14.73×10^{-3}	0	-14.7×10^{-3}
	299	299	299	299	-101.4×10^{-3}	-13.29×10^{-3}	0	-13.3×10^{-3}
From micrometer measurements					-82.0×10^{-3}	-10.70×10^{-3}	—	-10.7×10^{-3}

Note: Specimen was bowed and warped on removal from apparatus

TABLE 42

THERMAL EXPANSION OF VIRGIN MG-1, SILICONE-PHENOLIC IN THE Y DIRECTION MEASURED IN THE QUARTZ DILATOMETER

Specimen	Time	Specimen temperatures - K				Observed total elongation 10⁻³ cm	Observed unit elongation 10⁻³ cm/cm	Unit Elongation correction for dilatometer motion 10⁻³ cm/cm	Corrected specimen unit elongation 10⁻³ cm/cm
		Top	Middle	Bottom	Average				
Spec MG-1-QEXP-W-1 Run 5317-36-15 Density: 0.6138 gm/cm³		Initial length: 7.638 cm Final length: 7.438 cm				Initial weight: 5.9817 g Final weight: 5.7305 g			
	12:30	298	298	298	298	0.00	0.00	0.00	0.00
	1:37	338	339	339	339	7.14	0.93	0.01	0.95
	2:05	367	368	368	368	13.06	1.71	0.02	1.73
	2:20	423	424	425	424	43.56	5.70	0.05	5.75
	3:15	480	483	483	482	51.71	6.77	0.08	6.85
	3:50	532	535	536	504	59.36	7.77	0.11	7.88
	7:50	299	299	299	299	-112.83	-14.77	0.00	-14.77

123

TABLE 43

THERMAL EXPANSION OF VIRGIN MG-1, SILICONE-PHENOLIC IN THE Y DIRECTION
MEASURED IN THE QUARTZ DILATOMETER

Specimen	Time	Specimen temperatures - K				Observed total elongation 10⁻³ cm	Observed unit elongation 10⁻³ cm/cm	Unit elongation correction for dilatometer motion 10⁻³ cm/cm	Corrected specimen unit elongation 10⁻³ cm/cm
		Top	Middle	Bottom	Average				
Spec MG-1-QEXP-W-2 Run 5317-50-14 Density: 0.6020 gm/cm³		Initial Length: 7.7412 cm Final Length: 7.6045 cm				Initial Weight: 5.9503 g Final Weight: 5.6766 g			
	12:50	297	297	297	297	0.00	0.00	0.00	0.00
	1:03	112	107	102	107	-78.69	-10.17	0.05	-10.12
	1:10	154	146	142	148	-64.87	-8.38	0.01	-8.37
	1:15	178	173	166	172	-53.77	-6.95	0.00	-6.95
	1:21	207	200	196	201	-40.64	-5.25	-0.01	-5.26
	1:29	228	223	218	223	-30.23	-3.90	-0.02	-3.92
	1:55	258	255	252	255	-19.61	-2.53	-0.01	-2.54
	11:00	298	298	298	298	-4.78	-0.62	0.00	-0.62
	12:00	338	338	338	338	4.75	0.61	0.01	0.62
	12:30	366	366	366	366	7.01	0.91	0.02	0.93
	1:00	397	397	397	397	8.10	1.05	0.04	1.09
	1:30	423	423	423	423	8.26	1.07	0.05	1.12
	2:00	455	455	455	455	10.82	1.40	0.07	1.47
	2:40	483	483	483	483	8.05	1.04	0.08	1.12
	3:10	511	511	511	511	10.39	1.34	0.10	1.44
	3:45	534	534	534	534	9.58	1.24	0.11	1.35
	8:00	297	297	297	297	-113.23	-14.64	0.00	-14.63

TABLE 44

THERMAL EXPANSION OF MG-1, SILICONE-PHENOLIC, TO 1866 K AT A HEATING
RATE OF 10 K/MIN (MEASURED IN GRAPHITE DILATOMETER)

Time	Temperature K	Observed total elongation 10^{-3} cm	Observed unit elongation 10^{-3} cm/cm	Unit correction for dilatometer motion 10^{-3} cm/cm	Corrected unit expansion 10^{-3} cm/cm
	K-furnace No. 1; Dilatometer 125				
	Initial length: 3.480 cm				
	Initial weight: 7.130 g				
1:02	295	0.00	0.00	0.00	0.00
1:08	370	23.24	6.68	0.06	6.74
1:10	393	38.48	11.06	0.08	11.14
1:13	422	66.42	19.09	0.12	19.21
1:16	449	117.22	33.69	0.15	33.84
1:18	478	152.78	43.90	0.18	44.08
1:21	505	165.48	47.55	0.22	47.77
1:24	532	179.45	51.57	0.25	51.82
1:27	561	192.15	55.22	0.30	55.52
1:30	589	208.66	59.96	0.34	60.30
1:33	616	226.44	65.07	0.38	65.45
1:35	644	254.38	73.10	0.43	73.53
1:38	671 (1)	272.16	78.21	0.47	78.68
1:42	708	170.56	49.01	0.54	49.55
1:44	729	57.53	16.53	0.59	17.12
1:47	754 (2)	-50.42	-14.49	0.64	-13.85
1:50	784	-158.36	-45.51	0.69	-44.82
1:54	809	-192.66	-55.36	0.74	-54.62
1:56	839	-211.71	-60.84	0.80	-60.04
2:00	865	-282.58	-81.20	0.86	-80.34
2:03	894	-300.61	-86.39	0.92	-85.47
2:07	922	-328.55	-94.42	0.99	-93.43
2:10	949	-357.76	-102.81	1.04	-101.77
2:12	978	-393.32	-113.03	1.12	-111.91
2:16	733	-430.15	-123.61	1.18	-122.43
2:19	1033	-459.36	-132.01	1.25	-130.76
2:22	1061	-486.03	-139.67	1.32	-138.35
2:24	1089	-503.81	-144.78	1.40	-143.38
2:27	1116	-512.19	-147.19	1.48	-145.71
2:30	1144	-516.51	-148.43	1.56	-146.87
2:33	1172	-519.68	-149.34	1.62	-147.72
2:35	1200	-522.10	-150.04	1.72	-148.32
2:38	1228	-523.88	-150.55	1.79	-148.76
2:41	1255	-526.16	-151.20	1.87	-149.33
2:44	1283	-527.43	-151.57	1.97	-149.60
2:47	1311	-528.19	-151.79	2.05	-149.74
2:50	1338	-528.57	-151.90	2.13	-149.77
2:58	1422	-529.46	-152.15	2.40	-149.75
3:00	1450	-530.23	-152.37	2.49	-149.88
3:03	1477	-531.11	-152.63	2.58	-150.05
3:08	1594	-533.78	-153.39	2.97	-150.42
3:13	1636	-536.32	-154.12	3.12	-151.00
3:18	1686	-538.86	-154.85	3.29	-151.56
3:23	1736	-550.80	-158.28	3.47	-154.81
3:25	1766	-571.12	-164.12	3.58	-160.54
3:28	1797	-634.62	-182.37	3.69	-178.68
3:30	1830	-754.00	-216.68	3.81	-212.87
3:33	1861	-1002.92	-288.21	3.92	-284.29
3:34	1866	-1009.27	-290.03	3.93	-286.10
3:34	Power to furnace turned off.				

Notes:
(1) At this temperature the specimen indicated maximum expansion and began rapid outgasing.
(2) At this temperature the rapid outgasing of the specimen subsided.
(3) No final measurements were obtained due to specimen destruction.
(4) Temperatures measured with chromel/alumel thermocouples to 1477K and with optical pyrometer above this temperature.

TABLE 45

TOTAL NORMAL EMITTANCE OF MG-1 CHARRED AT 811 K

Spec No.	Time	Temp	Radiometer output millivolts	True temp K	Emittance
EM-1-811-10-3 Run 3908-25		Thermocouples			
	2:35	24.70 mv	0.081	868	0.85
	2:40	25.26 mv	0.086	881	0.84
	3:00	35.30 mv	0.181	1122	0.66
	3:10	35.17 mv	0.166	1119	0.66
	3:25	40.03 mv	0.220	1240	0.54
		Optical Pyrometer			
	3:25	1435°F	0.220	1095	0.88
	3:32	1445°F	0.224	1101	0.88
	3:50	2000°F	0.493	1478	0.62
EM-2-811-10-3 Run 3908-26		Optical Pyrometer			
		1730°F	0.359	1219	0.96
	4:00	2130°F	0.736	1555	0.74
	4:15	2480°F	1.208	1779	0.69
	4:15	2630°F	1.208	1932	0.52
EM-3-811-10-1 Run 3908-27		Optical Pyrometer			
	1:00	1500°F	0.182	1167	0.57
	1:30	1740°F	0.362	1299	0.75
	2:20	1935°F	0.505	1426	0.70
	2:40	2360°F	0.858	1733	0.55

TABLE 46

PERMEABILITY OF VIRGIN MG-45, SILICONE-PHENOLIC, IN PHENOLIC-GLASS HONEYCOMB
PARALLEL TO HONEYCOMB CELL, AT 297 K

Time	Permeating gas	Atmospheric pressure N/m²	Pressure drop through specimen $(P_2 - P_1)$ ΔP N/m²	Downstream gage pressure P_1 N/m²	Absolute mean specimen pressure P_m N/m²	Gas temp at flowmeter outlet K	Volumetric flow rate at atmospheric conditions Q_{STP} cm³/sec	(1) $\dfrac{P_m \Delta PM}{LRT\mu G}$ (cm⁻²)	(1) $\dfrac{G}{\mu}$ cm⁻¹
Specimen 6; A = 4.9876 cm²; L = 1.277 cm; Density = 0.2313 gm/cm³									
3:33	N₂	99.45 x 10³	13.51 x 10³	5.59 x 10³	106.73 x 10³	298	158	20.0 x 10³	209
3:34	N₂	99.45	13.51	5.59	106.73	298	158	20.0	209
3:35	N₂	99.45	27.01	7.59	113.69	298	318	21.3	421
3:36	N₂	99.45	27.01	7.59	113.69	298	318	21.3	421
3:37	N₂	99.45	40.52	11.32	120.82	298	473	22.7	626
3:38	N₂	99.45	40.52	11.32	120.82	298	473	22.7	626
3:39	N₂	99.45	54.03	16.67	128.11	298	644	23.6	853
3:40	N₂	99.45	54.03	16.67	128.11	298	645	23.6	854
4:02	He	99.45	33.68	5.97	116.93	298	370	21.2	620
4:03	He	99.45	33.68	5.97	116.93	298	370	21.2	620
4:05	He	99.45	50.65	7.34	125.51	298	600	20.6	101
4:07	He	99.45	50.65	7.34	125.51	298	600	20.6	101
4:08	He	99.45	67.54	9.08	134.13	298	850	20.8	143
4:10	He	99.45	67.54	9.08	134.13	298	850	20.8	143
4:13	He	99.45	84.42	11.90	142.84	298	1125	20.9	189
4:16	He	99.45	84.42	11.90	142.84	298	1120	21.0	188
4:18	He	99.45	101.30	15.50	151.65	298	1410	21.2	236
4:20	He	99.45	101.30	15.50	151.65	298	1410	21.2	236
4:23	He	99.45	118.20	20.00	160.54	298	1700	21.7	285
4:27	He	99.45	118.20	20.00	160.54	298	1730	21.4	290
3:22	He	98.87	16.88	2.96	107.58	291	172	20.6	288
12:49	N₂	98.69	67.47	24.00	134.80	297	832	24.0	1102
12:50	N₂	98.69	67.47	24.30	134.80	297	838	23.8	1110
12:52	N₂	98.69	80.97	33.50	142.48	297	1020	24.8	1351
12:54	N₂	98.69	80.97	33.70	142.48	297	1010	25.1	1338
12:55	N₂	98.69	87.80	39.80	146.50	297	1120	25.2	1483
12:58	N₂	98.69	87.86	40.20	146.63	297	1120	25.3	1483
Specimen 7; A = 5.0671 cm²; L = 1.2738 cm; Density = 0.2271 gm/cm³									
5:53	N₂	99.01	13.57	5.72	106.06	297	163	19.8	213
5:54	N₂	99.01	13.61	5.72	106.06	297	163	19.8	213
5:56	N₂	99.91	27.12	7.71	113.34	297	322	21.3	420
5:57	N₂	99.01	27.12	7.71	113.34	297	322	21.3	420
5:58	N₂	99.01	40.62	11.82	120.50	297	481	22.8	627
5:59	N₂	99.01	40.62	11.40	120.45	297	483	22.7	629
6:02	N₂	99.01	54.06	16.87	127.72	297	659	23.4	859
6:03	N₂	99.01	54.06	16.90	127.72	297	662	23.3	863
6:05	N₂	99.01	67.60	24.51	135.25	297	837	24.4	1091
6:06	N₂	99.01	67.57	24.41	135.23	297	840	24.3	1095
6:08	N₂	99.01	81.14	34.39	143.01	297	1022	25.4	1332
6:12	N₂	99.01	80.00	33.74	142.37	297	1018	25.0	1327
6:30	He	99.01	27.08	5.85	113.13	297	320	19.0	53
6:31	He	99.01	27.18	5.85	113.18	297	310	19.7	51
6:34	He	99.01	54.06	7.74	126.81	297	665	20.5	110
6:35	He	99.01	54.03	7.74	126.79	297	665	20.4	110
6:36	He	99.01	81.08	11.59	140.70	297	1095	20.7	181
6:37	He	99.01	81.08	11.64	140.70	297	1099	20.6	181
6:40	He	99.01	108.23	17.57	154.87	297	1555	21.4	257
6:41	He	99.01	108.16	17.59	154.84	297	1555	21.4	257

(1) $G = \dfrac{Q_{STP} \rho_{STP}}{A}$

TABLE 47

SUMMARY OF PERMEABILITY RESULTS FOR VIRGIN MG-45, SILICONE-PHENOLIC IN
PHENOLIC-GLASS HONEYCOMB, AND VIRGIN MG-58, PHENOLIC-NYLON
IN PHENOLIC-GLASS HONEYCOMB, PARALLEL TO HONEYCOMB CELL, AT 297 K

Material	Specimen	Density gm/cm^3	β, inertial flow coefficient cm^{-1}	α, viscous flow coefficient cm^{-2}	$K = \dfrac{1}{\alpha}$ Darcy's constant cm^2
MG-45	6	0.231	3300	20.5×10^6	4.9×10^{-8}
MG-45	7	0.227	3900	20.0×10^6	5.0×10^{-8}
MG-58	6	0.230	2200	11.5×10^6	8.7×10^{-8}
MG-58	7	0.225	2200	10.9×10^6	9.2×10^{-8}

Note: 1 darcy = $0.987 \times 10^{-8} cm^2$

128

TABLE 48

PERMEABILITY OF VIRGIN MG-58, PHENOLIC-NYLON IN PHENOLIC-GLASS HONEYCOMB, PARALLEL TO HONEYCOMB CELL, AT 297 K

Time	Permeating gas	Atmospheric pressure N/m²	Pressure drop through spec $(P_2 - P_1)$ ΔP N/m²	Downstream gage pressure P_1 N/m²	Absolute mean specimen pressure P_m N/m²	Gas temp at flowmeter outlet K	Volumetric flow rate at atmospheric conditions Q_{STP} cm³/sec	(1) $\dfrac{P_m \Delta P M}{LRT\mu G}$ cm⁻²	(1) $\dfrac{G}{\mu}$ cm⁻¹
Specimen 7; A = 4.9784 cm²; L = 1.2677 cm; Density = 0.2247 gm/cm³									
10:15	N₂	101.91x10³	13.51 x 10³	7.22 x 10²	109.38 x 10³	297	284	11.7 x 10⁶	370
10:17	N₂	101.91	27.01	14.18	116.83	297	563	12.6	734
10:21	N₂	101.91	40.52	25.63	124.70	297	855	13.3	1115
10:24	N₂	101.91	54.03	42.80	133.20	297	1132	14.3	1476
11:04	He	101.94	13.51	5.72	109.41	297	280	10.5	46
11:06	He	101.94	27.01	7.22	116.86	297	560	11.2	92
11:07	He	101.94	40.52	9.70	124.70	295	900	11.2	149
11:09	He	101.94	54.03	13.19	133.20	296	1244	11.5	205
11:14	He	101.94	67.54	17.92	137.50	296	1620	11.4	268
11:15	He	101.94	81.04	24.51	144.90	297	2010	11.6	332
11:16	He	101.94	94.55	32.72	152.49	297	2445	11.8	404
11:21	He	101.94	108.06	43.17	160.29	297	2910	11.9	480
3:00	He	99.95	13.51	6.59	107.32	296	250	11.6	41
3:03	He	99.95	13.51	6.59	107.32	296	250	11.6	41
3:38	He	99.95	13.51	4.23	107.13	296	244	11.8	40
Specimen 6; A = 5.027 cm²; L = 1.27 cm; Density = 0.2297 gm/cm³									
11:52	He	99.48	6.75	1.99	103.05	295	118	11.7	20
11:58	He	99.48	6.75	1.99	103.05	295	118	11.7	20
12:06	He	99.48	27.01	6.84	113.21	296	525	11.5	87
12:08	He	99.48	27.01	6.84	113.21	296	525	11.5	87
12:15	He	99.48	47.27	10.57	124.16	296	980	11.8	163
12:16	He	99.48	47.27	10.57	124.16	296	980	11.8	163
12:18	He	99.48	67.54	17.17	134.97	296	1505	12.0	250
12:19	He	99.48	67.54	17.42	134.97	296	1510	11.9	251
12:32	N₂	99.48	13.51	2.11	107.21	297	260	12.4	342
12:36	N₂	99.48	13.51	2.11	107.21	297	260	12.4	342
12:38	N₂	99.48	27.01	12.94	114.26	297	525	13.1	690
12:39	N₂	99.48	27.01	12.94	114.26	297	525	13.1	690
12:40	N₂	99.48	40.52	22.77	122.00	297	795	13.8	1045
12:42	N₂	99.48	40.52	22.77	122.00	297	805	13.7	1058
12:45	N₂	99.48	54.03	38.83	130.37	297	1087	14.4	1428
2:14	N₂	99.45	54.03	38.57	130.31	298	1055	14.8	1386

(1) $G = \dfrac{Q_{STP}\,\rho_{STP}}{A}$

129

TABLE 49

PERMEABILITY OF MG-1, SILICONE-PHENOLIC, CHARRED AT 811 K

Specimen 811-10-4, No. 1; A = 1.986 cm²; L = 1.712 cm; Density = 0.179 gm/cm³

Time	Permeating gas	Atmospheric pressure N/m²	Pressure drop through specimen ΔP N/m²	Downstream gage pressure Pi N/m²	Absolute mean specimen pressure Pm N/m²	Gas temp at flowmeter outlet K	Volumetric flow rate at atmospheric conditions Qstp cm³/sec	(2) $\frac{P_m \Delta PM}{LRT_uG}$ cm⁻²	(2) $\frac{G}{u}$ cm⁻¹	Flowmeter
9:42	He	99.48 × 10³	40.52 × 10³	5.7 × 10² (1)	120.31 × 10³	298	200	14.1 × 10⁶	84	FP-1/2-21 -G-10
10:00		99.55	47.28	10.9 (1)	124.28	299	240	14.2	101	
10:04		99.55	54.03	9.5 (1)	127.51	299	280	14.2	118	
10:08		99.55	60.78	6.0 (1)	130.53	299	310	14.8	131	
10:14		99.55	67.54	6.2	133.91	299	350	15.0	147	
10:16		99.55	74.29	6.3	137.30	299	415	14.2	175	
10:18		99.55	81.04	6.3	140.70	299	425	15.5	179	
10:19		99.55	87.80	6.5	144.09	299	455	16.1	192	
10:21		99.55	94.55	6.7	147.49	299	505	16.0	213	
10:23		99.55	101.30	7.0	150.89	299	540	16.4	227	
10:26		99.55	108.23	7.3	154.39	299	570	17.0	240	
10:33		99.55	115.08	7.6	157.85	299	615	17.1	259	
10:40		99.55	121.90	8.0	161.29	299	655	17.4	276	
12:53		99.52	6.75	1.1	103.00	299	33	12.2	139	FP-1/4-20 -G-5
12:57		99.52	13.51	1.1	106.38	299	61	13.6	26	
12:58		99.52	20.26	1.1	109.76	299	93	13.9	39	
12:59		99.52	27.01	1.2	113.15	299	124	14.3	52	
1:00		99.41	33.77	1.4	116.44	299	156	14.6	66	
1:01		99.41	40.52	1.7	119.85	299	191	14.7	80	
1:03		99.41	47.28	2.2	123.28	299	227	14.9	96	
1:04		99.41	54.03	2.5	126.68	299	269	14.7	113	
1:05		99.41	60.78	3.0	130.11	299	308	14.9	130	
10:47	N2	99.55	20.26	5.7	110.25	299	105	13.9	349	FP-1/2-21 -G-10
10:49		99.55	27.01	5.7	113.63	299	133	15.0	442	
10:51		99.55	33.76	5.9	117.02	299	158	16.3	525	
10:52		99.55	40.52	6.0	120.41	299	186	17.1	618	
10:54		99.55	47.34	6.3	123.85	299	215	17.8	714	
10:56		99.55	54.03	6.6	127.22	299	240	18.7	798	
10:38		99.11	60.78	7.4	130.24	299	283	18.23	941	
10:40		99.11	67.54	7.8	133.66	299	313	18.80	1041	
10:41		99.11	74.29	8.4	137.11	299	329	20.18	1094	
10:42		99.11	81.05	9.0	140.55	299	367	20.23	1221	
10:43		99.11	87.80	9.7	143.99	299	397	20.76	1321	
10:45		99.11	94.55	10.2	147.41	299	425	21.38	1414	
10:46		99.11	101.31	10.8	150.85	299	442	22.54	1470	
10:47		99.11	108.06	11.6	154.29	299	472	23.03	1570	
10:49		99.11	114.88	12.3	157.77	299	509	23.21	1693	
10:52		99.11	121.74	13.3	161.30	299	540	23.71	1796	
12:27		99.52	6.75	1.0	103.00	299	31	14.6	103	FP-1/4-20 -G-5
12:29		99.52	13.51	1.2	106.39	299	61	15.4	203	
12:43		99.52	20.26	1.9	109.83	299	91	15.9	302	
12:44		99.52	27.01	2.6	113.28	299	122	16.4	405	
12:46		99.52	33.77	3.5	116.75	299	147	17.5	488	

Notes:

1. Used valve downstream of flowmeter.
2. $G = \frac{Q_{stp}\rho_{stp}}{A}$

TABLE 50

PERMEABILITY OF MG-1, SILICONE-PHENOLIC, CHARRED AT 811 K

Specimen 811-10-4, No. 2; A = 1.988 cm²; L = 1.691 cm; Density = 0.182 gm/cm³

Time	Permeating gas	Atmospheric pressure N/m² ($\times 10^3$)	Pressure drop through specimen ΔP N/m² ($\times 10^3$)	Downstream gage pressure P_i N/m² ($\times 10^2$)	Absolute mean specimen pressure P_m N/m² ($\times 10^3$)	Gas temp at flowmeter outlet K	Volumetric flow rate at atmospheric conditions Q_{stp} cm³/sec	$\dfrac{P_m \Delta P M}{LRT \mu G}$ cm⁻² (1)	$\dfrac{G}{\mu}$ cm⁻¹ (1)	Flowmeter
5:41	He	99.18	6.75	1.1	102.67	300	30	13.6 $\times 10^6$	13	1/4-20-G-5
5:44		99.18	13.51	1.1	106.05	300	60	14.1	25	
5:45		99.18	20.26	1.1	109.42	300	91	14.3	38	
5:47		99.18	27.02	1.1	112.80	300	120	14.9	51	
5:48		99.18	33.77	1.4	116.20	300	157	14.7	66	
5:49		99.18	40.52	1.7	119.61	300	188	14.0	79	
6:57		99.15	40.52	13.1	120.72	300	205	14.0	86	
7:01		99.16	47.28	14.6	124.27	300	247	15.0	104	
7:02		99.16	54.03	17.4	127.96	300	270	15.3	114	
7:04		99.16	60.78	8.0	130.38	300	304	15.1	128	
7:05		99.16	67.54	6.3	133.59	300	350	15.3	147	
7:07		99.16	74.29	6.1	136.94	300	390	15.9	164	
7:08		99.16	81.05	6.3	140.35	300	420	15.9	177	
7:10		99.16	87.80	6.2	143.69	300	465	16.0	196	
7:12		99.16	94.59	6.9	147.15	300	510	15.8	215	
7:13		99.16	101.31	7.2	150.55	300	565	16.3	238	
7:14		99.16	108.23	7.5	154.04	300	600	16.2	252	
7:15		99.16	115.05	7.7	157.49	300	655	16.2	275	
7:17		99.16	121.91	8.9	161.02	300	710	15.0	299	
5:52	N_2	99.18	6.75	1.1	102.67	300	101	15.5	101	1/2-21-G-10
5:57		99.18	13.51	1.2	106.06	300	203	16.0	203	
5:58		99.18	20.26	1.6	109.47	300	304	16.0	304	
6:03		99.15	20.26	5.7	109.85	300	105	14.0	349	
6:06		99.15	27.02	5.7	113.22	300	145	13.9	482	
6:08		99.15	33.77	5.8	116.61	300	165	15.8	548	1/4-20-G-5
6:10		99.15	40.52	6.0	120.01	300	187	17.2	621	
6:12		99.15	47.28	6.3	123.42	300	218	17.7	724	
6:15		99.15	54.03	6.7	126.83	300	248	18.3	824	
6:17		99.15	60.78	7.1	130.25	300	281	18.6	934	
6:18		99.15	67.54	7.5	133.66	300	313	19.1	1040	
6:19		99.15	74.29	7.6	137.05	300	340	19.8	1130	
6:21		99.15	81.05	8.6	140.53	300	367	20.5	1219	
6:23		99.15	87.80	9.4	143.98	300	400	20.9	1329	
6:25		99.15	94.55	10.0	147.42	300	437	21.1	1452	
6:26		99.15	101.31	10.9	150.89	300	461	21.9	1532	
6:30		99.15	108.06	11.8	154.35	300	498	22.1	1655	
6:31		99.15	115.15	12.7	157.99	300	530	22.7	1761	
6:34		99.15	121.91	13.5	161.45	300	560	23.2	1860	

Note:

1. $G = \dfrac{Q_{stp}\rho_{stp}}{A}$

TABLE 51

BULK DENSITY OF VIRGIN MG-1, SILICONE-PHENOLIC

Specimen	Bulk density gm/cm^3
(Specimens for ASTM C177 guarded hot plate apparatus)	
Specimen 1 Disc 1	0.584
Disc 4	0.602
Specimen 2 Disc 2	0.598
Disc 3	0.604
Specimen 5 (thermal expansion)	0.608
Specimen 6 (thermal expansion)	0.600

TABLE 52

BULK DENSITY OF VIRGIN MG-45, SILICONE-
PHENOLIC IN PHENOLIC-GLASS HONEYCOMB

Specimen	Bulk density gm/cm^3
(Specimens for ASTM C177 guarded hot plate apparatus)	
Specimen 1 Disc 1 Disc 2	0.207 0.217
Specimen 2 Disc 3 Disc 4	0.213 0.206
Specimen 3 Disc 8 Disc 10	0.228 0.244
Specimen 4 Disc 9 Disc 11	0.228 0.218
Specimen 6 (permeability)	0.231
Specimen 7 (permeability)	0.227

133

TABLE 53

BULK DENSITY OF VIRGIN MG-58, PHENOLIC-NYLON IN
PHENOLIC-GLASS HONEYCOMB

Specimen	Bulk density gm/cm^3
(Specimens for ASTM C177 guarded hot plate apparatus)	
Specimen 1 Disc 1	0.238
Disc 2	0.226
Specimen 2 Disc 3	0.224
Disc 4	0.239
Specimen 6 (permeability)	0.230
Specimen 7 (permeability)	0.225

134

TABLE 54

SUMMARY OF BULK DENSITY MEASUREMENTS ON MG-1, SILICONE-PHENOLIC CHARRED IN FURNACE (MEASURED AT 298 K)

Specimen	Charring temp K	Bulk density gm/cm^3	Apparatus used for evaluations
811-10-4	811	0.156	Radial inflow
811-10-6	811	0.168	Radial inflow
	Average =	0.162	
1000-10-A3	1000	0.198	ASTM C177
1000-10-A4	1000	0.203	ASTM C177
1000-10-A11	1000	0.187	ASTM C177
1000-10-A12	1000	0.201	ASTM C177
1000-10-R13	1000	0.189	Radial inflow
1000-10-6	1000	0.171	Radial inflow
	Average =	0.192	
1500-10-A1	1500	0.200	ASTM C177
1500-10-A2	1500	0.206	ASTM C177
1500-10-A9	1500	0.189	ASTM C177
1500-10-10	1500	0.189	ASTM C177
1500-10-R16	1500	0.180	Radial inflow
1500-10-R19	1500	0.181	Radial inflow
	Average =	0.191	
1644-10-A7	1644	0.180	ASTM C177
1644-10-A8	1644	0.180	ASTM C177
1644-10-A13	1644	0.158	ASTM C177
1644-10-A14	1644	0.167	ASTM C177
1644-10-5	1644	0.178	Radial inflow
1644-10-6	1644	0.177	Radial inflow
	Average =	0.173	

TABLE 55

SUMMARY OF BULK DENSITY MEASUREMENTS ON CHARS OF MG-45
AND MG-58 PREPARED IN NASA ARC-JET (MEASURED AT 298 K)

Material and Disc No.	Note on box	Charring time sec	Bulk density gm/cm^3
Values of gross char (filler and honeycomb)			
MG-45-S2	---	110	0.154
MG-45-S3	---	110	0.196
MG-45-U1	---	110	0.145
		Average =	0.165
MG-58-M2	0.8	150	0.138
MG-58-N2	0.8	150	0.146
MG-58-S2	0.8	150	0.138
		Average =	0.141
Values for filler only			
MG-58-Q3	1.5	150	0.160
MG-58-Q3	1.5	150	0.159
MG-58-T4	0.8	150	0.368
MG-58-T4	0.8	150	0.340
		Average =	0.257

136

TABLE 56

SUMMARY OF "TRUE" DENSITY MEASUREMENTS
ON VIRGIN MG-1, MG-45 AND MG-58

| Material | "True" density-gm/cm^3 | | | Remarks |
	Liquid pycnometer	Helium pycnometer by NASA Langley	Calculated	
MG-1	1.05[1] 1.11[2]	1.19	1.14	Material contains 19% microballoons and 8% silica eccospheres
MG-45	0.98[1]	-	1.24	Material contains 78% microballoons
MG-58	0.99[1] 1.20[3]	-	1.26	Material contains 60% microballoons

Notes:

1. Water as pycnometer fluid with Tergitol TNN
   wetting agent
2. Ethanol as pycnometer fluid. Light fraction
   separated from sample by flotation
3. Specimen pulverized in liquid nitrogen

TABLE 57

CALCULATED TRUE DENSITIES OF VIRGIN MG-1,
MG-45 AND MG-58

A. True densities of constituents (from NASA Langley)

   Silicone elastomer (RTV 602) — 1 gm/cm^3
   phenolic (cured)   — 1.28 gm/cm^3
   nylon   — 1.1 gm/cm^3
   quartz   — 2.08 gm/cm^3
   dimethyl oil   — 1 gm/cm^3

B. Calculation of true density (see Table 1 for percentages)

   MG-1

$$\frac{1}{\frac{0.60}{1.00} + \frac{0.19}{1.28} + \frac{0.16}{2.08} + \frac{0.05}{1}} = 1.14$$

   MG-45

$$\frac{1}{\frac{0.18}{1} + \frac{0.78}{1.28} + \frac{0.04}{2.08}} = 1.24$$

   MG-58

$$\frac{1}{\frac{0.90}{1.28} + \frac{0.10}{1.1}} = 1.26$$

C. Porosity calculations

Material	Calculated true density gm/cm^3	Measured "true" density gm/cm^3	Measured bulk density gm/cm^3	Calculated porosity %	Porosity from quantitative microscopy %
MG-1	1.14	1.15	.584/.608	47/49	--
MG-45	1.24	0.98	.206/.244	80/85	97
MG-58	1.26	1.20	.224/.239	81/82	85

138

TABLE 58

SUMMARY OF "TRUE" AND APPARENT DENSITY MEASUREMENTS
ON CHARS OF MG-1, MG-45 AND MG-58

Material number	Char disc number	Charring time sec	"True" density on pulverized material gm/cm³ Helium pycnometer	"True" density on pulverized material gm/cm³ Liquid pycnometer	Apparent density on bulk material with helium pycnometer gm/cm³	Average density gm/cm³	Remarks
MG-1 (furnace char)	-- -- -- -- --	1800 1800 1800		2.07 1.63		1.85	1000 K char 1644 K char
MG-45 (arc-jet char)	G1 U2	150 110		2.24 2.17		2.21	honeycomb honeycomb
	G1 U2 O1 O1	150 110	1.67 1.68	1.54 1.15		1.51	filler filler filler filler
	P1 P1				0.77 0.74	0.76	filler filler
MG-58 (arc-jet char)	Q3 T4	150 150		1.98 1.73		1.86	honeycomb honeycomb
	Q3 T4 K4 K4	150 150	1.60 1.62	1.52 1.23		1.47	filler filler filler filler
	U2 U2				0.59 0.60	0.60	filler filler

Notes for measurements with liquid pycnometer:

1. ASTM Procedure C-135-66 used for measurements. Ethanol used as pycnometer fluid.
2. All samples ground to pass 325 mesh screen (44 microns) prior to measurements.
3. All samples ground to a black powder except MG-58, T4, which was gray.
4. All samples contained some material which was less dense than ethanol as well as denser material. Sample MG-58, T4, had the least of this less dense material.

139

TABLE 59

SUMMARY OF INFORMATION ON TRUE DENSITY,
BULK DENSITY AND POROSITY FOR MG-1, MG-45 AND MG-58

Material	(1) Calculated true density (gm/cm^3)	(2) Measured "true" density (gm/cm^3)	(3) Measured bulk density (gm/cm^3)	Calculated porosity (%)	Total porosity from quantitative microscopy (%)
Virgin MG-1	1.14	1.17	0.584/0.608	47/49[1]	-
Virgin MG-45	1.24	0.98	0.206/0.244	80/85[1]	97
Virgin MG-58	1.26	0.99	0.224/0.239	81/82[1]	85
Charred MG-1	1.87	1.85	0.162/0.192	90/91[1]	85
Charred MG-45	-	1.51[3]	0.145/0.196	87/90[2]	90
Charred MG-58	-	1.47[3]	0.138/0.146	90/91[2]	85

Notes:

1. Based on (1) and (3)
2. Based on (2) and (3)
3. True density values used for charred MG-45 and MG-58 are for filler only and bulk density values are for honeycomb and filler.

140

TABLE 60

BULK DENSITY FOR MG-1 MATERIAL

Spec No.	Bulk Density gm/cm^3	Spec No.	Bulk Density gm/cm^3	Spec No.	Bulk Density gm/cm^3
C1a	.6077	C31a	.6063	T26a	.6057
C2a	.6095	C32a	.6073	T27a	.6100
C3a	.5971	C33a	.5988	T28a	.6095
				T29a	.6060
C4a	.6026	C34a	.6047	T30a	.5905
C5a	.6036	C35a	.6042		
C6a	.5923	C36a	.5946	T31a	.6059
				T32a	.6082
C7a	.5990	T1a	.6084	T33a	.6084
C8a	.6009	T2a	.6108	T34a	.6066
C9a	.5902	T3a	.6114	T35a	.5918
		T4a	.6068		
C10a	.6038	T5a	.5896		
C11a	.6071				
C12a	.5931	T6a	.6051		
		T7a	.6086		
C13a	.6068	T8a	.6097		
C14a	.6095	T9a	.6039		
C15a	.5976	T10a	.5925		
				Note: Specimens	
C16a	.6057	T11a	.6042	are arranged in	
C17a	.6121	T12a	.6078	each grouping in	
C18a	.5930	T13a	.6084	accordance with	
		T14a	.6067	their "c" direction	
C19a	.6001	T15a	.5863	location in the	
C20a	.6031			billet. The first	
C21a	.5906	T16a	.6061	specimen listed in	
		T17a	.6107	each group was at	
C22a	.6046	T18a	.6114	the top of the	
C23a	.6080	T19a	.6086	billet.	
C24a	.5975	T20a	.5938		
C25a	.6031	T21a	.6072		
C26a	.6062	T22a	.6090		
C27a	.5918	T23a	.6104		
		T24a	.6091		
C28a	.6053	T25a	.5897		
C29a	.6071				
C30a	.5955				

141

TABLE 61

TENSILE DATA FOR MG-1 MATERIAL

Determinations and Loading	Temp K	Loading Rate 10⁻³N/m²/sec	Specimen Number	Bulk density gm/cm³	Ultimate[1] strength 10⁸N/m²	Initial[1] elastic modulus 10⁸N/m²	Total unit axial strain 10⁻³cm/cm	Sonic[2] velocity "b" direction cm/µsec	Failure location	Remarks
Tensile a	500	172	MG-1-1B-T8a4	.6097	.192	.0099	26.3	.1139	lower yoke	outgassing 372 F .071" strain during heating
			MG-1-1B-T18a4	.6114	.192	.0099	25.8	.1152	lower yoke	outgassing 372 F .073" strain during heating
			MG-1-1B-T19a4	.6086	.185	.0120	---	.1096	lower yoke	failed from weight of load train upon reaching 500 K
			MG-1-1B-T30a4	.5905	.185	---	23.1	.1101	upper yoke	outgassing 372 F .076" strain during heating
			Average	.6050	.190	.0109	25.1	.1122		
	450	172	MG-1-1B-T14a4	.6067	.112	.0070	20.0	.1146	upper yoke	.072" strain during heating
			MG-1-1B-T16a4	.6061	.152	.0108	18.7	.1101	gage	.066" strain during heating
			MG-1-1B-P26a4	.6057	.126	.0074	22.3	.1140	upper yoke	.061" strain during heating
			Average	.6062	.130	.0084	20.3	.1129		
	400	172	MG-1-1B-T13a4	.6084	.132	.0134	18.8	.1077	upper yoke	.032" strain during heating
			MG-1-1B-T21a4	.6072	.145	.0098	22.5	.1101	gage	.034" strain during heating
			MG-1-1B-T35a4	.5918	.159	.0104	23.0	.1002	tangent	.033" strain during heating
			Average	.6025	.145	.0112	21.4	.1060		
	350	172	MG-1-1B-T15a4	.5863	.211	.0238	16.1	.1109	gage	.015" strain during heating
			MG-1-1B-T22a4	.6090	.186	.0238	13.2	.1100	upper yoke	
			MG-1-1B-T34a4	.6066	.138	.0262	9.5	.0985	upper yoke	
			Average	.6006	.178	.0246	12.9	.1065		
	300	172	MG-1-1B-T12a4	.6078	.185	.0424	9.6	.1100	lower yoke	
			MG-1-1B-T24a4	.6091	.227	.0476	8.1	.1091	lower yoke	
			MG-1-1B-T32a4	.6082	.260	.0645	8.6	.0998	gage	
			Average	.6084	.224	.0515	8.8	.1063		
	250	172	MG-1-1B-T9a4	.6039	---	---	---	---		broken in handling
			MG-1-1B-T17a4	.6107	.216	.0805	7.7	.1022	upper yoke	
			MG-1-1B-T28a4	.6095	.250	.0799	8.8	.1011	gage	
			MG-1-1B-T29a4	.6060	.281	.0529	13.9	.1130	upper yoke	
			Average	.6075	.249	.0711	10.1	.1054		
	200	172	MG-1-1B-T11a4	.6042	3.200	.604	10.9	.1103	gage	broken in handling — re-loaded
			MG-1-1B-T23a4	.6104	2.970	.572	6.2	.1072	lower yoke	slipped in grip - re-loaded
			MG-1-1B-T25a4	.5897	1.560	.624	---	.1120	upper grip	failed in upper grip strength not included in average
			MG-1-1B-T27a4	.6100				.1110		
			Average	.6024	3.085	.600	8.5	.1101		
	150	172	MG-1-1B-T6a4	.6051	8.960	---	---	.1160	gage	broken in handling re-loaded
			MG-1-1B-T20a4	.5938	4.500	.957	8.5	.1088	lower yoke	<2.2 kgm preload applied at 200 K σ_a & ε_a not included in average
			MG-1-1B-T33a4	.6059	4.500	1.470	4.8	.1114	lower yoke	<4.5 kgm preload applied at 200 K σ_a & ε_a not included in average
			MG-1-1A-T36a4	.6084	2.330	1.300	1.6	.1017		broken in handling reloaded
			MG-1-1A-T37a4	.6182	5.860	1.150	7.9	---	tangent	
			Average	.6063	7.910	1.219	8.2	.1095		

Notes:

1. Strength values corrected by +.018 x 10⁸N/m² for stress induced by extensometers.

2. Velocity measurement made in the center of the gage section.

142

TABLE 62

TENSILE DATA FOR MG-45 MATERIAL

Determination and Loading	Temp K	Loading Rate $10^3 N/m^2/sec$	Specimen Number	Bulk density gm/cm^3	Ultimate[2] strength $10^6 N/m^2$	Initial elastic modulus $10^6 N/m^2$	Total unit axial strain 10^{-3} cm/cm	.2% Yield strength $10^6 N/m^2$
Tensile a	300	172	MG-45-2-T1a1[1]	.2308	.404	57.3	12.5	.333
			MG-45-3-T2a1	.2308	.437	34.3	23.1	.267
			MG-45-5-T4a1	.2298	.446	48.9	11.5	.426
			MG-45-3-T5a1	.2300	.489	27.4	26.4	.314
			Average	.2303	.444	41.9	18.4	.333
Tensile b	300	172	MG-45-2-T10b1	.2250	.098	12.5	6.7	----
			MG-45-3-T11b1	.2346	.072	9.6	5.5	----
			MG-45-4-T12b1	.2423	.073	11.3	6.6	----
			MG-45-5-T13b1	.2332	.158	21.6	7.3	----
			Average	.2338	.100	13.8	6.5	----

Notes:
1. 12.2 cm radius at end of gage section
2. Strength values corrected by +.018 x $10^6 N/m^2$ for stress induced by extensometers

TABLE 63

TENSILE DATA FOR MG-58 MATERIAL

Loading direction	Temp K	Stress rate 10³N/m²/sec	Specimen Number	Gage sect area cm²	Bulk Density B.D.¹ gm/cm³	A.D.¹ gm/cm³	Ultimate strength 10⁶N/m	Initial elastic modulus 10⁶N/m	Total unit axial strain 10⁻³cm/cm	Failure location
Tensile a	294	172	MG-58-5-T1a1	3.63	.2150	.2075	.550	84	7.5	Gage
		172	MG-58-5-T5a1		.2152	.2068	.585	80	8.6	Tangent
		172	MG-58-2-T9a1		.2144	.2067	.447	72	7.4	Gage
			Average		.2149	.2070	.527	79	7.8	
		172	MG-58-5-T3a2	6.45	.2217	.2136	.826	128	6.4	Radius
		172	MG-58-5-T4a2		.2240	.2159	.888	146	7.1	Gage
		172	MG-58-2-T7a2		.2148	.2076	.524	Not Obtained		Gage
			Average		.2202	.2124	.746	137	6.8	
		172	MG-58-5-T2a3	10.09	.2122	.2047	.295	88	5.8	Gage
		172	MG-58-5-T6a3		.2265	.2184	.550	155	7.5	Tangent
		172	MG-58-2-T8a3		.2152²	.2078²	.482	72	7.3	Gage
			Average		.2180	.2103	.509	105	6.9	
			Overall Average		.2177	.2099	.594	103	7.2	
Tensile a	294	172	MG-58-2-T10a1³	3.63	.2174	—	.426ᵇ	97	4.3	
Tensile b	294	172	MG-58-3-T30b1	3.63	.2303	.2226	.245	45	7.4	Gage
		172	MG-58-3-T34b1		.2172	.2101	.289	40	12.1	Gage
		172	MG-48-4-T38b1		.2329	.2252	.275	38	7.2	Radius
			Average		.2268	.2193	.270	41	8.9	
		172	MG-58-3-T32b2	6.45	.2356	.2278	.365	44	5.7	Tangent
		172	MG-58-3-T33b2		.2247	.2172	.248	39	5.7	Tangent
		—	MG-58-4-T36b2		.2199	.2127	Not Run			
			Average		.2267	.2192	.307	42	5.7	
		172	MG-58-3-T31b3	10.09	.2263	.2192	.269	39	3.5	Tangent
		172	MG-58-3-T35b3		.2213	.2141	Not Run			
		172	MG-58-4-T37b3		.2233	.2164	.275	38	3.6	Tangent
			Average		.2236	.2166	.272	38.5	3.5	
			Overall Average		.2257	.2184	.281	40	6.5	
Tensile b	294	172	MG-38-4-T39b1³	3.63	.2217	—	.292ᵇ	54	5.1	Tangent

Notes:

1. BD - before drying; AD - after drying
2. Small amount of material missing from the end of this specimen
3. Undried specimen
4. Strength value corrected by +.018 x 10⁶ N/m² for stress induced by extensometers

144

TABLE 64

COMPRESSIVE DATA FOR MG-1 MATERIAL

Determination and loading direction	Temp K	Loading rate 10³ N/m²/sec	Specimen Number	Bulk density gm/cm³	Ultimate strength 10⁶ N/m²	Initial elastic modulus 10⁹ N/m²	Total unit axial strain 10⁻³ cm/cm	Sonic velocity "b" direction cm/µsec	Remarks
Compressive a	500	172	MG-1-1B-C11a	.6071	.610	.0114	79.4	.0868	Specimen slipped in loading fixture. Values not included in average.
			MG-1-1B-C18a	.5930	.557	.0191	58.4	.0874	
			MG-1-1B-C22a	.6046	.599	.0156	69.4	.0874	
			MG-1-1B-C25a	.6031	.525	.0140	55.0	.0780	
			Average						
	450	172	MG-1-1B-C10a	.6019	.560	.0162	60.9	.0849	Specimen slipped in loading fixture. Values not included in average.
			MG-1-1B-C17a	.6038	.466	.0087	72.0	.0871	
			MG-1-1B-C27a	.6121	.396	.0168	52.6	.0984	
			MG-1-1B-C32a	.5918	.418	.0156	55.4	.0908	
			MG-1-1B-C33a	.6073	.400	---	---	.0861	Stress-strain not obtained. Recorder malfunction.
			Average	.5988	.414	.0208	48.0	.0775	
	400	172	MG-1-1B-C 9a	.6028	.407	.0177	52.0	.0860	
		172	MG-1-1B-C12a	.5902	.386	.0179	52.2	.0866	
		>172	MG-1-1B-C11a	.5931	.382	.0209	51.4	.0945	High stress rate
		172	MG-1-1B-C20a	.6068	.438	.0196	43.8	.0942	Stress-strain not obtained. Recorder malfunction.
			Average	.6031	.358	---	---	.0686	
	350	172	MG-1-1B-C 8a	.5983	.391	.0195	49.1	.0860	
			MG-1-1B-C15a	.6009	.442	.0131	62.8	.0675	
			MG-1-1B-C19a	.5976	.501	.0469	37.8	.0900	
			Average	.6001	.442	.0270	48.2	.0715	
	300	172	MG-1-1B-C 7a	.5995	.462	.0290	49.6	.0763	
			MG-1-1B-C14a	.5990	.621	.0297	48.0	.0726	
			MG-1-1B-C21a	.6095	.631	.0308	46.4	.0965	
			Average	.5906	.593	.0322	45.6	.0861	
	250	172	MG-1-1B-C 6a	.5997	.615	.0309	46.7	.0851	
			MG-1-1B-C29a	.5923	.988	.0403	71.0	.0945	
			MG-1-1B-C34a	.6071	.988	.0517	53.0	.0864	
			Average	.6047	.935	.0634	46.0	.0777	
	200	172	MG-1-1B-C 5a	.6014	.988	.0460	62.0	.0862	Failed in foot. Values not included in averages
			MG-1-1B-C23a	.6036	2.95	.374	51.7	.0812	Failed in foot. Values not included in average
			MG-1-1B-C26a	.6080	7.22	.592	36.2	.0854	
			MG-1-1B-C28a	.6062	6.42	.535	31.7	.0861	
			MG-1-1B-C31a	.6053	5.35	.516	51.3	.0851	
			MG-1-1B-C36a	.6063	7.66	.526	33.2	.0955	Failed in foot. Values not included in average
			Average	.5946	2.99	.450	41.7	.0765	
	150	172	MG-1-1B-C 4a	.6040	7.10	.551	33.7	.0850	Failed in foot. Values not included in average
			MG-1-1B-C30a	.6026	35.2	1.140	36.8	.0853	
			MG-1-1B-C35a	.5955	38.6	1.390	36.4	.0865	
			MG-1-1B-C	.6042	31.8	1.360	43.5	.0760	
			Average	.6008	35.2	1.30	38.9	.0826	

TABLE 65

COMPRESSIVE DATA FOR MG-45 MATERIAL

Determination and loading direction	Temp K	Loading rate 10^3 N/m²/sec	Specimen Number	Bulk density	Ultimate strength[1] 10^6 N/m²	.05% Yield strength[3] 10^6 N/m²	0.2% Yield strength 10^6 N/m²	Initial elastic modulus 10^6 N/m²	Axial strain at ultimate strength 10^{-3} cm/cm
Compressive a	300	172	MG-45-2-C 1a2	.2213	.343	.280	.286	34.7	56.6
			MG-45-3-C 2a2	.2198[1]	.219	.128	.150	20.5	83.3
			MG-45-4-C 5a2	.2337	.254	.086	.095	15.5	71.8
			MG-45-2-C 6a2	.2214	.306	.276	.284	28.1	62.0
			Average	.2240	.280	.192	.204	24.7	68.9
Compressive a	300	172	MG-45-2-C 7a2	.2177	.340	---	.277	51.7	41.0
			MG-45-2-C 8a2	.2163	.286	---	.243	43.6	26.1
			Average	.2170	.313	---	.260	47.6	33.5
Compressive b	300	172	MG-45-2-C10b2	.2093	.312	.088	.116	7.0	133
			MG-45-3-C11b2	.2179	.305	.131	.153	12.0	157
			MG-45-5-C12b2	.2101	.247	.094	.238	9.3	173
			Average	.2187	.288	.104	.132	9.4	154
Compressive b	300	172	MG-45-2-C14b2	.2151	---	---	.237	11.3	---
			MG-45-2-C15b2	.215	---	---	.258	13.5	---
			Average	.2183	---	---	.247	12.4	---

Notes: 1.   Small amount of material missing from this specimen
         2.   Compressive block
         3.   .05% Yield strength included to permit comparison with MG-58

146

TABLE 66

COMPRESSIVE DATA FOR MG-58 MATERIAL

Loading and direction	Temp K	Stress rate 10³N/m²/sec	Specimen Number	Gage sect Area cm²	Bulk Density B.D.[1] gm/cm³	Bulk Density A.D.[1] gm/cm³	Ultimate strength 10⁸N/m²	.05% Yield strength 10⁸N/m²	Initial elastic modulus 10⁶N/m²	Total unit axial strain 10⁻³cm/cm
Compressive a	294	1375	MG-58-5-C5a1	1.61	.2310	.2246	.860	.755	79	14.1
		172	MG-58-5-C6a1		.2388[2]	.2321[2]	1.170	.825	172	9.2
		172	MG-58-5-C7a1		.2423	.2353	1.000	.825	162	8.4
			Average		.2374	.2307	1.010	.802	138	10.6
		172	MG-58-5-C2a2	3.63	.2180	.2115	.620	.550	90	8.8
		172	MG-58-5-C4a2		.2325[2]	.2255[2]	1.070	.755	191	6.5
		668	MG-58-2-C9a2		.2073	.2014	.300	.300	37	7.5
		172	MG-58-2-C12a2		.2502	.2454	1.490	.895	168	10.8
		172	MG-58-2-C13a2		.2361	.2316	1.030	.620	122	10.9
			Average		.2288	.2231	.902	.624	122	8.9
		334	MG-58-5-C1a3	6.45	.2284	.2014	Not obtained			
			MG-58-5-C3a3		.2181	.2116	.585	.550	67	9.8
			MG-58-5-C8a3		.2470	.2398	Not obtained			
		172	MG-58-2-C10a3		.2451	.2408	Broken in machining			
			MG-58-2-C11a3		.2337	.2293	.895	.550	102	11.3
			Average		.2345	.2246	.740	.550	85	10.6
			Overall Average		.2330	.2254	.902	.663	119	9.7
Compressive a	294	172	MG-58-2-C14a2³	3.63	.2405	-----	.752	Not obtained	138	Not obtained
Compressive b	294	668	MG-58-3-C34b1	1.61	.2260	.2201	---	.340	11.1	---
		172	MG-58-3-C35b1		.2299	.2243	---	.480	44.2	---
		172	MG-58-3-C36b1		.2284	.2222	---	.210	38.9	---
			Average		.2281	.2222		.343	31.4	
		334	MG-58-3-C31b2	3.63	.2348	.2284	---	.210	44.3	---
		172	MG-58-3-C33b2		.2324	.2259	---	.410	37.4	---
			MG-58-4-C38b2		.2247	.2189	---	Not obtained	Not obtained	---
			Average		.2306	.2244		.310	40.9	
		172	MG-58-3-C30b3	6.45	.2433[2]	.2368[2]	---	.550	72.9	---
		172	MG-58-3-C32b3		.2314	.2253	---	.410	51.9	---
		172	MG-58-3-C37b3		.2310	.2243	---	.410	34.4	---
			Average		.2352	.2288		.457	53.1	
			Overall Average		.2313	.2251		.378	41.9	
Compressive B	294	172	MG-58-4-C39b2³	3.63	.2407	-----	---	.836	88	---

Notes:

1. BD - before drying   AD - after drying
2. Small amount of material missing from foot of this specimen
3. Undried specimen

147

TABLE 67

COMPARISON OF MECHANICAL PROPERTIES OF
SILICONE-PHENOLIC AND PHENIC-NYLON

Property[4]	Tensile		Compressive	
	Silicone[1] phenolic (MG-1)	Phenolic[2] nylon	Silicone[3] phenolic (MG-1)	Phenolic[2] nylon
Ultimate Strength in 10^6 N/m^2	0.22	9.90	0.62	24.2
Elastic Modulus in 10^9 N/m^2	0.052	1.12	0.032	0.75

Notes:

1. Table 61, this report.

2. Reference 2.

3. Table 64, this report.

4. Test temperature - room temperature

MG-58, Phenolic-Nylon
in Phenolic-Glass Honeycomb
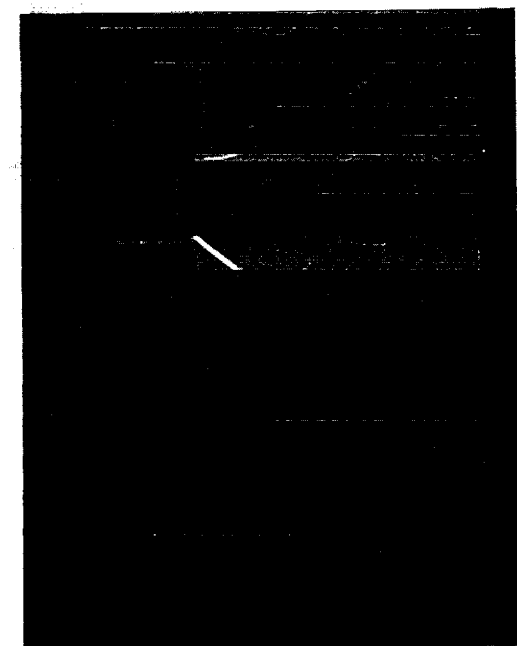
MG-45, Silicone Elastomer
in Phenolic-Glass Honeycomb
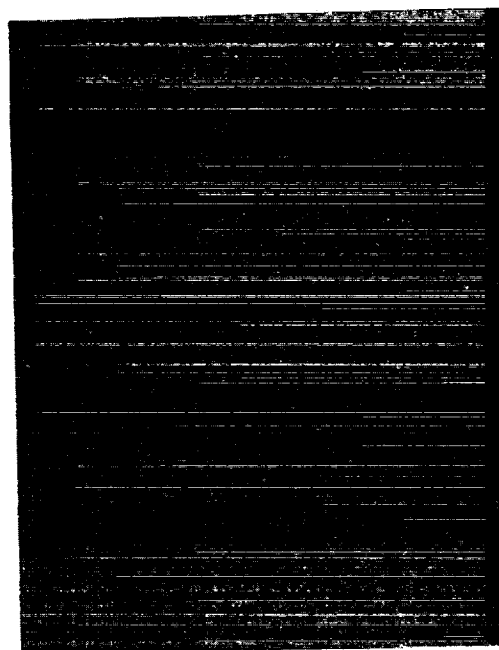
MG-1, Silicone Elastomer

Figure 1. Pictures of Virgin MG-1, MG-45 and MG-58 Ablative Materials

149

100 microns

(a) Virgin Material
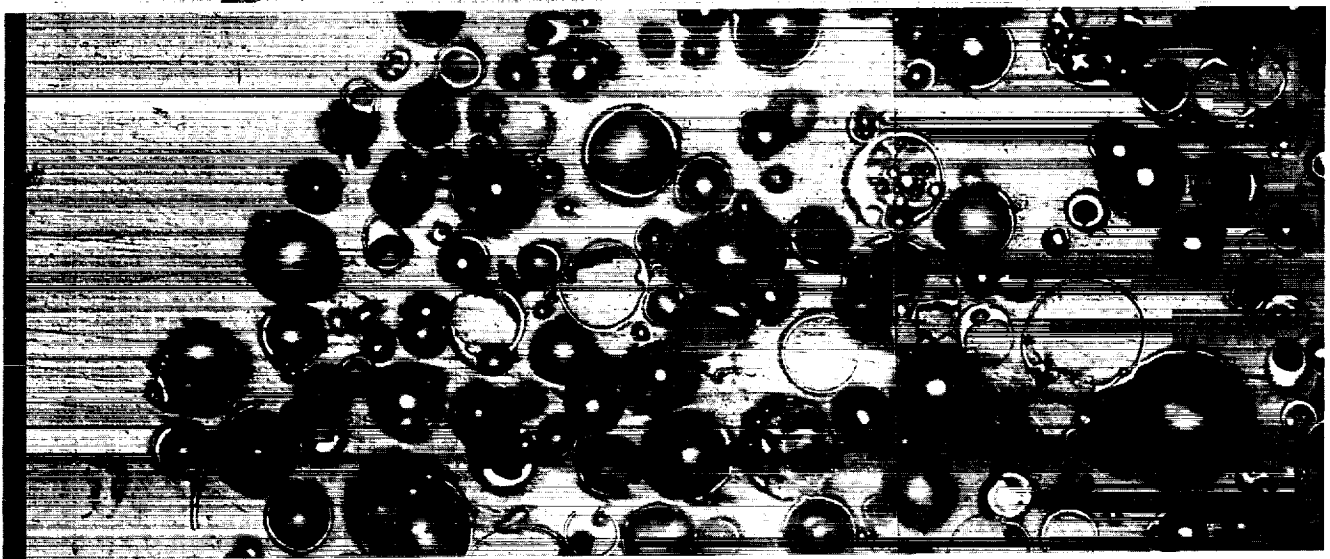
(b) Arc-Jet Char

Figure 2. Photomicrographs at 169X of MG-45, Silicone-Phenolic in
Phenolic-Glass Honeycomb, (material vacuum impregnated with
Bakelite EPL2795 and HYSOL H2-3404 hardener)
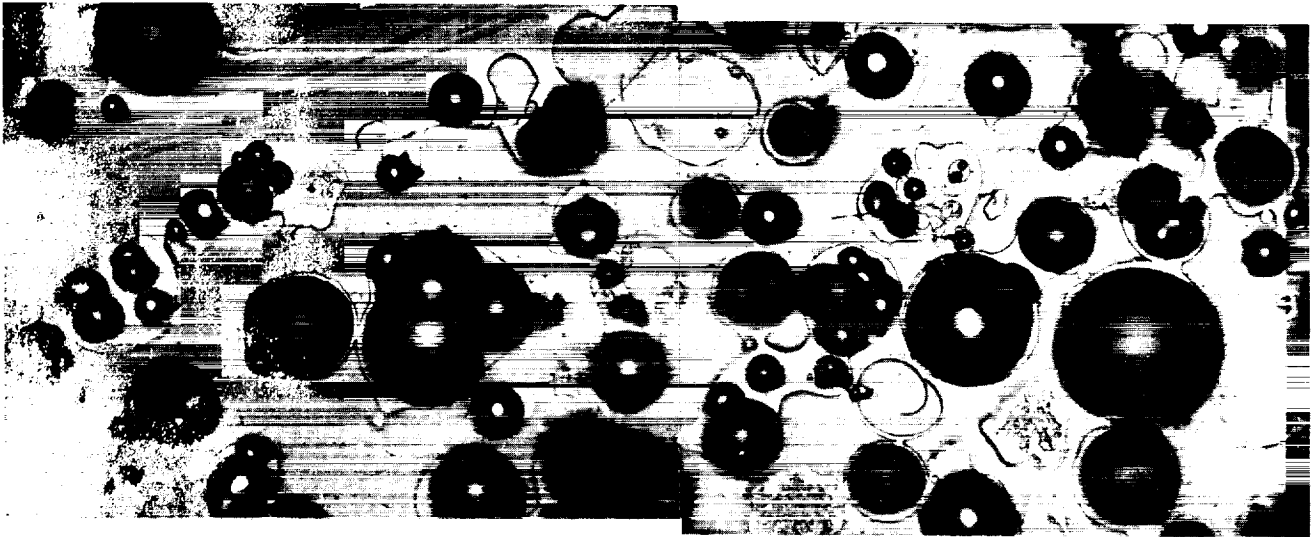
(a) Virgin Material

(b) Arc-Jet Char

Figure 3. Photomicrographs at 188X of MG-58, Phenolic-Nylon in Phenolic-Glass Honeycomb, (material vacuum impregnated with Bakelite ERL2795 and HYSOL H2-3404 hardener)

151

Spec 1644-10-A-14 After Charring at 1644 K.
Note that Inhomogeneity Persisted After Charring.

Spec 1644-10-A-14 (3" Dia) Before
Charring. Note Black Spot which was
Hard and Rubbery.

Spec 1750-10-R-9 After Charring at 1750 K.
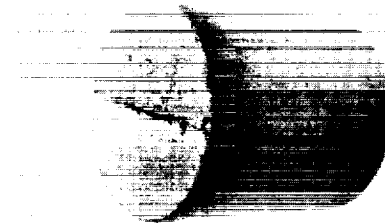
Spec 1644-10-R-12 After Charring at 1644 K.

Figure 4. Pictures of chars prepared at 10 K/min from MG-1
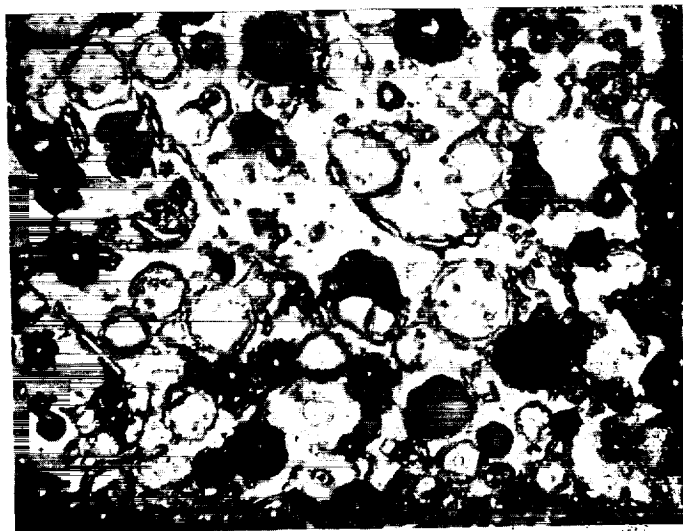
(a) Charred to 811 K in furnace at 10 K/min
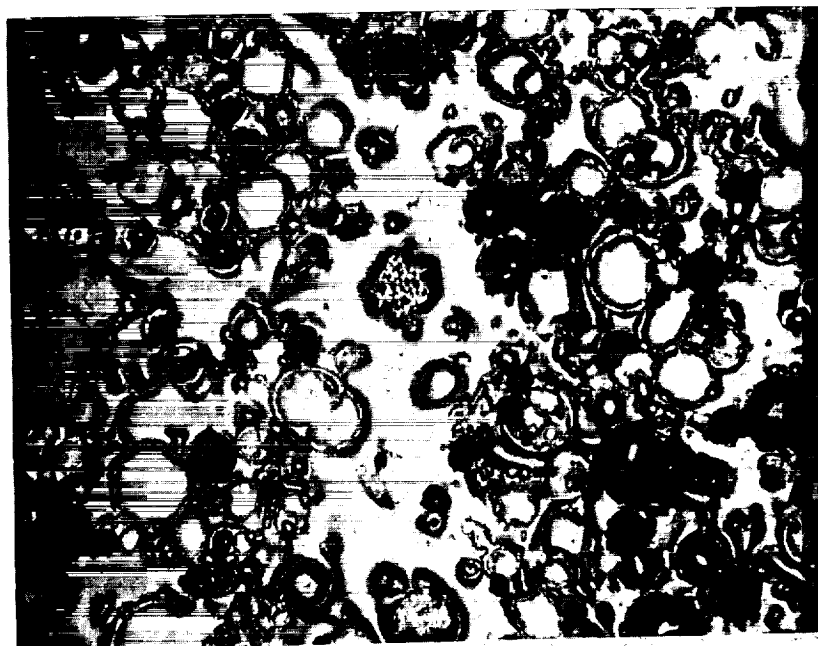
(b) Charred to 1561 K by immersing in
     furnace preheated to 1561 K

Figure 5. Photomicrographs at 95X of MG-1, Silicone-Phenolic,
           charred in furnace (material impregnated with Bakelite
           ERL2795 and HYSOL H2-3404 hardener)
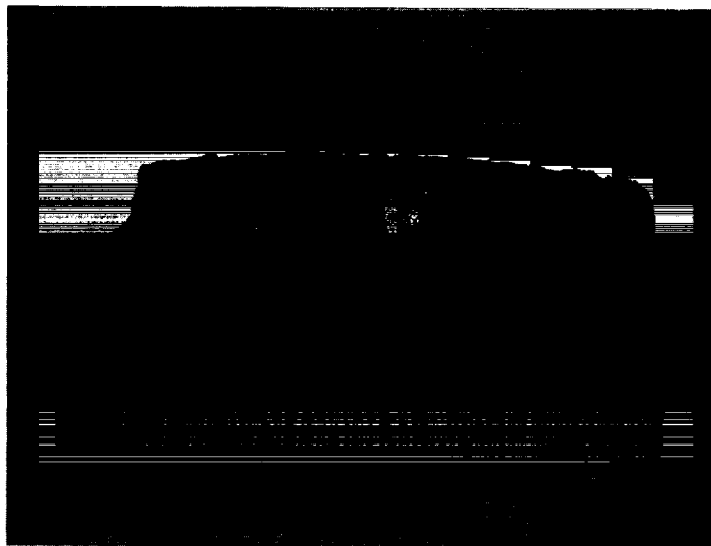
Char Disc K4

Figure 6. Picture of section through MG-58, Phenolic-Nylon in Phenolic-Glass Honeycomb, charred in arc-jet

154
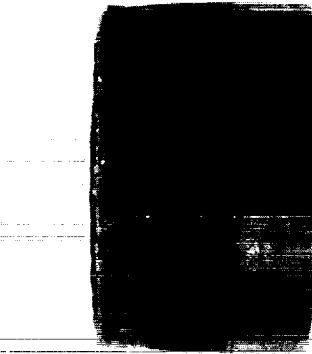
Disc L2

Disc L2

Disc X1

Disc X1
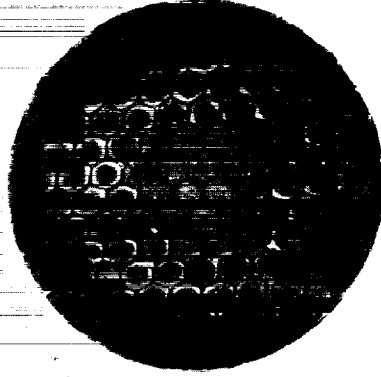
Figure 7. Pictures of MG-58, charred in NASA arc-jet

155
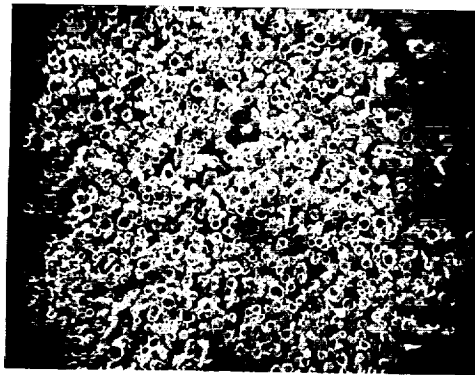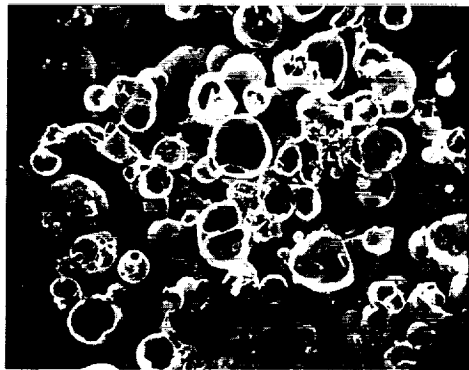
1000 microns

200 microns

50 microns

Figure 8. Pictures made with scanning electron microscope of MG-58, Phenolic-Nylon, charred in arc-jet
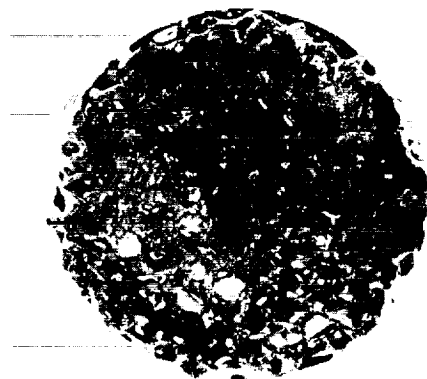
MG-58

MG-58

MG-45, Disc Q1
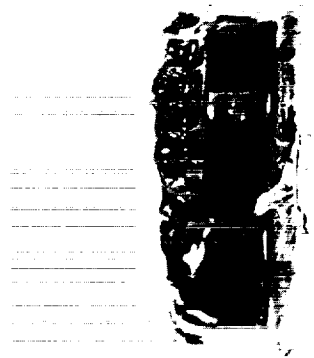
MG-58

MG-58

Figure 9. Pictures of MG-45 and MG-58 charred in NASA arc-jet, impregnated with polyalphamethylstyrene

X Direction

Y Direction

10.2 cm
(4")

20.4 cm
(8")
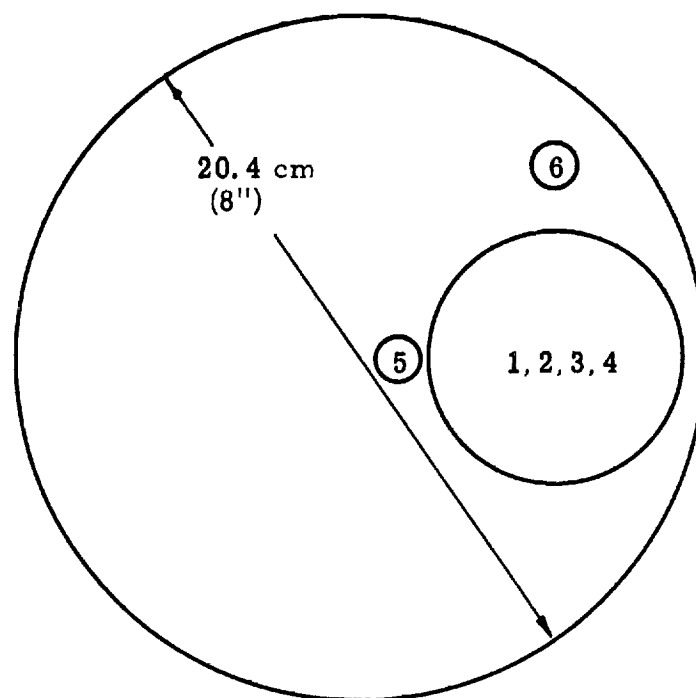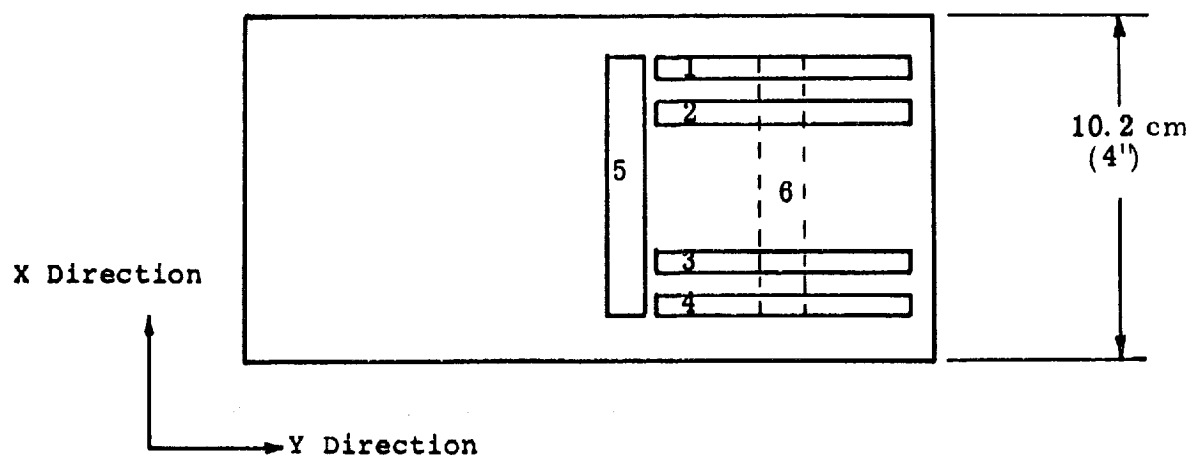
1, 2, 3, 4 - Discs for ASTM conductivity
5, 6 - Thermal expansion specimens

Figure 10. Cutting plan for billet of virgin MG-1, Silicone-Phenolic

158

1, 2, 3, 4 - ASTM Thermal Conductivity Specimens 1 and 2
5, 6, 7 - Permeability Specimens
8, 9, 10, 11 - ASTM Thermal Conductivity Specimens 3 and 4 of MG-45

3 and 4

A   A

5   1 and 2

38.1 cm (15 in.)

8, 9, 10, 11   6

7

8
9
10
11

5   1

2

3.18cm ($1\frac{1}{4}$ in.)

Typical Permeability Specimens

Typical ASTM Thermal Conductivity Specimens
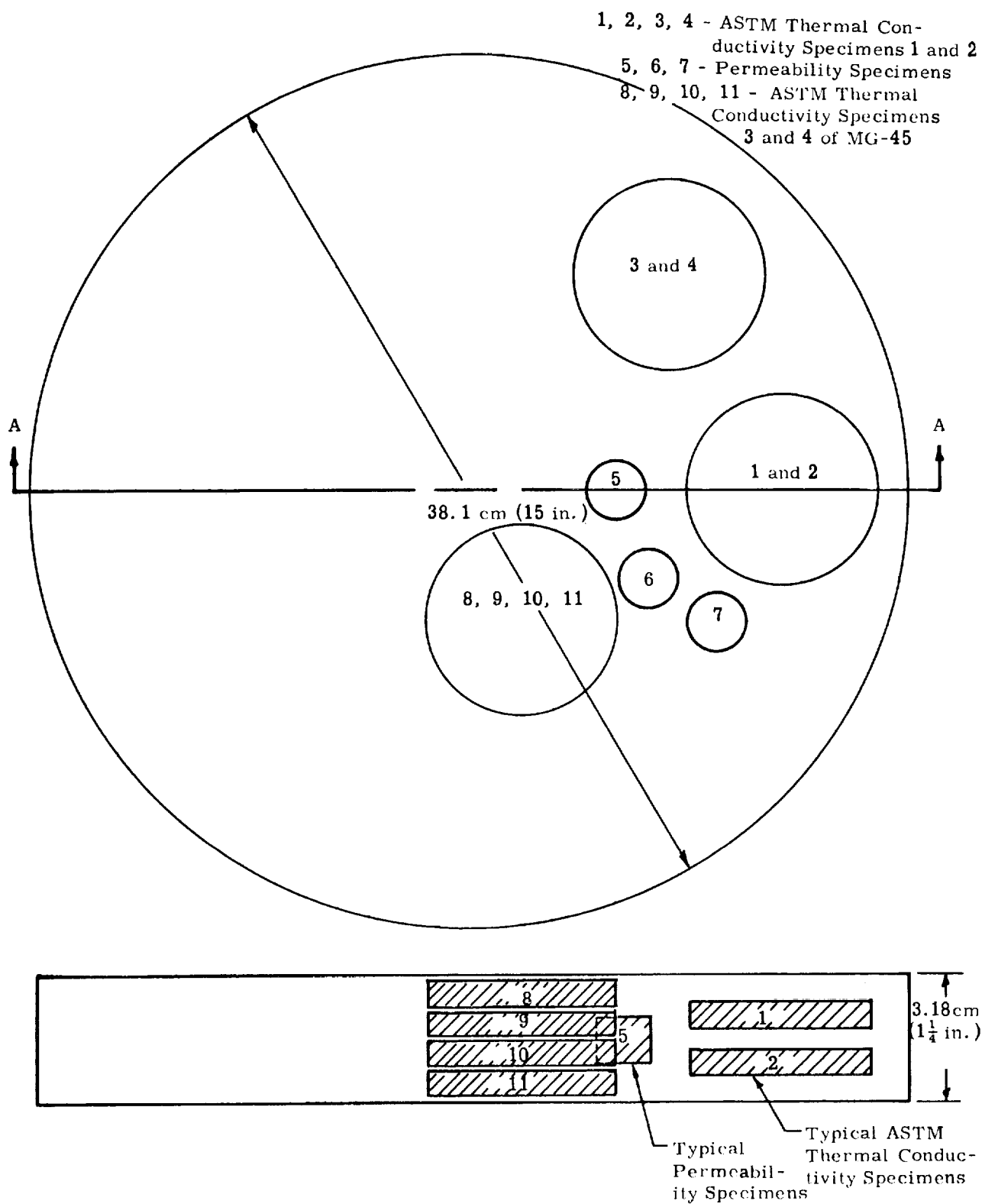
Figure 11.   Cutting plan for billets of virgin MG-45 and MG-58

159
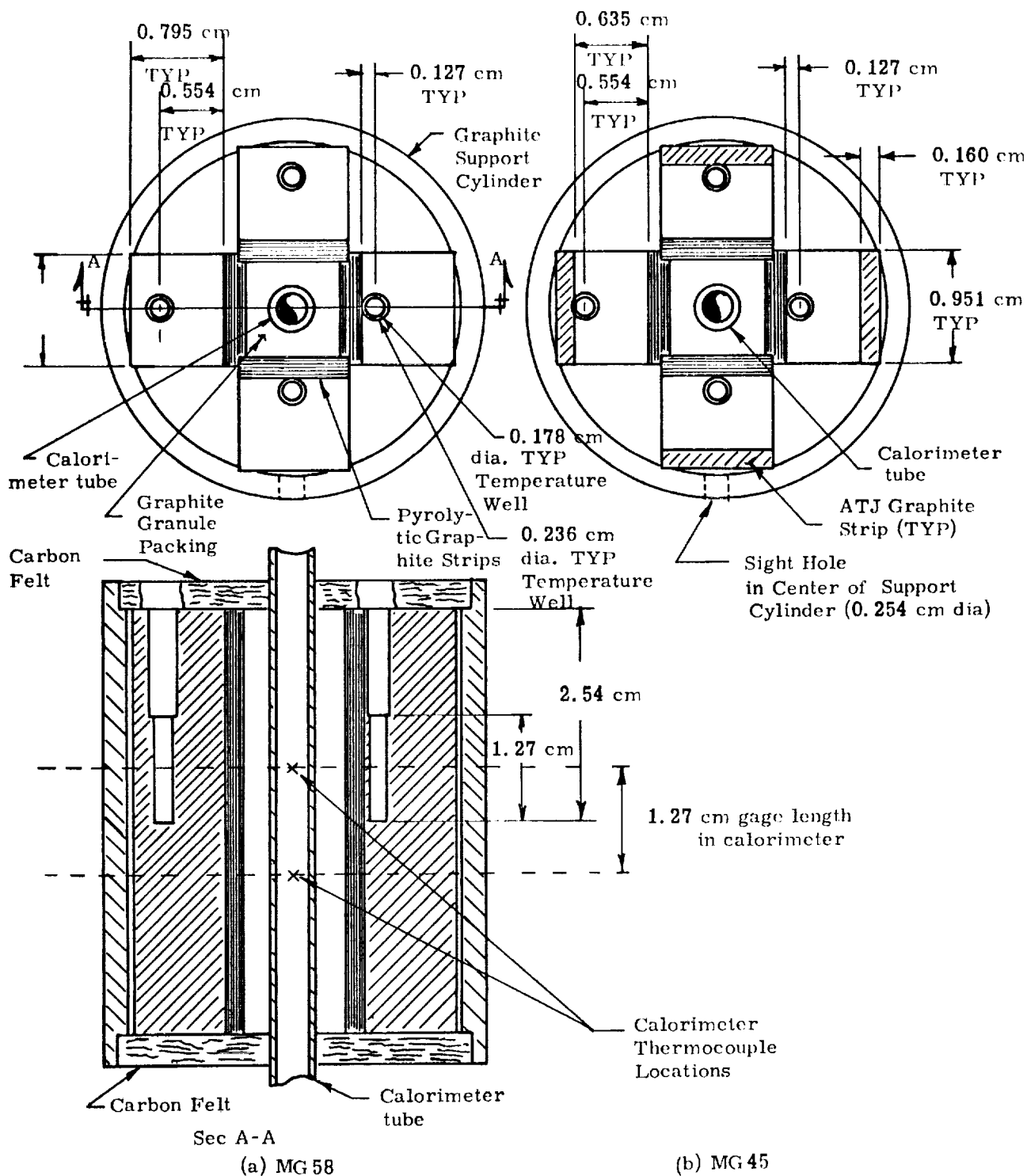
Figure 12. Configurations of specimens for radial inflow measurements on chars of MG-45 and MG-58
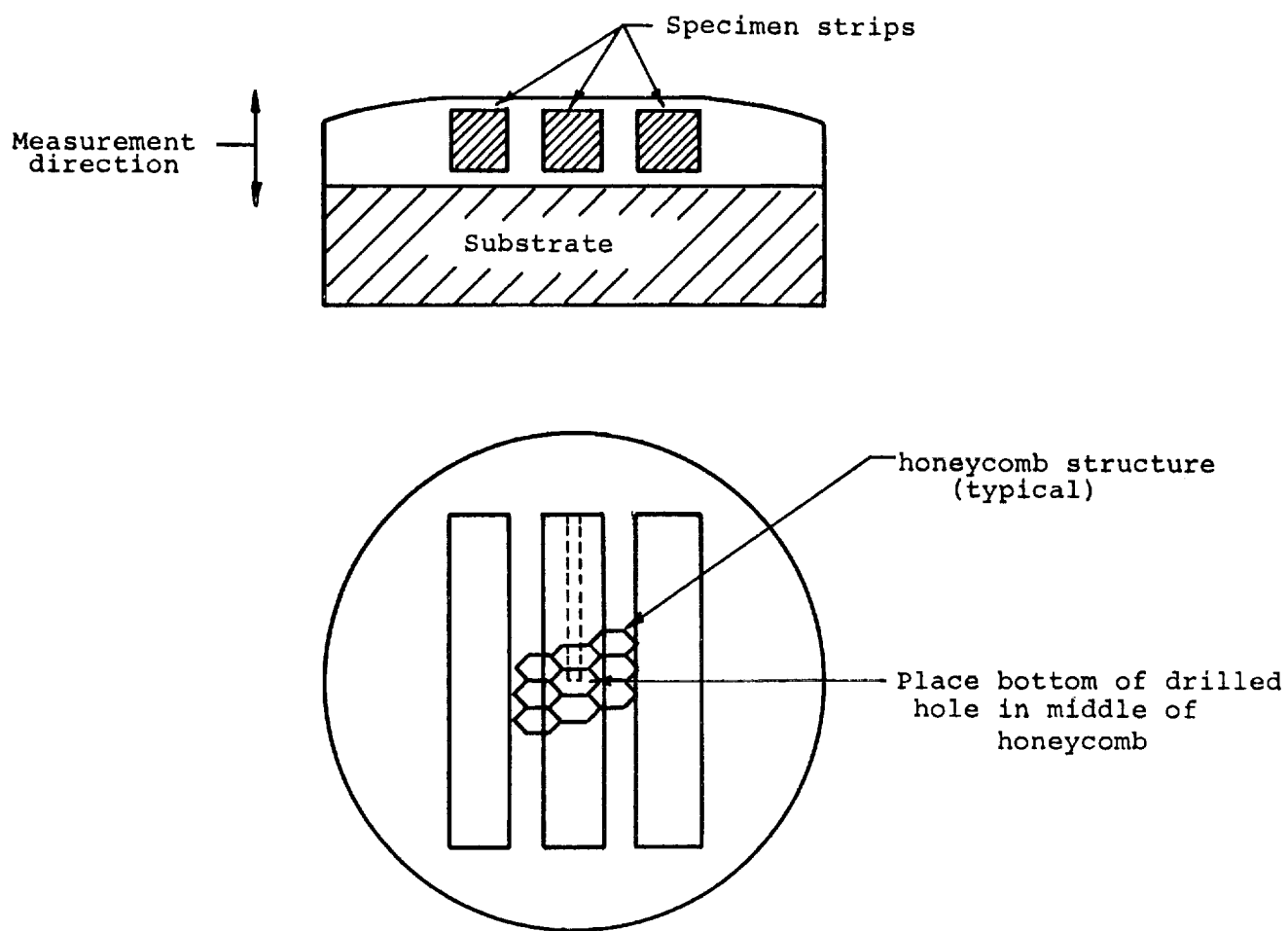
Figure 13. Cutting plan used to obtain strip specimens for radial inflow apparatus from impregnated arc-jet discs of MG-45 and MG-58

161
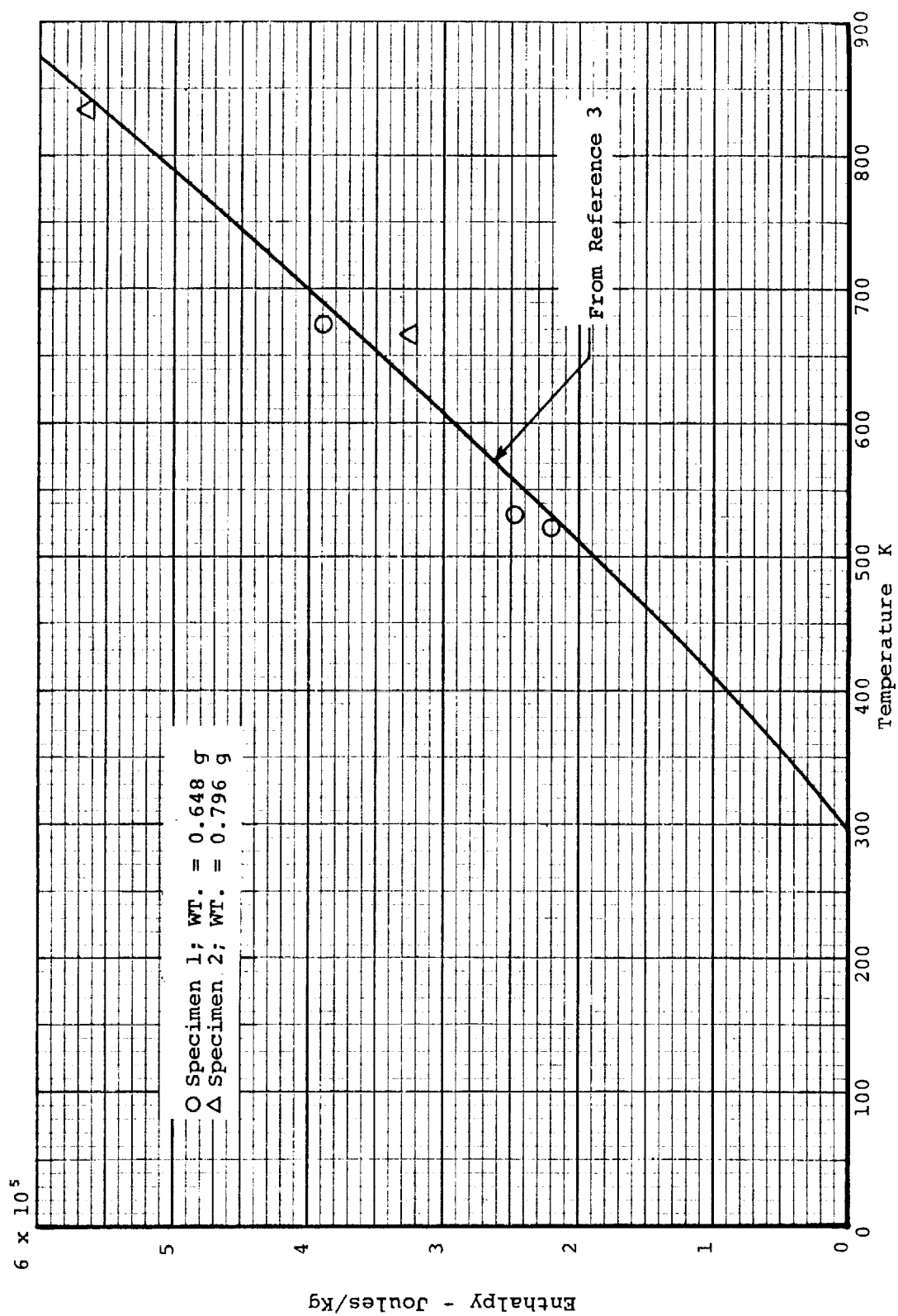
Figure 14. Calibration of aluminum foil used as sample holders for evaluations in adiabatic calorimeter on charred MG-1
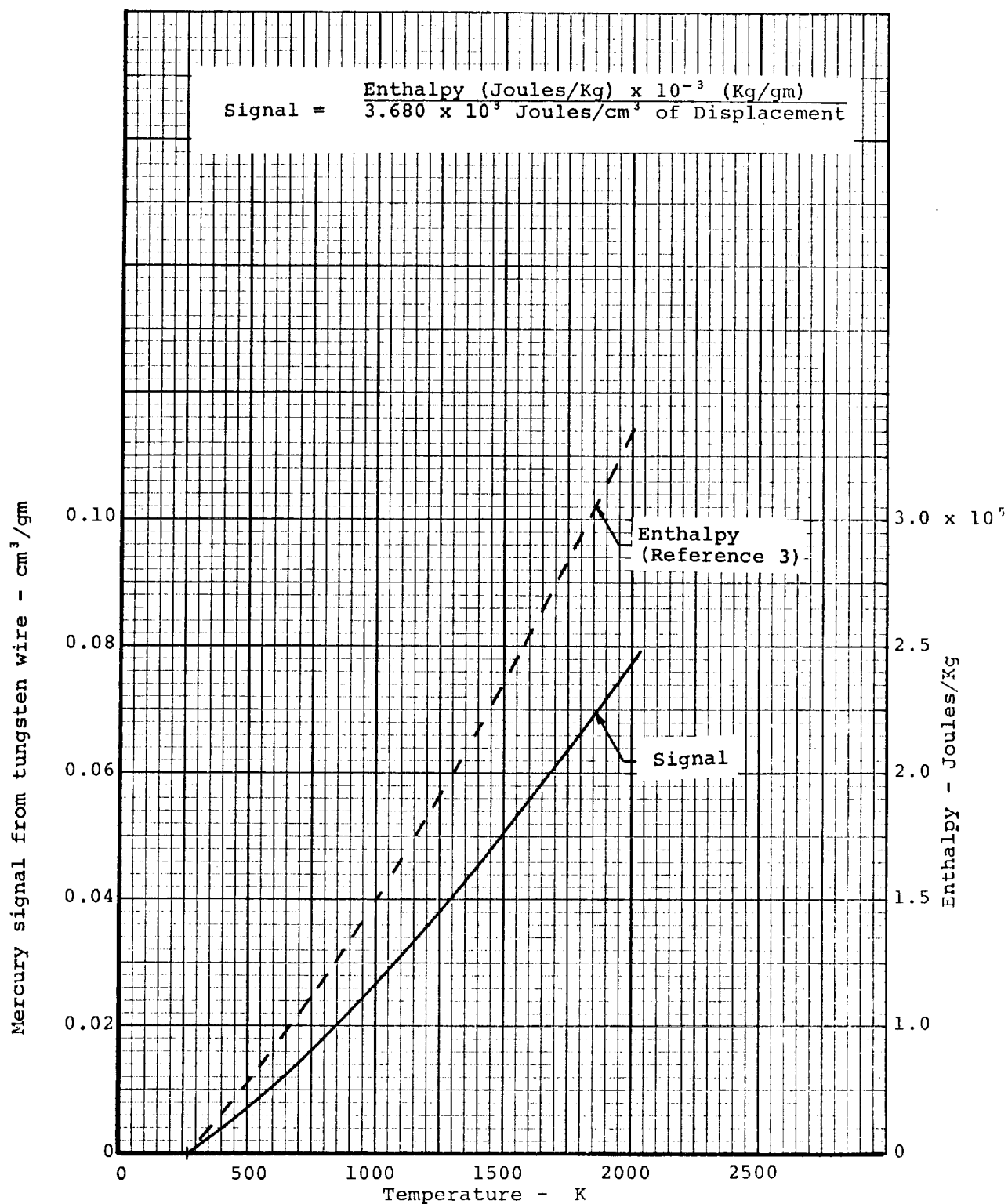
Figure 15.   Correction for tungsten wire used to hold drop
             cup together

163

Q3 **T4**
Coated Uncoated
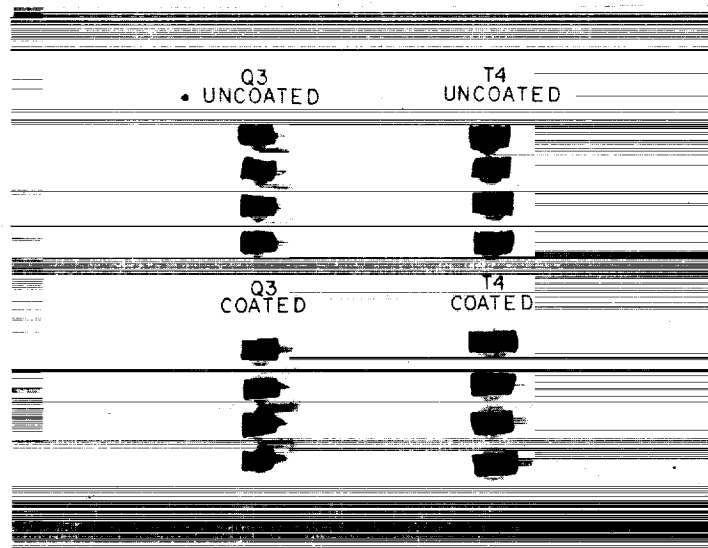
Figure 16. Pictures of filler of char of MG-58 before and
after wax-coating for bulk density measurements

36 ga. wire (0.005")

50

Scale - smallest divisions = 0.05 mL

Meniscus

0

Weight

Samples (wax coated)

Water with Tergitol ®
TNN added as wetting agent
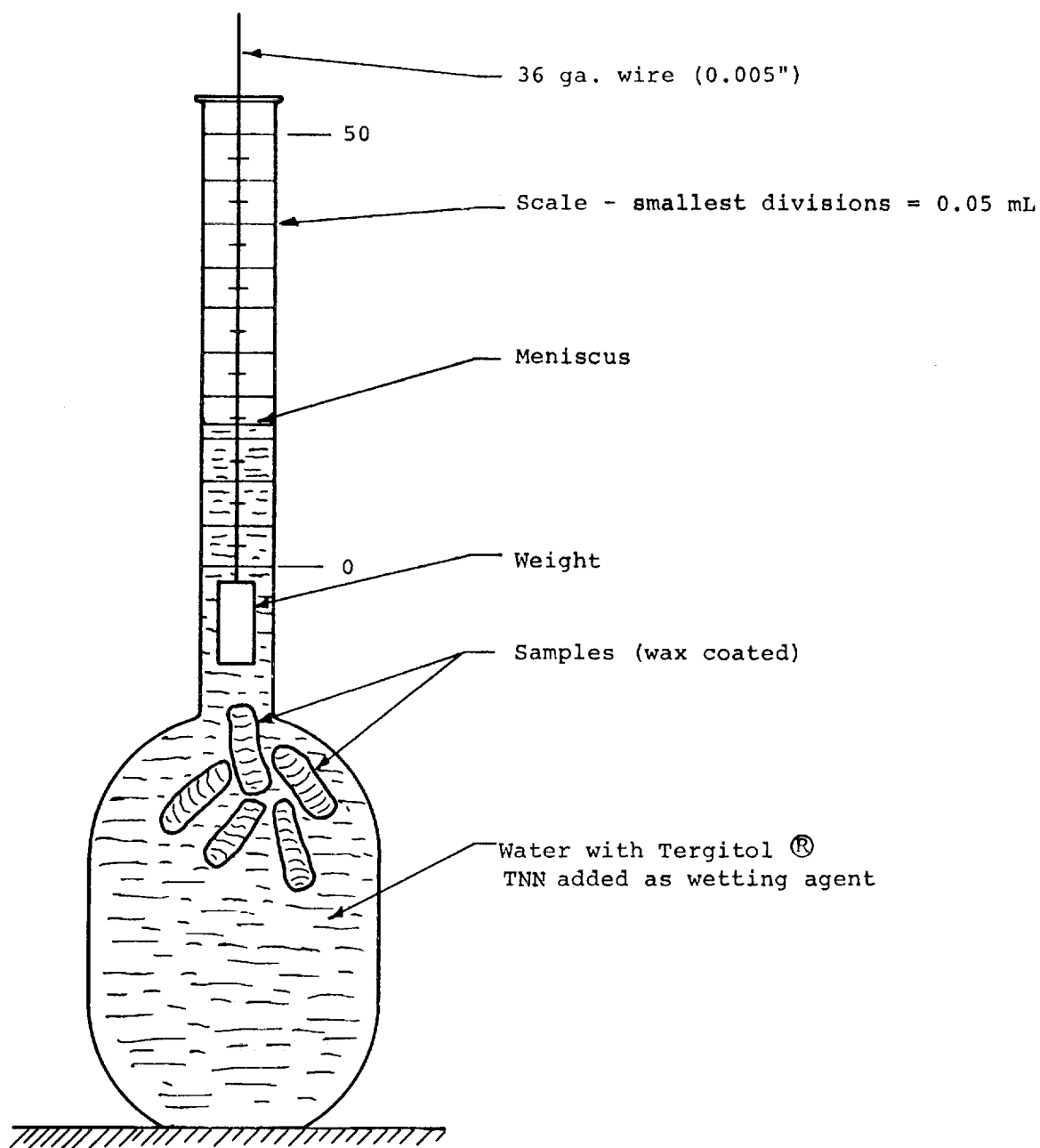
Experimental Apparatus

Procedures used:

1. Get initial reading with weight immersed in water
2. Remove weight - add samples
3. Submerge samples and weight
4. Read displacement above initial reading
5. Remove sample - replace weight - check initial readings (initial and final readings were within 0.025 mL)

Figure 17. Experimental apparatus for determination of bulk density of the filler of the charred MG-58.
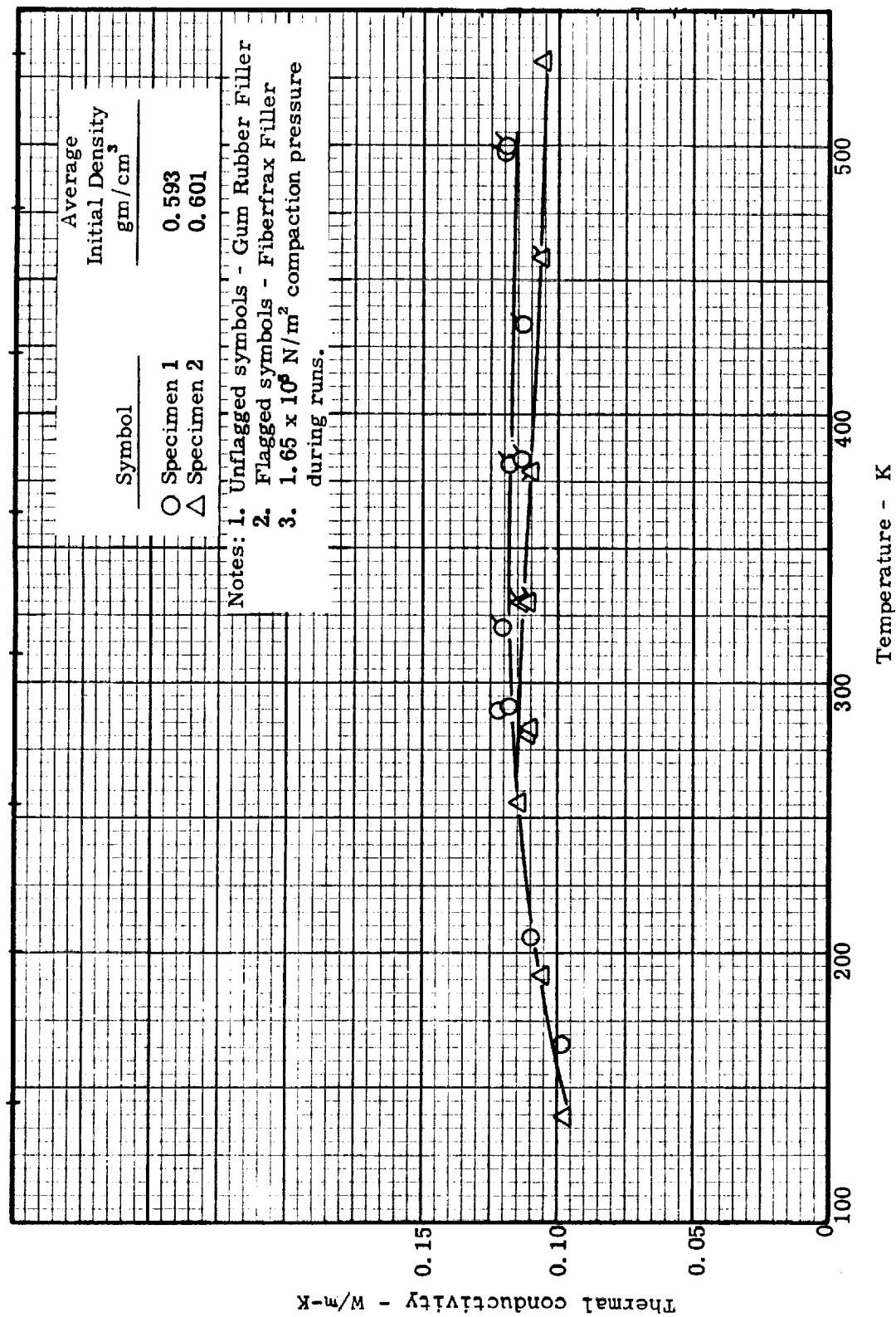
Figure 18. Thermal conductivity of virgin MG-1, Silicone-Phenolic

166
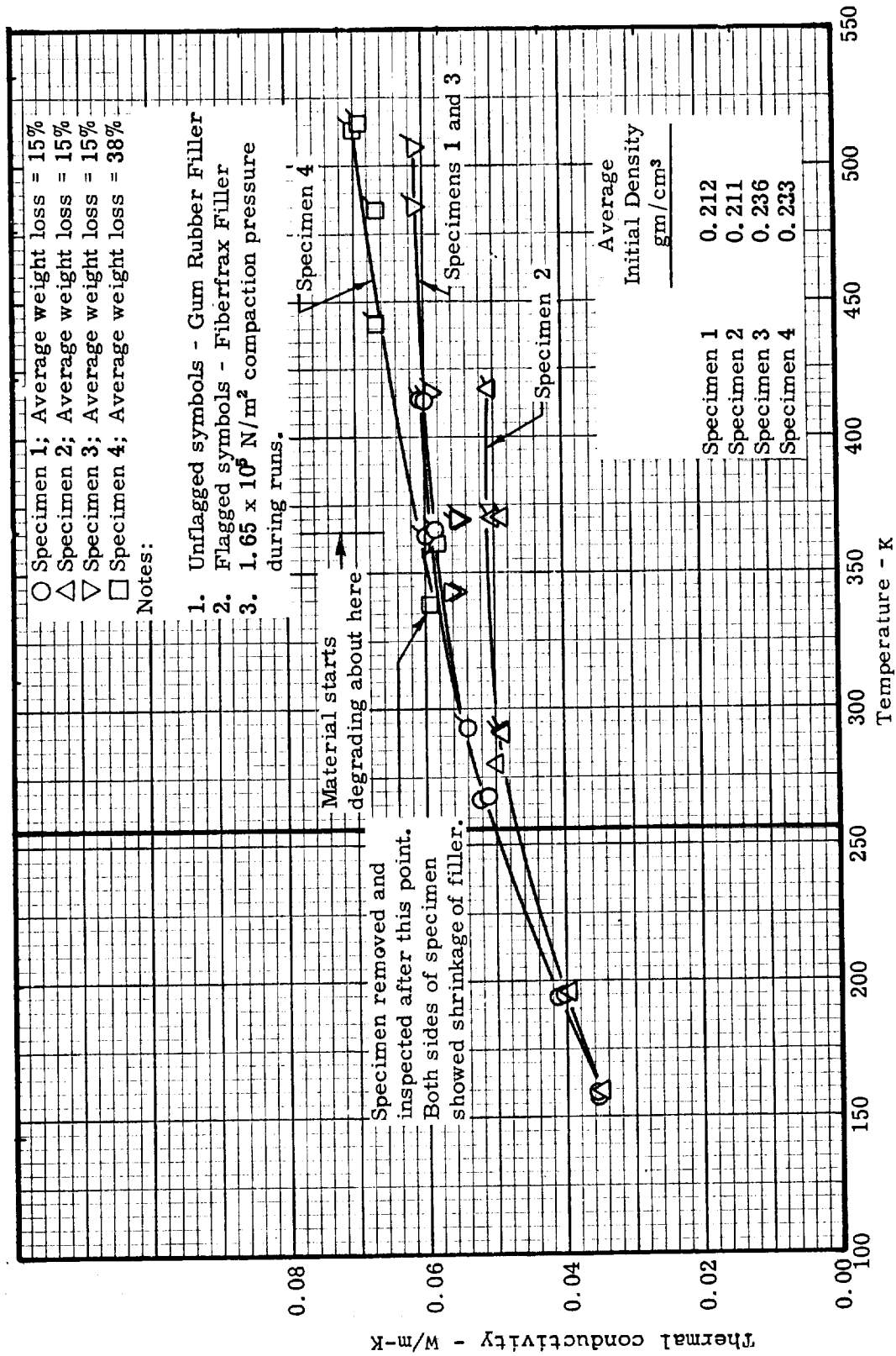
Figure 19. Thermal conductivity of virgin MG-45, Silicone-Phenolic in Phenolic-Glass Honeycomb

167
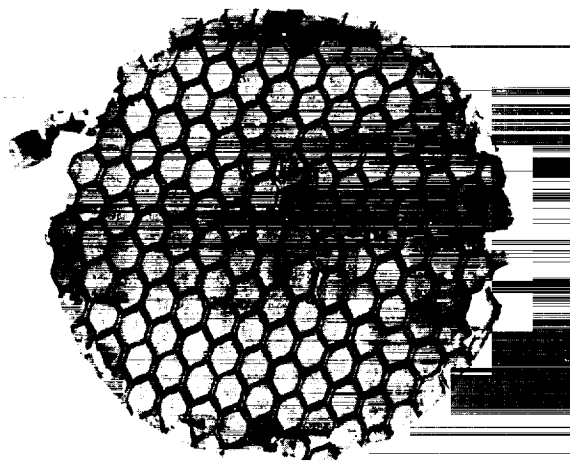
(a) Hot Face of Specimen - Exposed
to 574°K (577°F) (Note Shrinkage
of Filler)
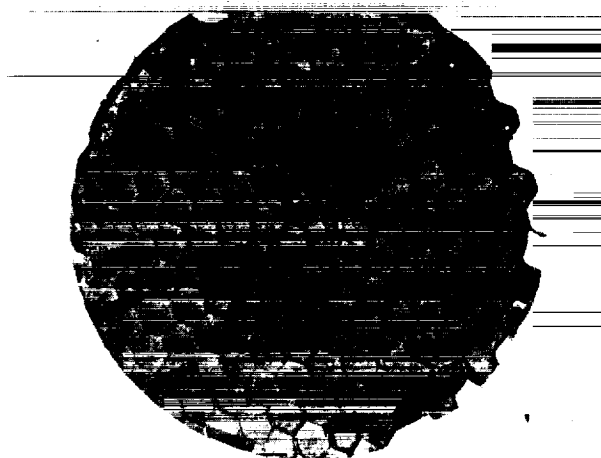
(b) Cold Face of Specimen - Exposed
to 454°K (357°F)

Figure 20.   Pictures of Virgin MG-45, Silicone-Phenolic in Phenolic-
Glass Honeycomb, thermal conductivity specimen after
exposure in ASTM C177 guarded hot plate apparatus

168
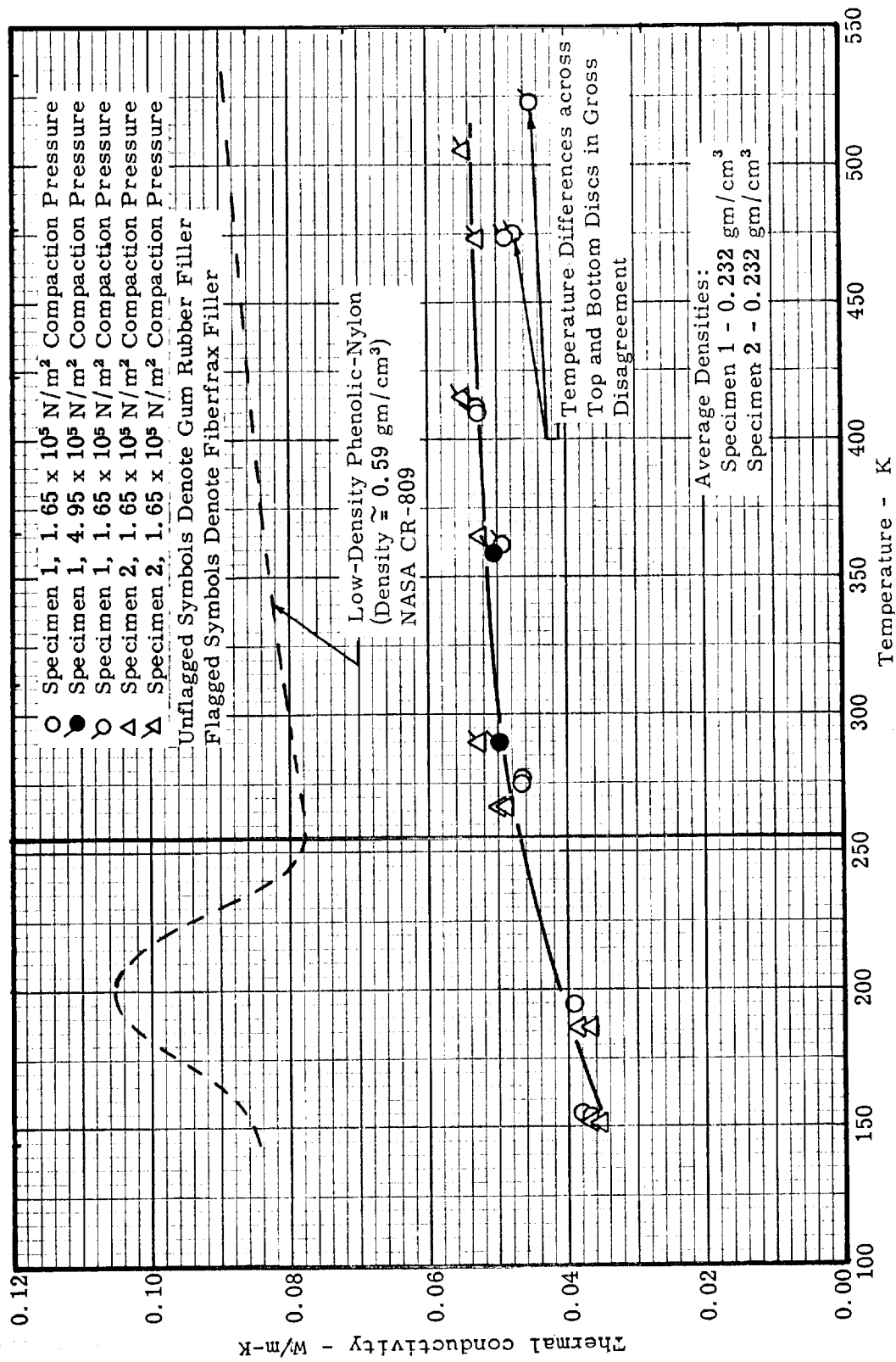
Figure 21. Thermal conductivity of Virgin MG-58, Phenolic-Nylon in Phenolic-Glass Honeycomb
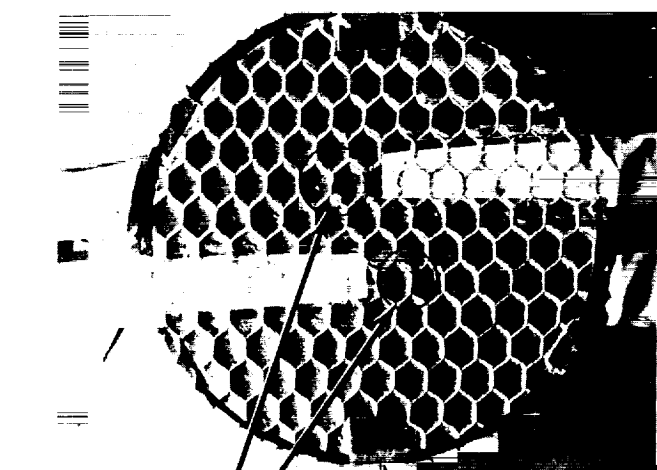
Thermocouple Getters Located under Foil at These Locations

Shim Stock for Gage Thickness Measurement

(a) Hot Face of Specimen Showing Instrumentation Covered by 0.0012 cm (0.0005 in.) Thick Aluminum Foil
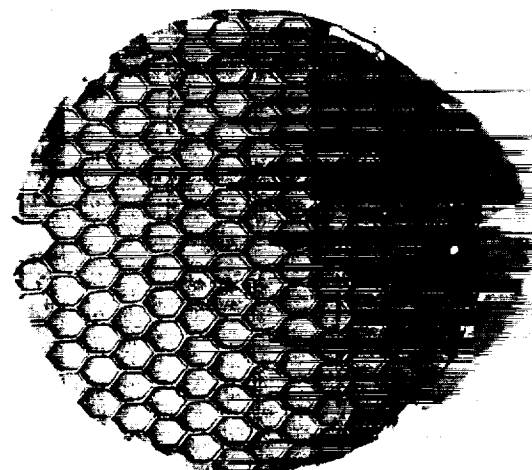
(b) Hot Face of Specimen - Exposed to 581°K (585°F) (Note Shrinkage of Filler)

(c) Cold Face of Specimen - Exposed to 465°K (377°F)

Figure 22.   Pictures of virgin MG-58, Phenolic-Nylon in Phenolic-Glass Honeycomb, thermal conductivity specimen after exposure in ASTM C177 guarded hot plate apparatus

170
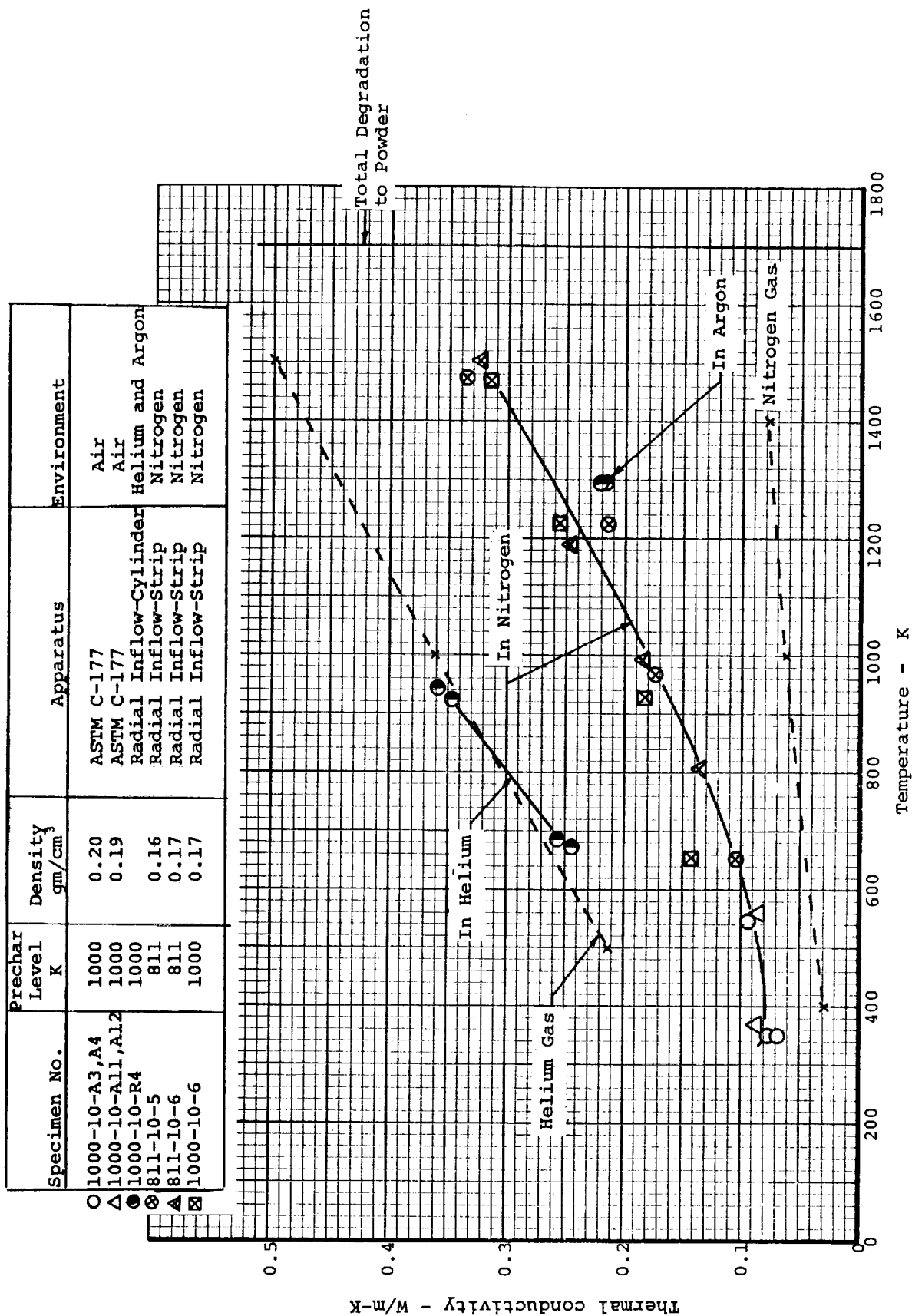
Figure 23. Thermal conductivity of MG-1 charred at 811 and 1000 K

171
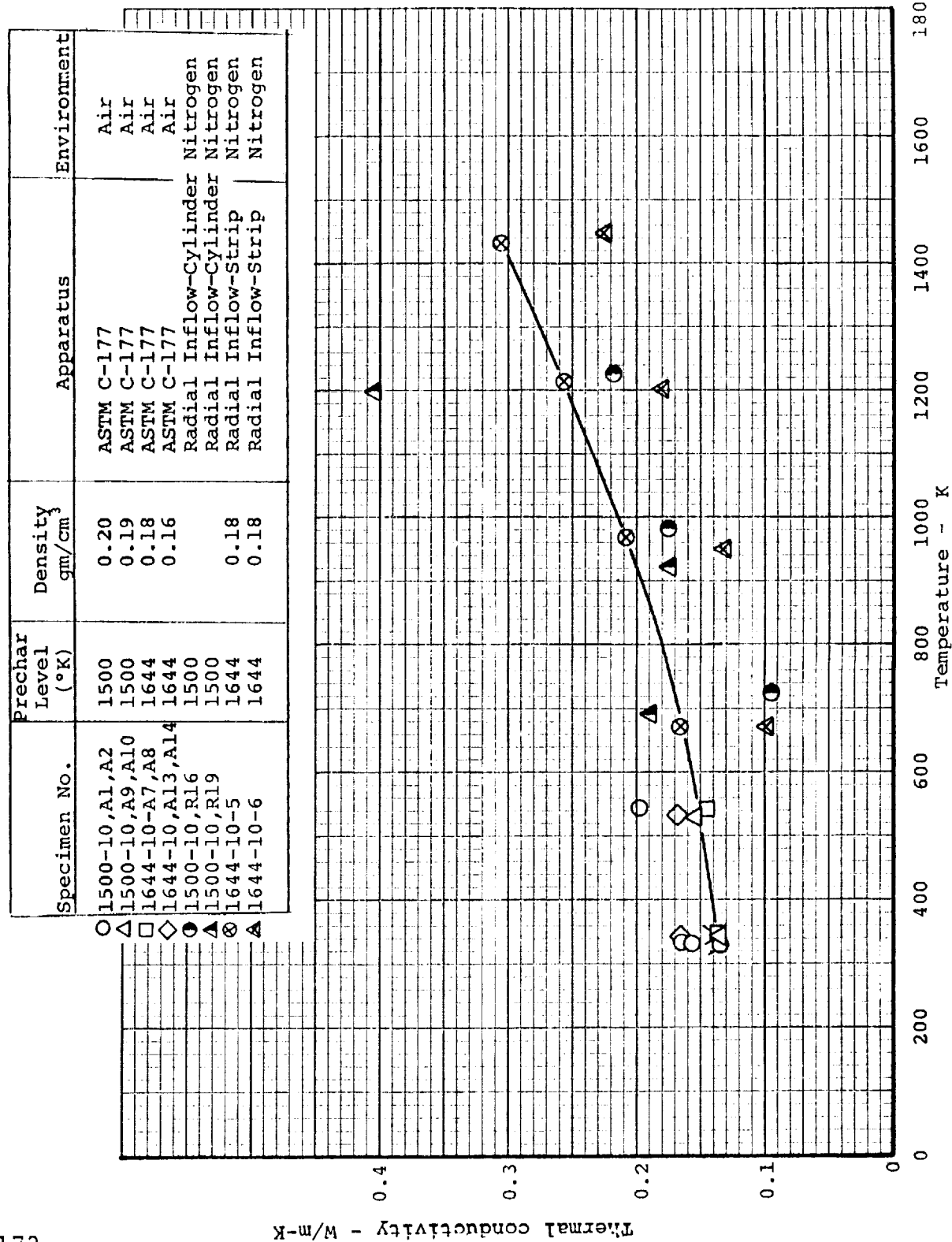
Figure 24. Thermal conductivity of MG-1 charred at 1500 and 1644 K
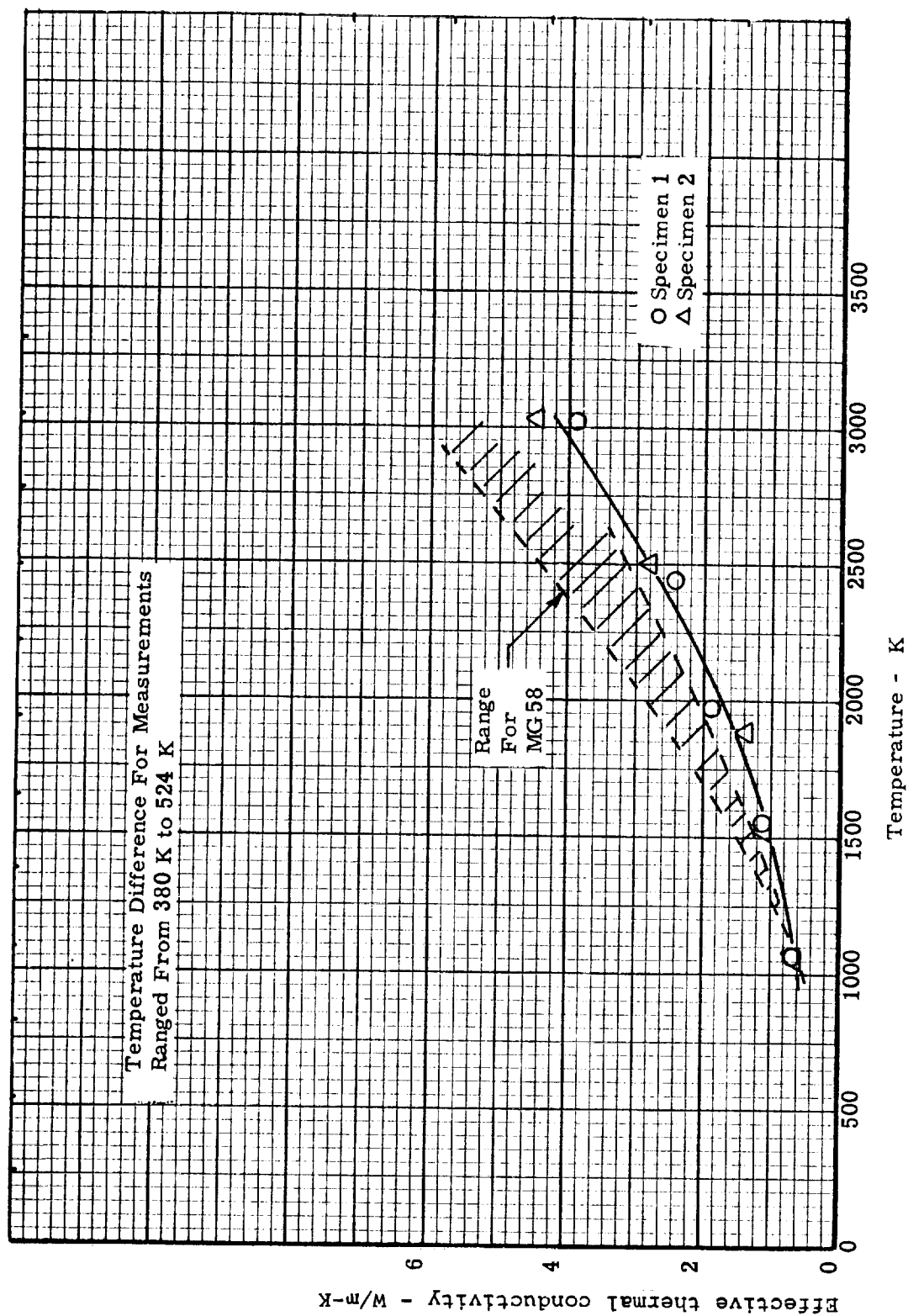
Figure 25. The effective thermal conductivity of MG-45, Silicone-Phenolic in Phenolic-Glass Honeycomb, charred in NASA arc-jet

173
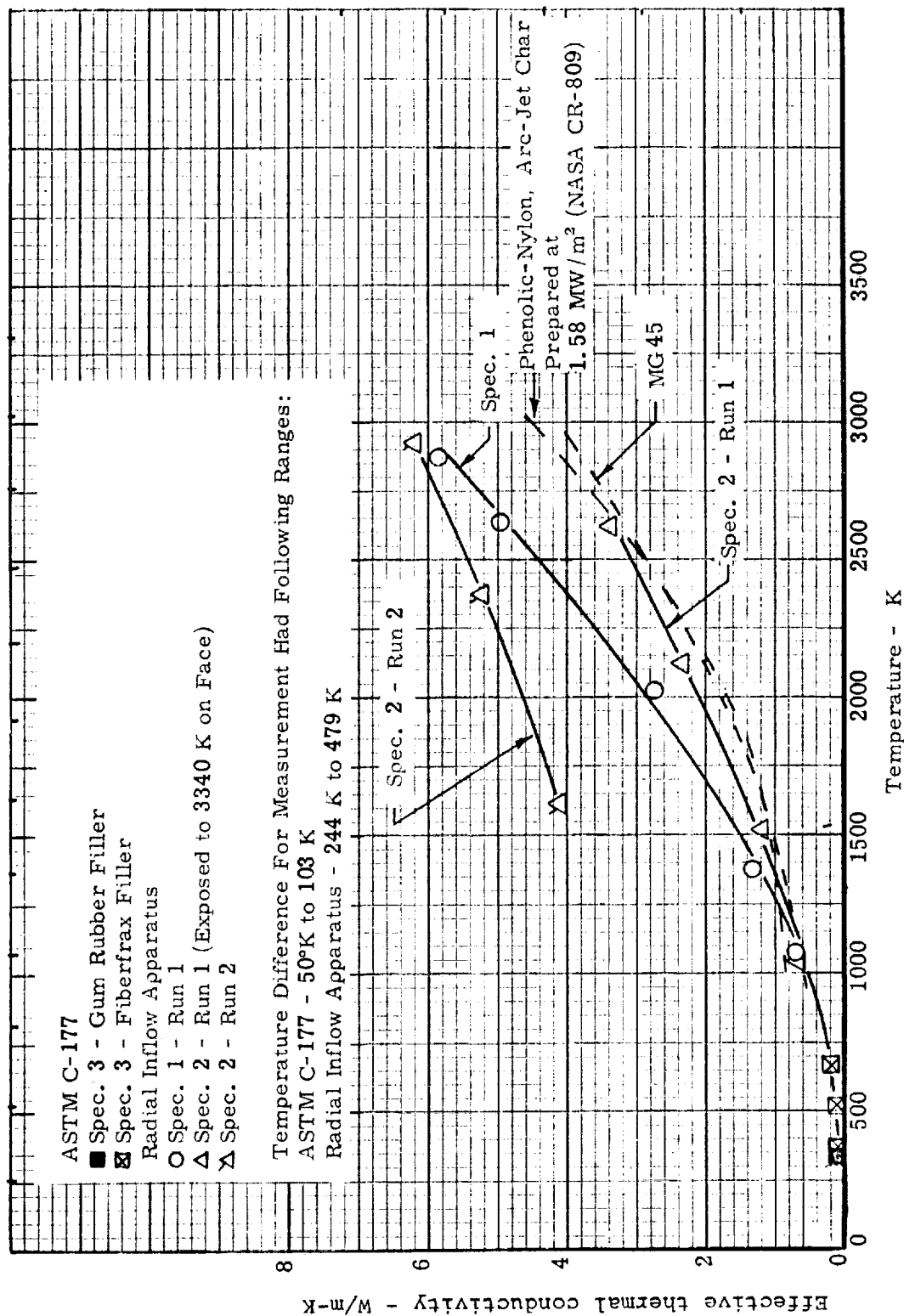
Figure 26. The effective thermal conductivity of MG-58, Phenolic-Nylon in Phenolic-Glass Honeycomb, charred in NASA arc-jet

174

Heat capacity graph (top):

O Graphical calculation
X Analytical solution

$$HC = 1.385 \times 10^3 + 0.360T - \frac{8.395 \times 10^6}{T^2}$$

(valid from 200K to 500 K)

Enthalpy graph (bottom):

X Analytical solution

$$h_{273} = 1.385 \times 10^3 T + 0.180\ T^2 + \frac{8.755 \times 10^6}{T} - 4.200 \times 10^5$$

(valid from 200K to 500 K)

○ Specimen 1
□ Specimen 2
△ Specimen 3
◬ Specimen 3A
◇ Specimen 4
◈ Specimen 4A

Note: Specimens 3A and 4A were taken from Specimens 3 and 4, respectively.
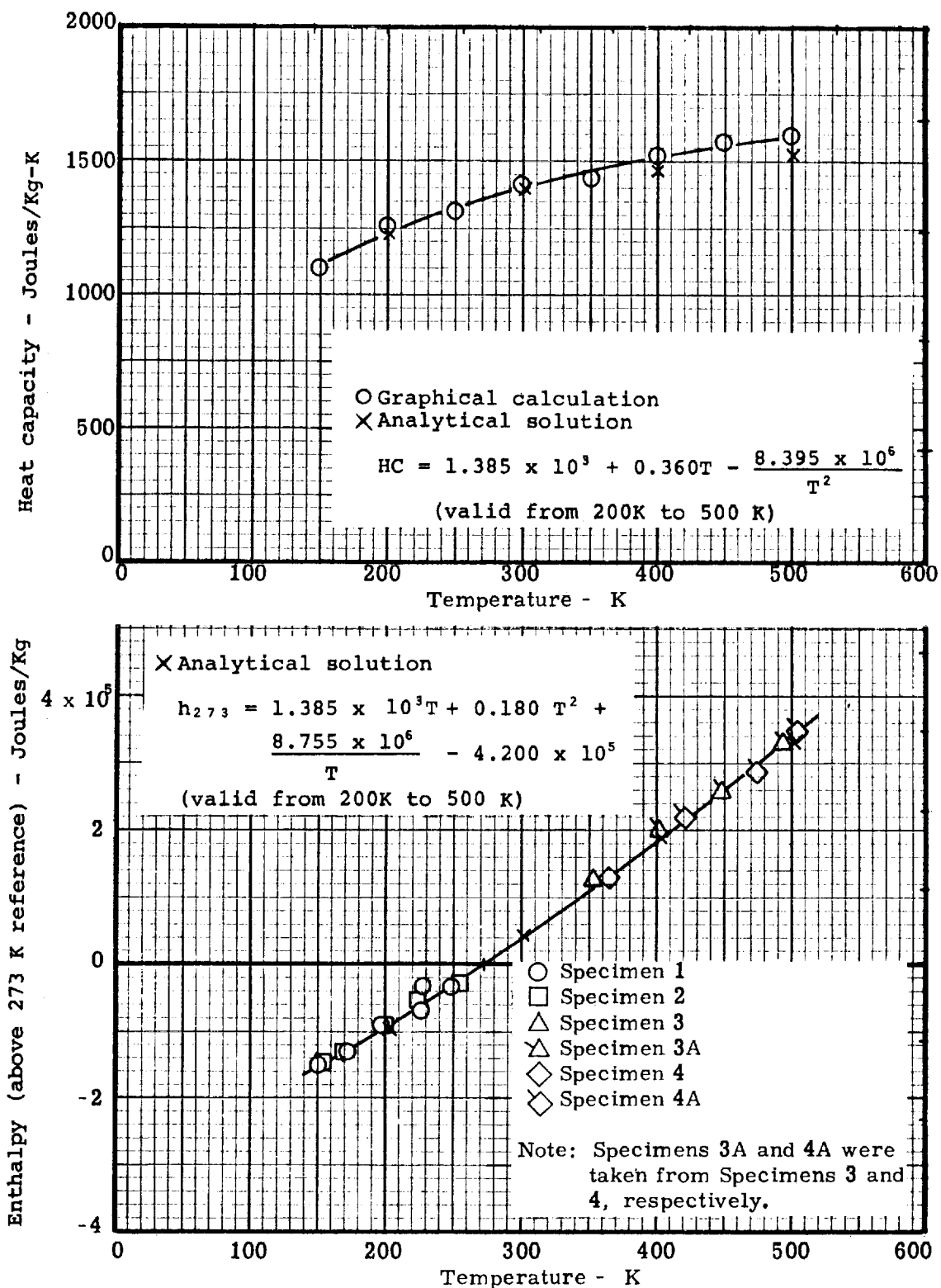
Figure 27. Enthalpy and heat capacity of virgin MG-1, Silicone-Phenolic

175
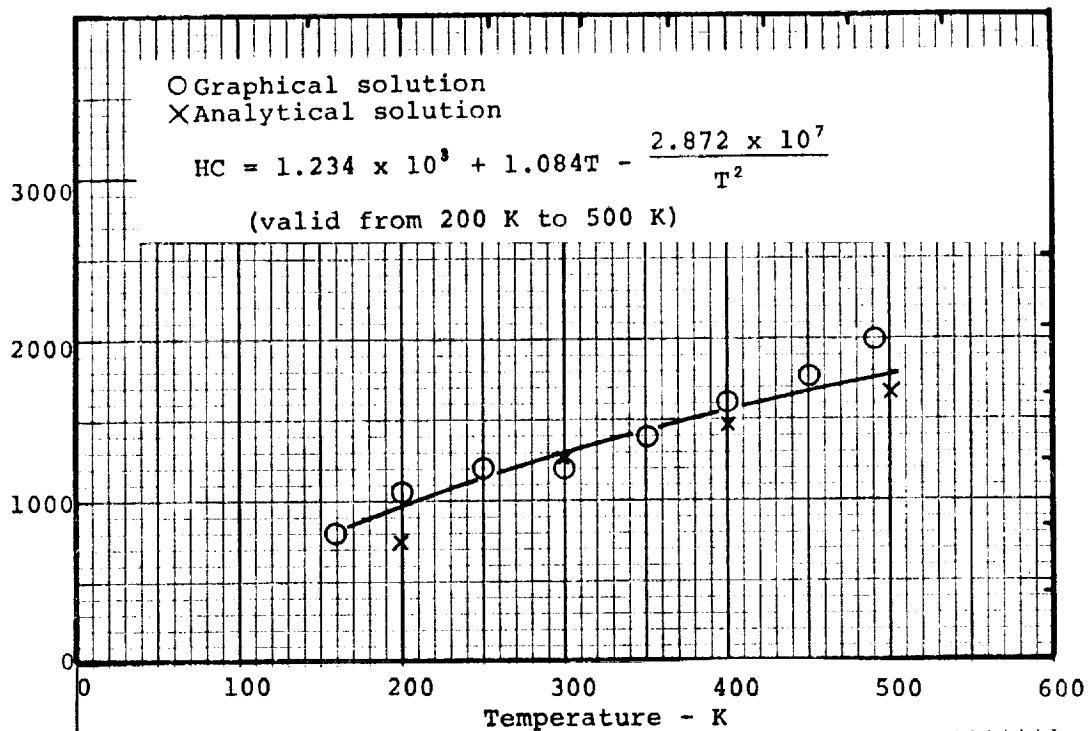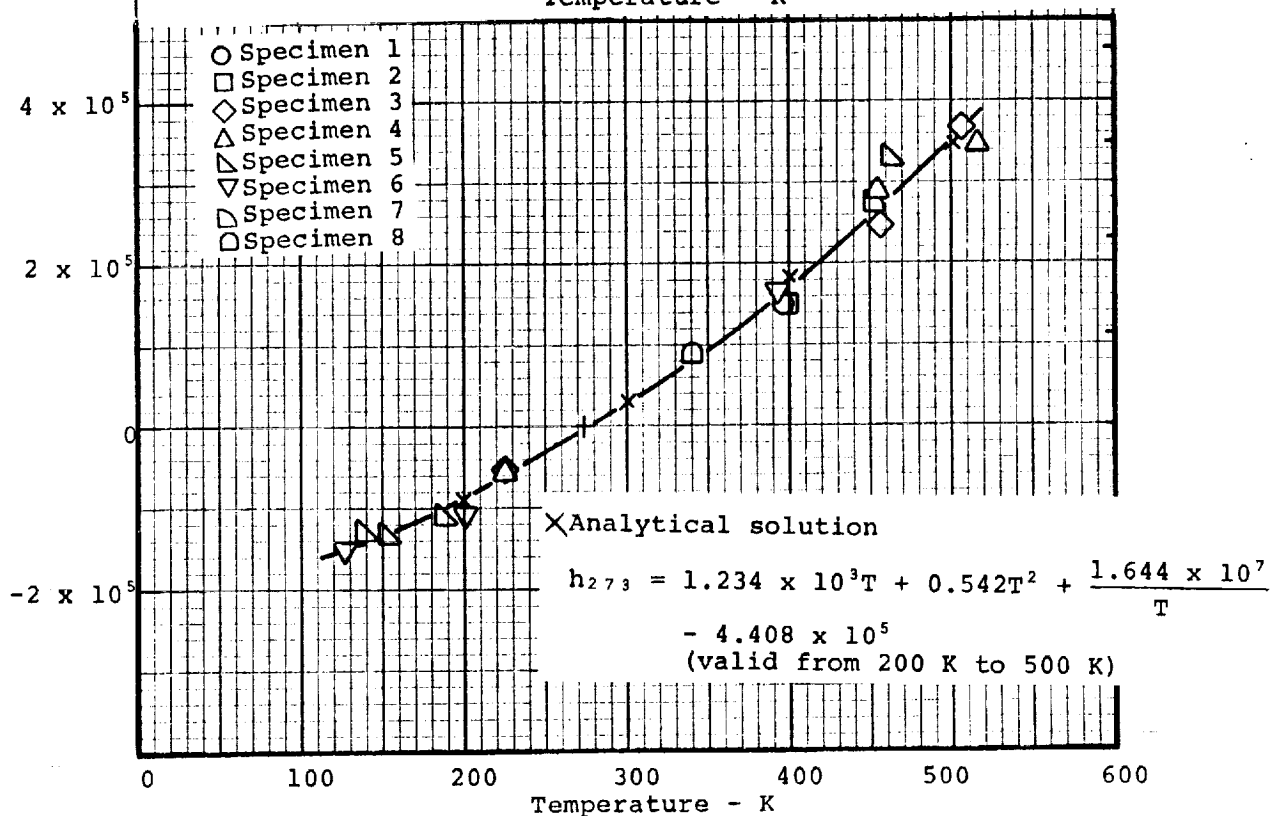
Figure 28. Enthalpy and heat capacity of virgin MG-45, Silicone-Phenolic in Phenolic-Glass Honeycomb
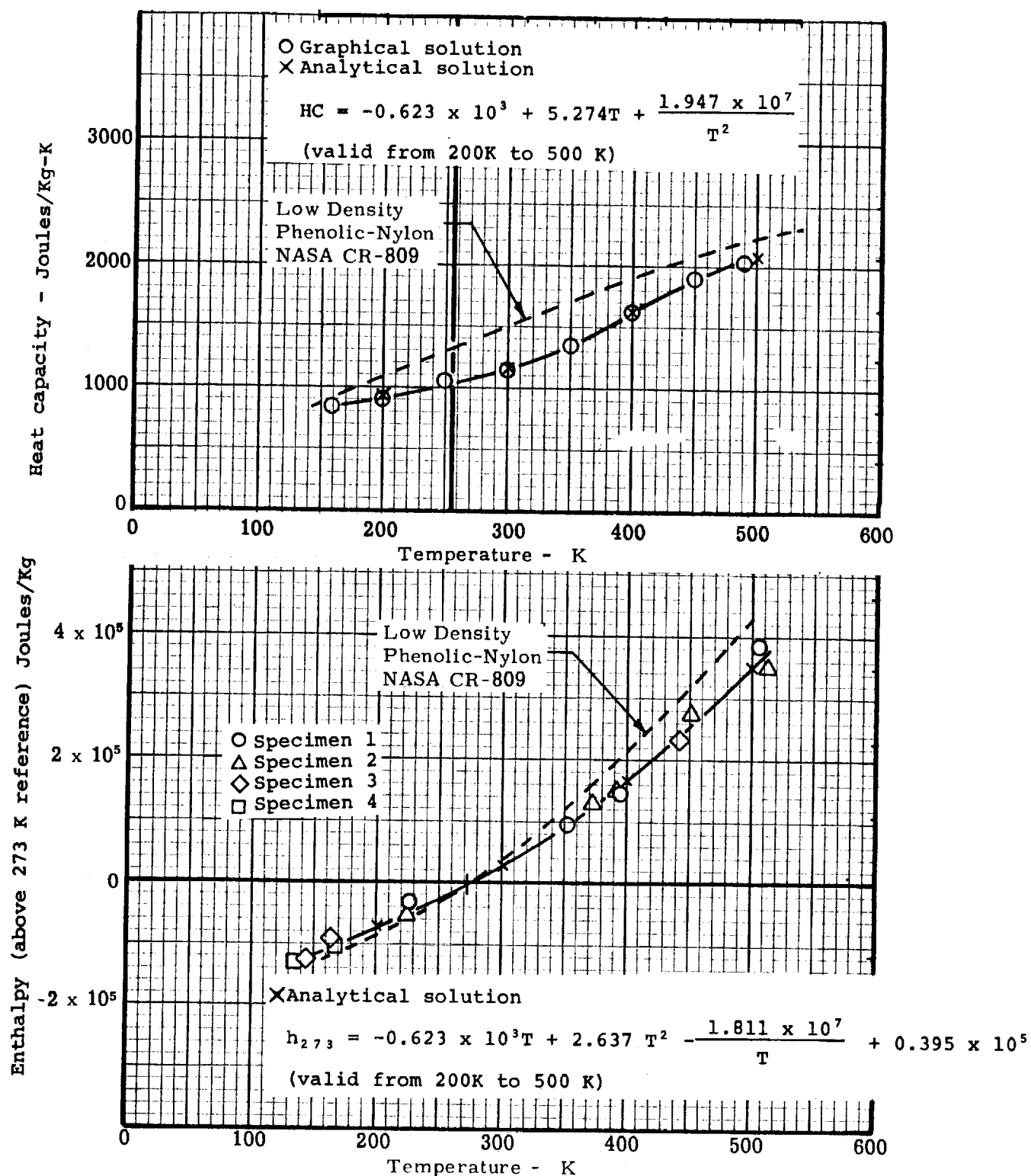
Figure 29. Enthalpy and heat capacity of virgin MG-58, Phenolic-Nylon in Phenolic-Glass Honeycomb

The upper graph shows Heat capacity - Joules/Kg-K versus Temperature - K:

○ Graphical solution
✗ Analytical solution

$$HC = -0.623 \times 10^3 + 5.274T + \frac{1.947 \times 10^7}{T^2}$$

(valid from 200K to 500 K)

Low Density Phenolic-Nylon NASA CR-809

The lower graph shows Enthalpy (above 273 K reference) Joules/Kg versus Temperature - K:

Low Density Phenolic-Nylon NASA CR-809

○ Specimen 1
△ Specimen 2
◇ Specimen 3
□ Specimen 4

✗ Analytical solution

$$h_{273} = -0.623 \times 10^3 T + 2.637\ T^2 - \frac{1.811 \times 10^7}{T} + 0.395 \times 10^5$$

(valid from 200K to 500 K)

177

Top figure:

MG-45, charred
in NASA arc-jet

Virgin MG-1

Heat capacity – Joules/Kg-K

O Graphical Solution
X Analytical Solution

$$HC = 1.676 \times 10^3 + 1.064 \times 10^{-3}T - \frac{1.717 \times 10^8}{T^2}$$
(equation valid from 500 K to 1500 K)

Temperature – K

Bottom figure:

<u>Adiabatic Calorimeter</u>

● Specimen 1
▲ Specimen 2

<u>Ice Calorimeter</u>
O Specimen 1
△ Specimen 2
◇ Specimen 1000-10-3 #1
□ Specimen 1000-10-3 #2

Flags denote data obtained
after exposure at maximum
temperature level

X Analytical Solution

$$h_{273} = 1.676 \times 10^3 T + 0.532 \times 10^{-3}T^2$$
$$+ \frac{1.081 \times 10^8}{T} - 8.532 \times 10^5$$

(equation valid from 500 K to 1500K)

MG-45, Silicone Elastomer, Charred
in NASA Arc-Jet

Enthalpy – Joules/Kg

Temperature – K

Figure 30.   Enthalpy and heat capacity of MG-1, Silicone-Phenolic, charred at 1000 K

178
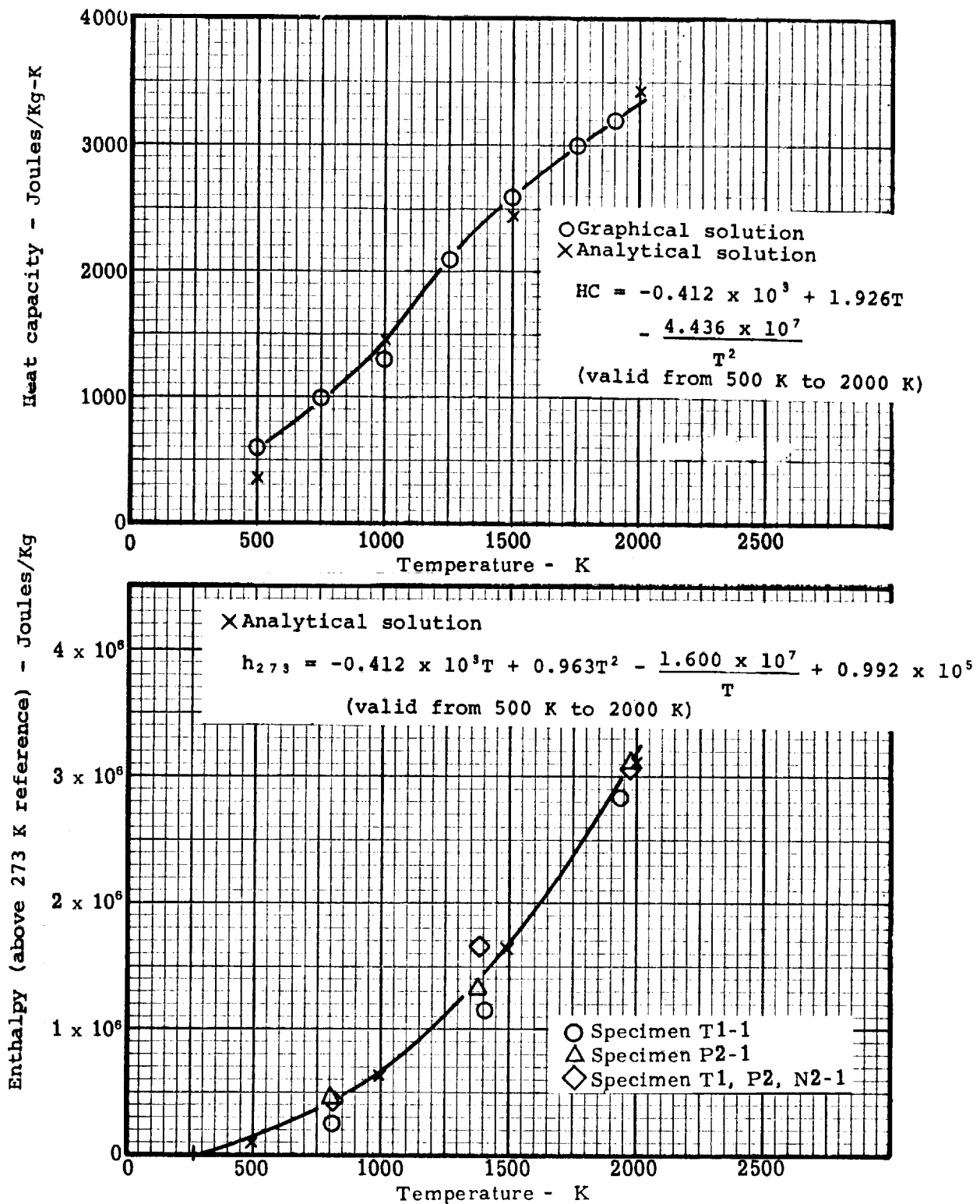
Figure 31. Enthalpy and heat capacity of MG-45, Silicone-Phenolic in Phenolic-Glass Honeycomb, charred in NASA arc-jet

179
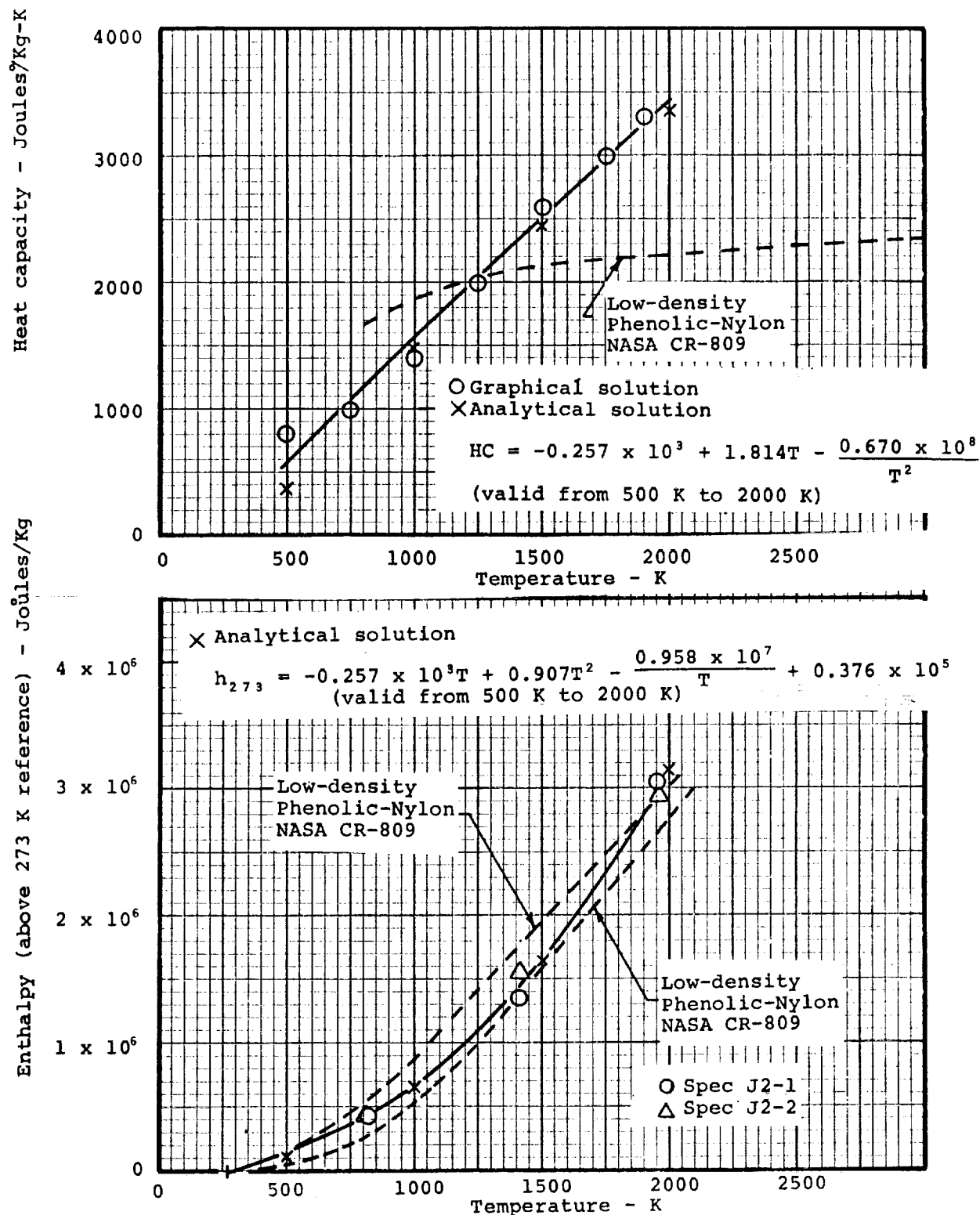
Figure 32. Enthalpy and heat capacity of MG-58, Phenolic-Nylon
in Phenolic-Glass Honeycomb, charred in NASA arc-jet

180
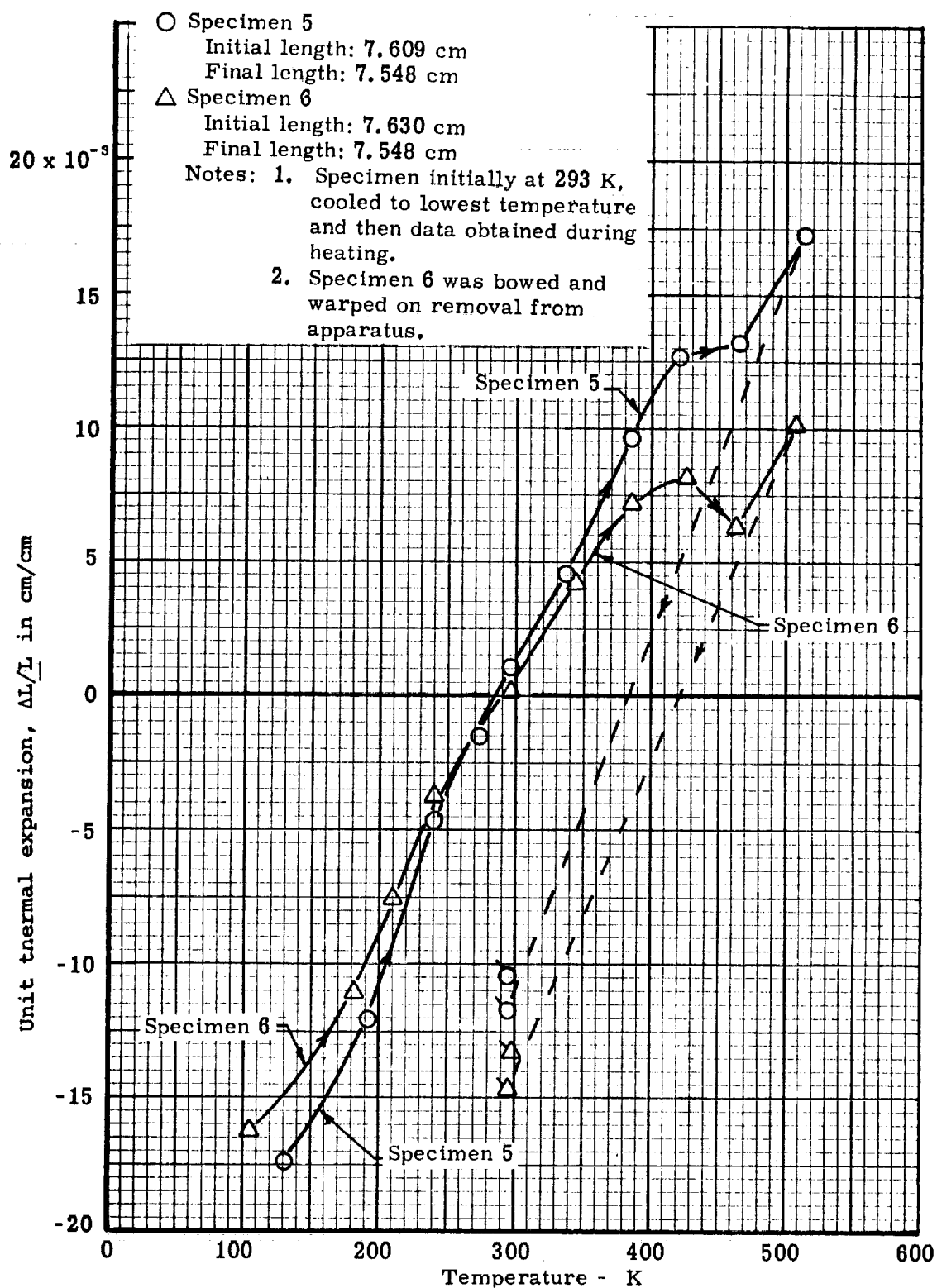
Figure 33. Thermal expansion of virgin MG-1, Silicone-Phenolic, in the X Direction

181
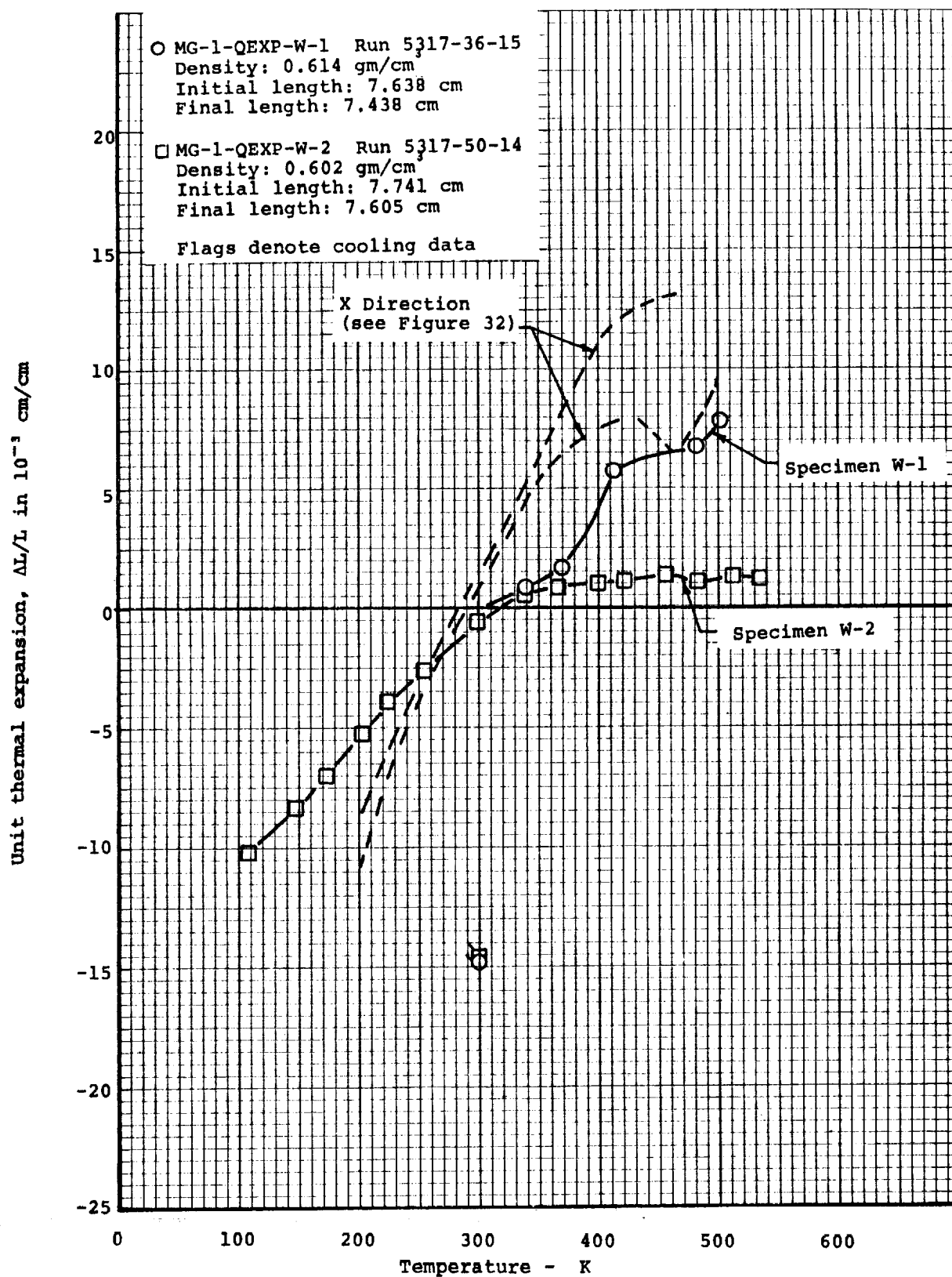
Figure 34. Thermal expansion of MG-1, Silicone-Phenolic, in the Y Direction

182
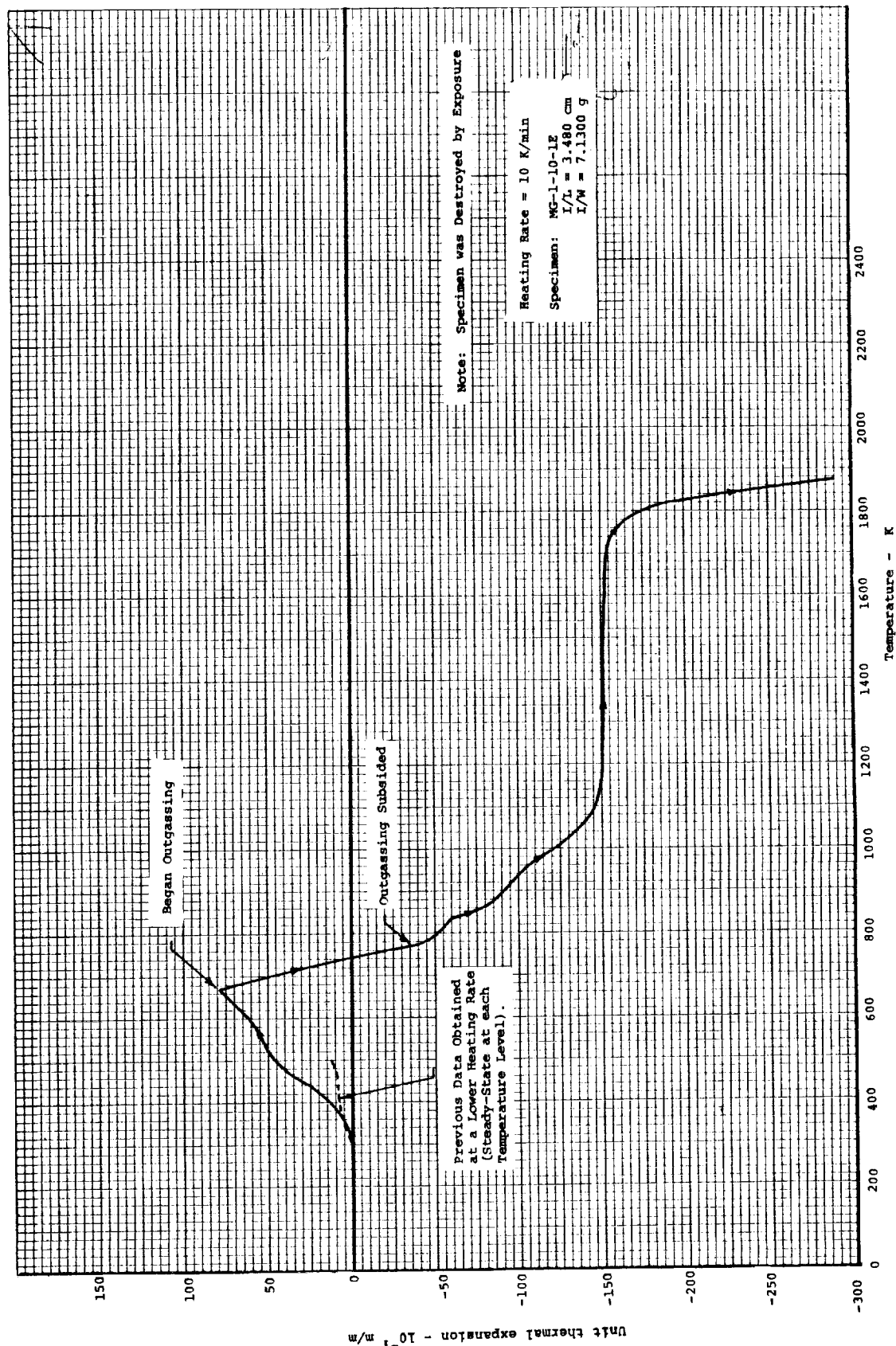
Figure 35. Thermal expansion of virgin MG-1, Silicone-Phenolic, at a constant temperature-rise rate of 10 K/min

183
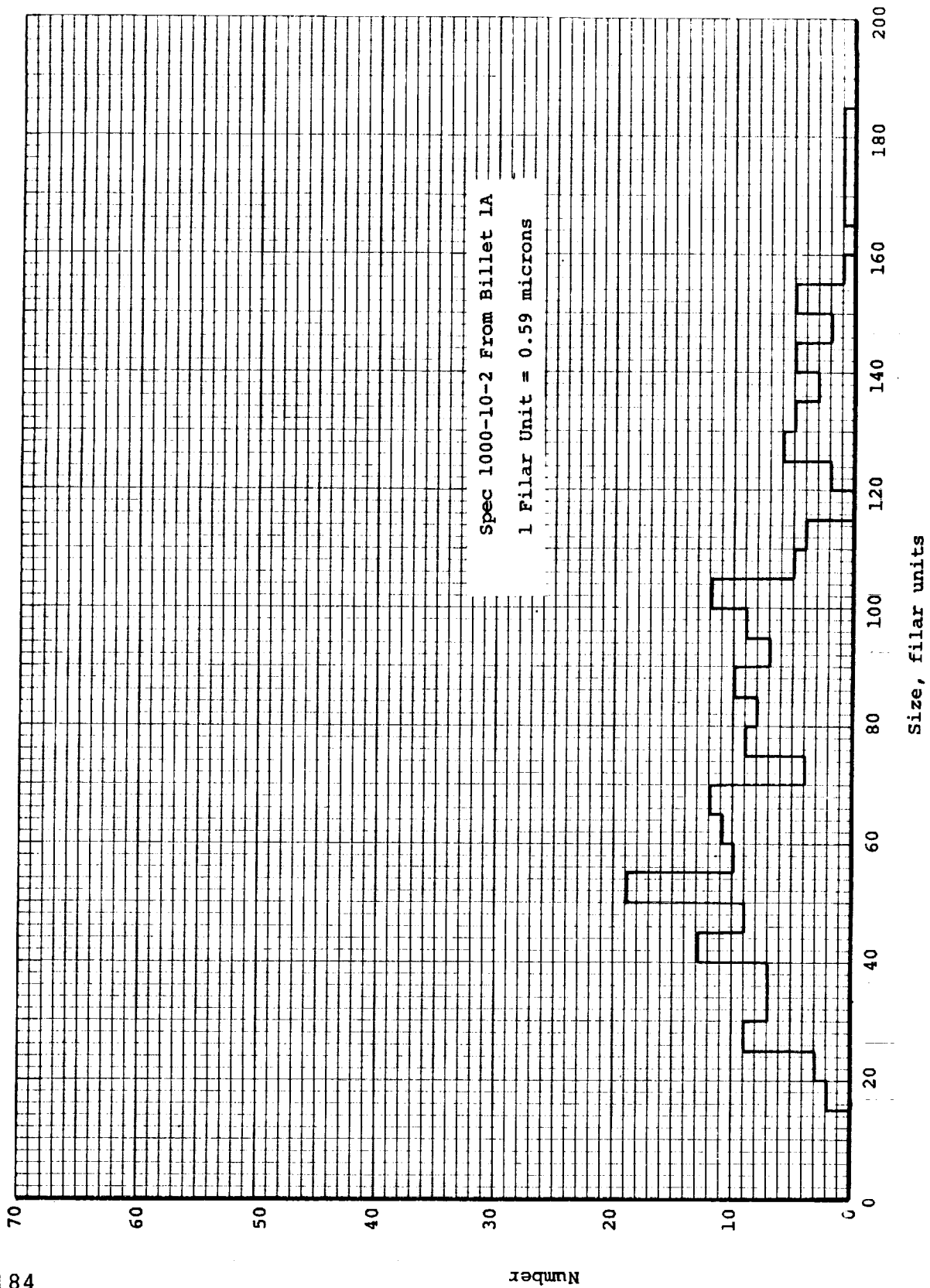
Figure 36. Distribution of unfilled microballoon diameters measured on a plane section through MG-1 charred at 1000 K
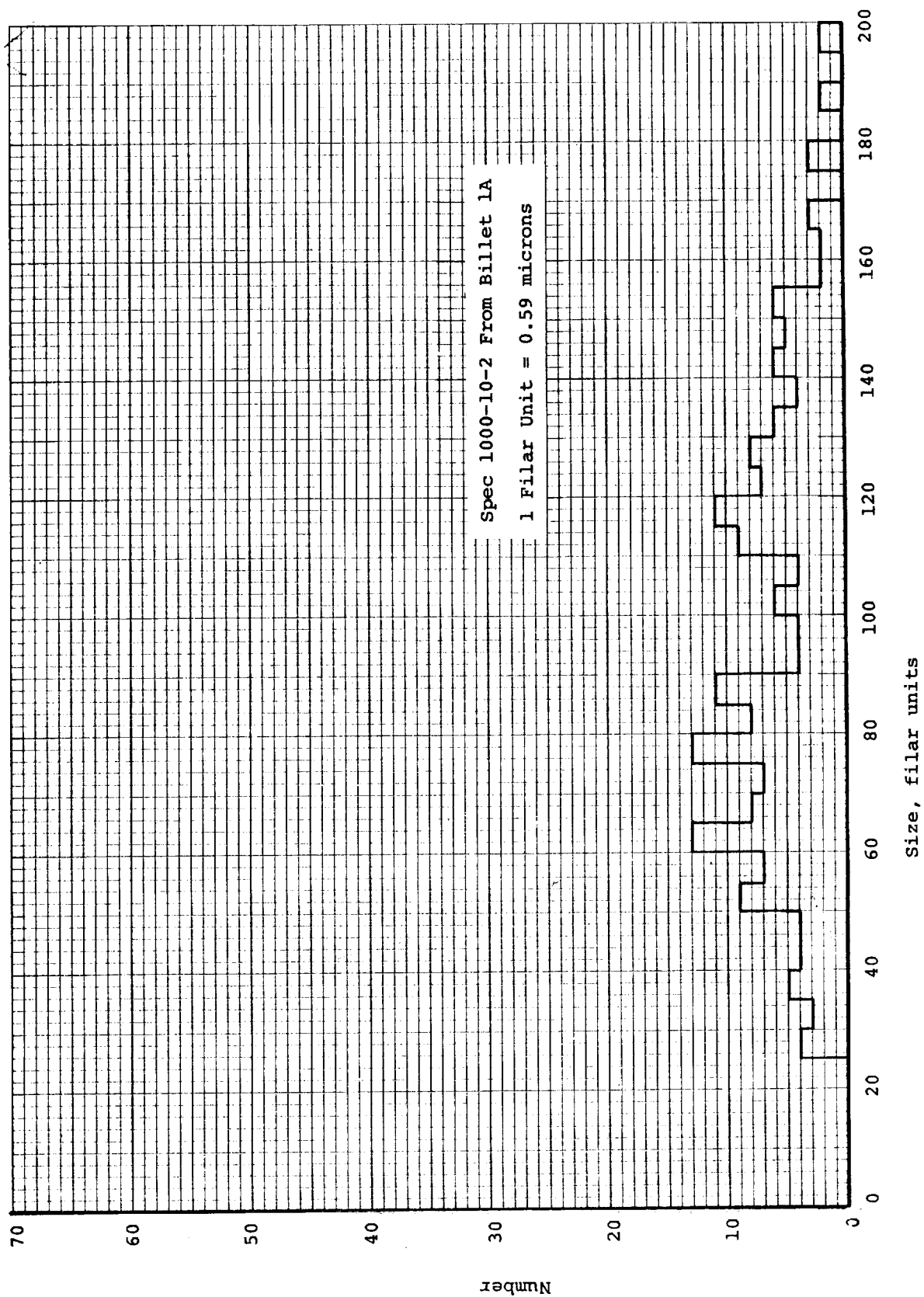
Figure 37. Distribution of filled microballoon diameters measured on a plane section through MG-1 charred at 1000 K

185
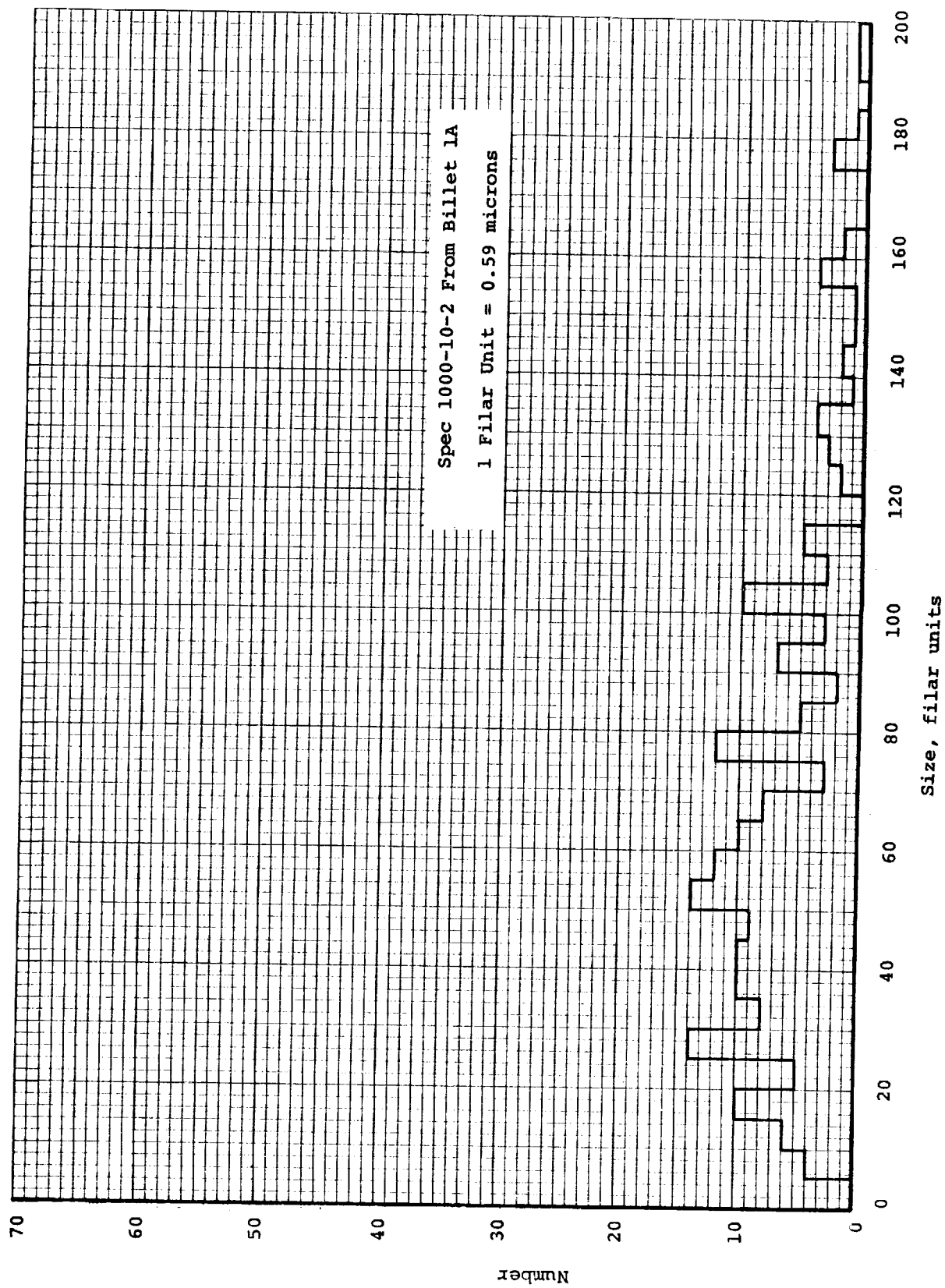
Figure 38. Distribution of open porosity measured on a plane section through MG-1 charred at 1000 K

186
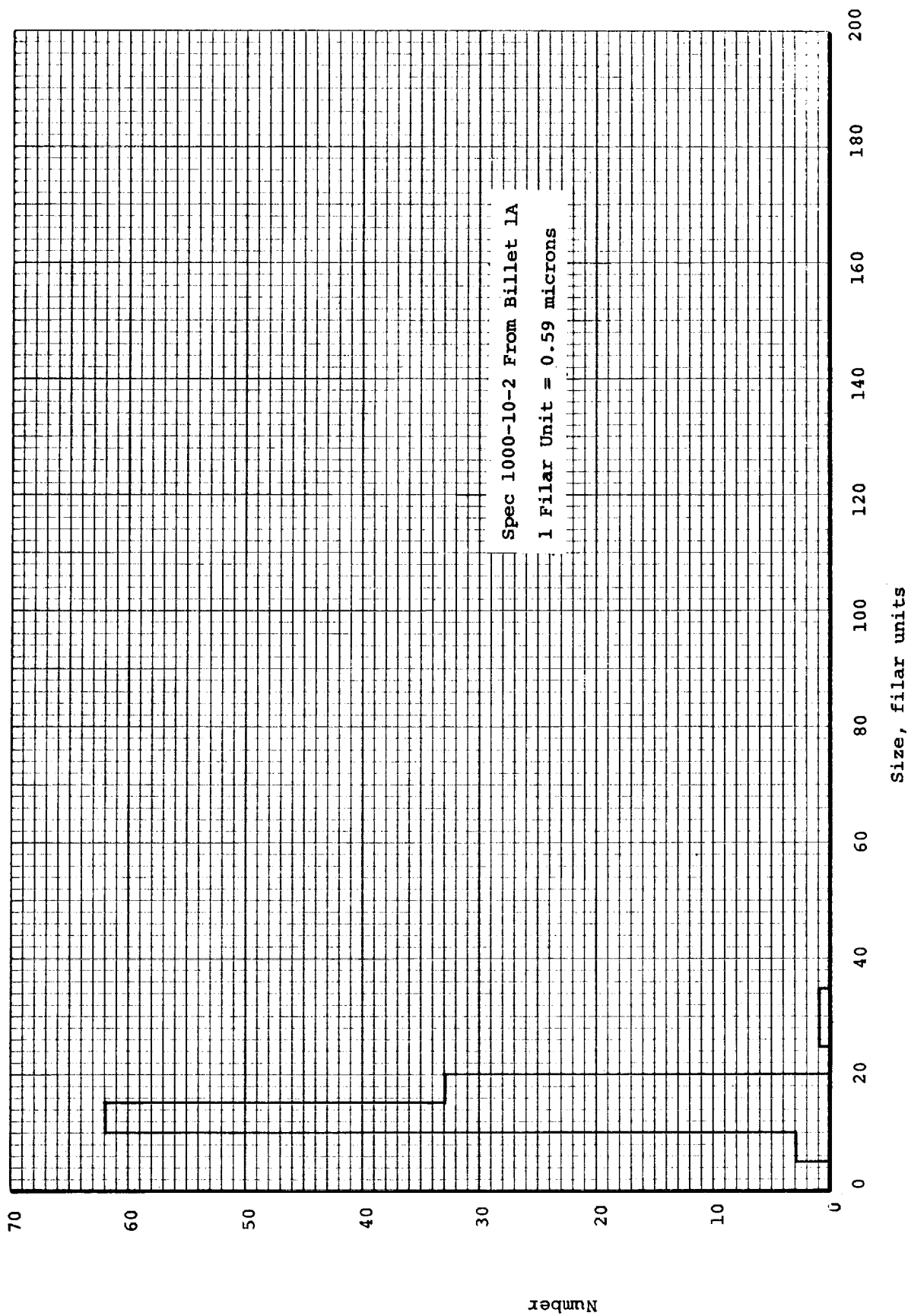
Figure 39. Distribution of fiber diameters measured on a plane section through MG-1 charred at 1000 K

Spec 1000-10-2 From Billet 1A

1 Filar Unit = 0.59 microns

Size, filar units

Number

187
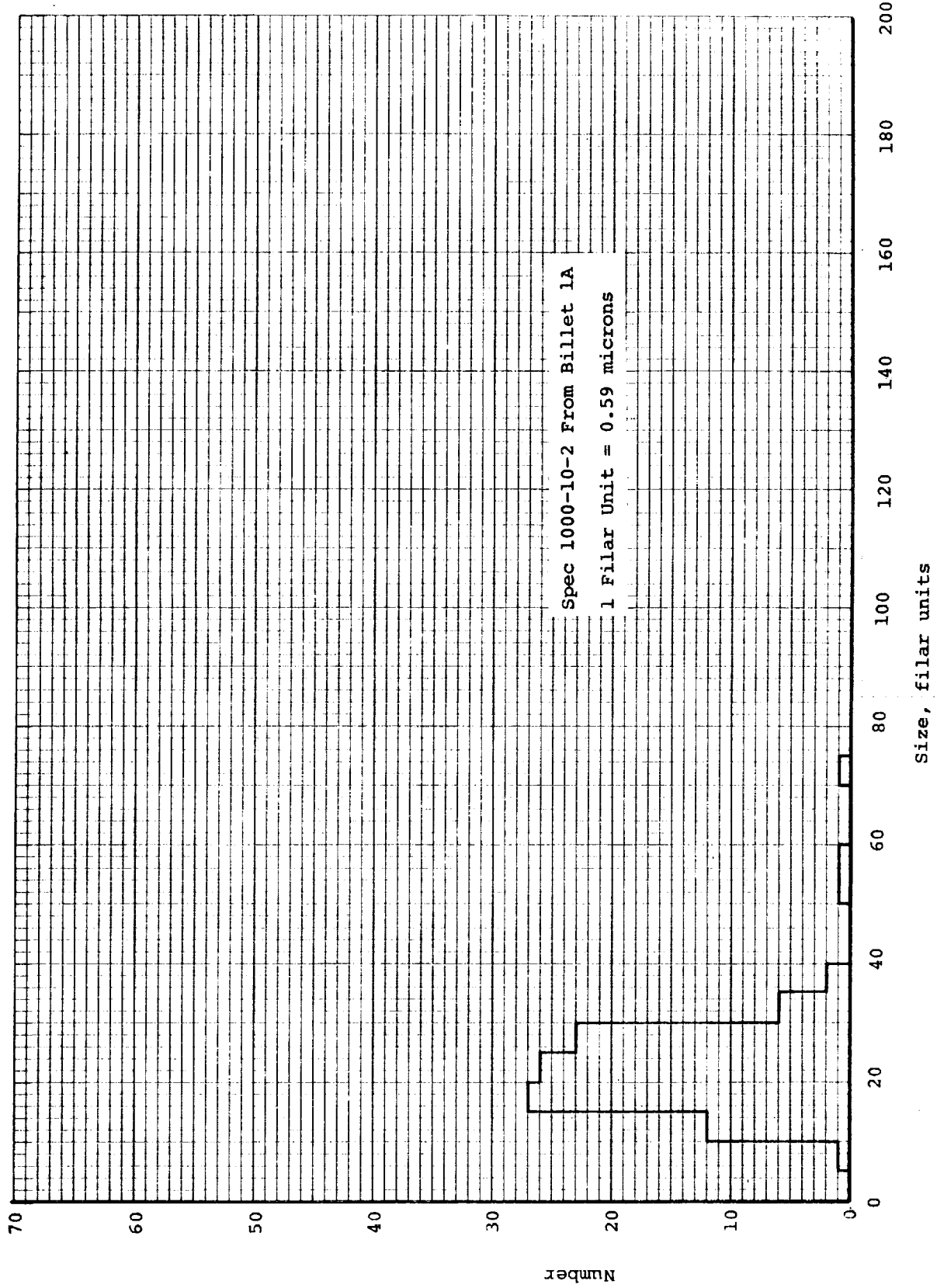
Figure 40. Distribution of small solid particles (not considered wall material) on a plane section through MG-1 charred at 1000 K

188
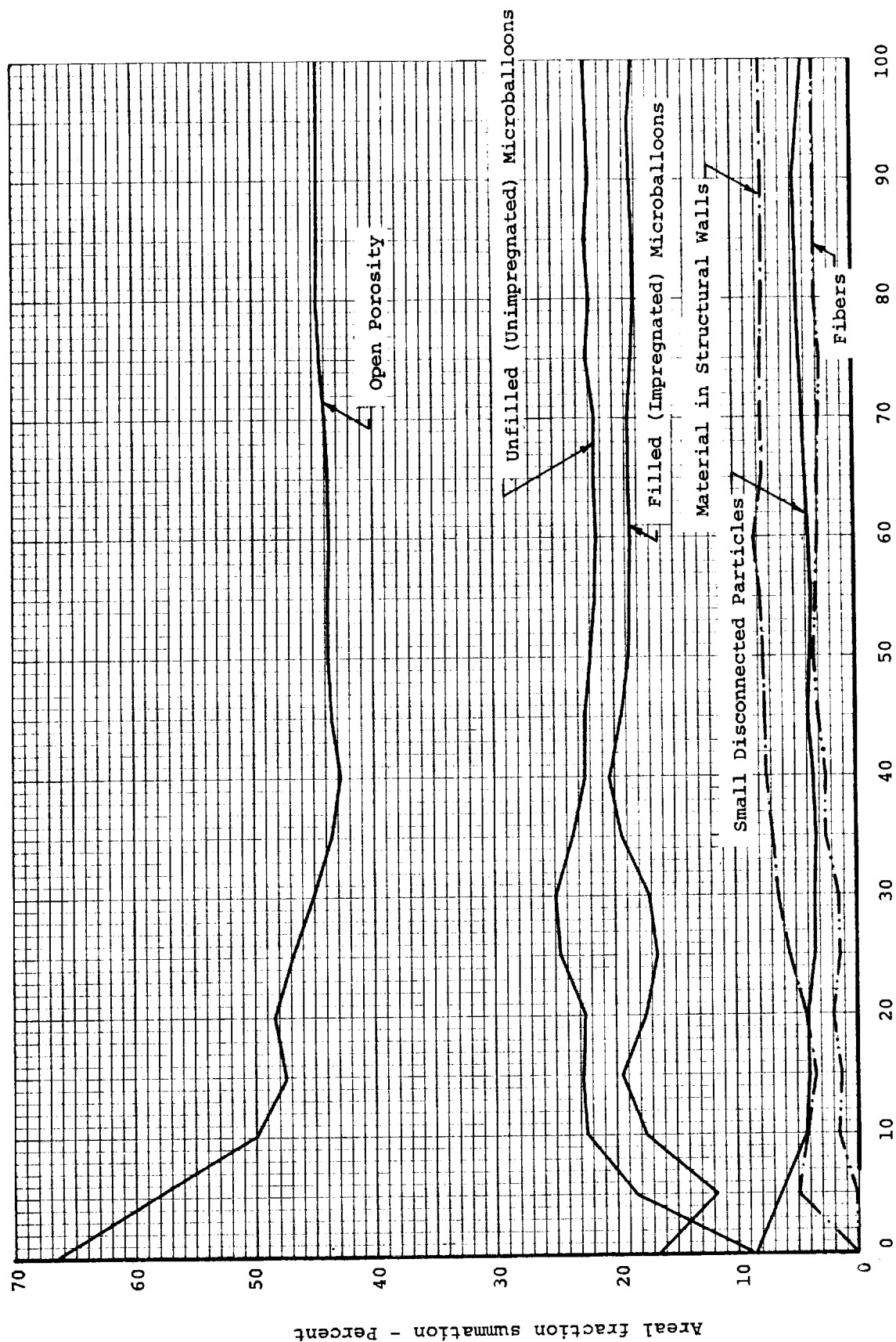
Figure 41. Analysis of point count showing percent summation as a function of points applied for constituents of MG-1 which was charred at 1000 K and vacuum impregnated

189

1 Filar Unit = 0.43 microns

Empty Microballoons

Filled Microballoons
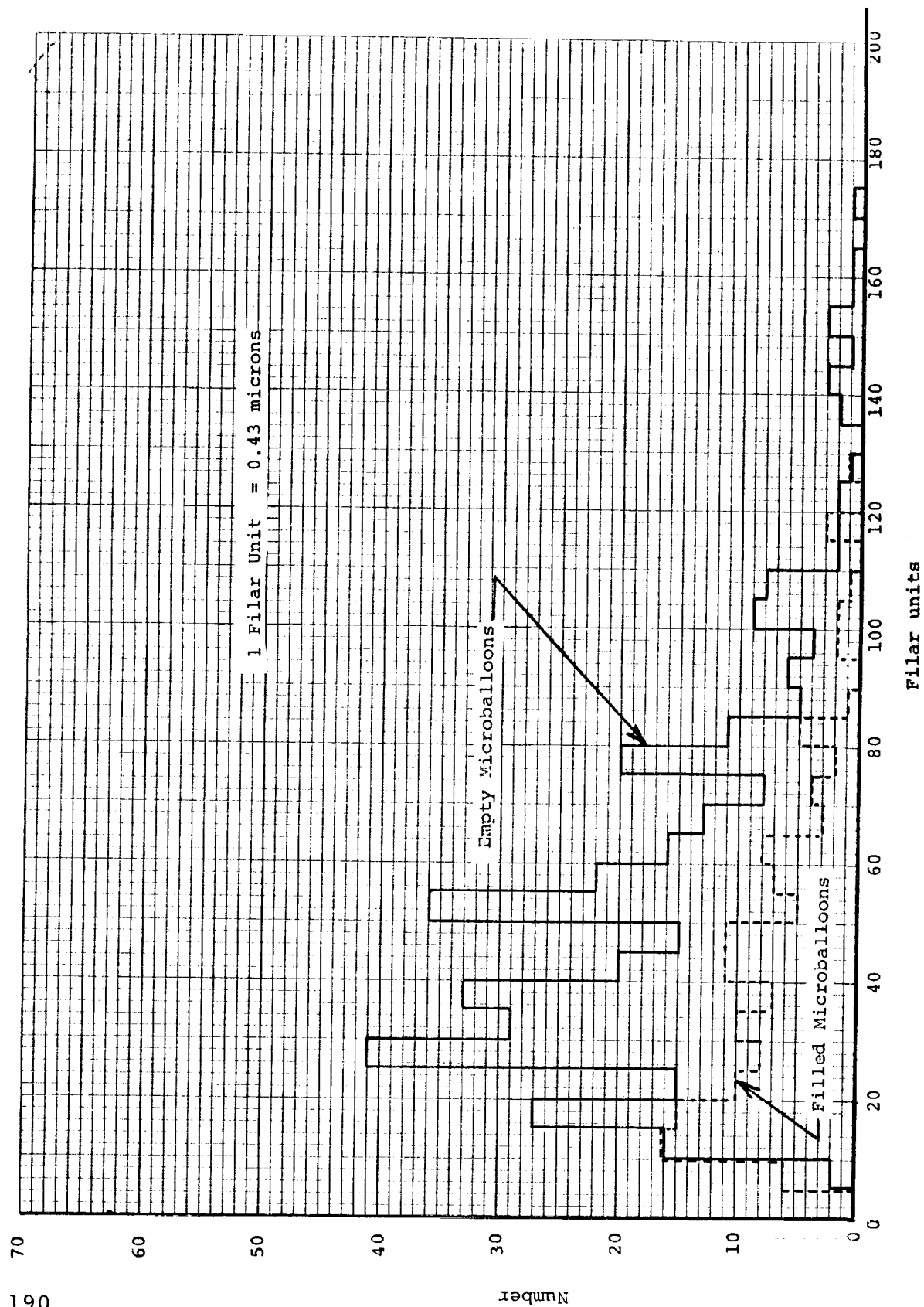
Figure 42. Distribution of microballoon diameters measured on a plane section through the MG-45 virgin material

190
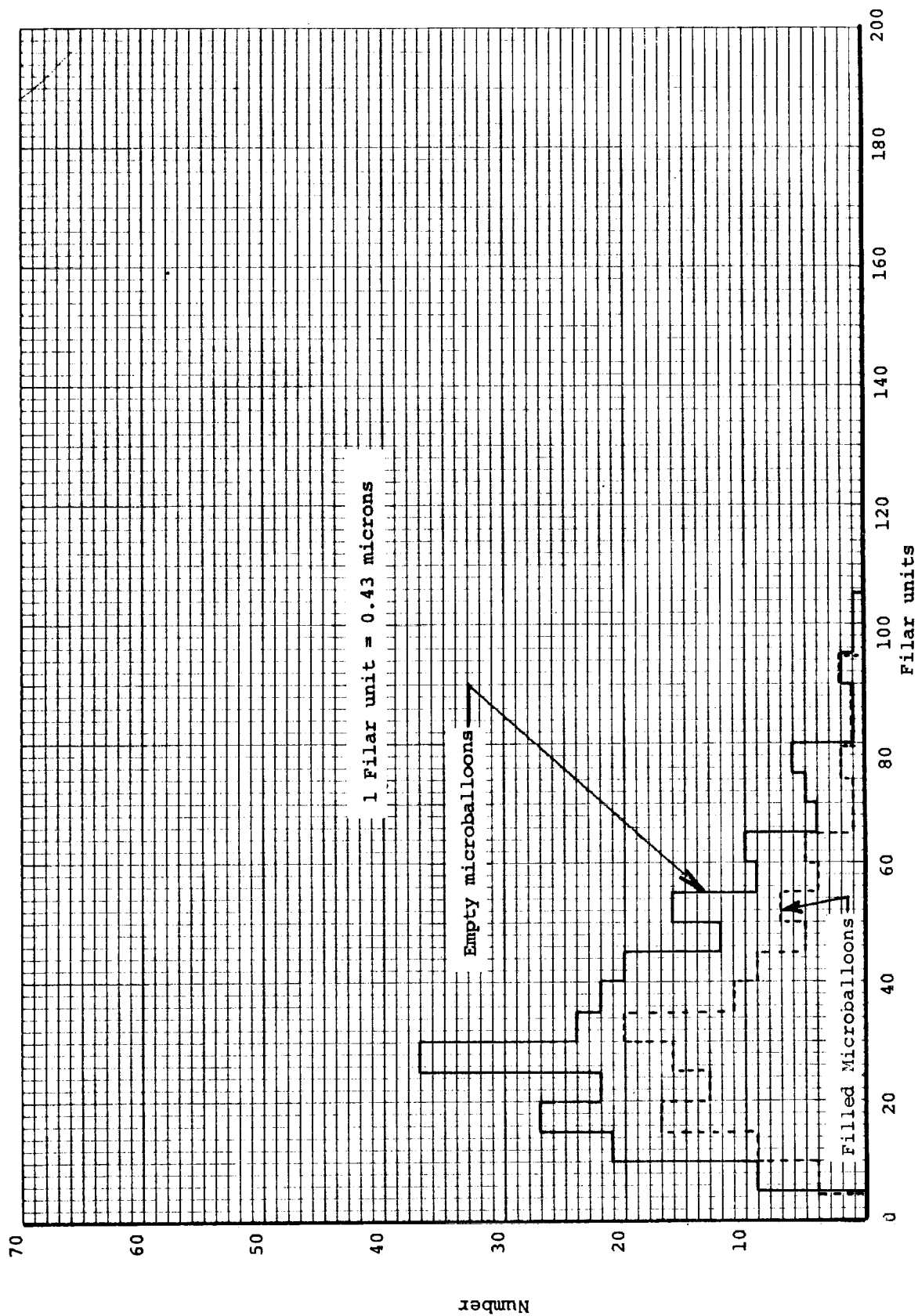
Figure 43. Distribution of microballoon diameters measured on a plane section through the MG-45 charred material

191
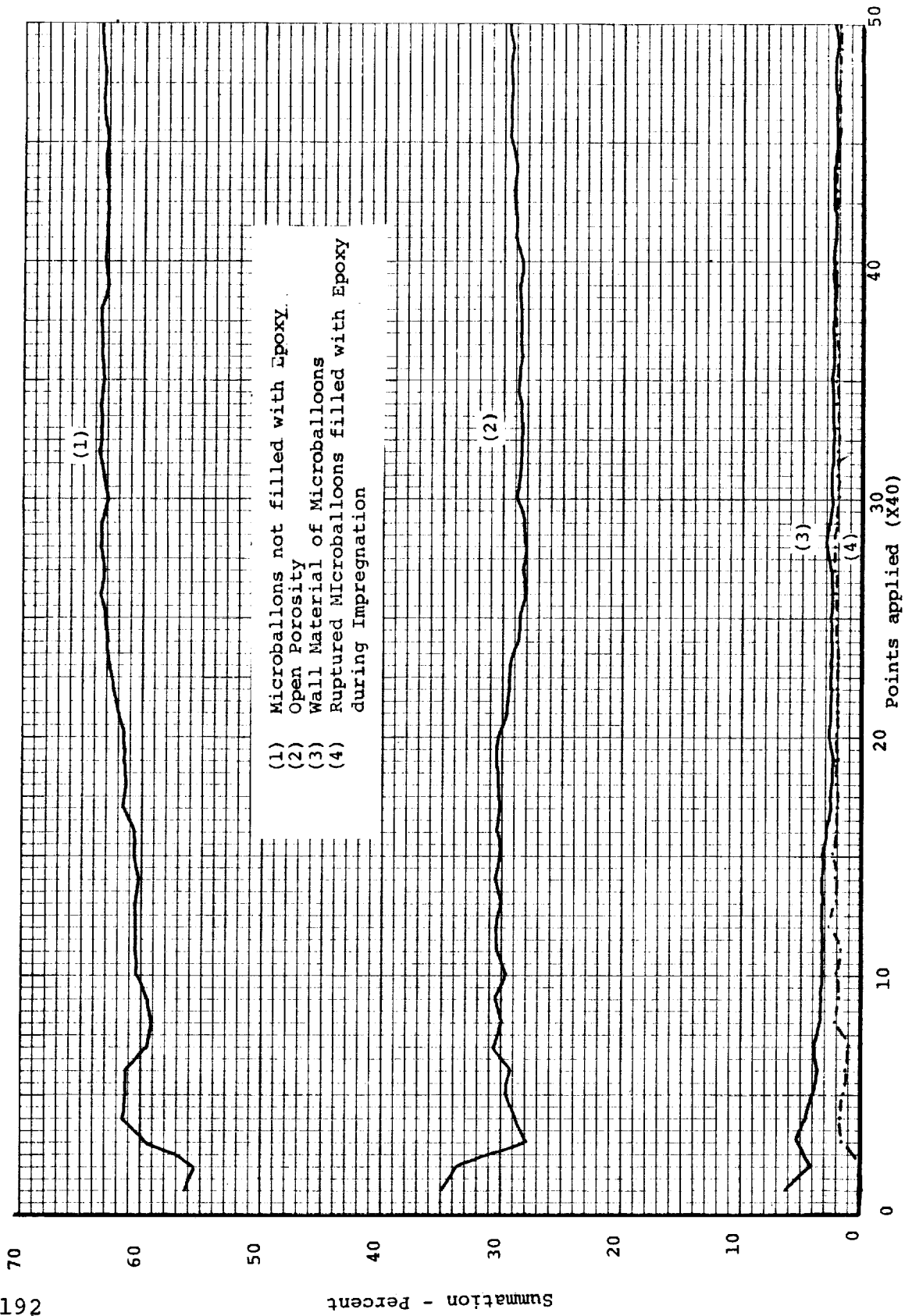
Figure 44. Analysis of point count showing percent summation as a function of points applied for constituents of vacuum impregnated MG-45 virgin material

(1) Microballons not filled with Epoxy.
(2) Open Porosity
(3) Wall Material of Microballoons
(4) Ruptured Microballoons filled with Epoxy during Impregnation
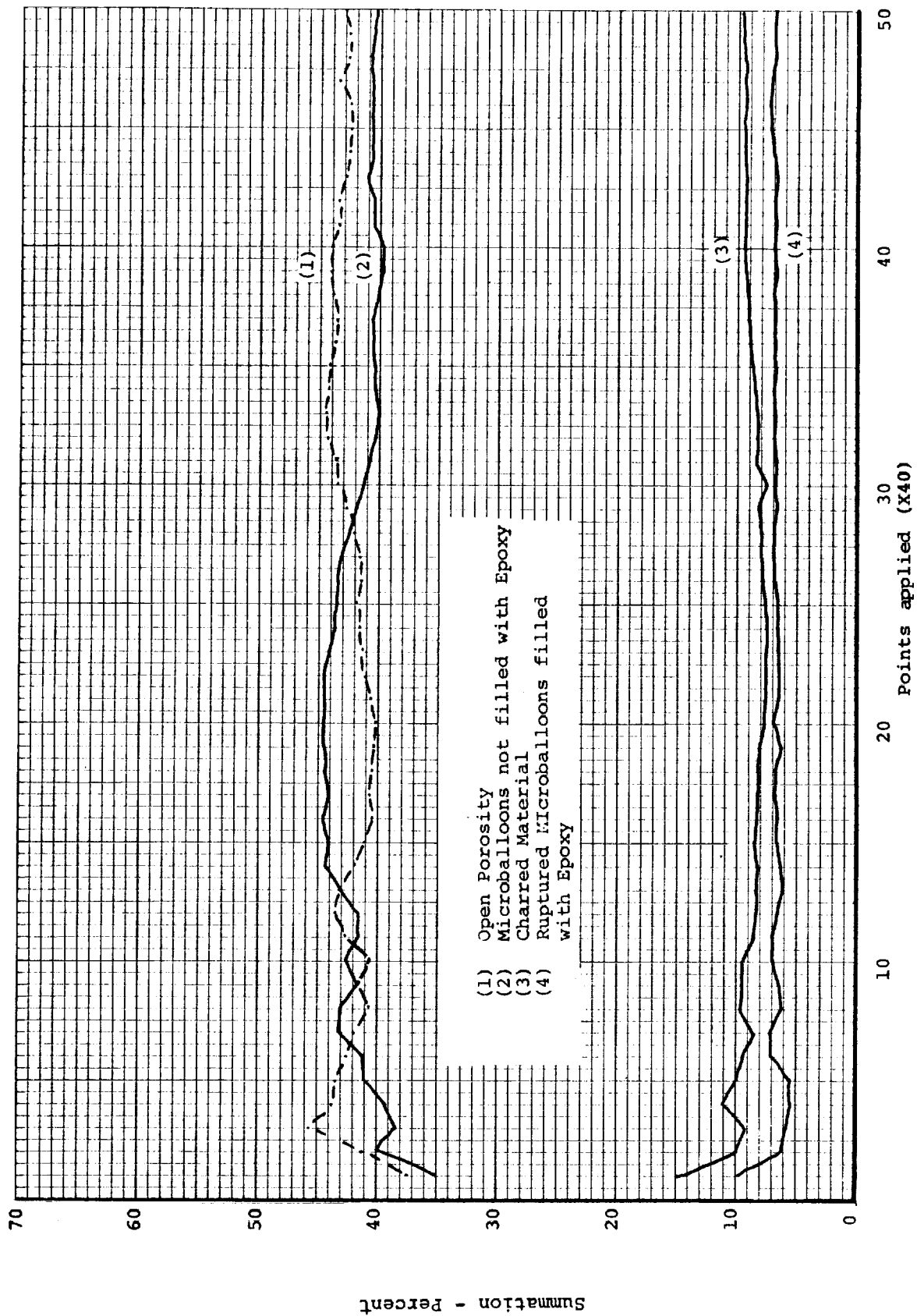
Figure 45. Analysis of point count showing percent summation as a function of points applied for constituents of vacuum impregnated MG-45 charred material

193
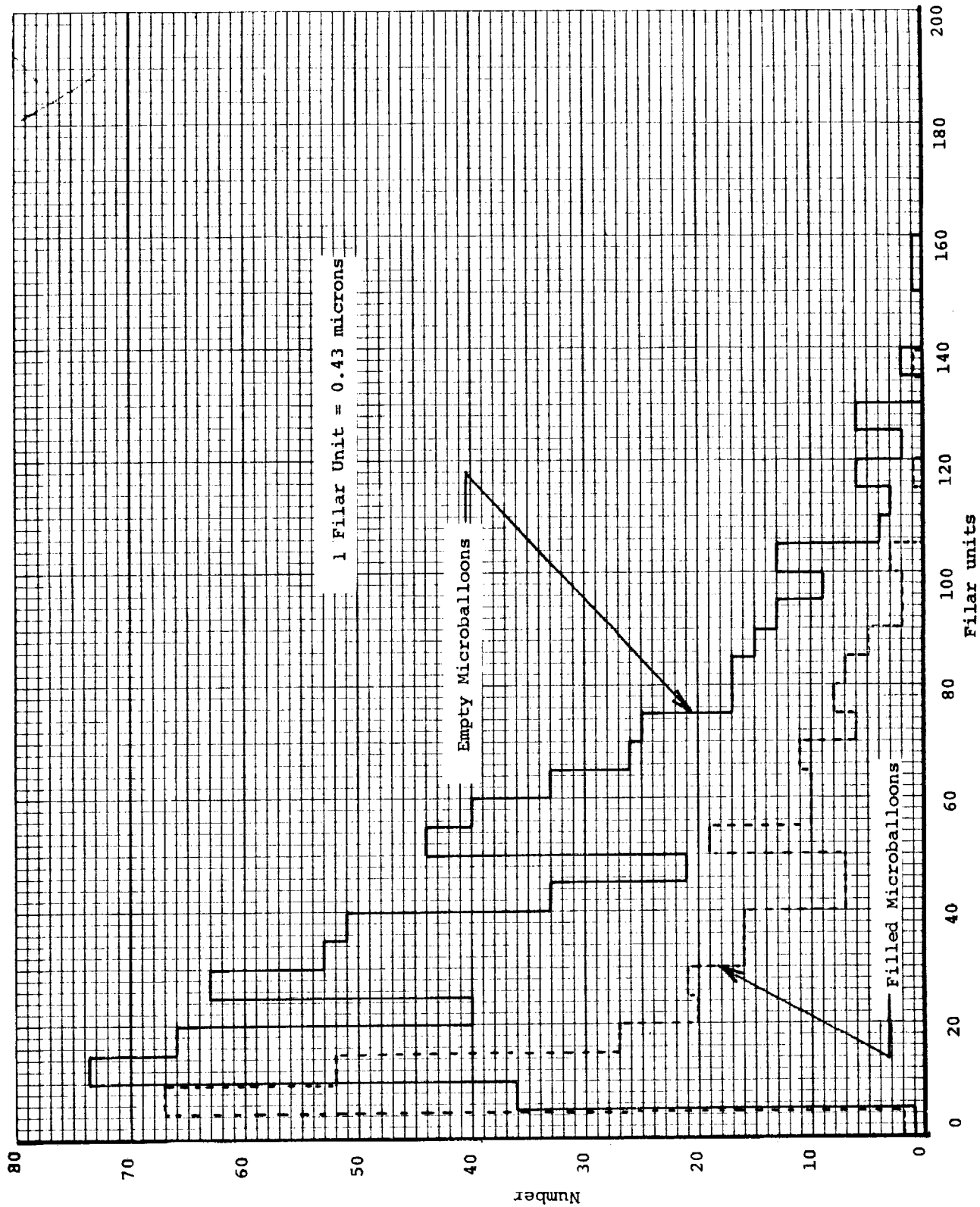
Figure 46. Distribution of microballoon diameters measured on a plane section through the MG-58 virgin material

194
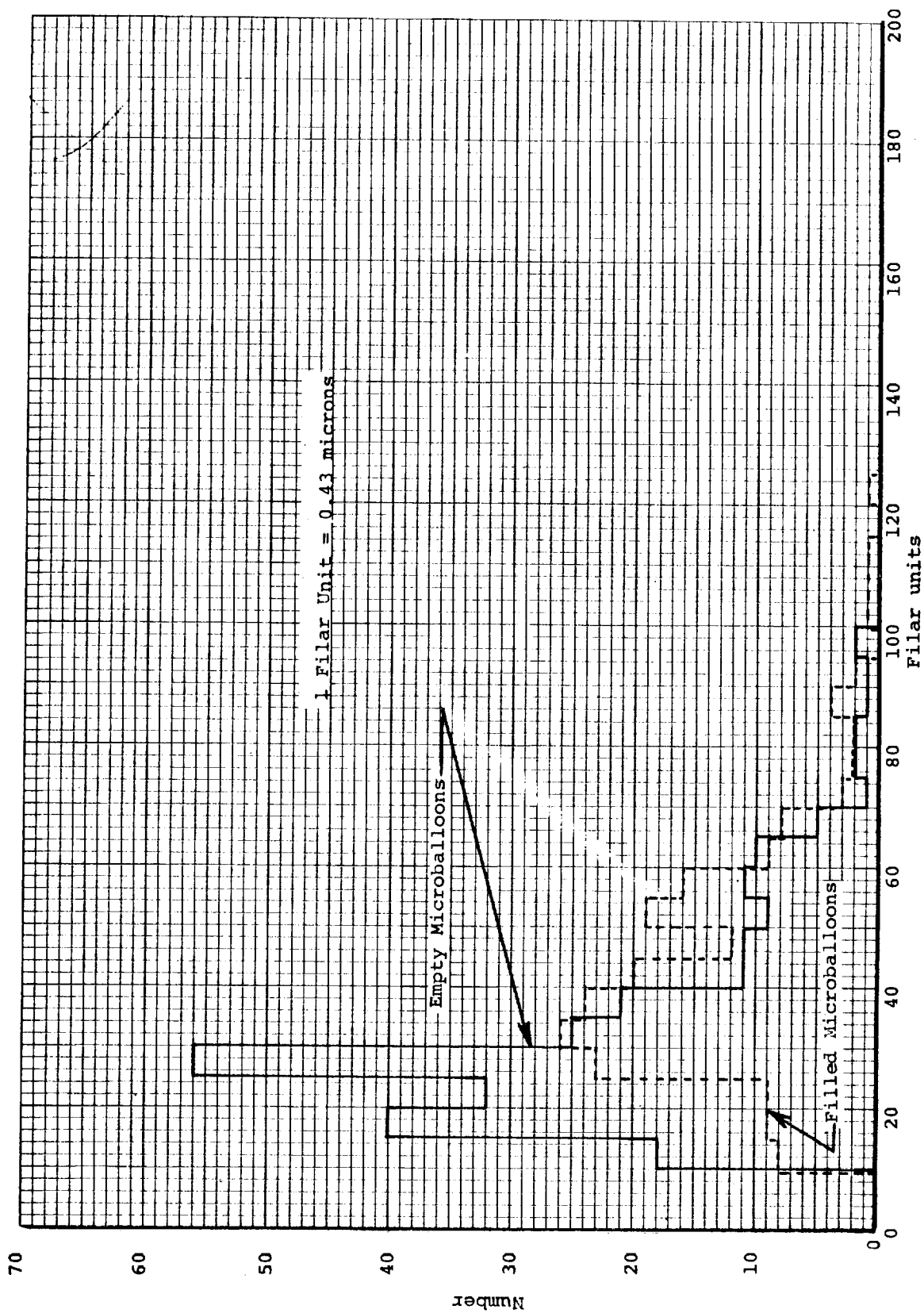
Figure 47. Distribution of microballoon diameters measured on a plane section through the MG-58 charred material

195
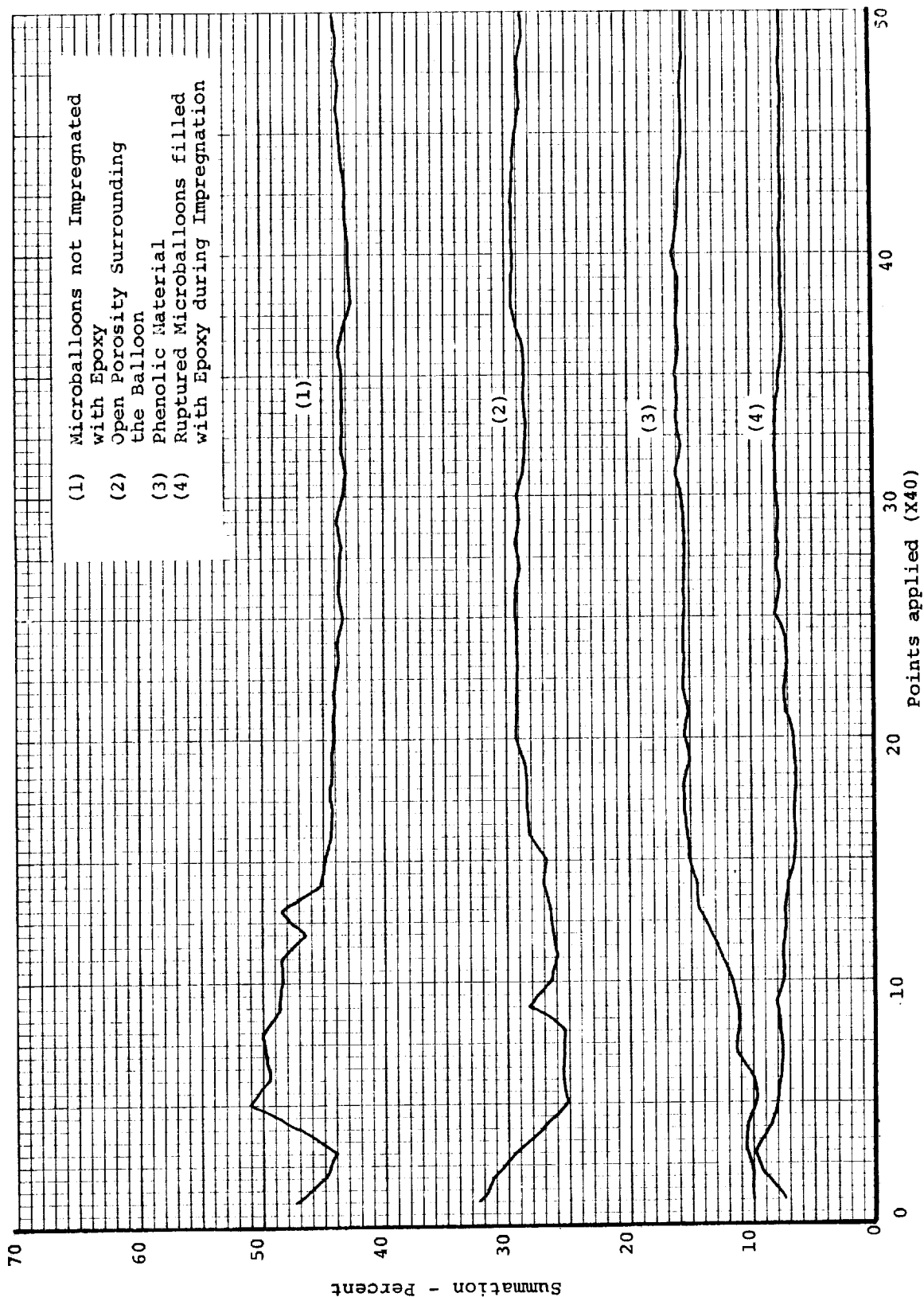
Figure 48. Analysis of point count showing percent summation as a function of points applied for constituents of vacuum impregnated MG-58 virgin material
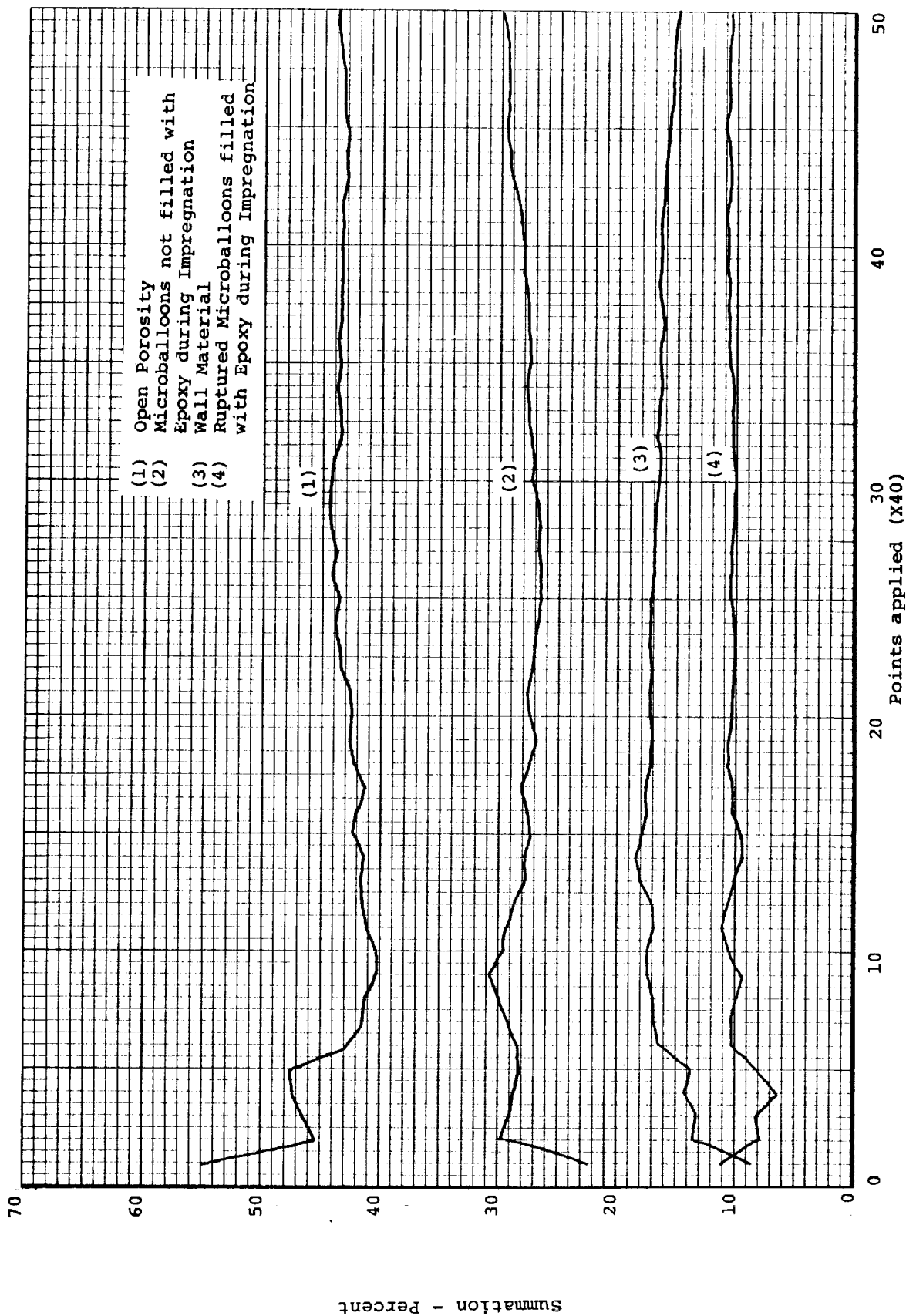
Figure 49. Analysis of point count showing percent summation as a function of points applied for constituents of vacuum impregnated MG-58 charred material
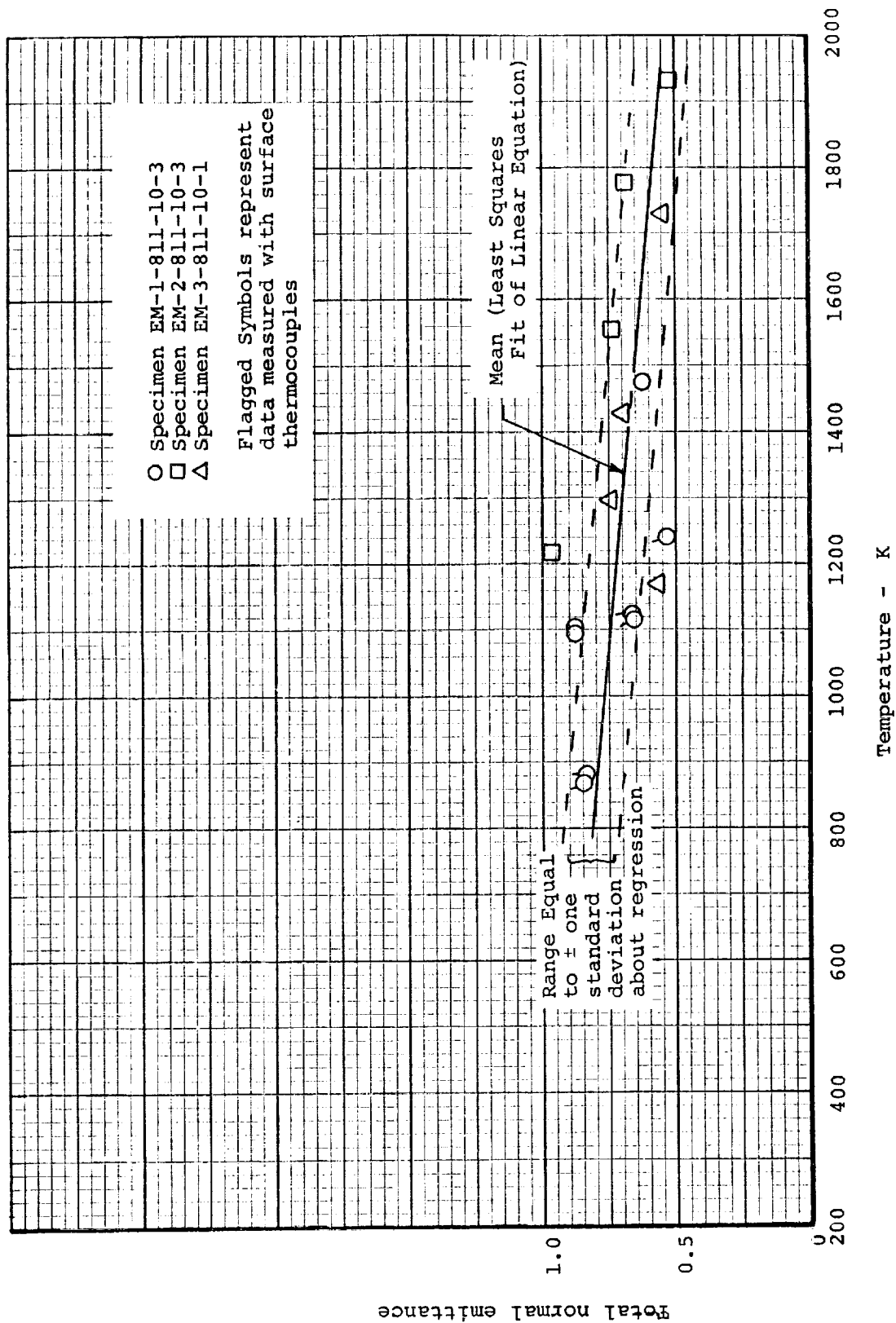
Figure 50. The total normal emittance of MG-1 charred at 811 K

198
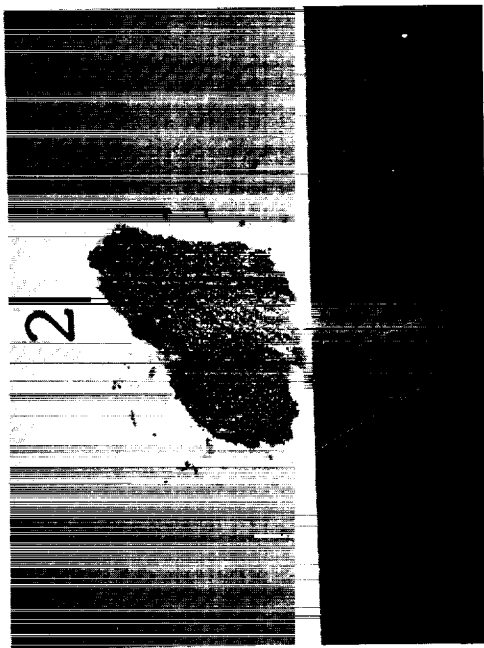
Spec EM-2-811-10-3

Spec EM-1-811-10-3

Spec EM-3-811-10-1

Figure 51. Photographs of the emittance specimens from MG-1 charred at 1000 K after exposure to temperature during the runs

199
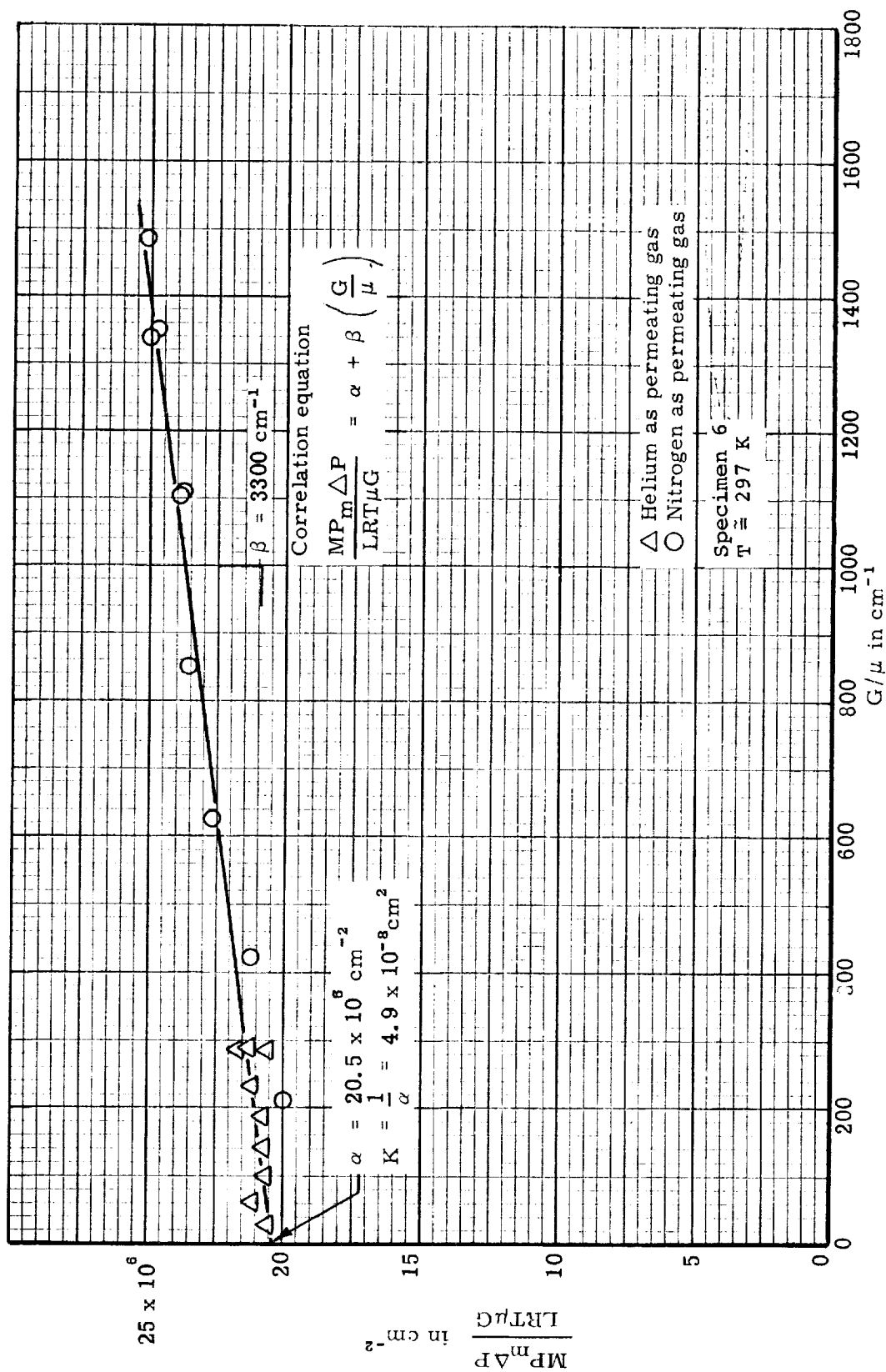
Figure 52. Cornell-Katz correlation of permeability data for virgin MG-45, Silicone-Phenolic in Phenolic-Glass Honeycomb, parallel to honeycomb cell

200

$$\frac{MP_m \Delta P}{LRT \mu G} = \alpha + \beta \left(\frac{G}{\mu}\right)$$

Correlation equation

$\beta = 3900 \text{ cm}^{-1}$

$\alpha = 20.0 \times 10^8 \text{ cm}^{-2}$

$K = \frac{1}{\alpha} = 5.0 \times 10^{-8} \text{cm}^2$

△ Helium as permeating gas
○ Nitrogen as permeating gas

Specimen 7
$T \cong 297$ K

$\frac{MP_m \Delta P}{LRT \mu G}$ in cm^{-2}

25×10^8
20
15
10
5
0

G/μ in cm^{-1}

0   200   400   600   800   1000   1200   1400   1600   1800
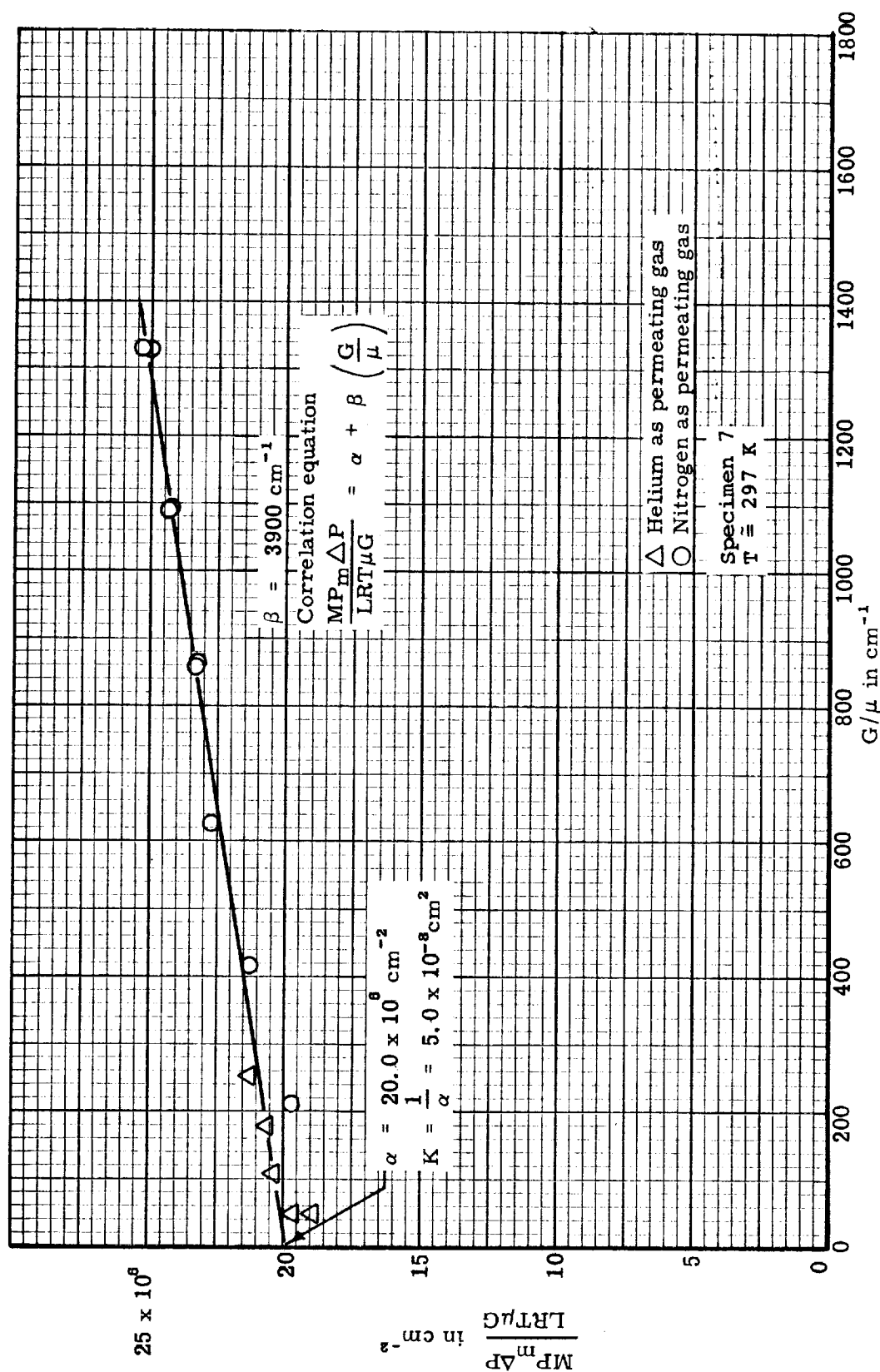
Figure 53. Cornell-Katz correlation of permeability data for virgin MG-45, Silicone-Phenolic in Phenolic-Glass Honeycomb, parallel to honeycomb cell
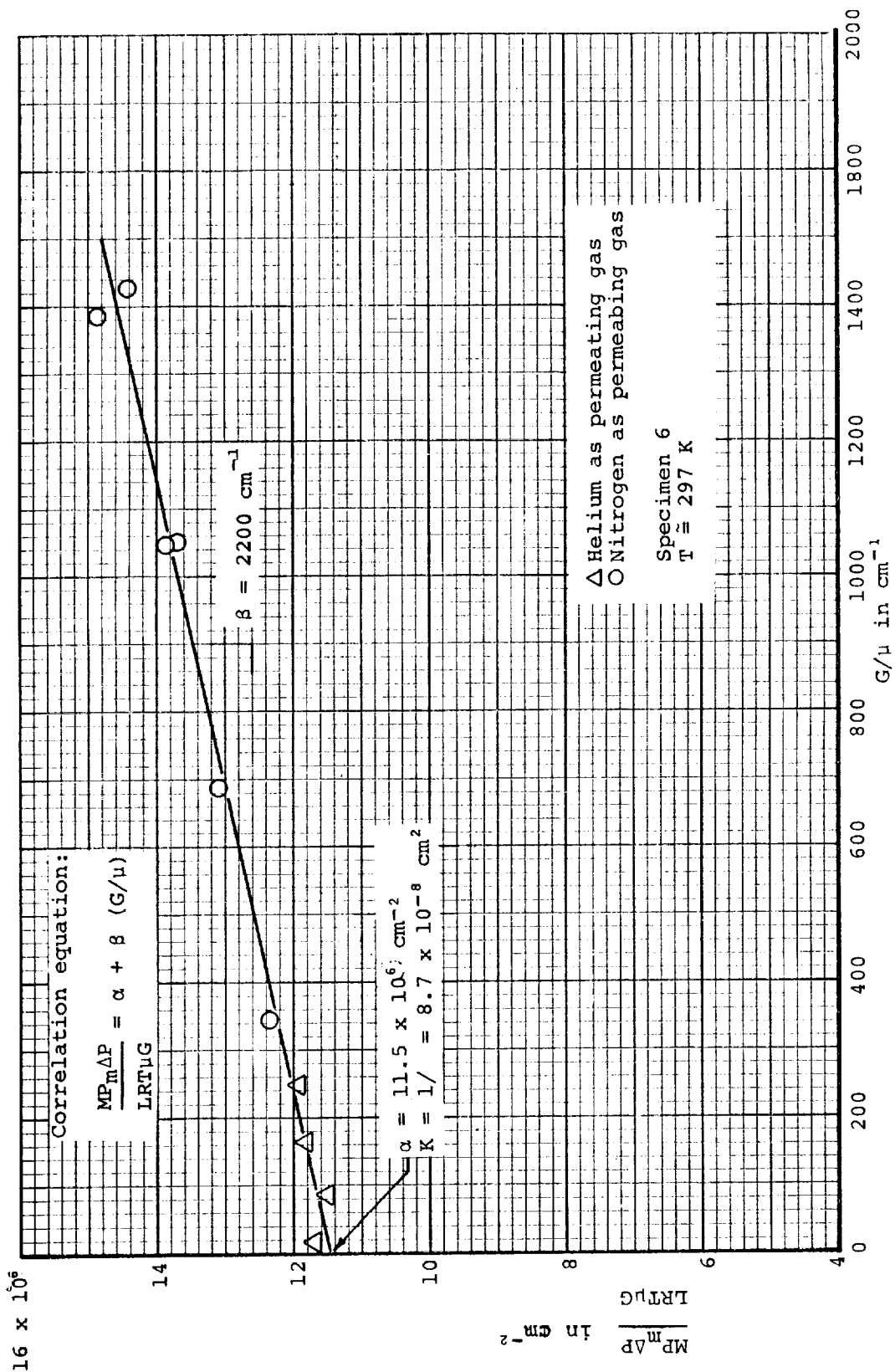
Figure 54. Cornell-Katz Correlation of permeability data for virgin MG-58, Phenolic-Nylon in Phenolic-Glass Honeycomb, parallel to honeycomb cell

202
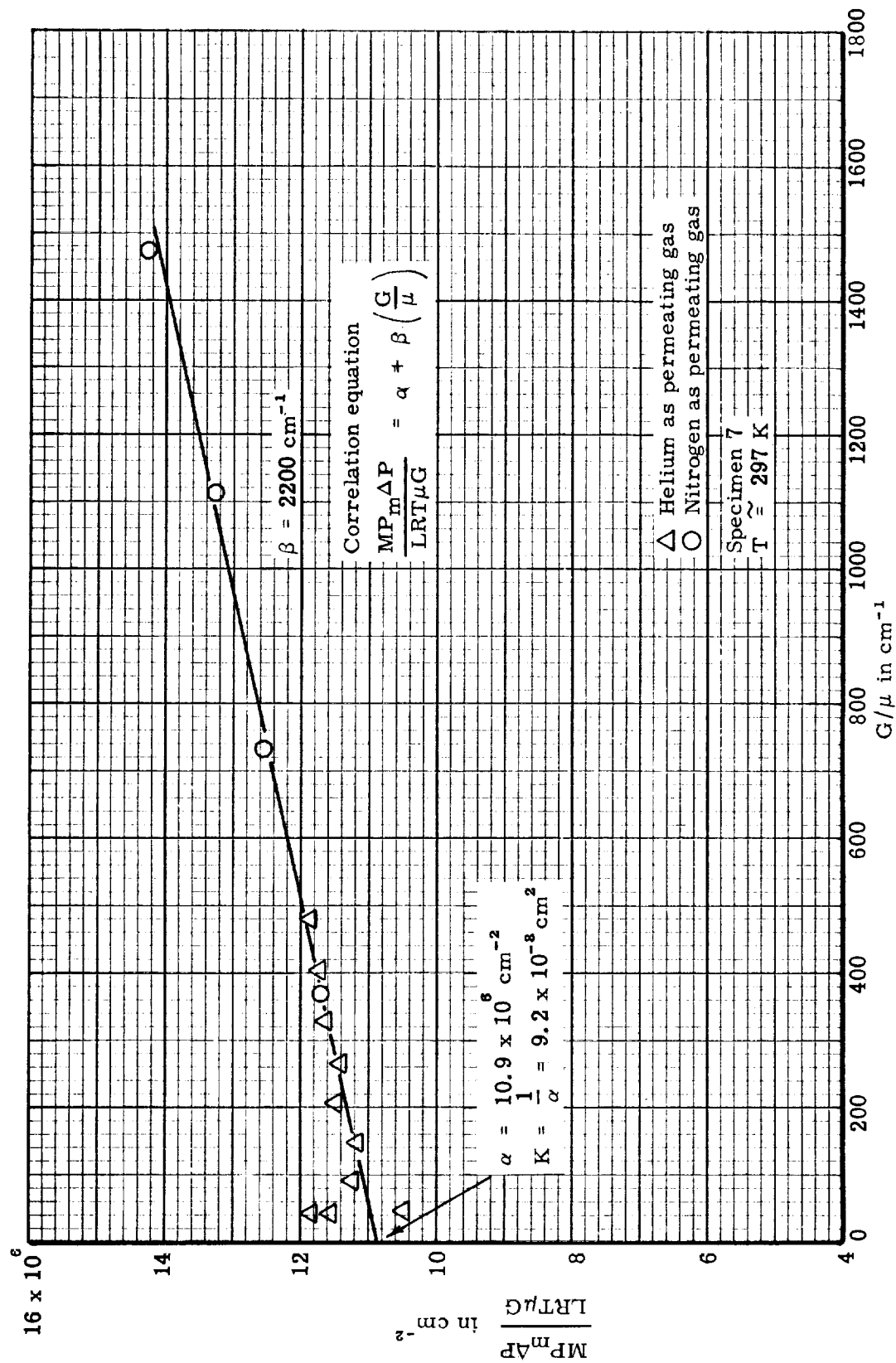
Figure 55. Cornell-Katz correlation of permeability data for virgin MG-58, Phenolic-Nylon in Phenolic-Glass Honeycomb, parallel to honeycomb cell
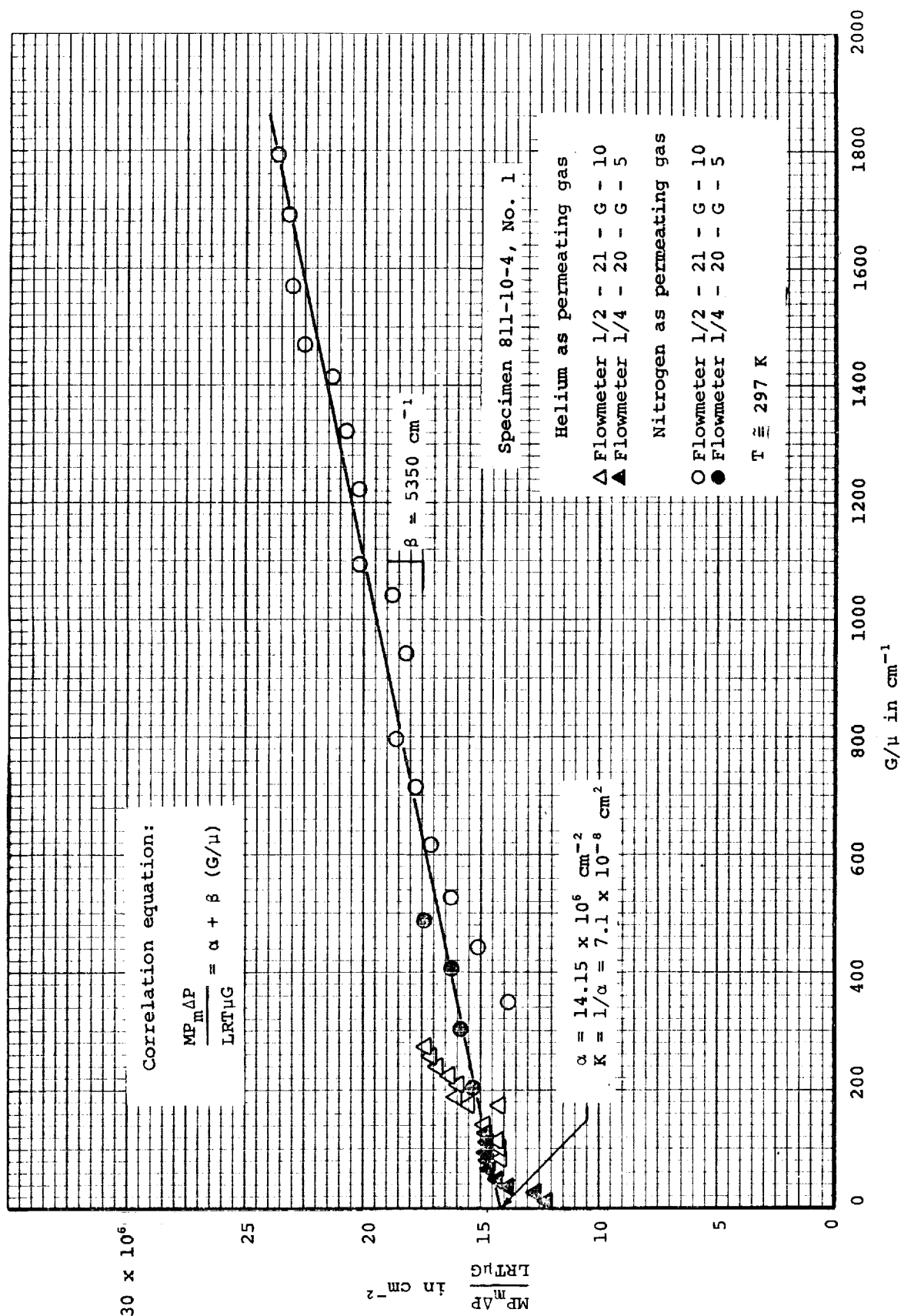
Figure 56. Cornell-Katz Correlation of permeability data for MG-1 charred in a furnace at 811 K

204
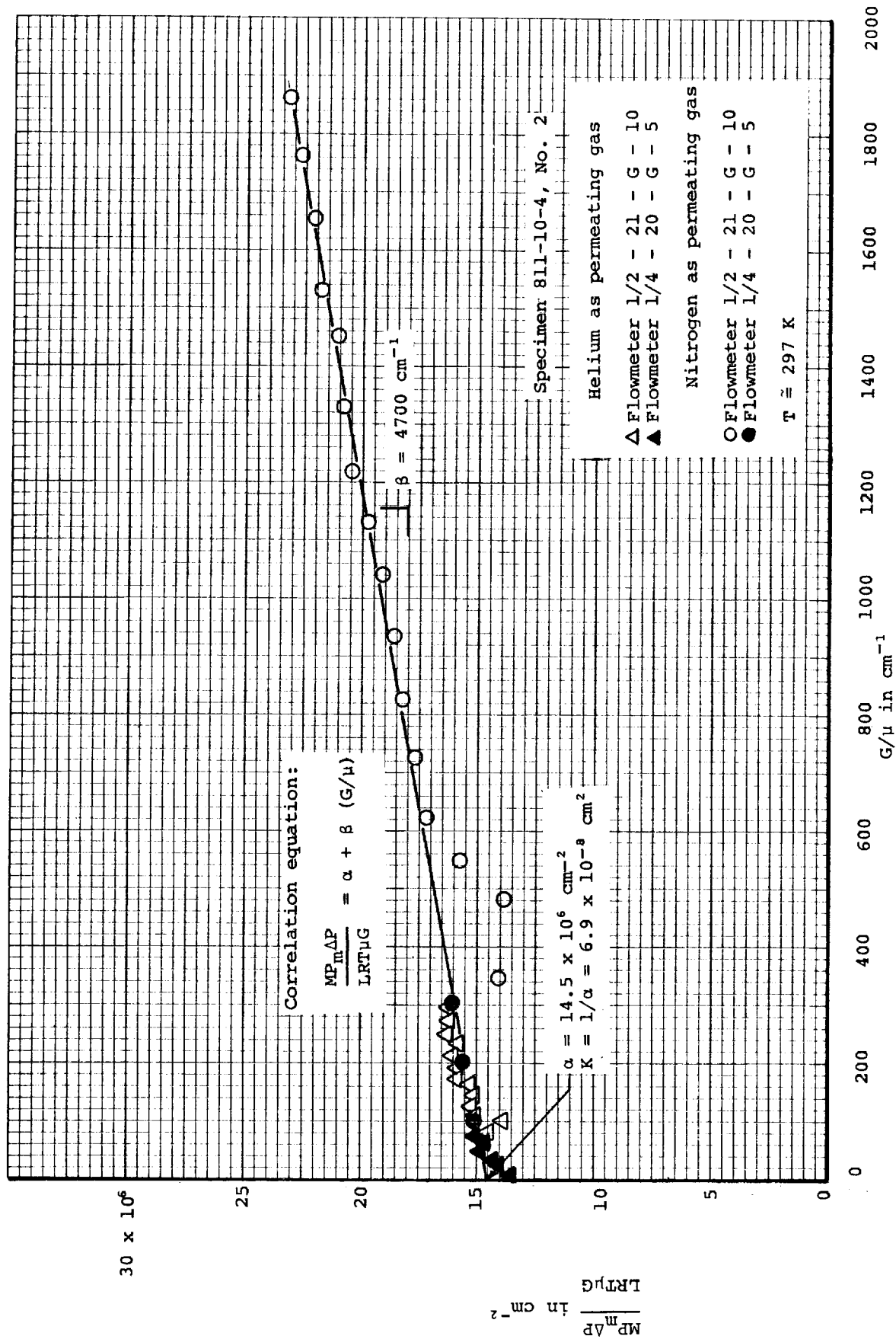
Figure 57. Cornell-Katz Correlation of permeability data for MG-1 charred in a furnace at 811 K

205

Silicone rubber
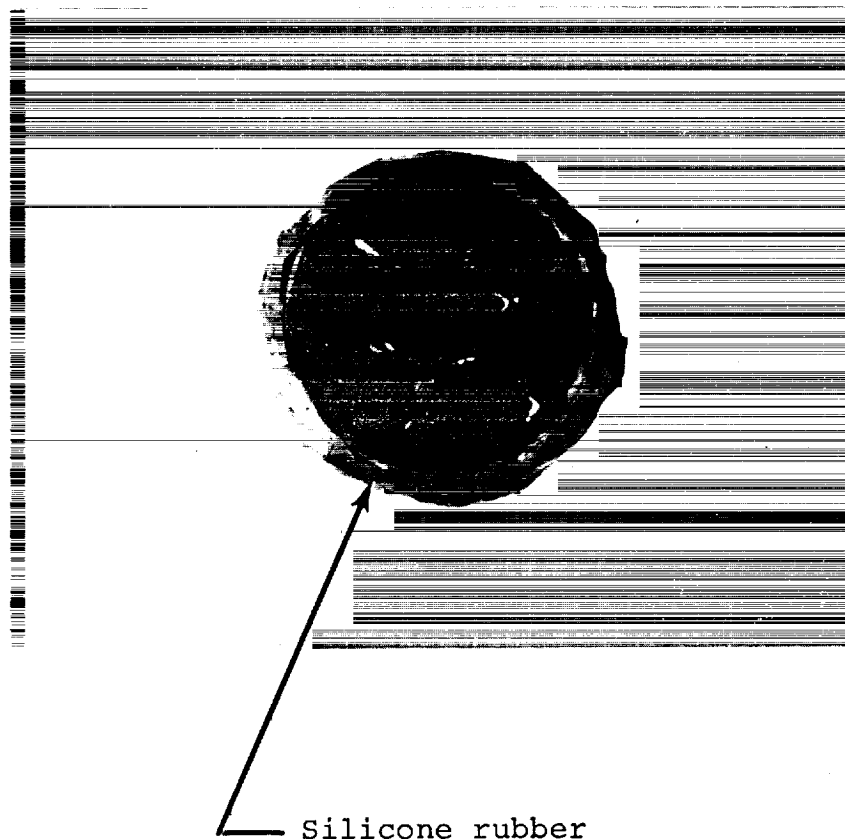
Note: Light areas inside specimen are gaps between
filler and honeycomb

Figure 58. Picture of permeability specimen of MG-58, Phenolic-Nylon
in Phenolic-Glass Honeycomb, charred in arc-jet

206
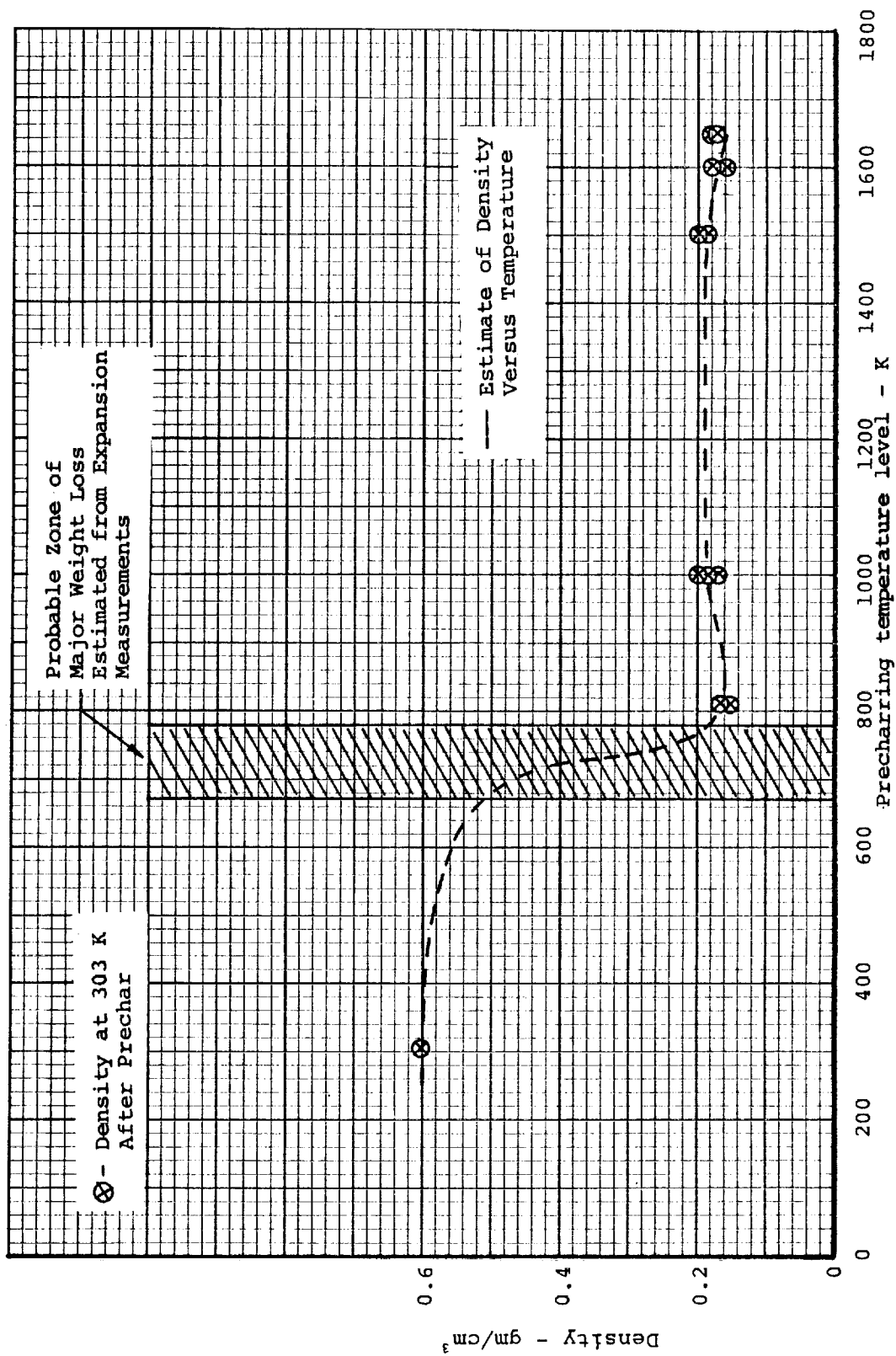
Figure 59. Estimate of bulk density of MG-1 char during ablation

207
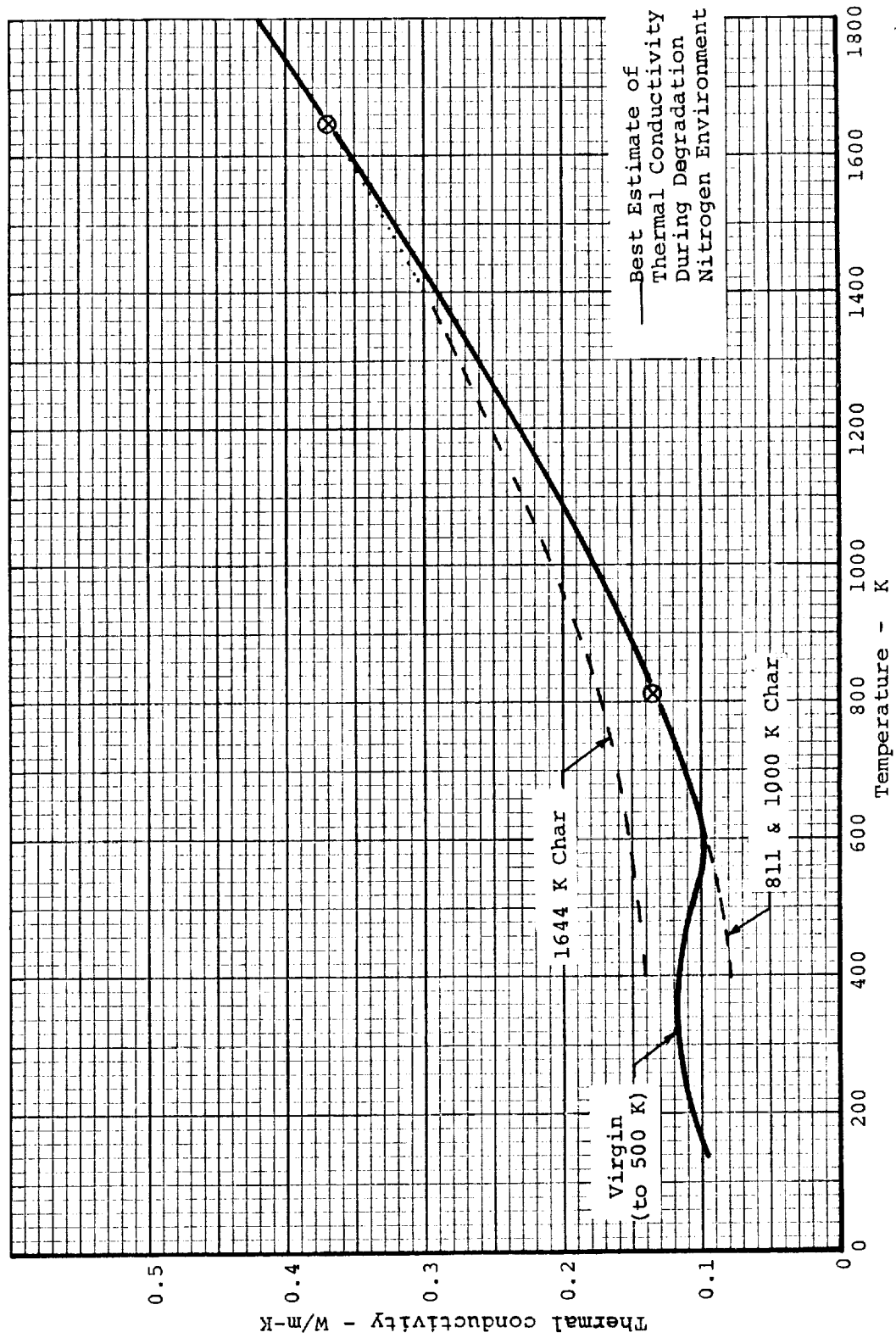
Figure 60. Best estimate of thermal conductivity of MG-1 char during degradation

208
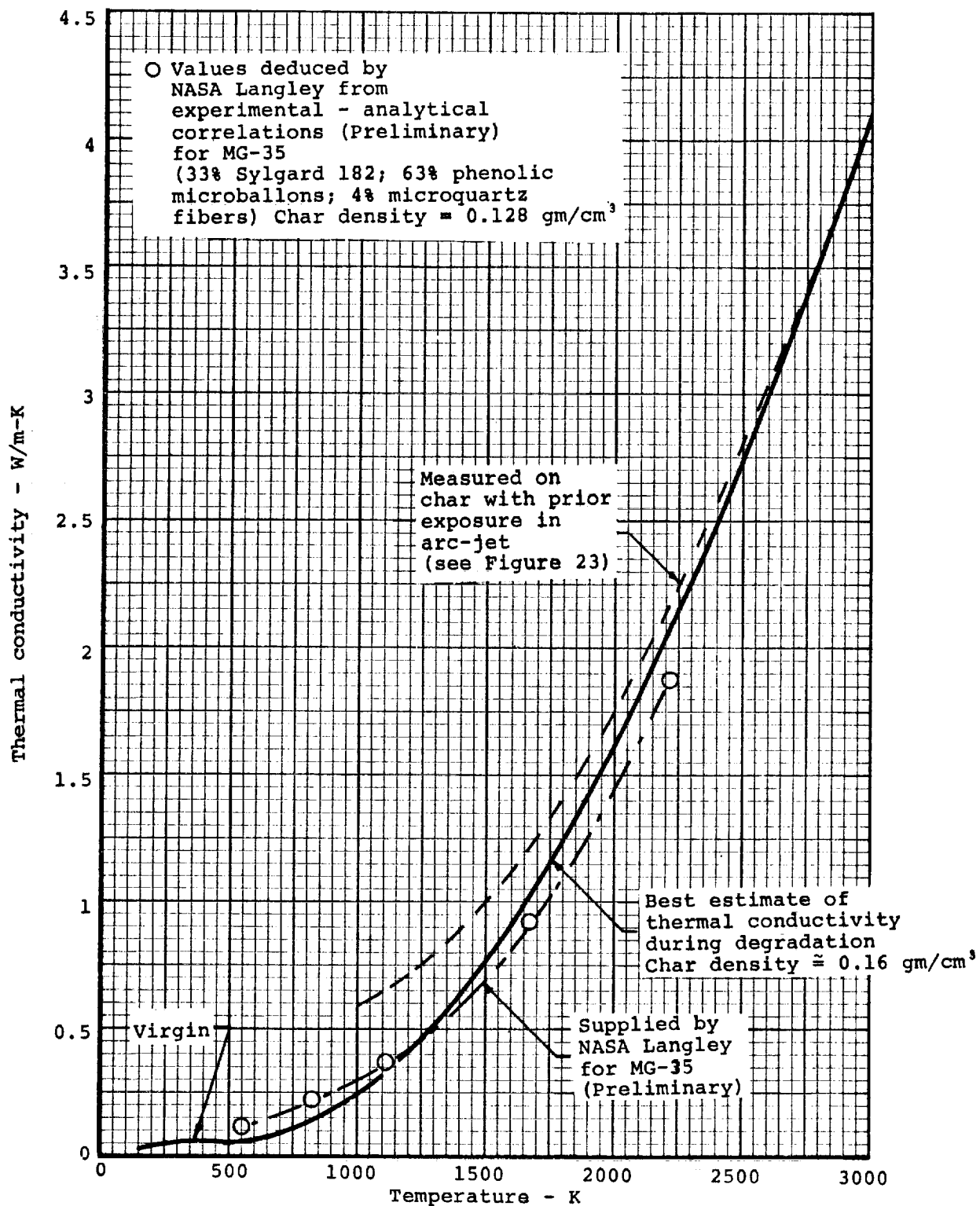
Figure 61. Best estimate of thermal conductivity during degradation of MG-45, Silicone-Phenolic in Phenolic-Glass Honeycomb
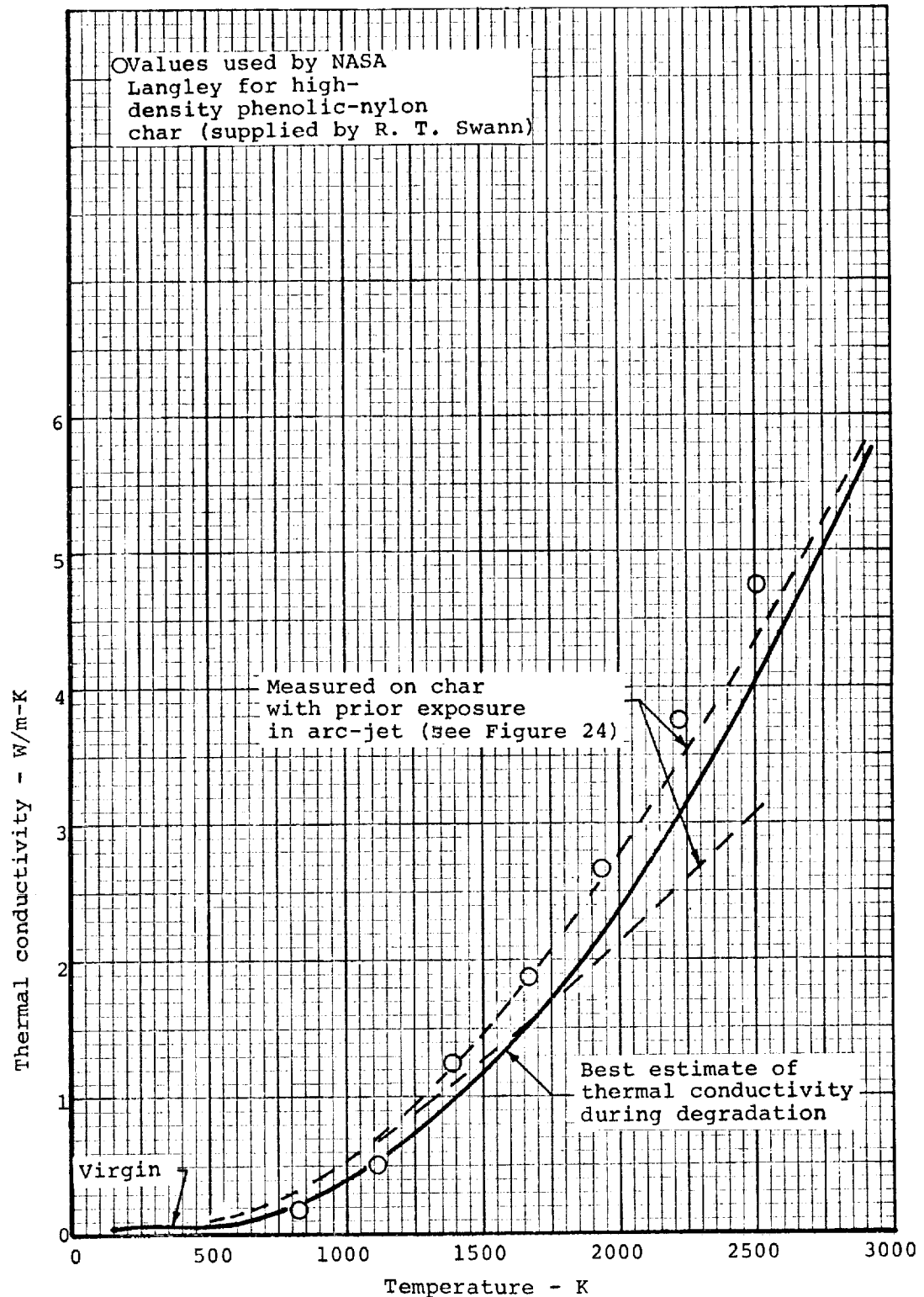
Figure 62. Best estimte of thermal conductivity during degradation
of MG-58, Phenolic-Nylon in Phenolic-Glass Honeycomb

210
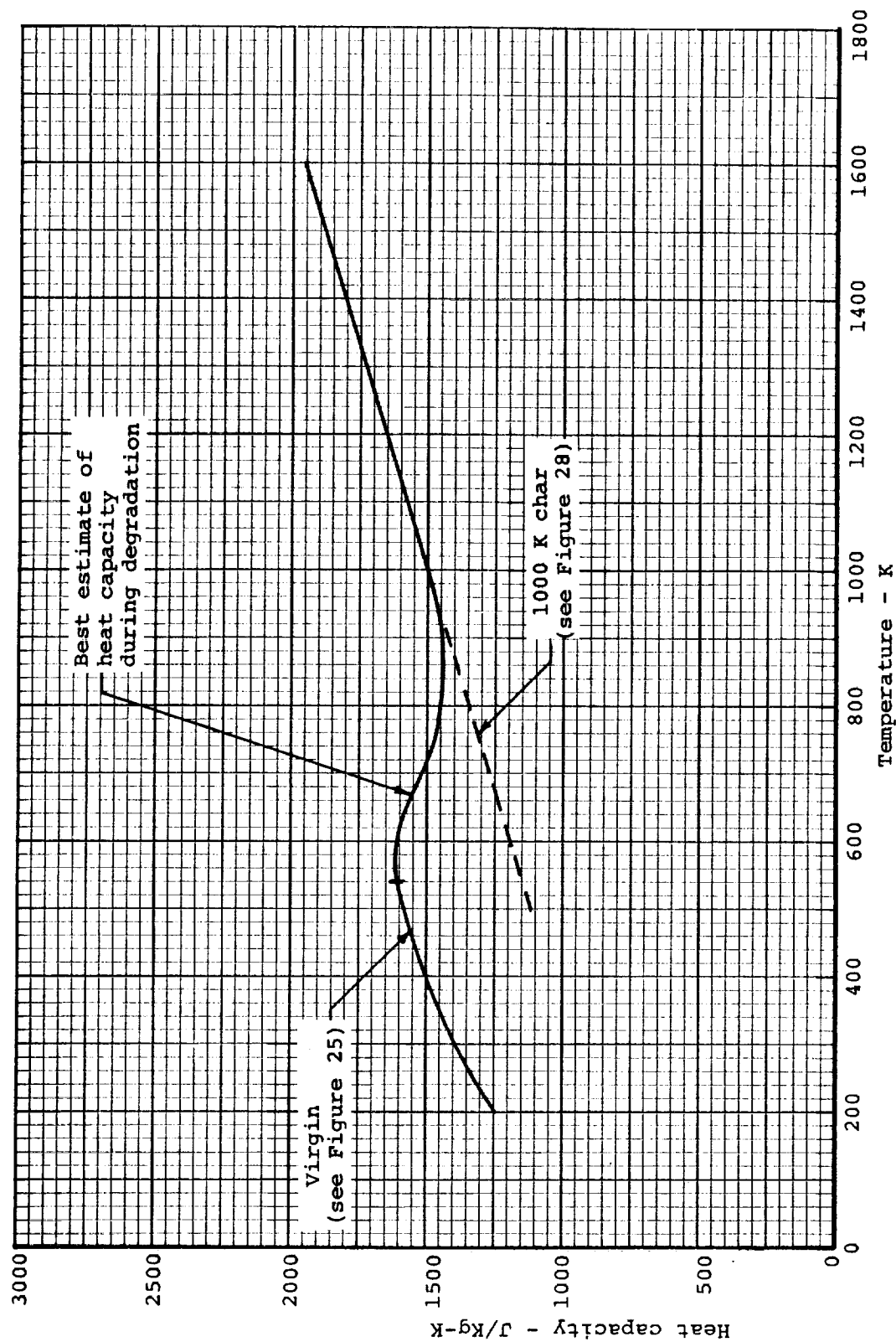
Figure 63. Best estimate of heat capcity during degradation of MG-1, Silicone-Phenolic

211
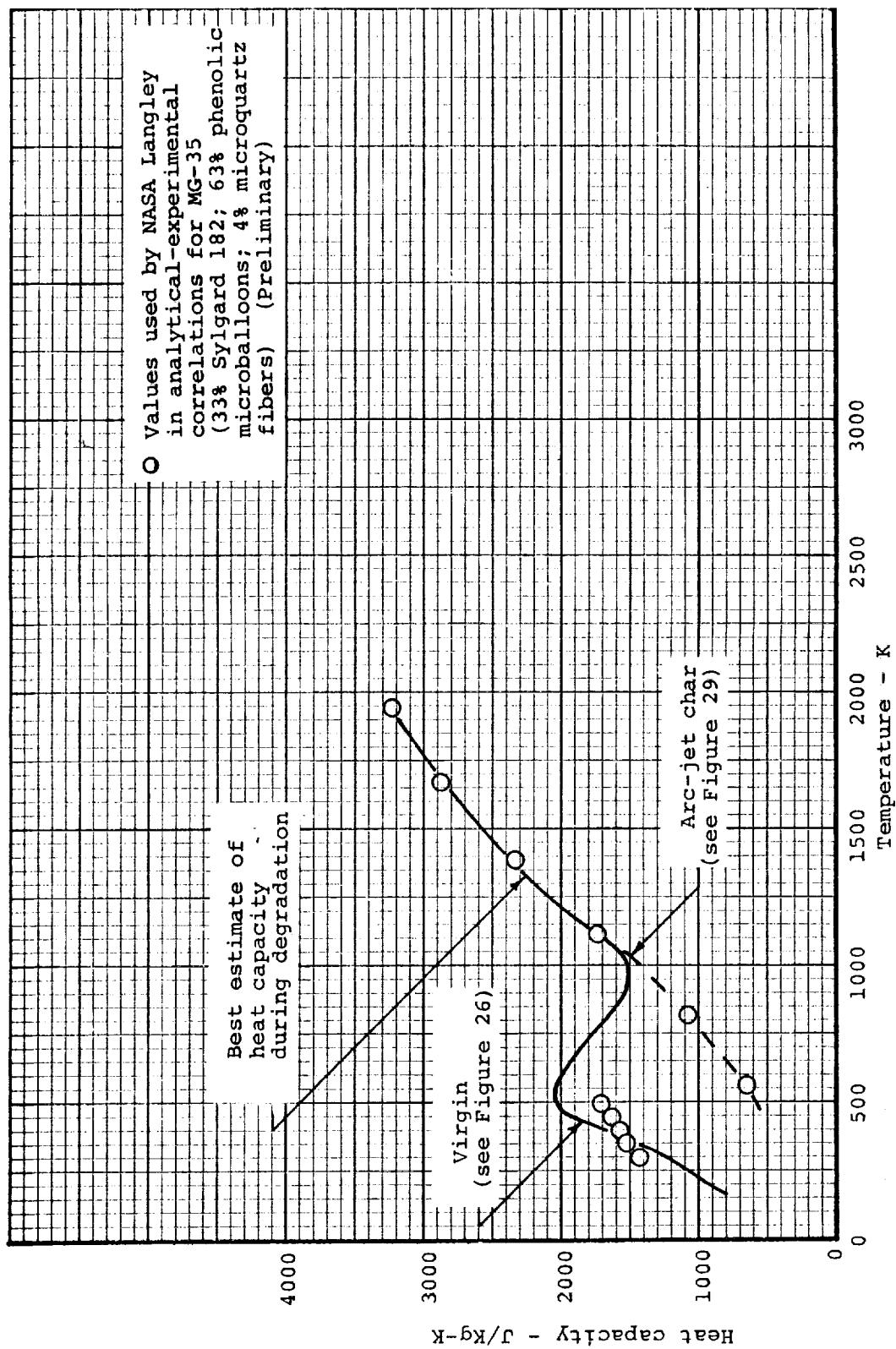
Figure 64. Best estimate of heat capacity during degradation of MG-45, Silicone-Phenolic in Phenolic-Glass Honeycomb

212
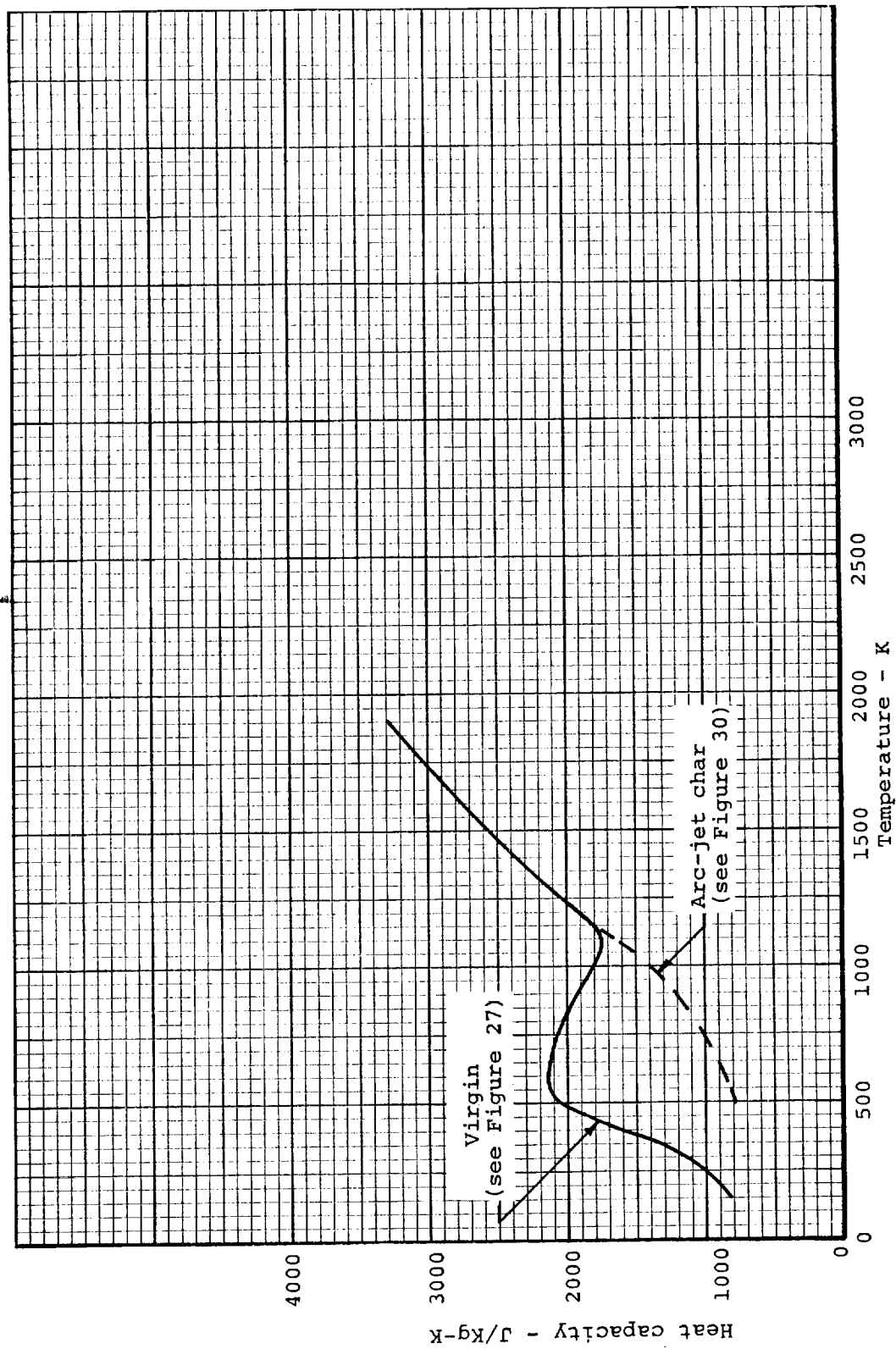
Figure 65. Best estimate of heat capacity during degradation of MG-58, Phenolic-Nylon in Phenolic-Glass Honeycomb

213
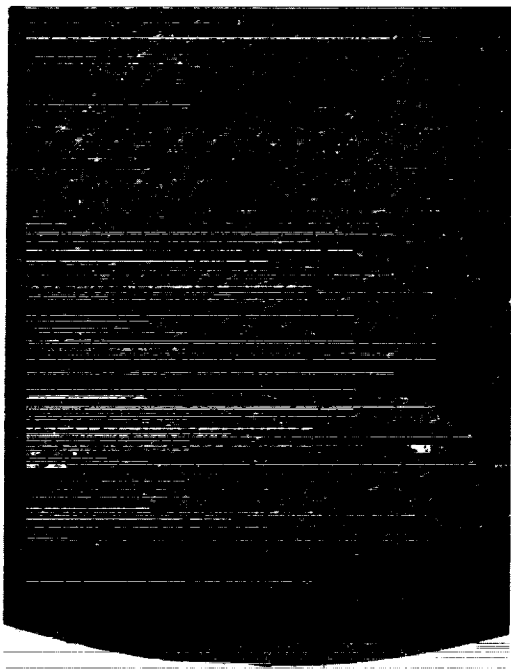
a. MG-58 Material Cake 2
   (label side) showing
   severely delaminated area
   Plane of picture is a b plane

b. Specimen MG-58-2-C9a2
    showing delaminations and
    honeycomb misalignment.
    Specimen was taken from
    area in cake 2 diametrically
    opposite that shown in
    Figure a. Plane of picture
    is ab plane.
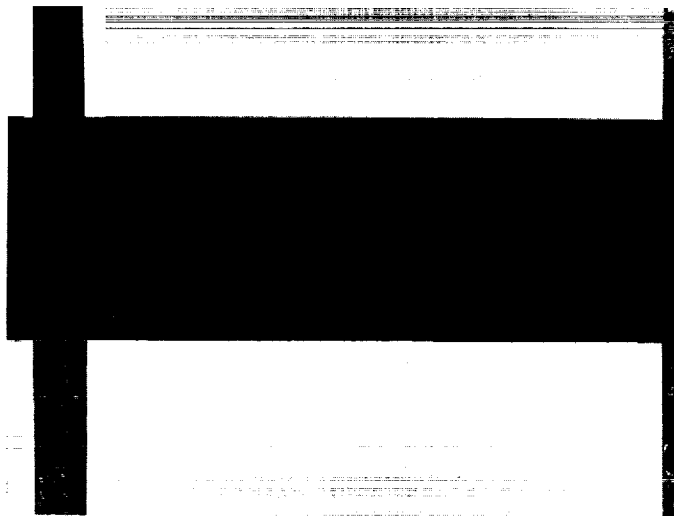
c. Specimen MG-58-3-T35b3 showing delaminations.
    Horizontal line resulted from slag inclusion.
    Plane of picture is bc plane.

Figure 66. Photographs showing MG-58 material condition (all 1X)

Specimen MG-45-3-C2a2
Delaminations indicated are
average for MG-45 material.
Also note honeycomb misalignment
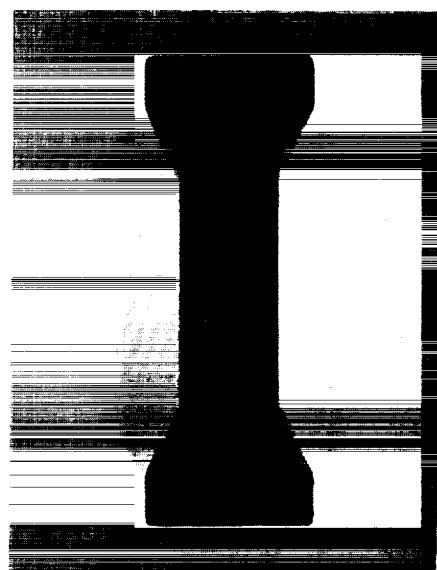
Specimen MG-45-5-Cl2b2

Figure 67. Photographs of specimens of MG-45 material showing disparates

215
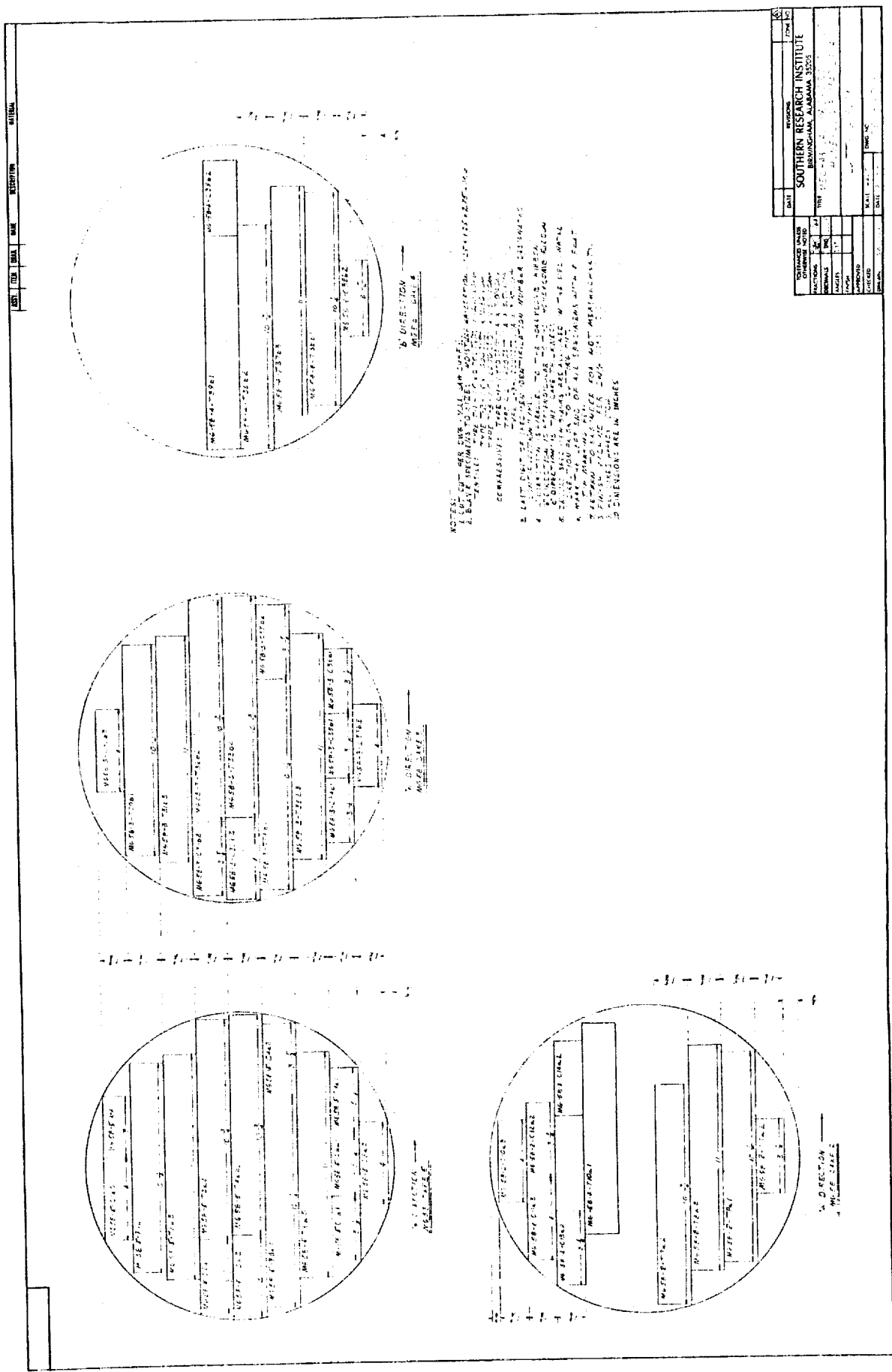
Figure 68.   MG-58 material cutting plans
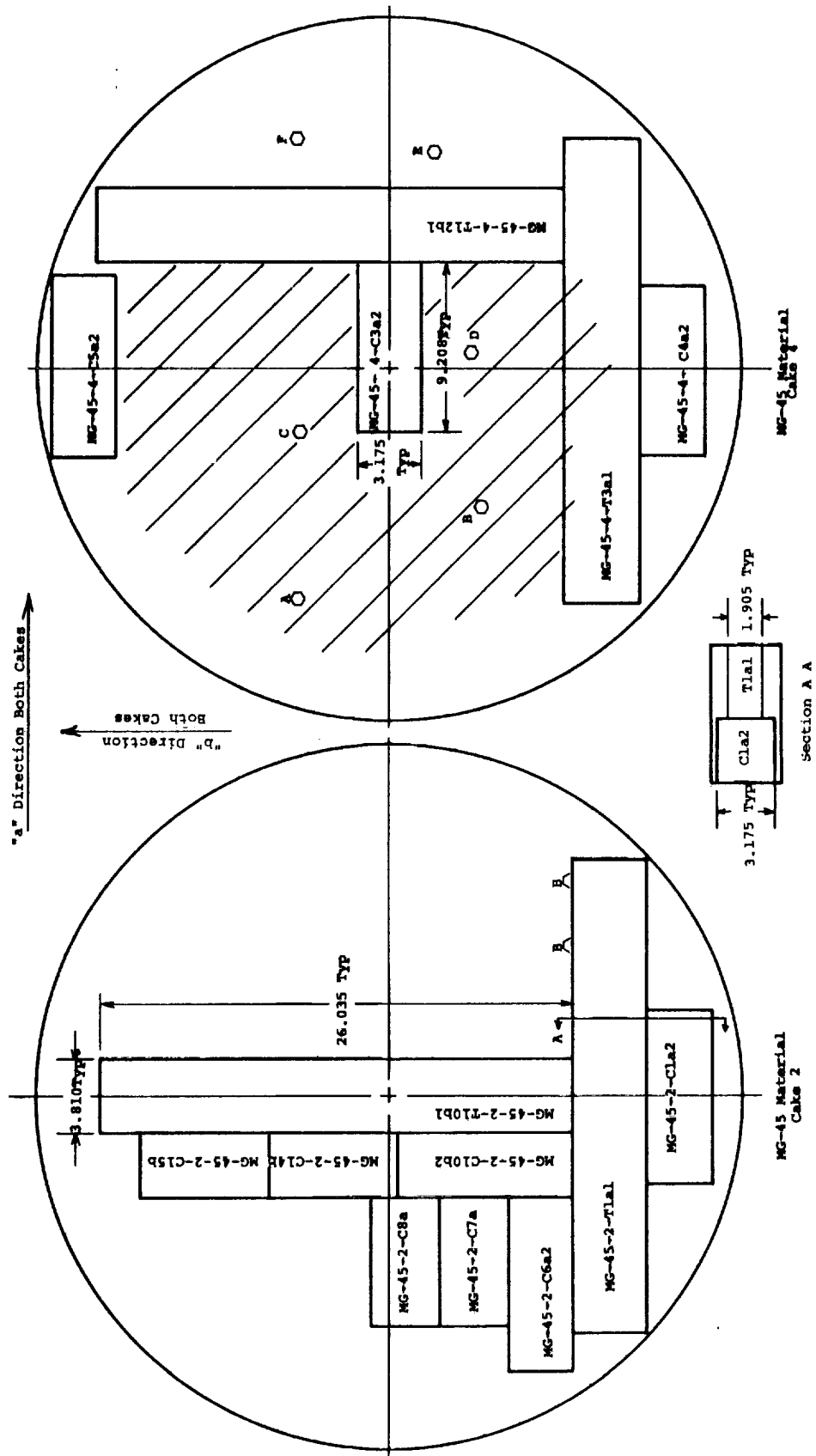
Figure 69. Cutting plan for MG-45 Material - cakes 2 and 4
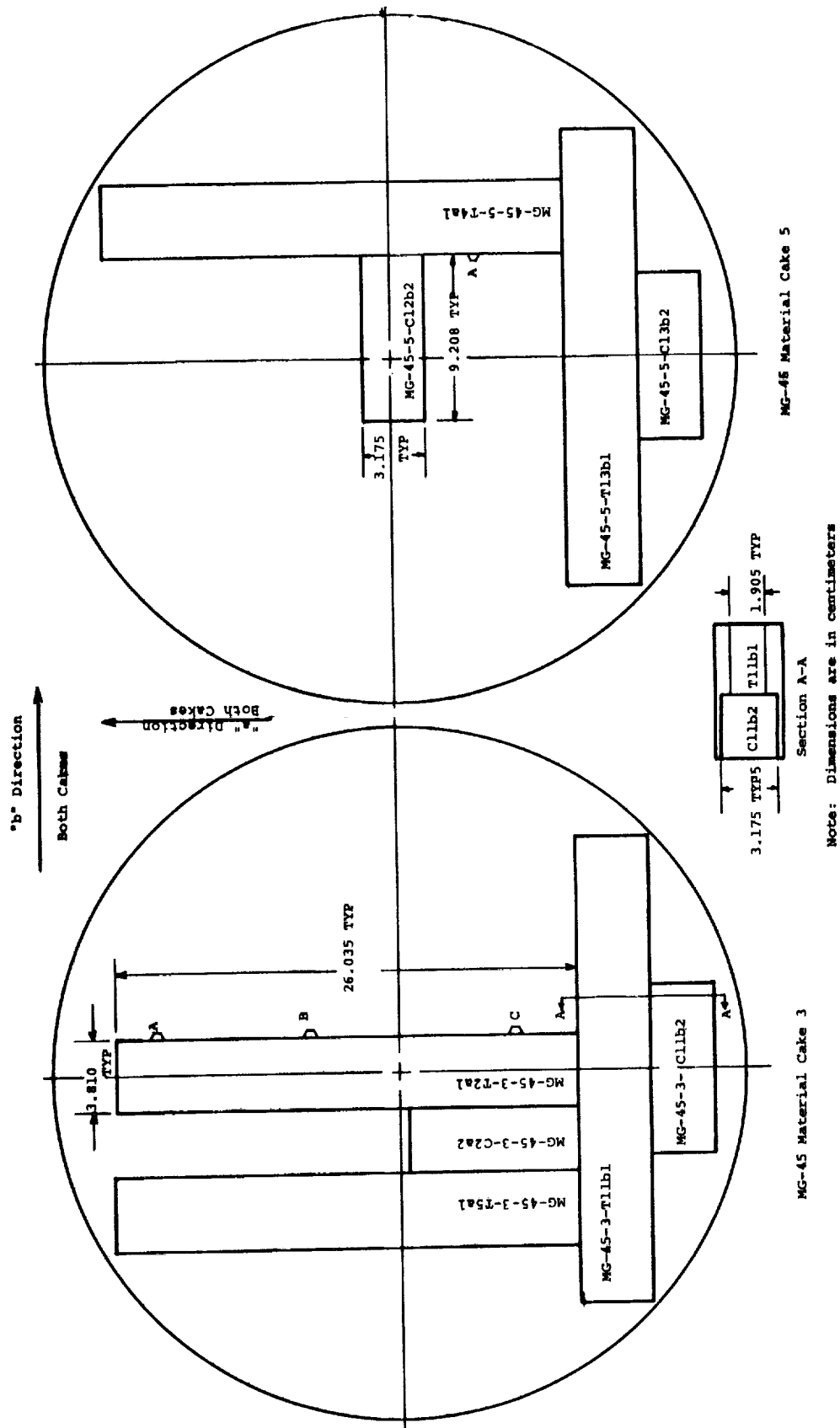
Figure 70. Cutting plan for MG-45 Material – cakes 3 and 5

MG-45 Material Cake 3

MG-45 Material Cake 5

"b" Direction
Both Cakes

"a" Direction
Both Cakes

Section A-A

Note: Dimensions are in centimeters

218

Typical Tier-Tensile Specimen Blanks

Typical Tier Compressive Specimen Blank

Figure 71. MG-1 Material cutting plan

Billet MG-1-1B

Notes: 1. Dimensions in centimeters
        2. Tensile specimen blanks T6a through T10a are 22.225 cm long

219

Section A-A

MG-1-1A-T36a4

MG-1-1A-T37a4

"a" Direction

MG-1-1A-T36a4 and T37a4

"b" Direction
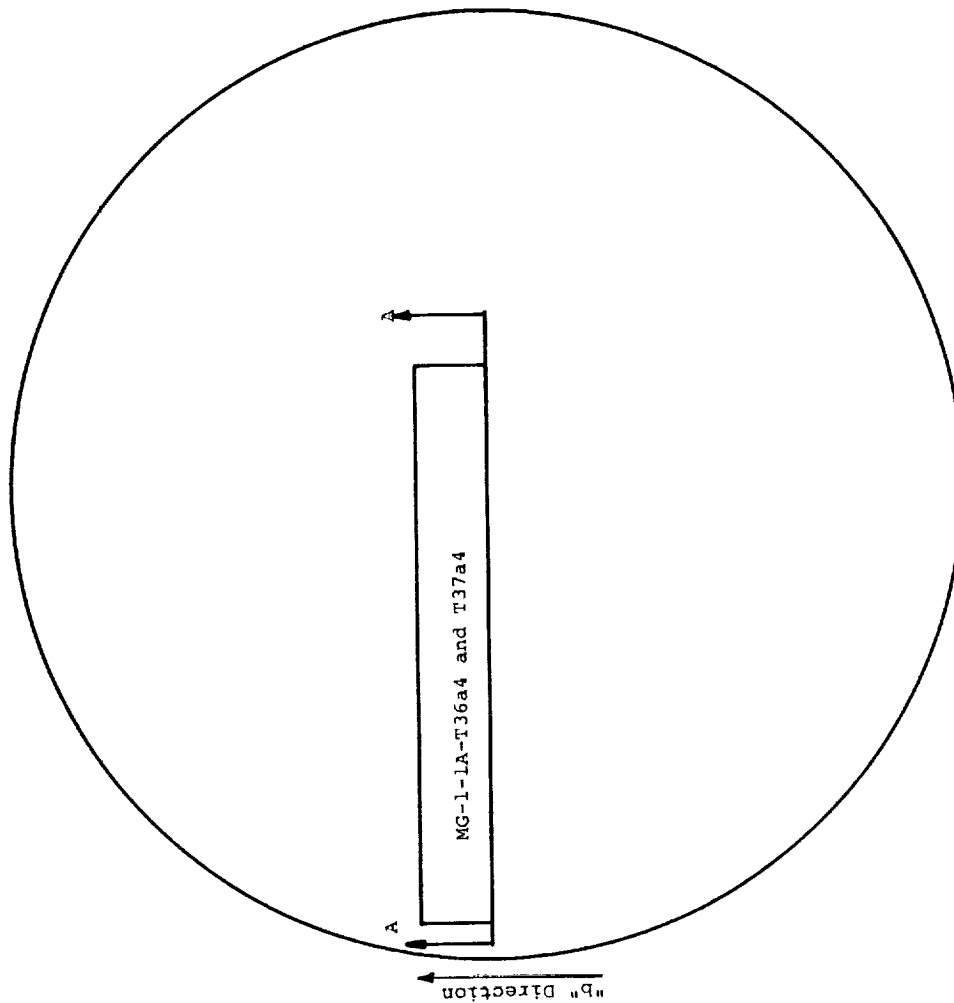
A

Billet MG-1-1A

Figure 72. MG-1 Material cutting plan
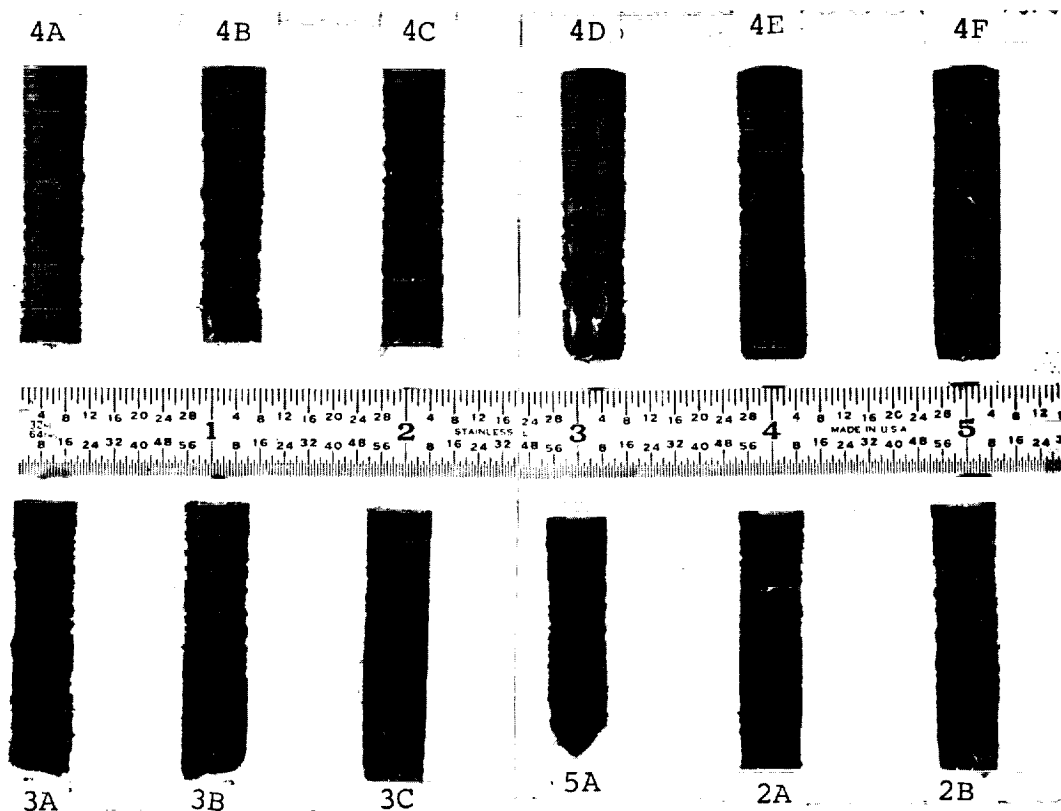
Shown are "cells" of silicone-phenolic filler material taken from each of the MG-45 billets. The number designates the billet from which the materials were taken, while the letter denotes the locations within the billet as shown on the cutting plans (Figures 69 and 70). The cells taken from Billet 4 are complete cells, while those taken from the other billets are only partial cells taken adjacent to cuts made while fabricating specimen blanks.

Note that Cells 4A and 4D contain numerous voids, while the number of voids in Cells 4B, 4C and 4E appear to be representative of cells taken from Billets 2, 3 and 5.

Figure 73. Photograph of silicone-phenolic filler material fiber from MG-45 billets

221

Note: Specimen dried in thermostatically controlled oven for 24 hrs at 377 K

Specimen MG58-5-MA	Before Drying	Immediately After Drying
Moisture Content =		4.96 %
length	6.178 cm	6.175 cm
width	3.178 cm	3.151 cm
thickness	3.178 cm	3.270 cm
weight	14.371 gm	13.657 gm
bulk density	.2303 gm/cm³	.2213 gm/cm³

Black point is density before drying.

Bulk density in gm/cm³

.2500 .2400 .2300 .2200 .2100 .2000

0   12 hrs   24 hrs   10 days   20 days   30 days

Time after removal from oven

Figure 74. Moisture absorption test

Threaded Steel Rod to Fixed
Upper Crosshead

Universal Joint

Chain

Loading Fixture

Gage Point Yoke

Steatite Contact Arms

Steel Spring

SR-4 Strain Gages

Electrical Leads to
Recorder

Specimen

Lower Moveable Crosshead
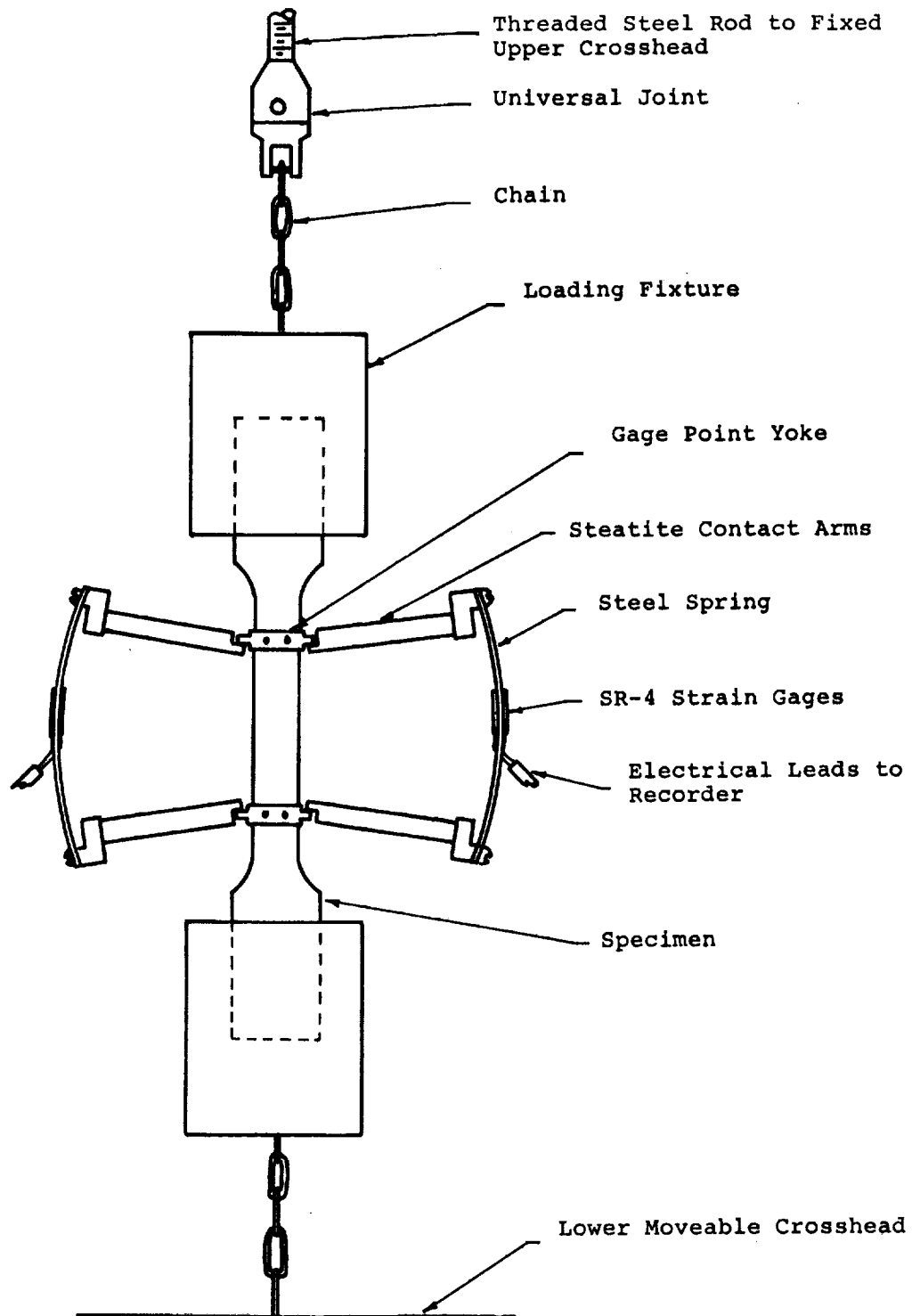
Figure 75. "Clip-on" extensometers used to monitor axial strains
and tensile load train

Figure 76. MG-58 material specimen configuration

1.27

2.54

8.255

5.715

22.225

1.27 Dia

10.16 R
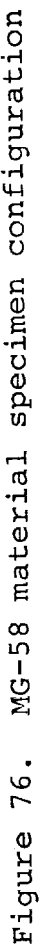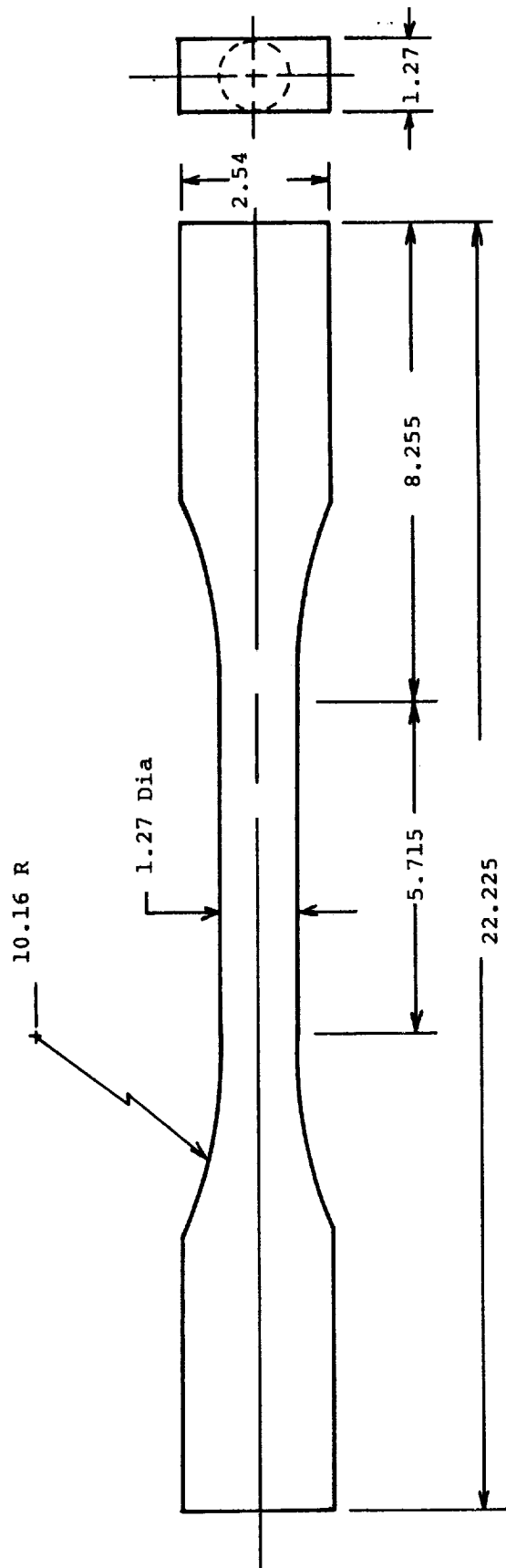
Notes:

1. Dimensions are in centimeters
2. Diameters true and concentric to within .005
3. Do not undercut radii at tangent points
4. Faces to be flat and parallel to $\mathbf{\mathcal{G}}$
5. Tolerances: ±.005

Figure 77. Tensile specimen configuration for MG-1 Material (configuration T-4)
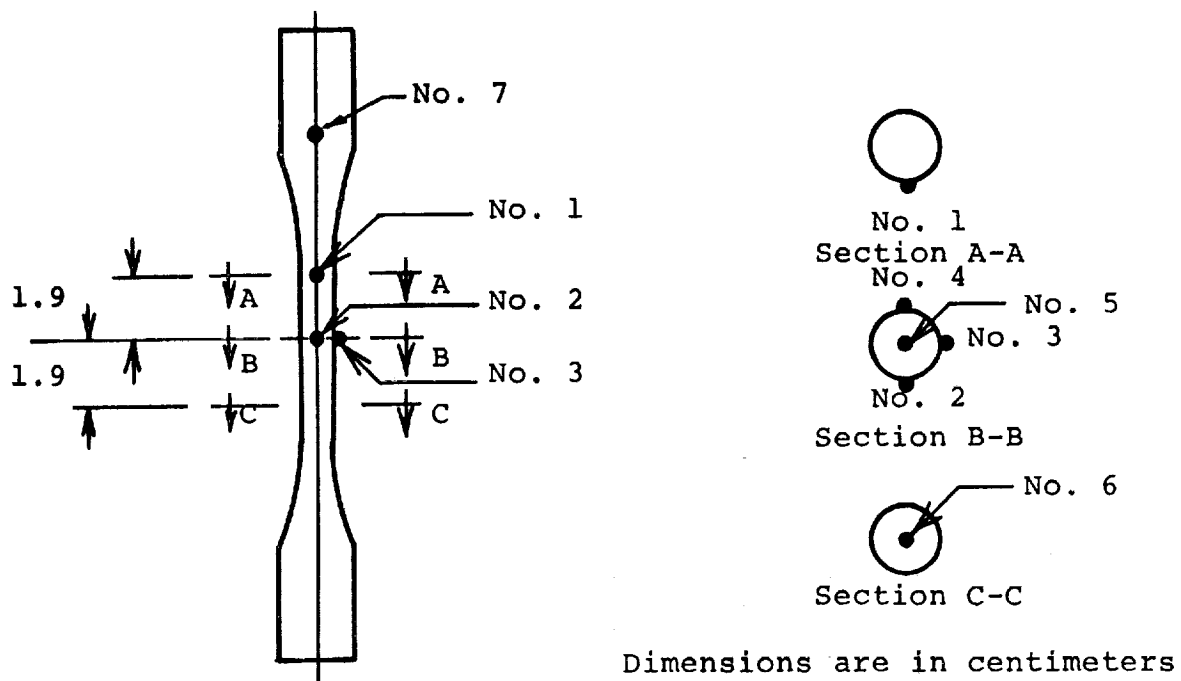
Figure 78. Thermocouple locations for determining heating rates for MG-1 tensile specimen
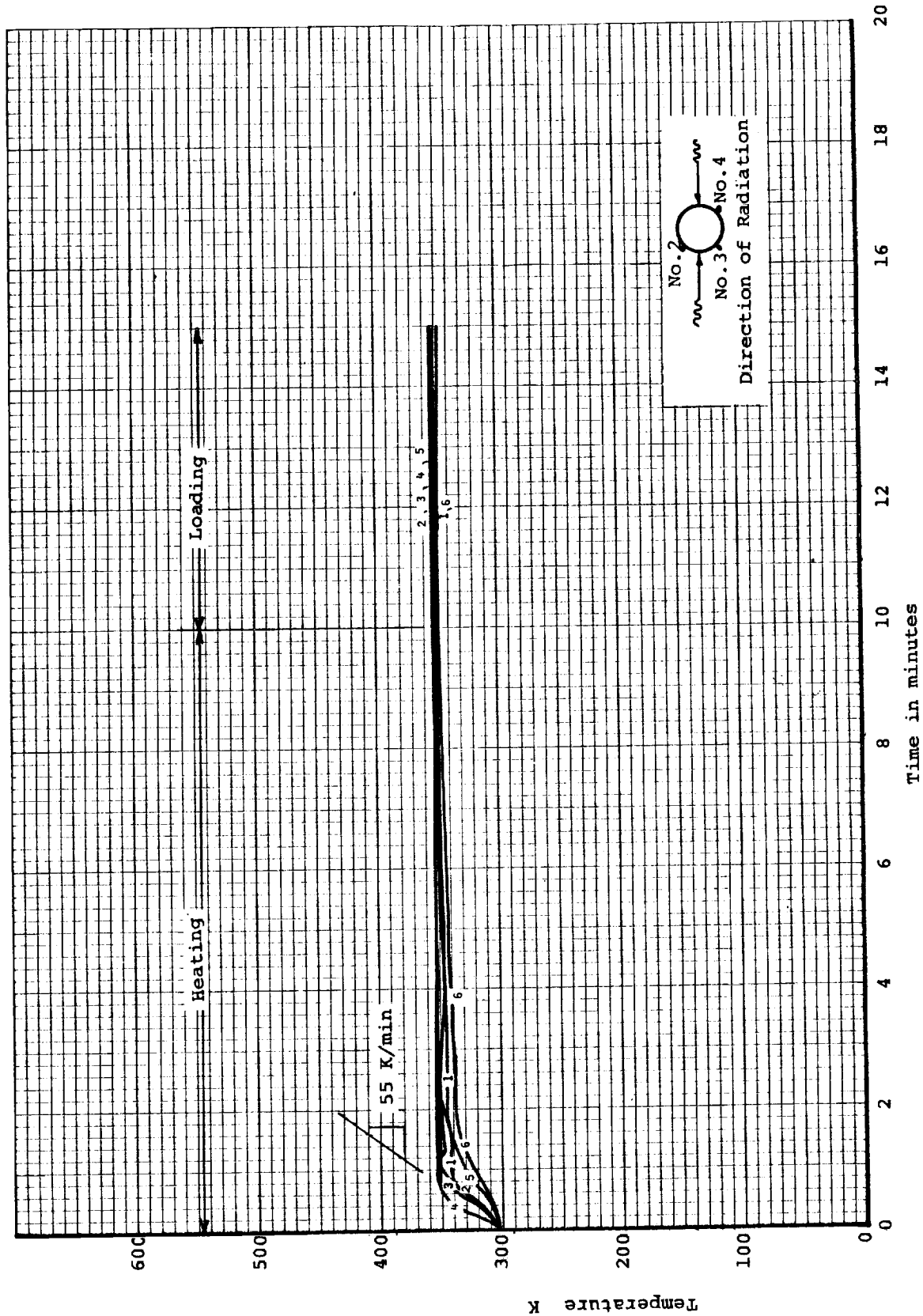
Figure 79. Typical heating curve for MG-1 tensile specimen - 55 K/min to 350 K

227

Figure 80. Typical heating curve for MG-1 tensile specimen - 55 K/min to 400 K
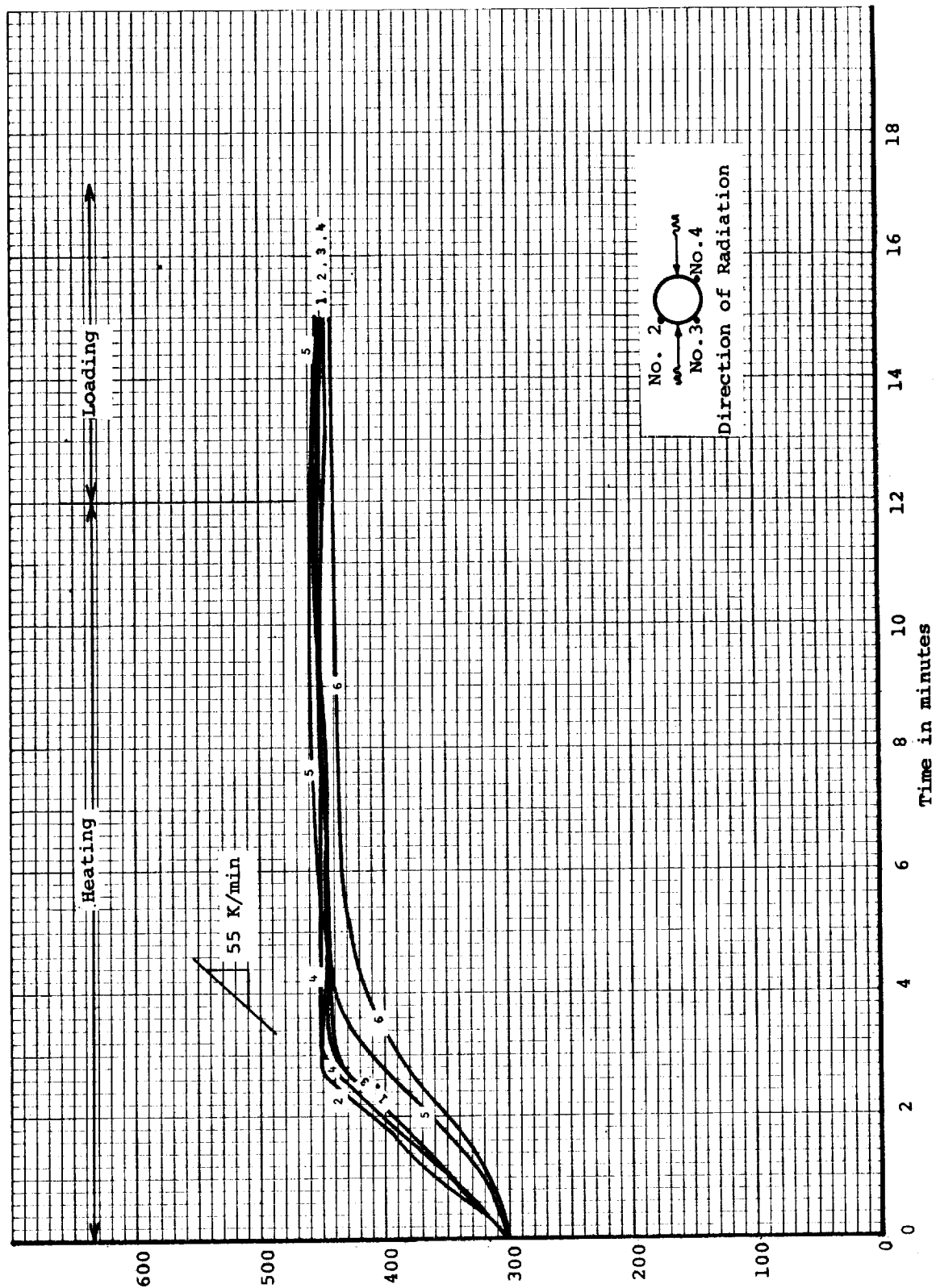
Figure 81. Typical heating curve for MG-1 tensile specimen - 55 K/min to 450 K

229
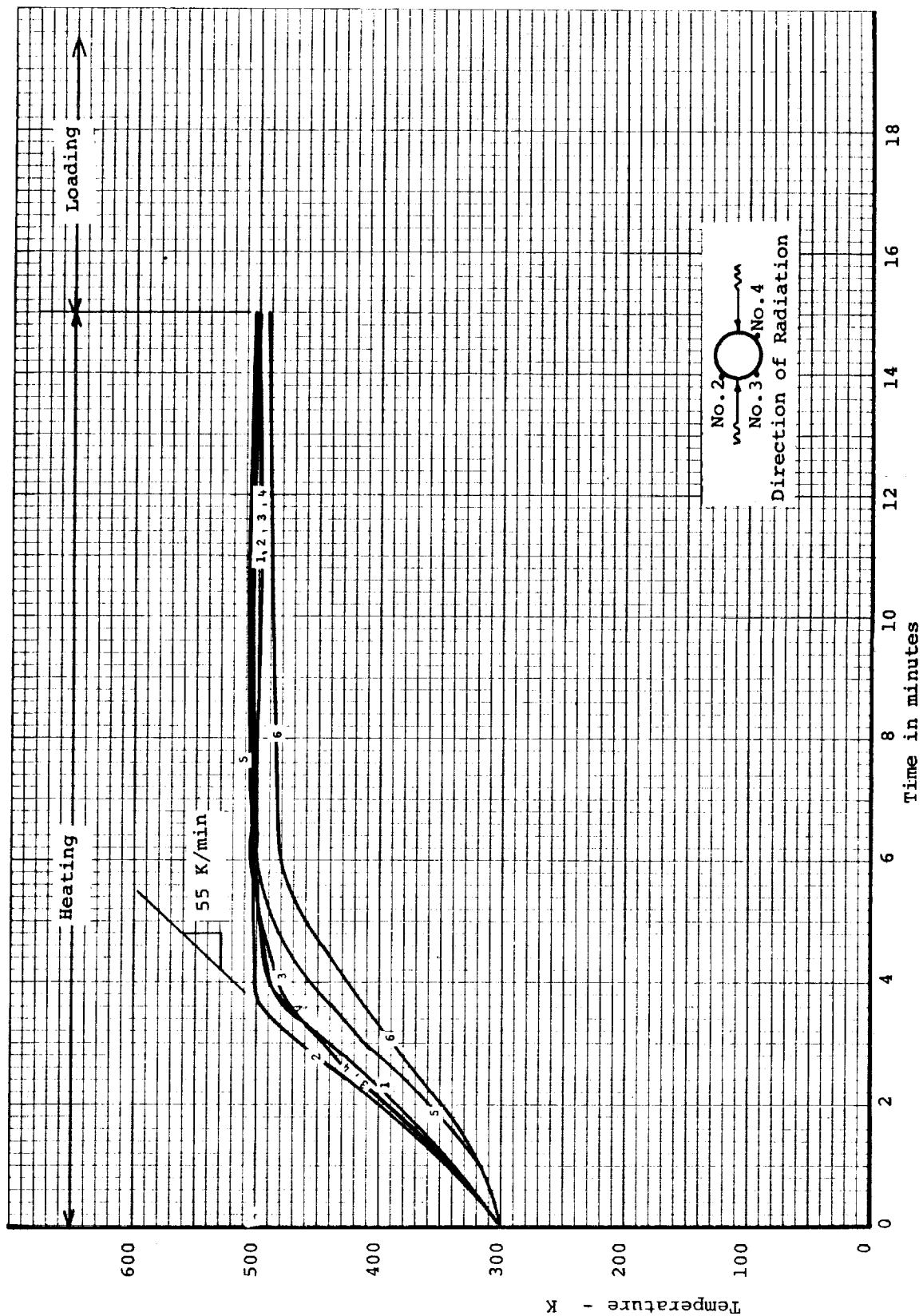
Figure 82. Typical heating curve for MG-1 tensile specimen - 55 K/min to 500 K
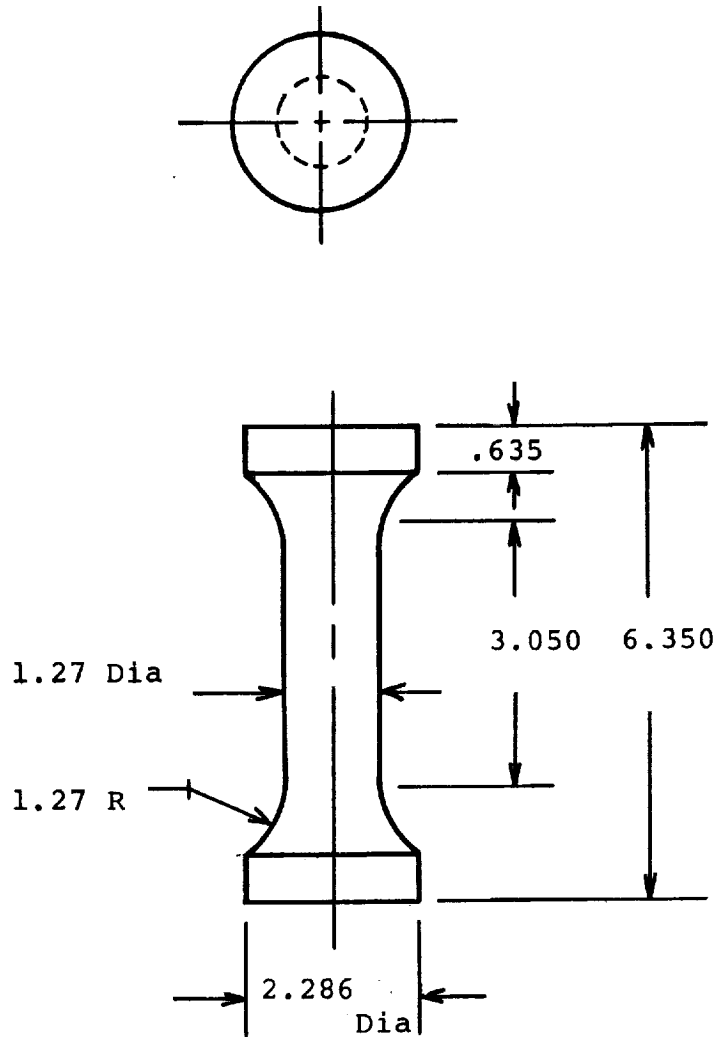
Notes:
1. Dimensions are in centimeters
2. All diameters true and concentric to within .005
3. Ends flat and perpendicular to ₵ to within .005
4. Do not undercut radii at tangent points
5. Tolerances are: ±.005 on all dimensions

Figure 83. Compressive specimen configuration for MG-1 Material
(configuration C-4)

Dimensions are in centimeters
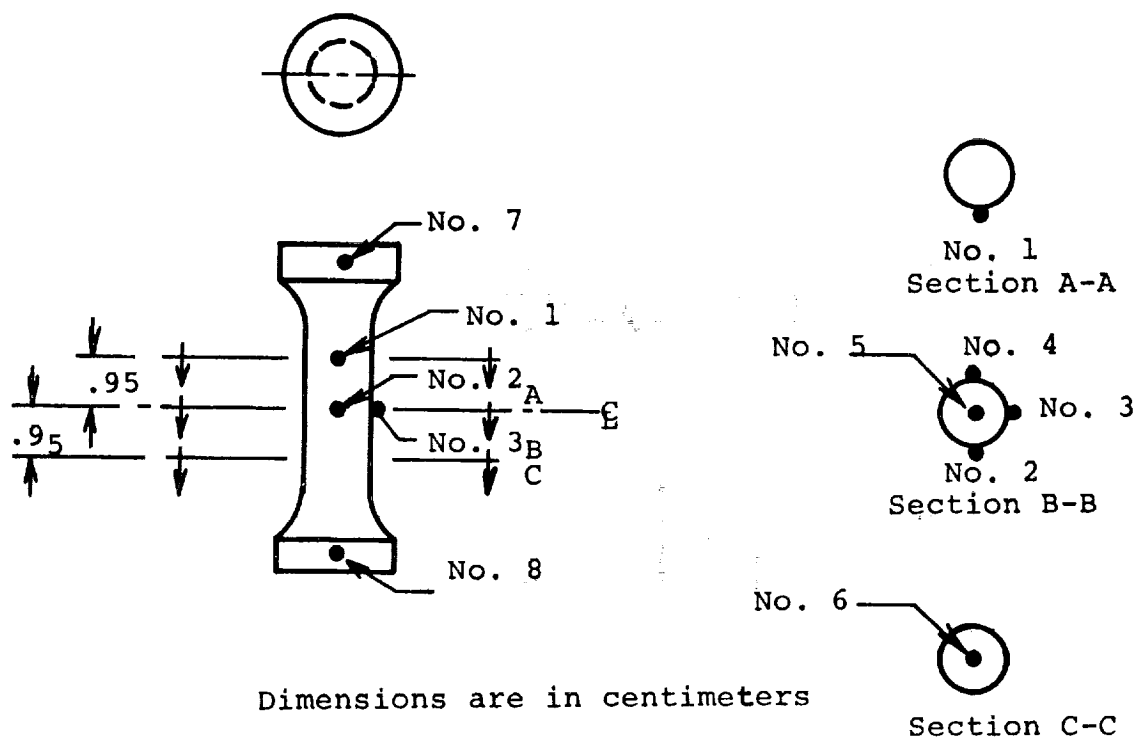
Figure 84. Thermocouple locations for determining heating rates for MG-1 compressive specimens

232
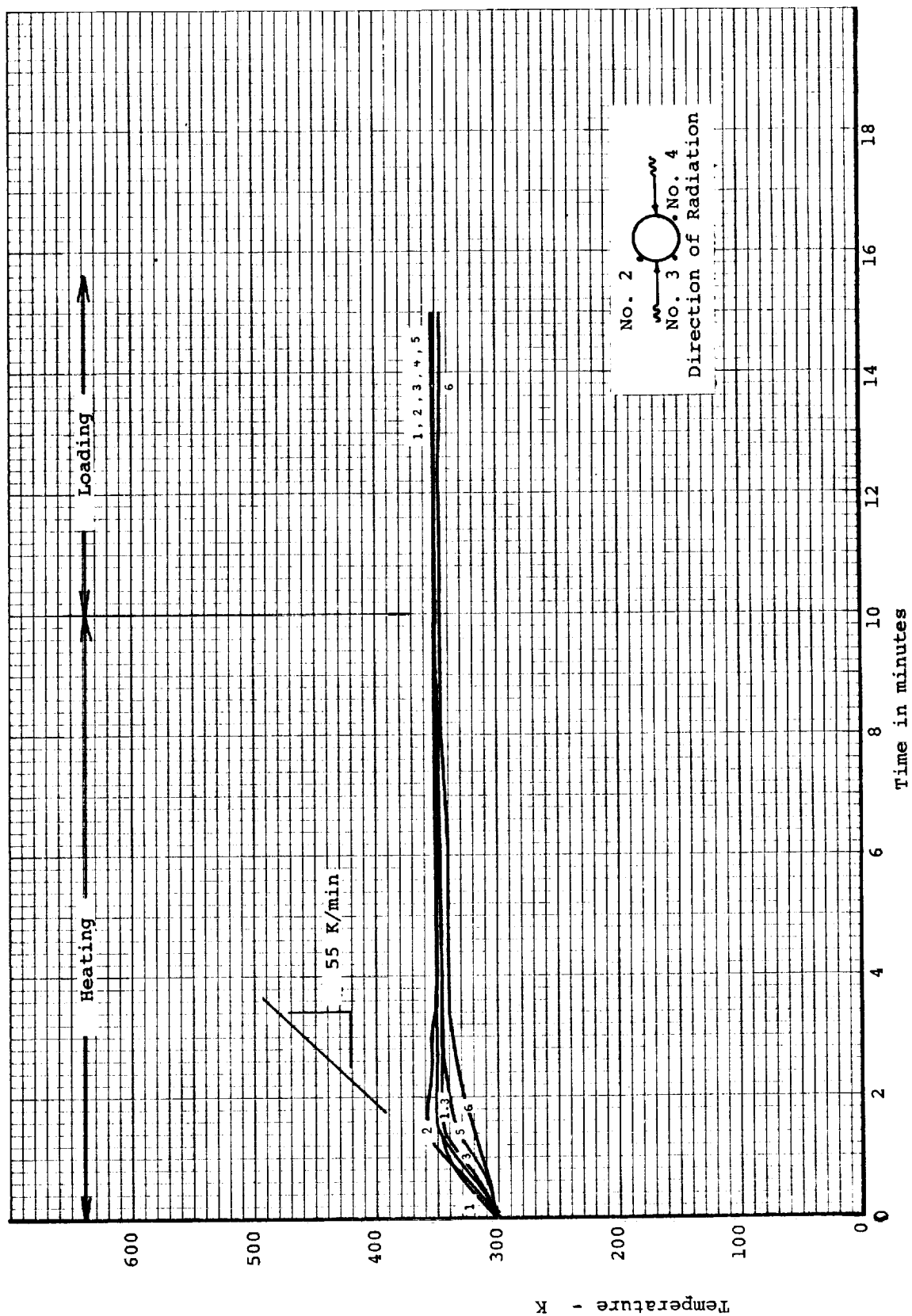
Figure 85. Typical heating curve for MG-1 compressive specimen - 55 K/min at 350 K

233
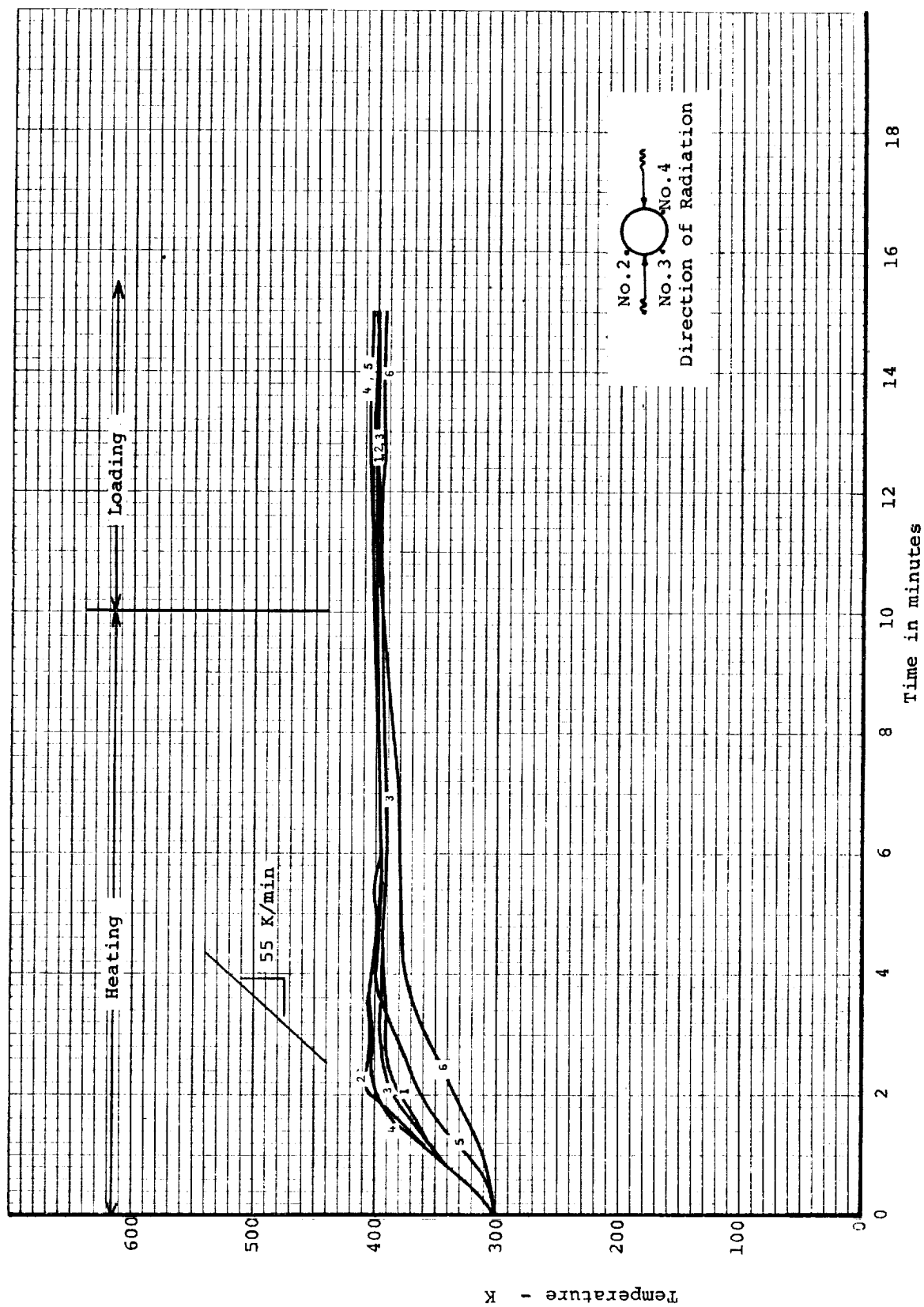
Figure 86. Typical heating curve for MG-1 compressive specimen – 55 K/min to 400 K

234
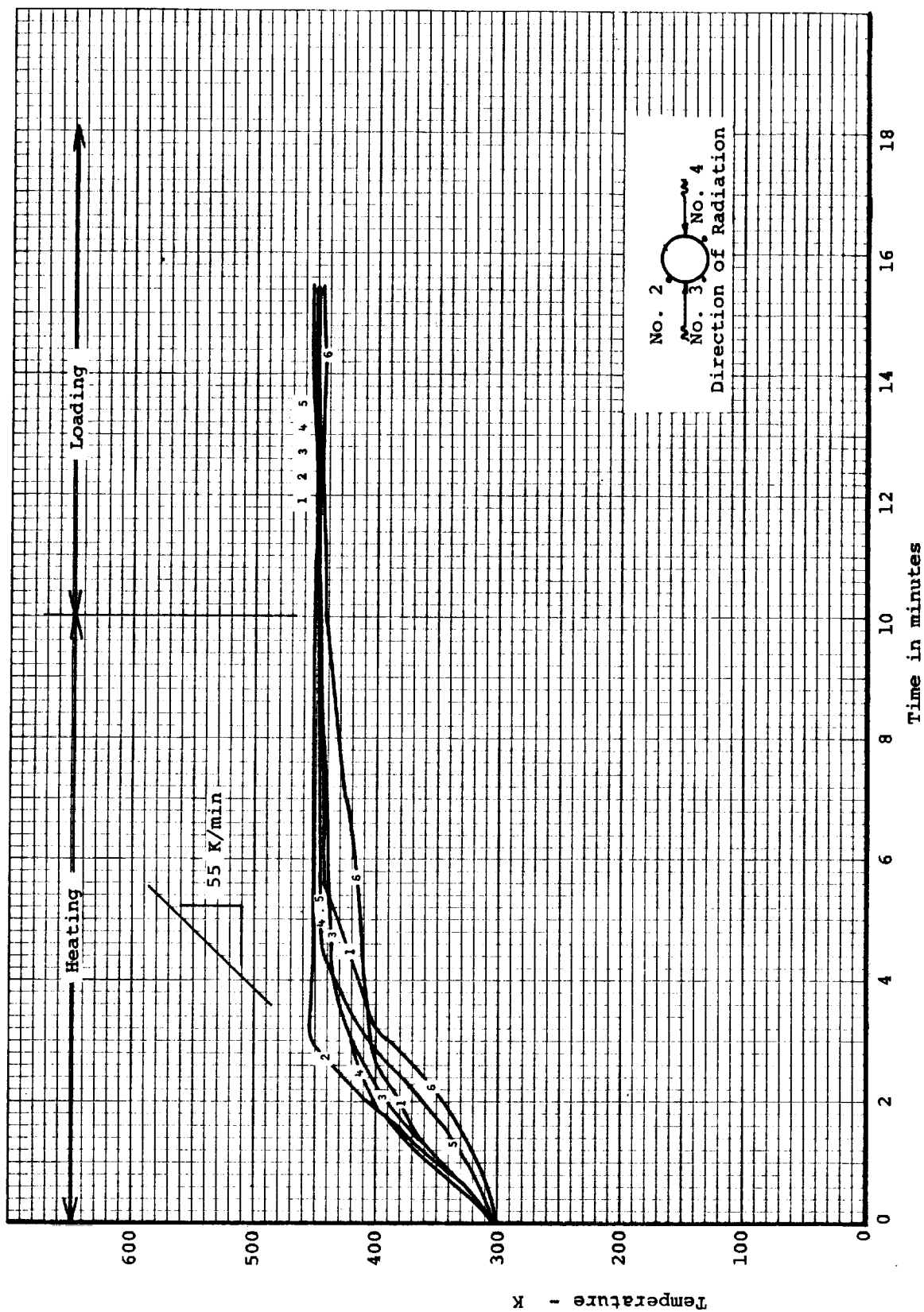
Figure 87. Typical heating curve for MG-1 compressive specimen - 55 K/min to 450 K

235
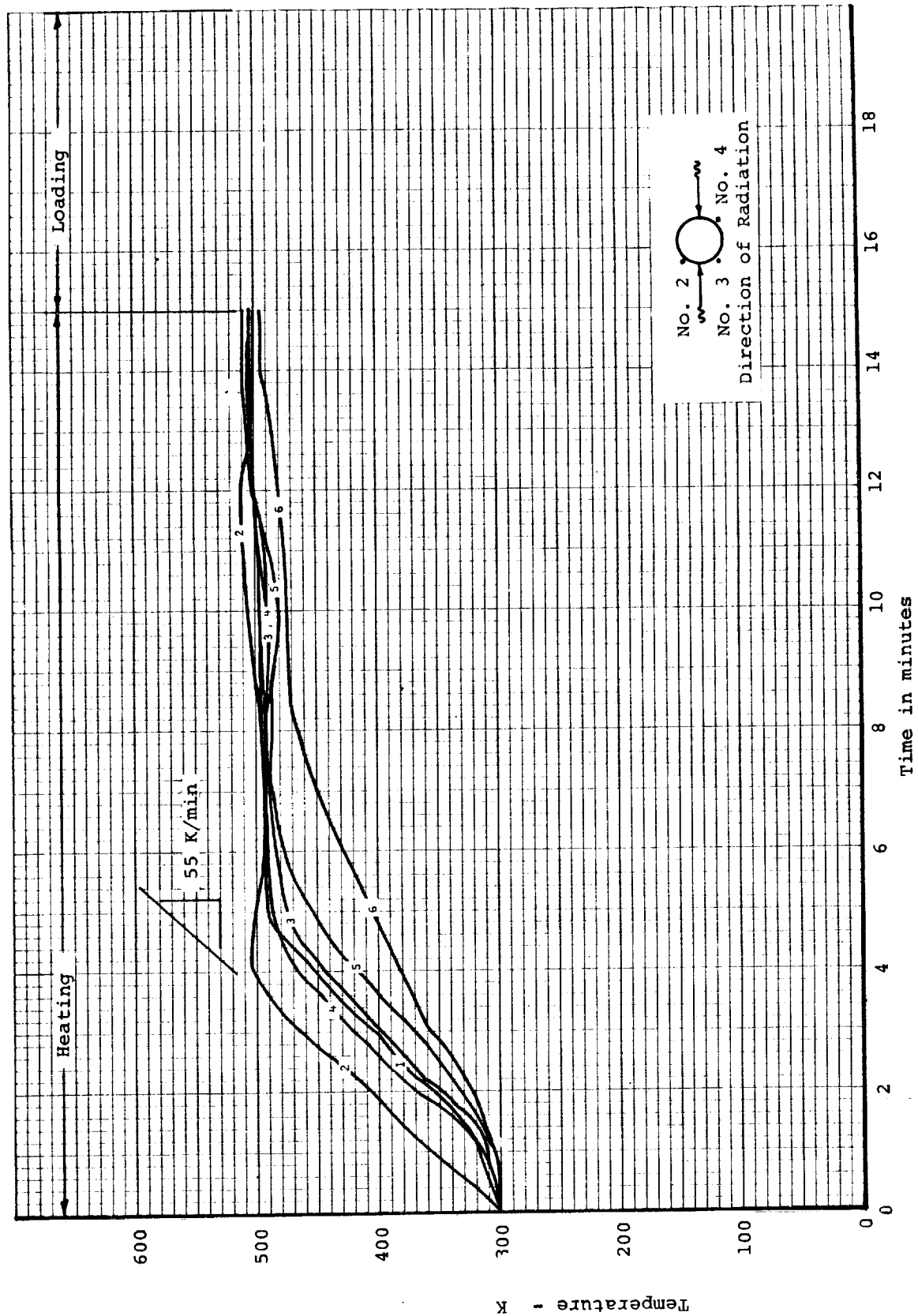
Figure 88. Typical heating curve for MG-1 compressive specimen – 55 K/min to 500 K

236
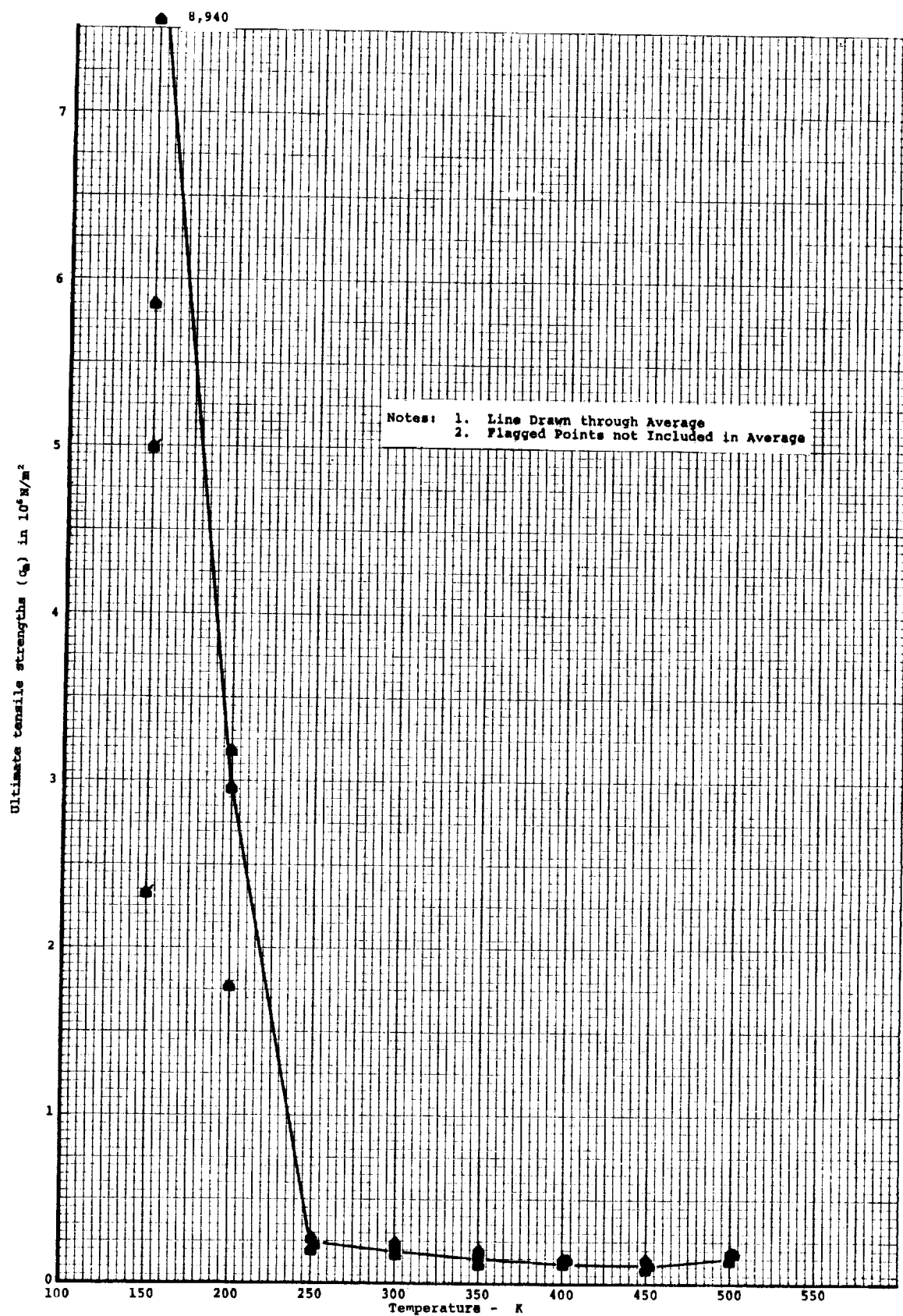
Figure 89. Ultimate tensile strength versus temperature for MG-1 Material

237
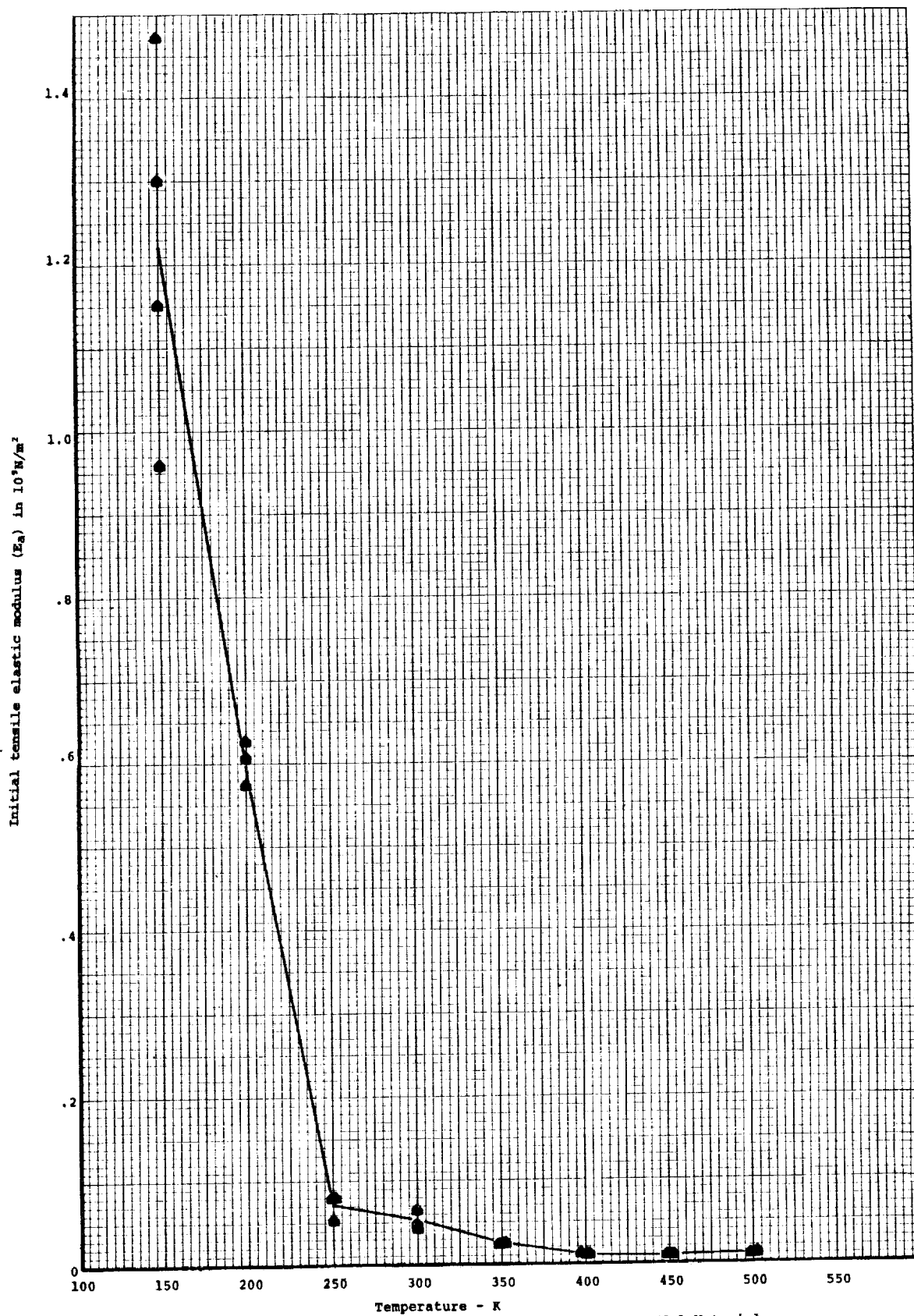
Figure 90. Initial tensile elastic modulus versus temperature for MG-1 Material

238
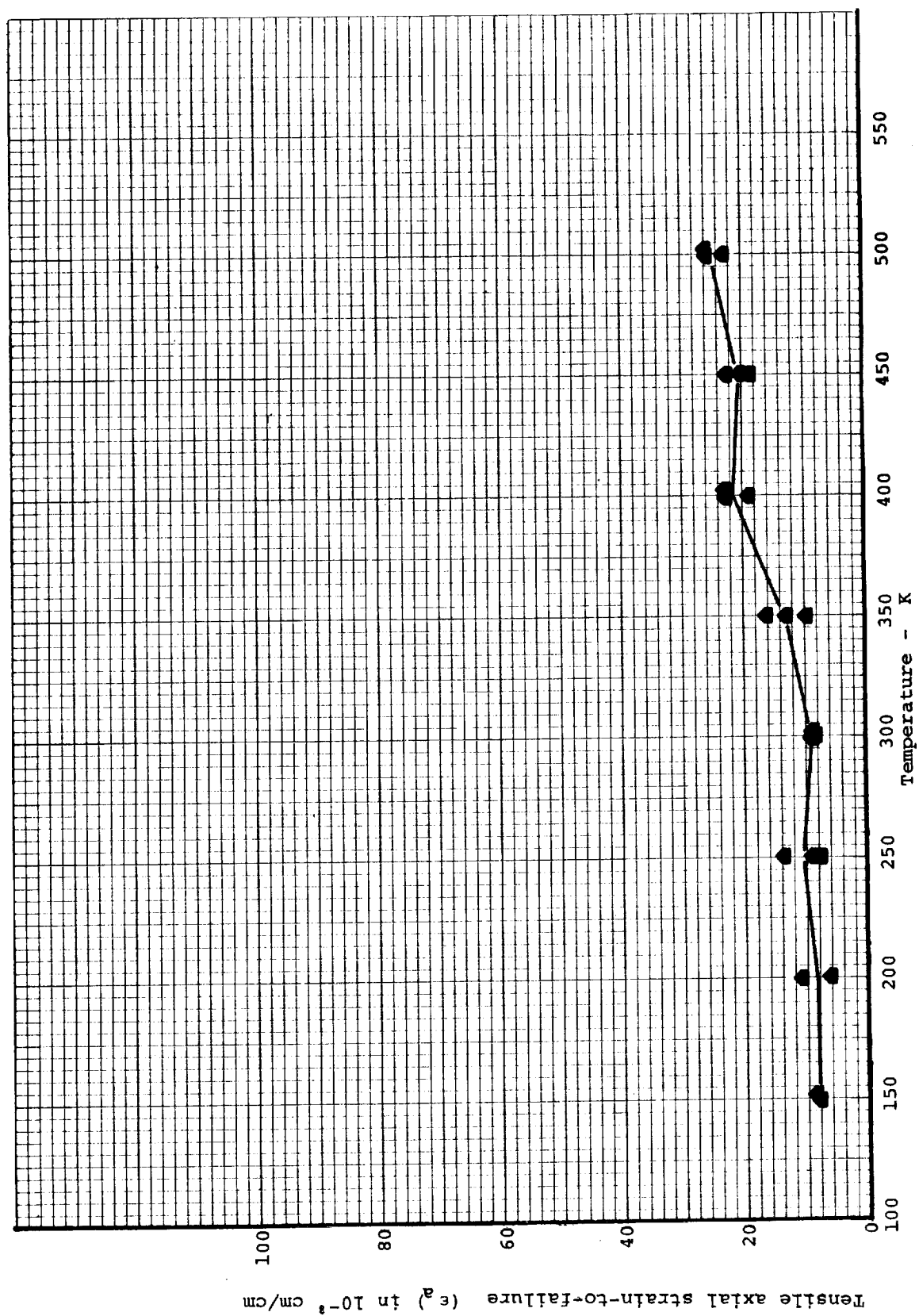
Figure 91. Tensile axial strain-to-failure versus temperature for MG-1 Material
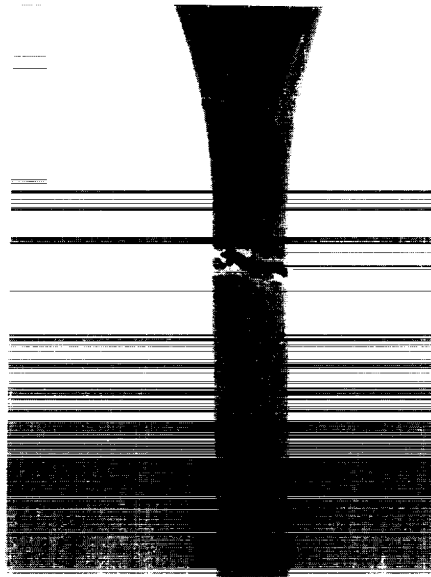
Specimen MG-1-1B-T32a4
300°K Test Temperature
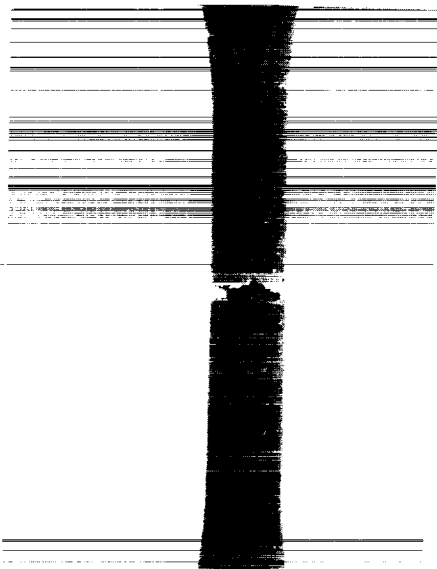
Specimen MG-1-1B-T20a4
150°K Test Temperature
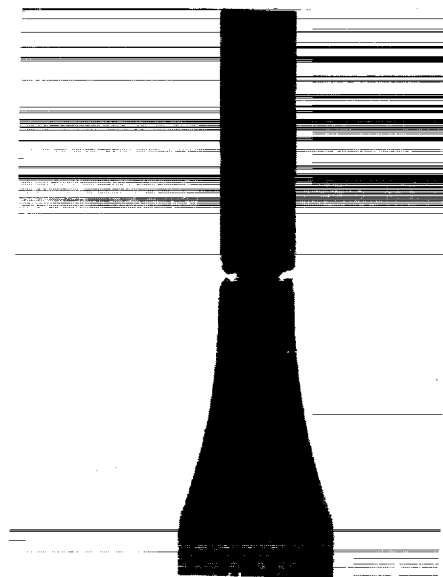
Specimen MG-1-1B-T18a4
500°K Test Temperature
Note darkening of speci-
men due to heating effects

Figure 92.   Typical failed specimens - MG-1 material

The graph contains the following labels and data:

SRI Run No: 2050-1-T-49
Material: MG-1
Specimen No: MG-1-1B-T8a4
Temperature: 500 K
Loading Direction: a
Stress Rate: 172 x 10³N/m²/sec
Specimen Gage Section: 1.27 Dia

Fracture
(26.3, .174)

$E_a = .0099 \times 10^9 \text{N/m}^2$

Unit axial strain in 10^{-3} cm/cm

Tensile stress in 10^6N/m²
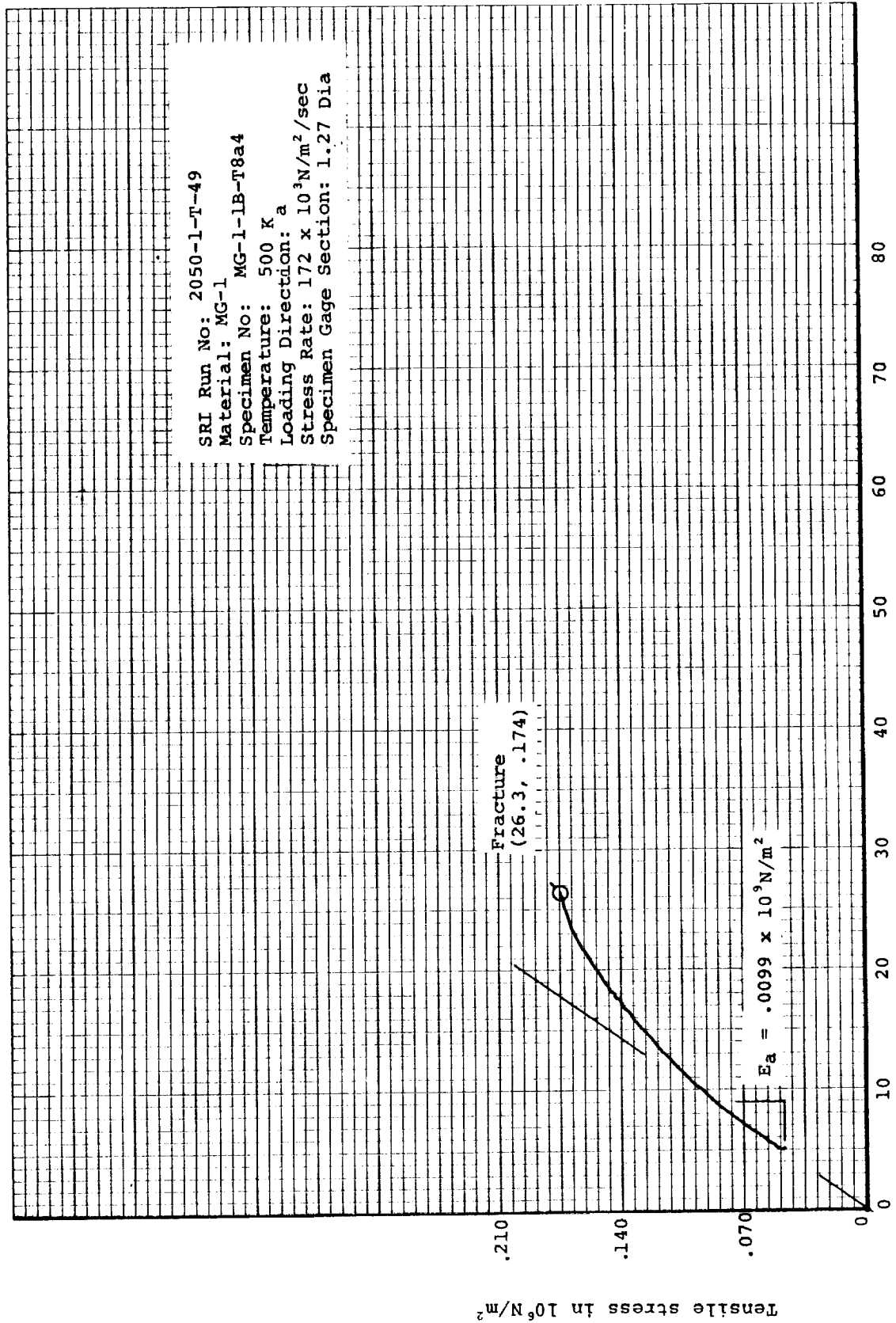
Figure 93. Typical "a" direction tensile stress-strain curve for MG-1 Material 500 K

241
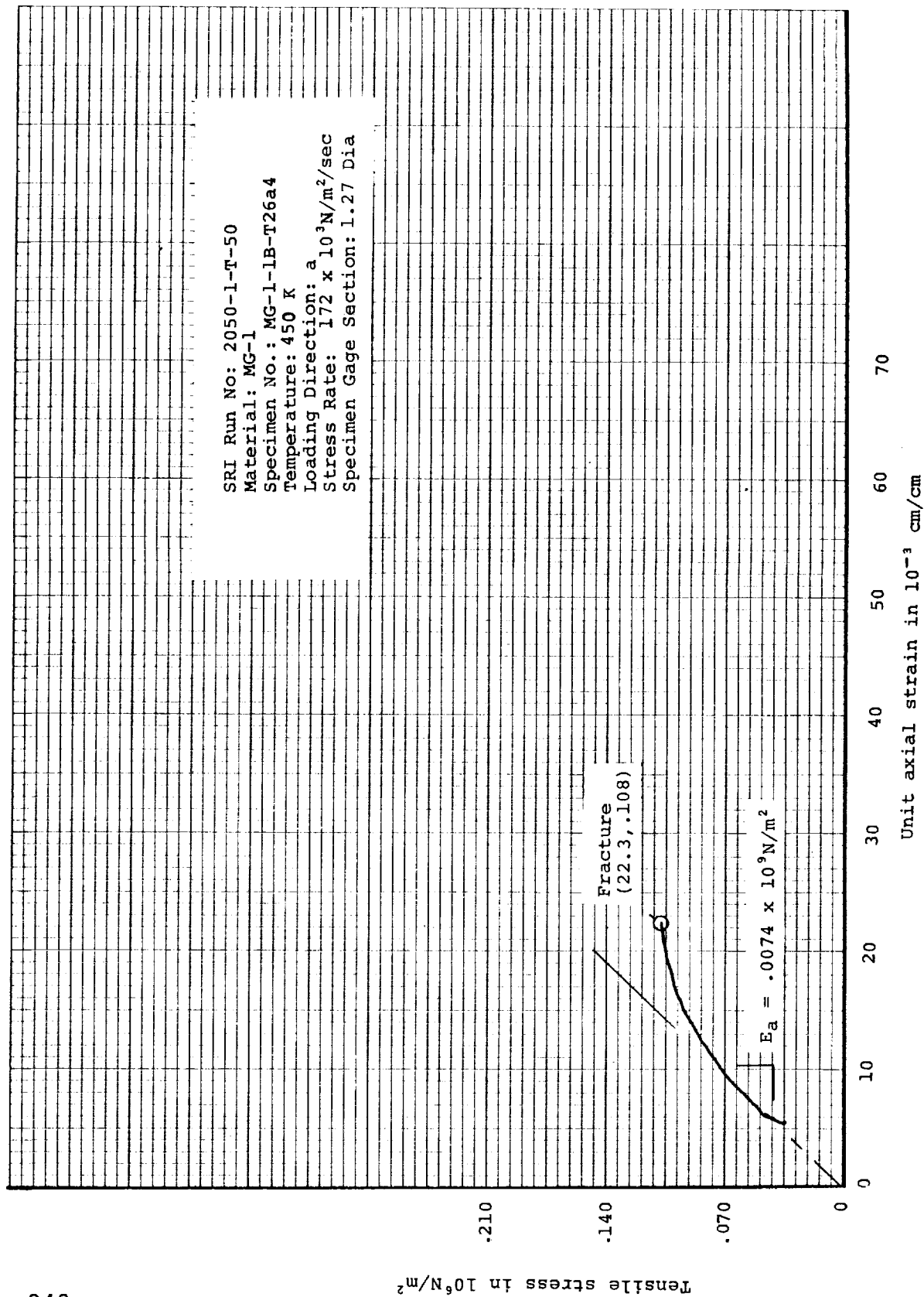
Figure 94. Typical "a" direction tensile stress-strain curve for MG-1 Material 450 K
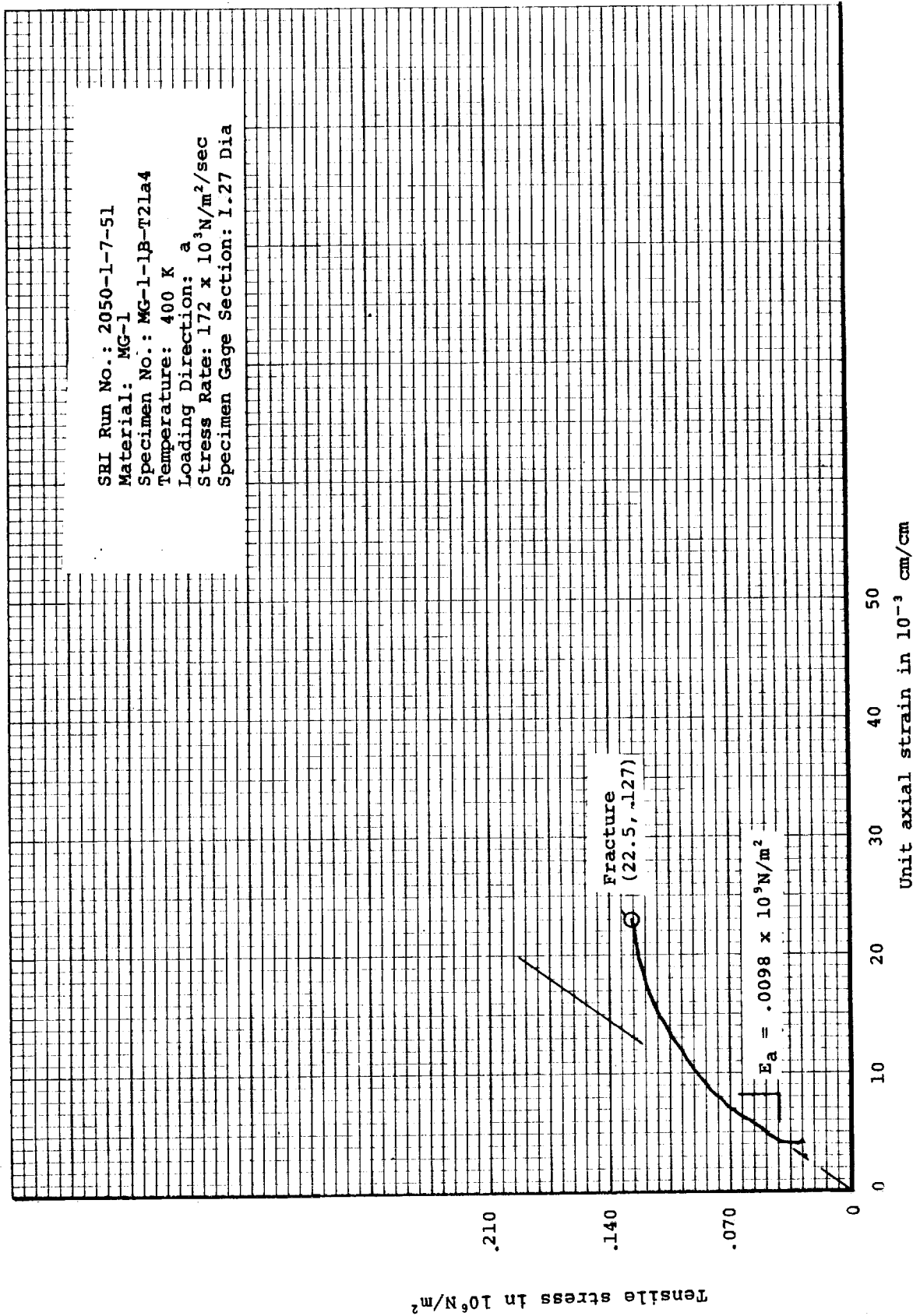
Figure 95. Typical "a" direction tensile stress-strain curve for MG-1 Material at 400 K

243

The graph contains the following labels and annotations:

SRI Run No.: 2050-1-T-42
Material: MG-1
Specimen No.: MG-1-1B-T15a4
Temperature: 350 K
Loading Direction: a
Stress Rate: 172 x 10^3 N/m²/sec
Specimen Gage Section: 1.27 Dia

Fracture
(16.1, .193)

E_a = .0238 x 10^9 N/m²

Tensile stress in 10^6 N/m²

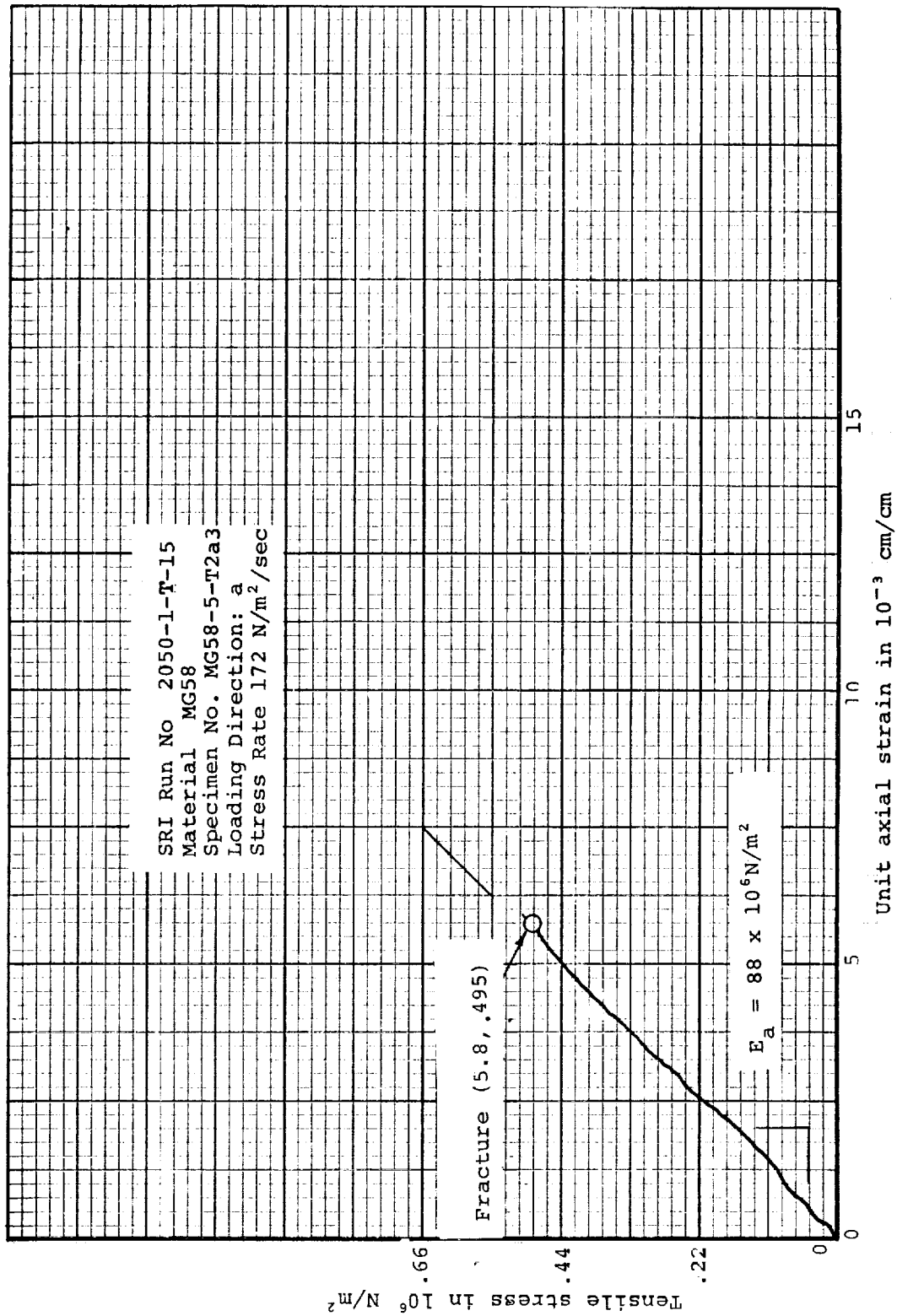Unit axial strain in 10^{-3} cm/cm
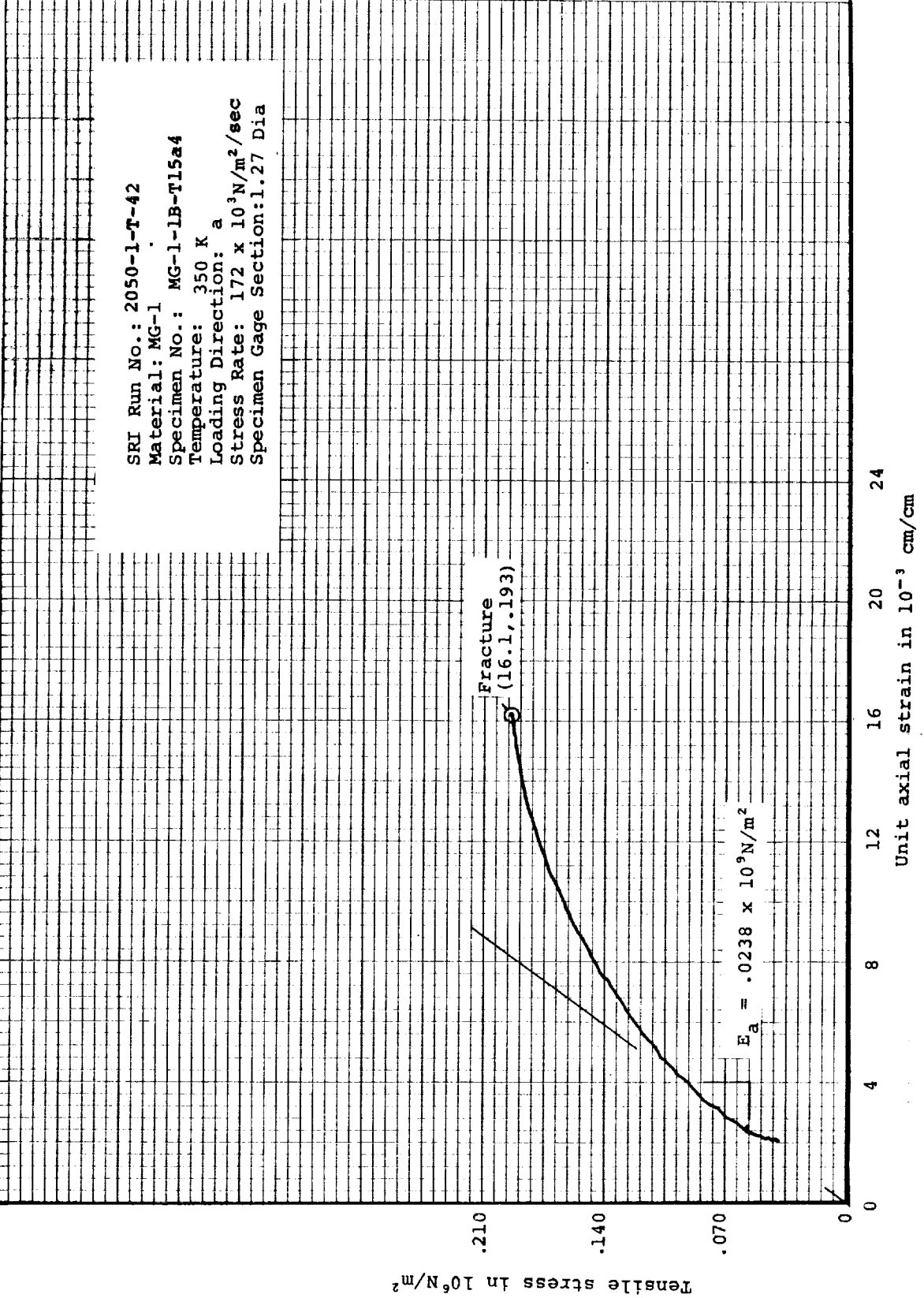
Figure 96. Typical "a" direction tensile stress-strain curve for MG-1 material at 350 K

244
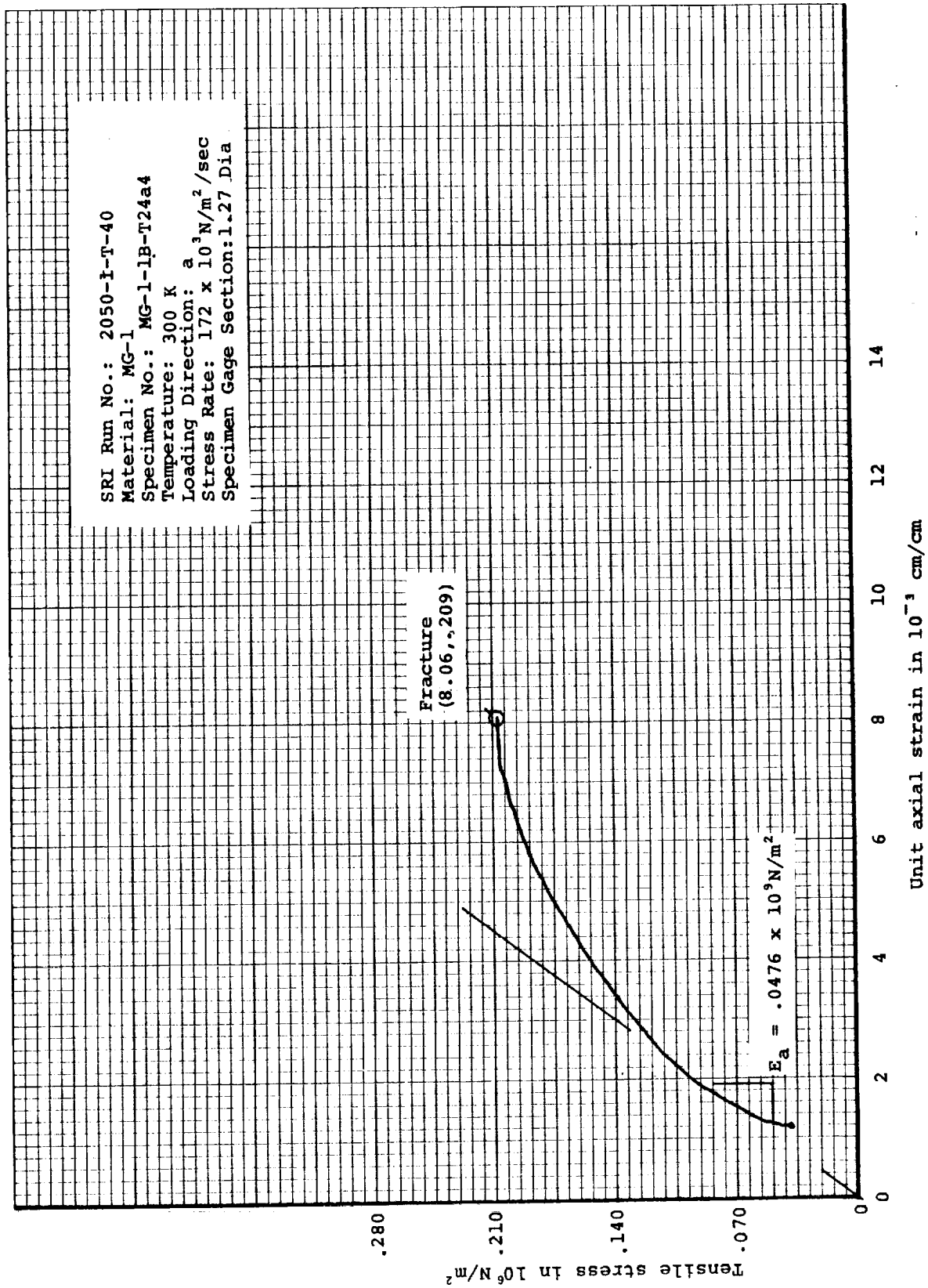
Figure 97. Typical "a" direction tensile stress-strain curve for MG-1 material at 300 K

245

The following information appears within the figure:

SRI Run No.: 2050-1-T-30
Material: MG-1
Specimen No.: MG-1-1B-T28a4
Temperature: 250 K
Loading Direction: a
Stress Rate: 172 x 10³N/m²/sec
Specimen Gage Section: 1.27 Dia

Fracture
(8.85, .232)

$E_a = .0799 \times 10^9 \text{N/m}^2$

Unit axial strain in 10^{-3} cm/cm

Tensile stress in 10^6N/m²
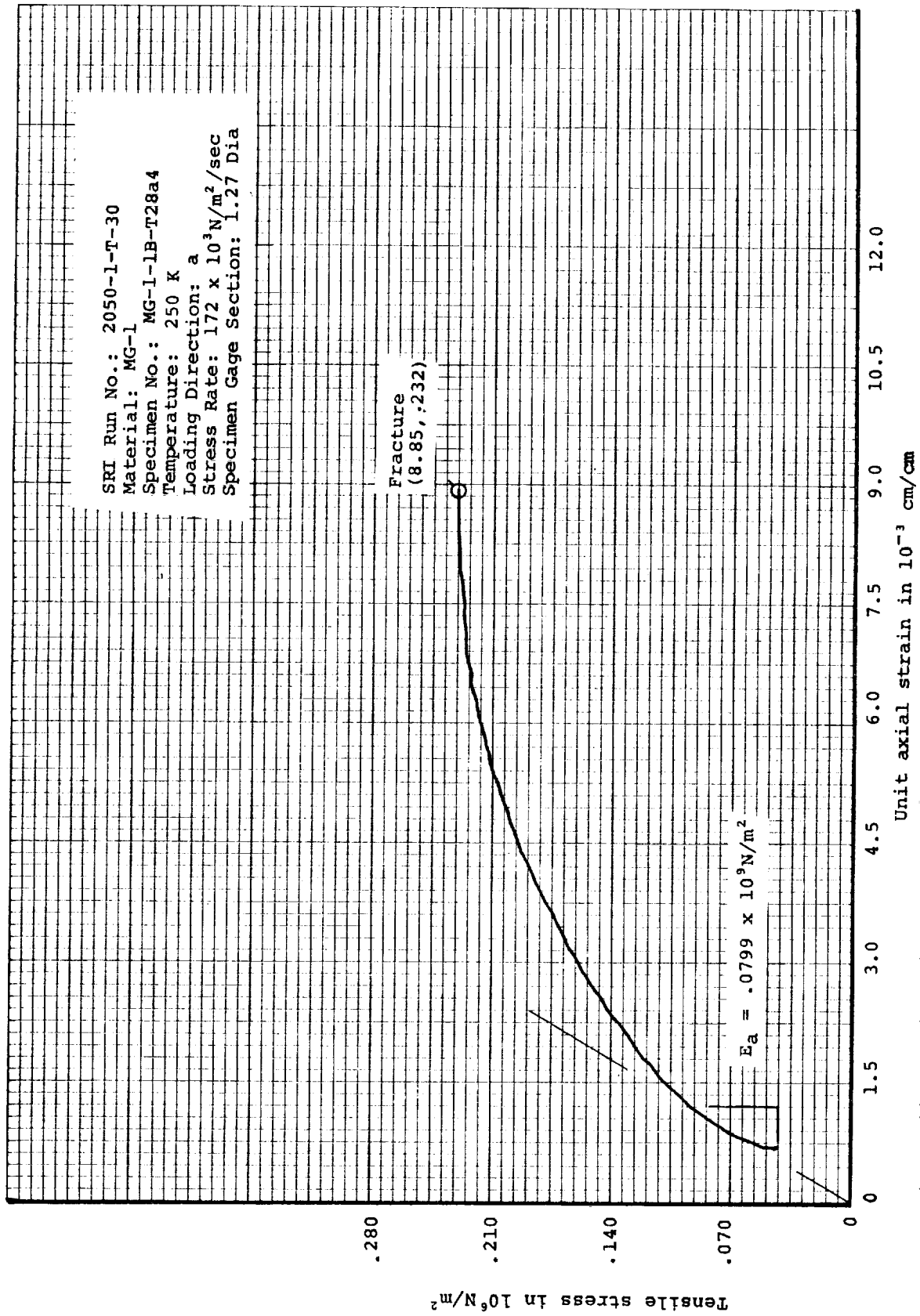
Figure 98. Typical "a" direction tensile stress-strain curve for MG-1 material at 250 K

246
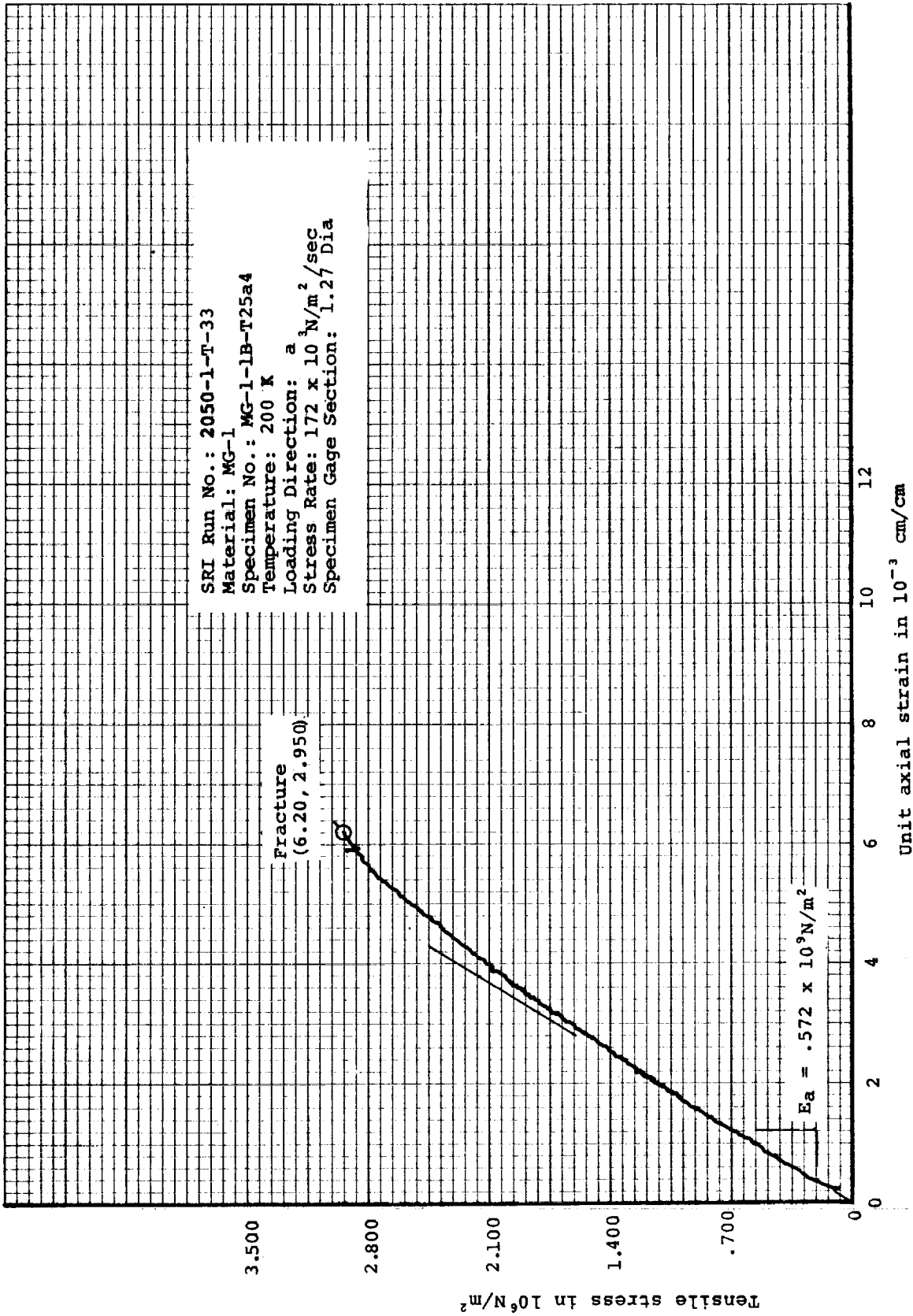
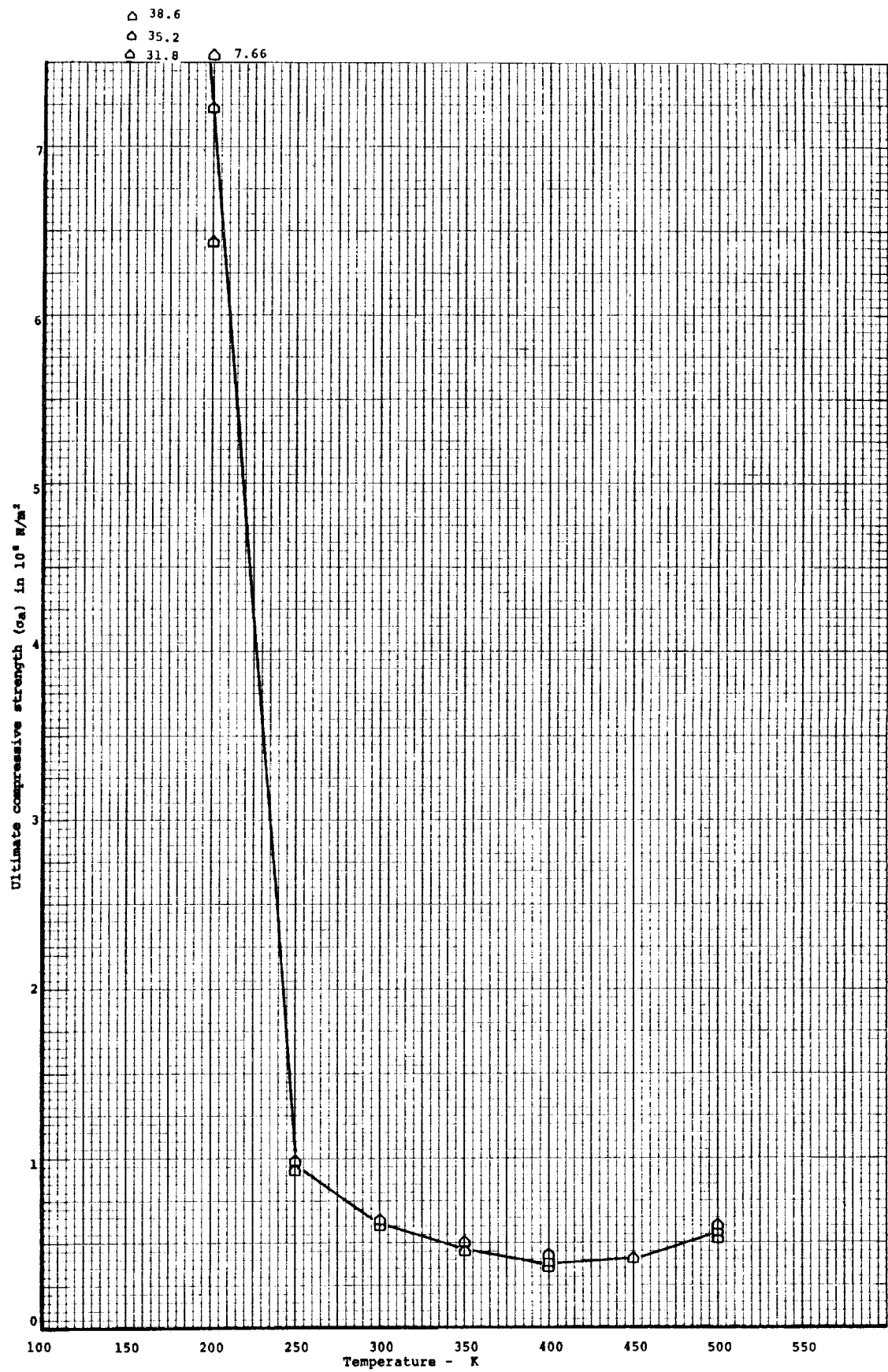Figure 99. Typical "a" direction tensile stress-strain curve for MG-1 Material at 200 K

SRI Run No.: 2050-1-T-33
Material: MG-1
Specimen No.: MG-1-1B-T25a4
Temperature: 200 K
Loading Direction: a
Stress Rate: 172 x 10³ N/m²/sec
Specimen Gage Section: 1.27 Dia

Fracture
(6.20, 2.950)

$E_a = .572 \times 10^9 \text{N/m}^2$

Tensile stress in 10^6N/m^2

Unit axial strain in 10^{-3} cm/cm
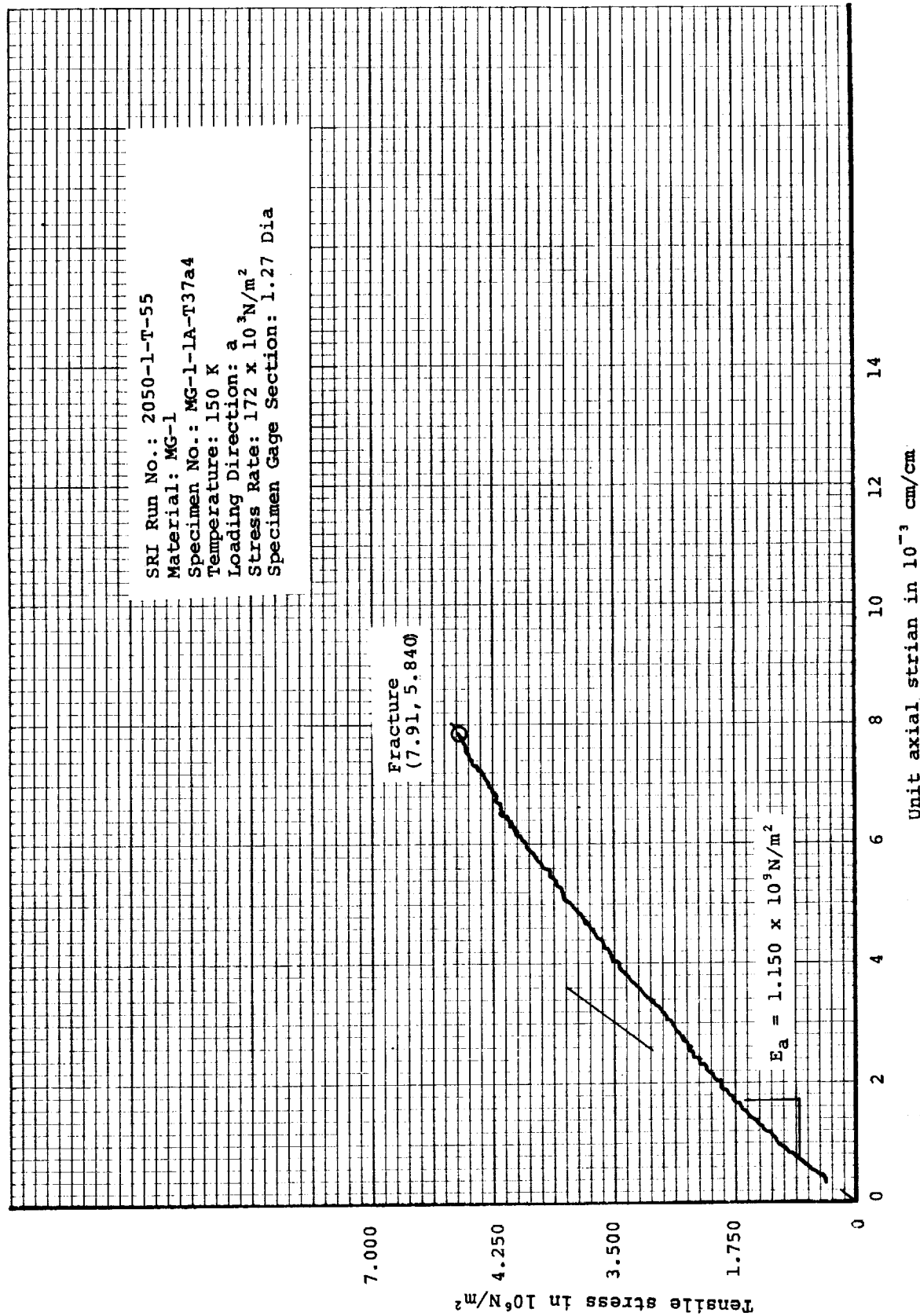
Figure 100. Typical "a" direction tensile stress-strain curve for MG-1 material at 150 K

SRI Run No.: 2050-1-T-55
Material: MG-1
Specimen No.: MG-1-1A-T37a4
Temperature: 150 K
Loading Direction: a
Stress Rate: 172 x 10³N/m²
Specimen Gage Section: 1.27 Dia

Fracture
(7.91, 5.840)

$E_a = 1.150 \times 10^9 \text{N/m}^2$

Unit axial strian in 10⁻³ cm/cm

Tensile stress in 10⁶N/m²

248
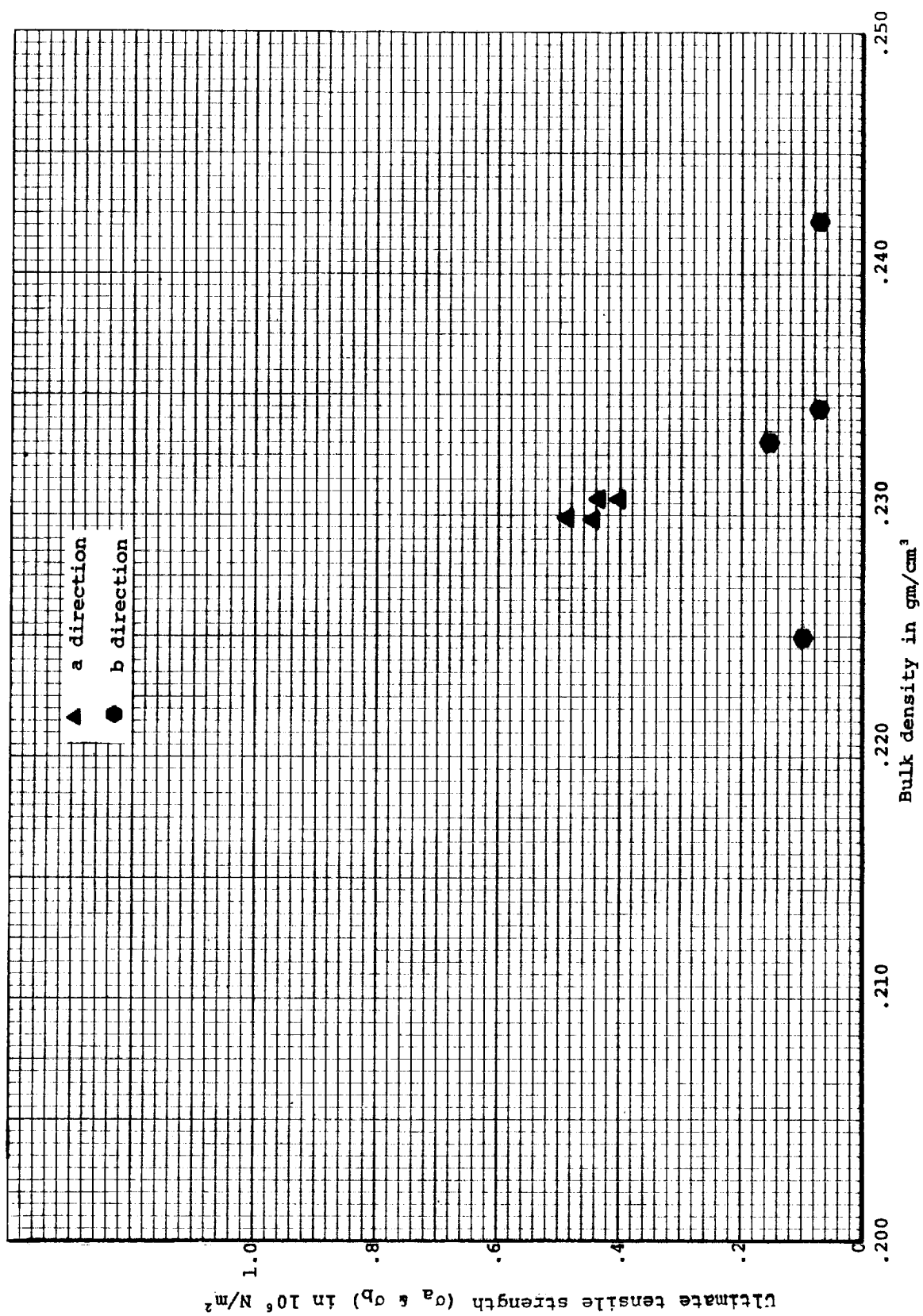
Figure 101. Ultimate tensile strength versus bulk density for MG-45 material

249
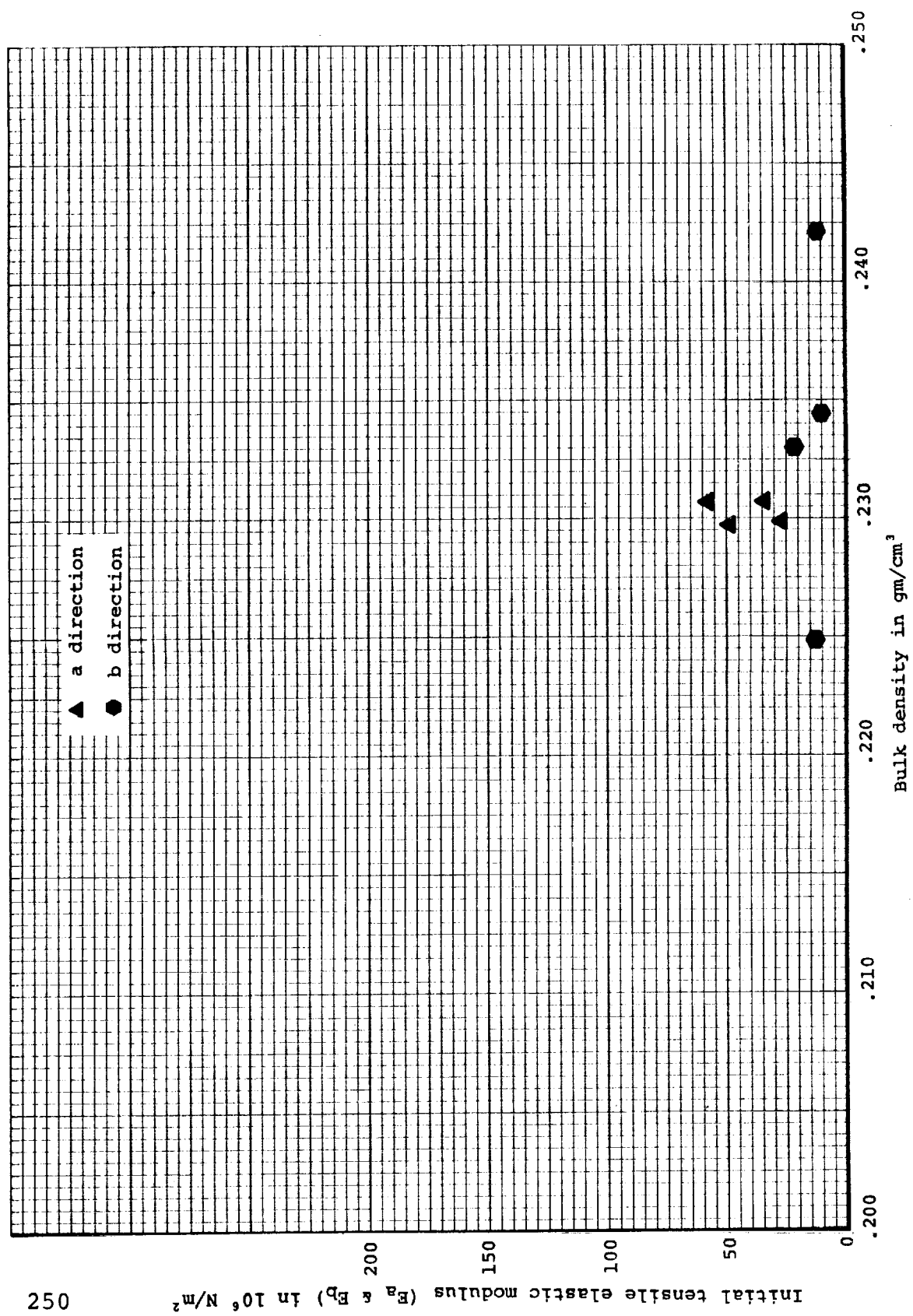
Figure 102. Initial tensile elastic modulus versus bulk density for MG-45 Material

250
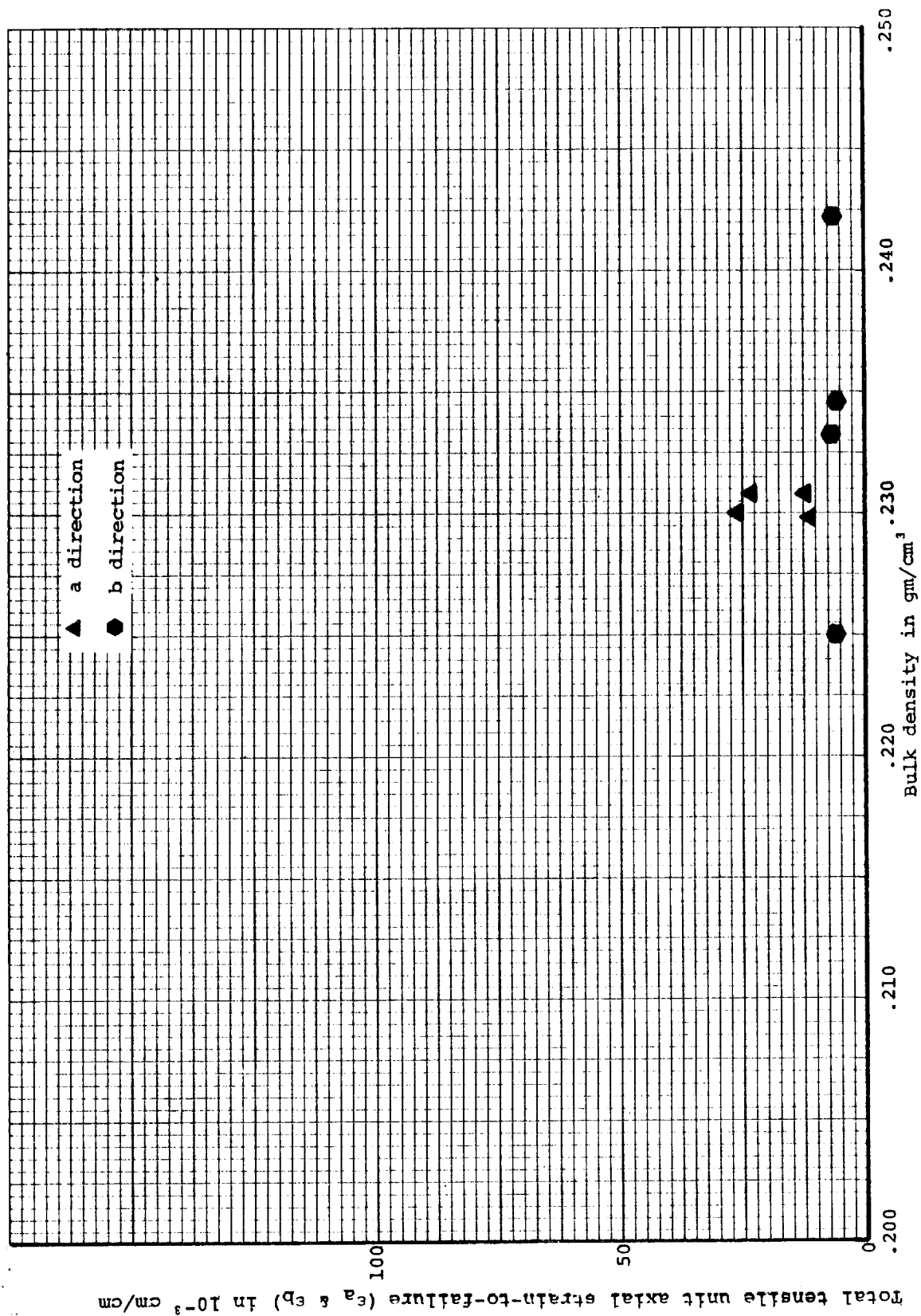
Figure 103. Total tensile unit axial strain-to-failure versus bulk density for MG-45 Material

Specimen MG-45-3-T11bl
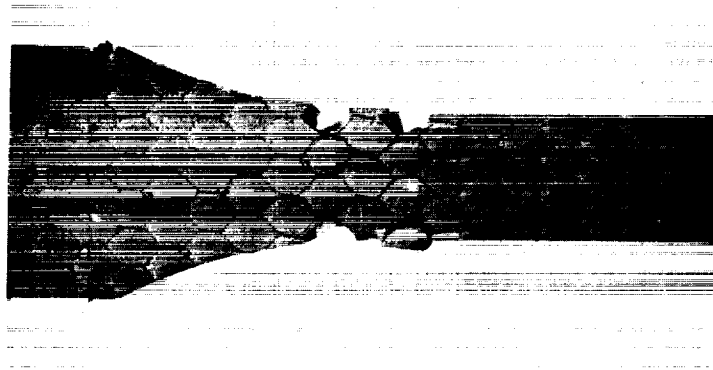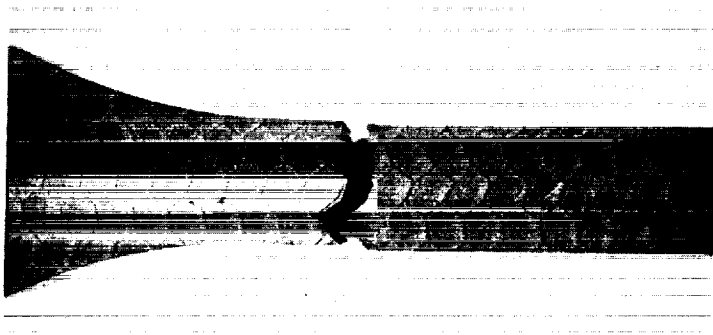
Specimen MG-45-5-T13bl
Note honeycomb misalignment

Specimen MG-45-5-T4al
Note honeycomb misalignment
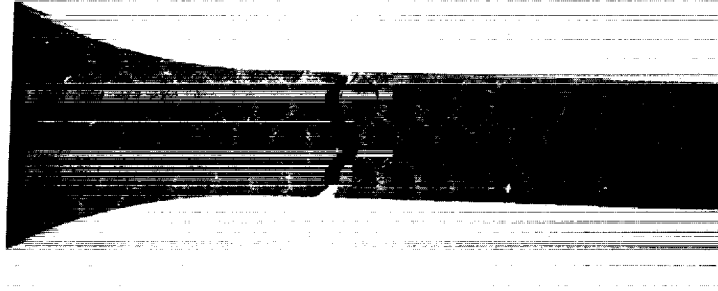
Figure 104. Photographs of typical failed MG-45 tensile specimens
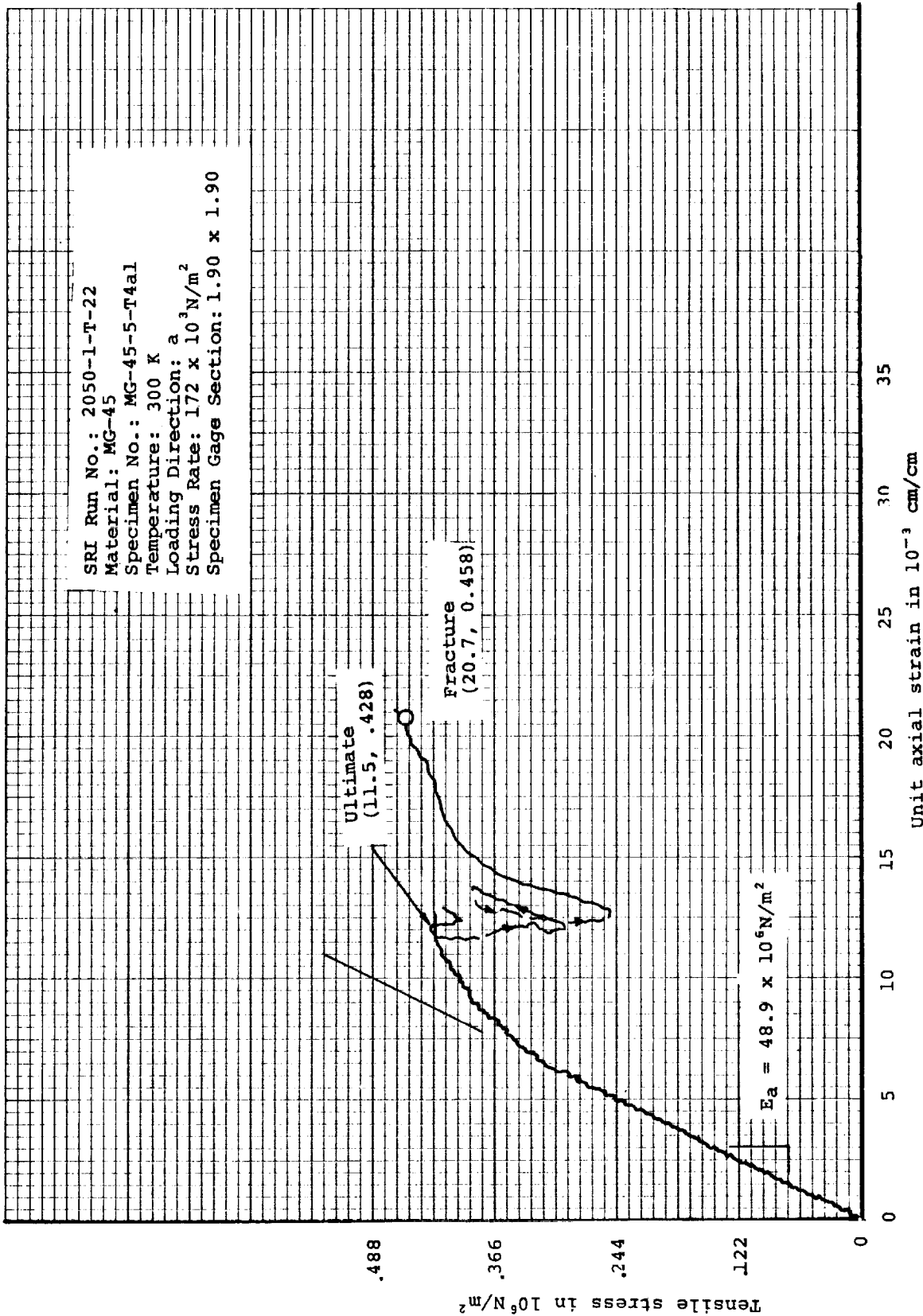
Figure 105. Typical "a" direction tensile stress-strain curve for MG-45 Material

The figure contains the following labeled information:

SRI Run No.: 2050-1-T-22
Material: MG-45
Specimen No.: MG-45-5-T4al
Temperature: 300 K
Loading Direction: a
Stress Rate: 172 x 10^3 N/m^2
Specimen Gage Section: 1.90 x 1.90

Ultimate (11.5, .428)

Fracture (20.7, 0.458)

$E_a = 48.9 \times 10^6$ N/m^2

Unit axial strain in 10^{-3} cm/cm

Tensile stress in 10^6 N/m^2

SRI Run No.: 2050-1-T-27
Material: MG-45
Specimen No.: MG-45-2-T10b1
Temperature: 300 K
Loading Direction: b
Stress Rate: 172 x 10^3 N/m^2
Specimen Gage Section: 1.90 x 1.90

E_a = 12.5 x 10^6 N/m^2

Fracture
(6.7, .0795)

Unit axial strain in 10^{-3} cm/cm

Tensile stress in 10^6 N/m^2

Figure 106. Typical "b" direction tensile stress-strain curve for MG-45 Material
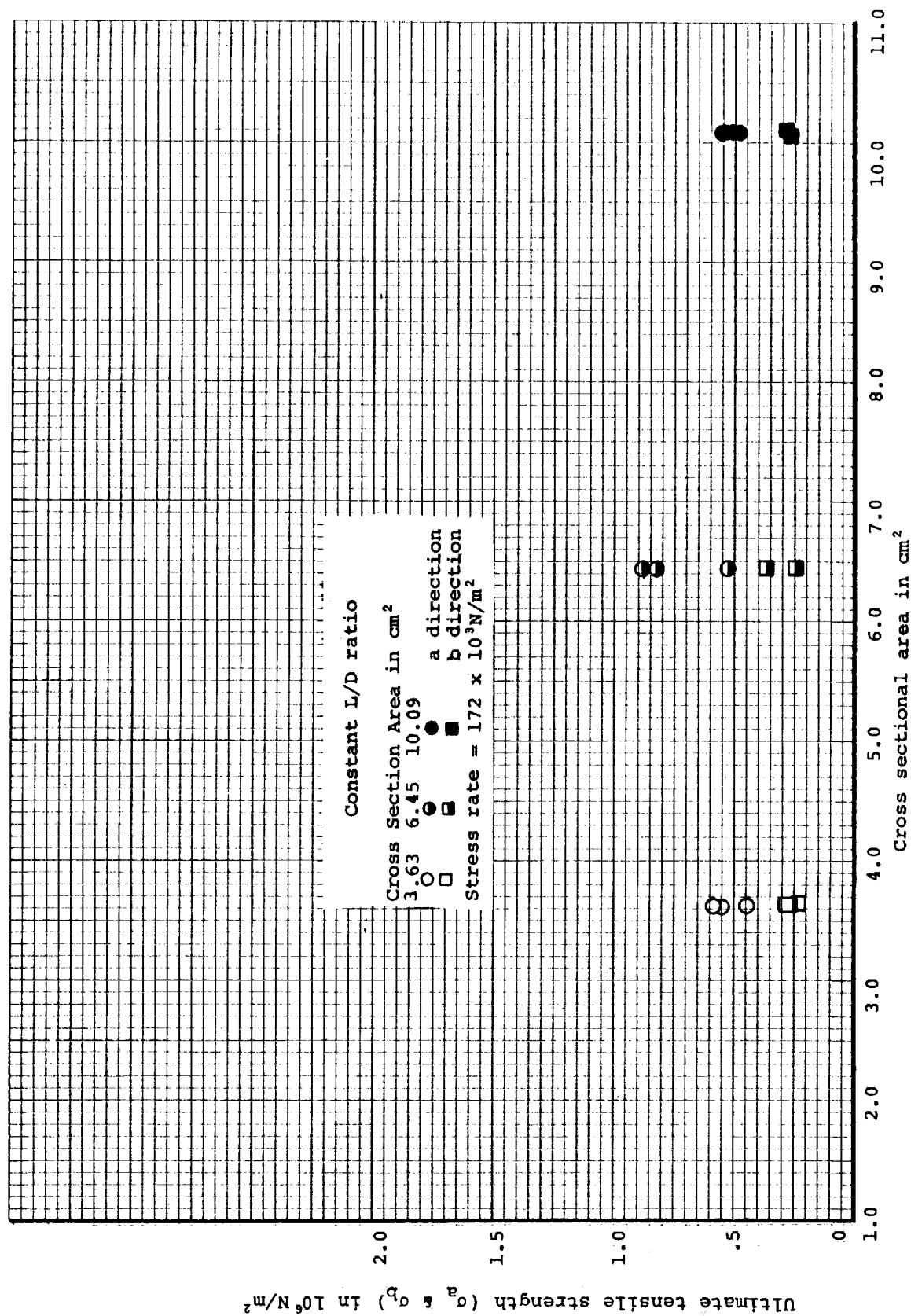
Figure 107. Ultimate tensile strength versus cross-sectional area for MG-58 Material
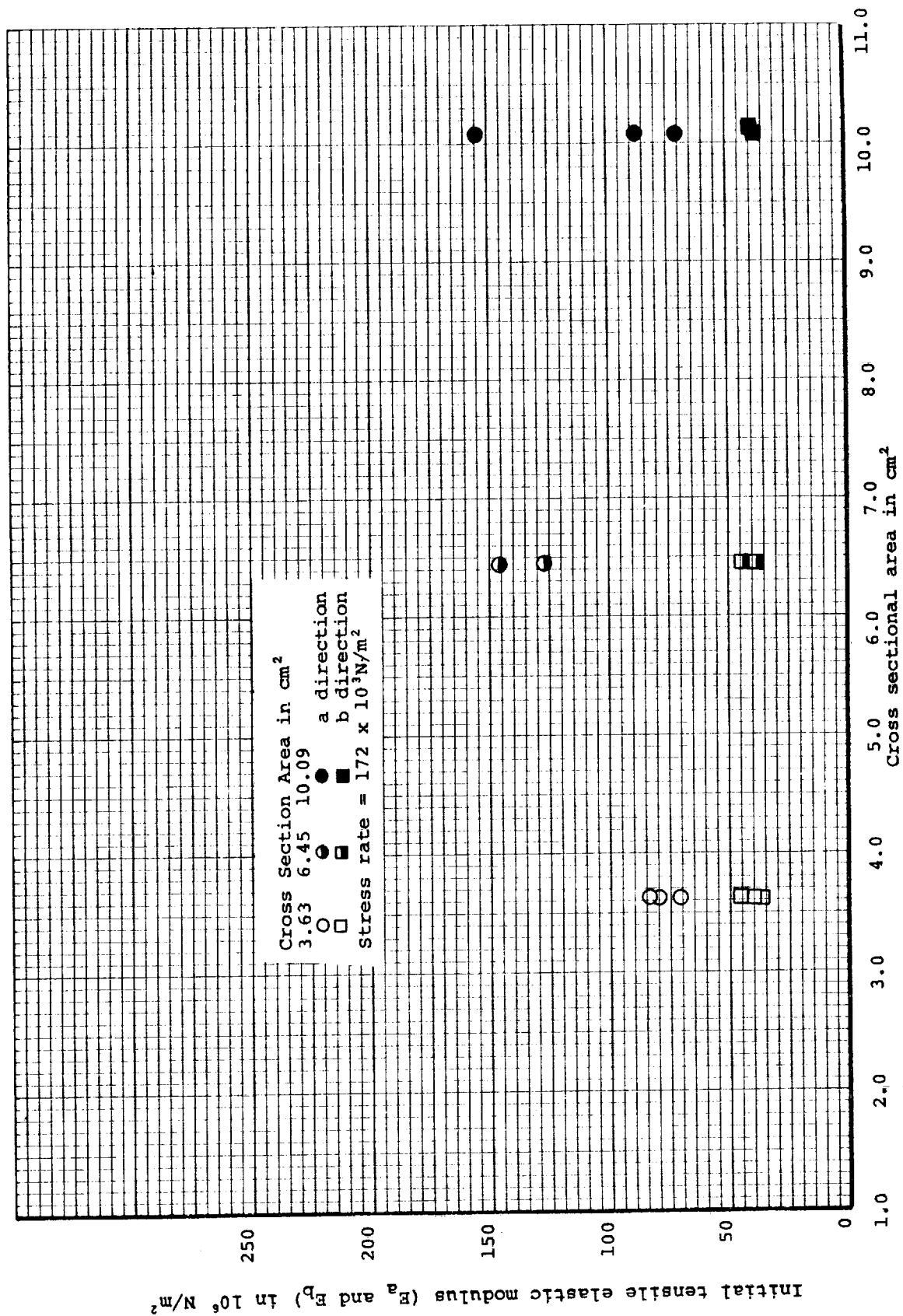
Figure 108. Initial tensile elastic modulus versus cross-sectional area for MG-58 material

256
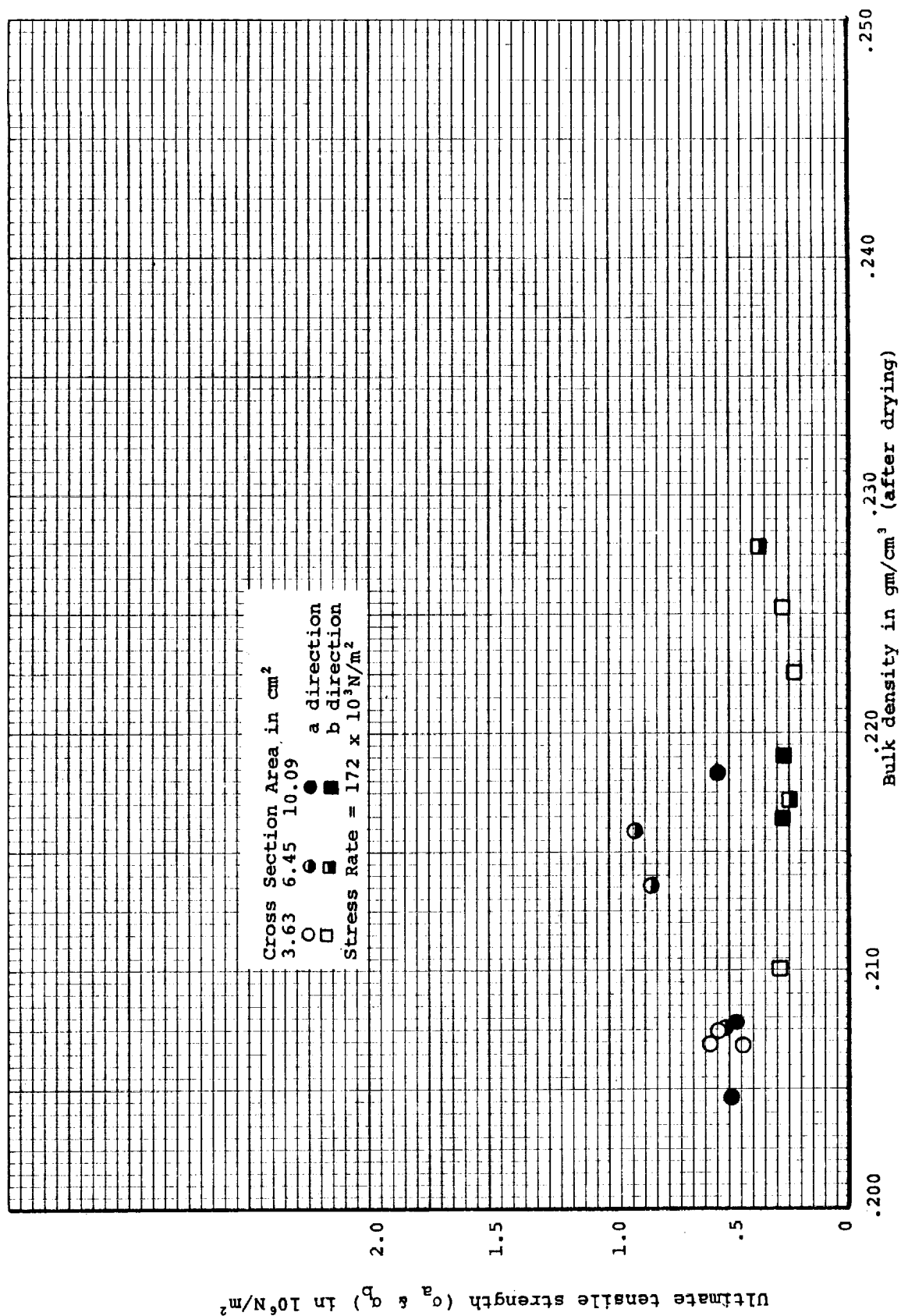
Figure 109. Ultimate tensile strength versus bulk density for MG-58 material

257
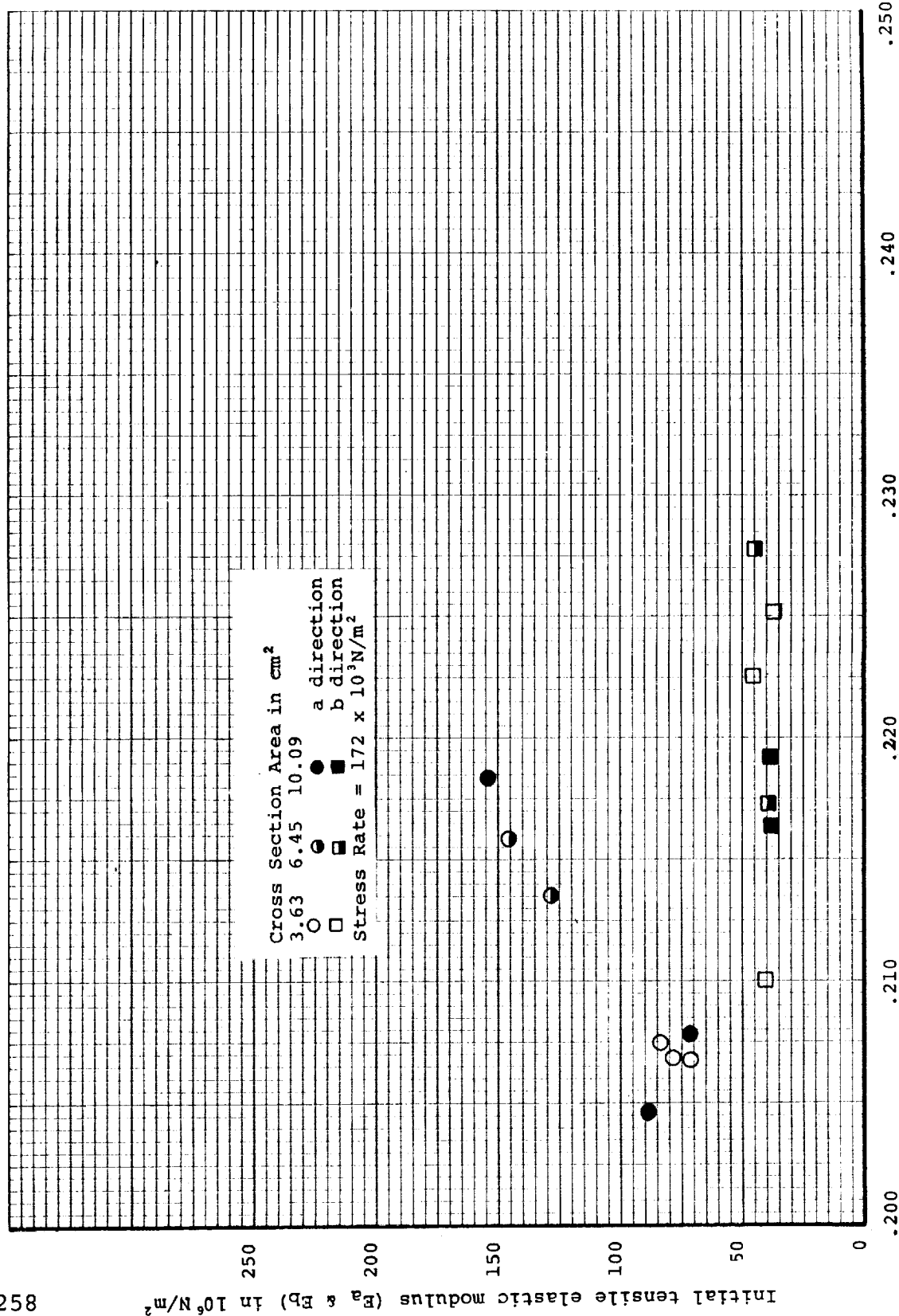
Figure 110. Initial tensile elastic modulus versus bulk density for MG-58 material
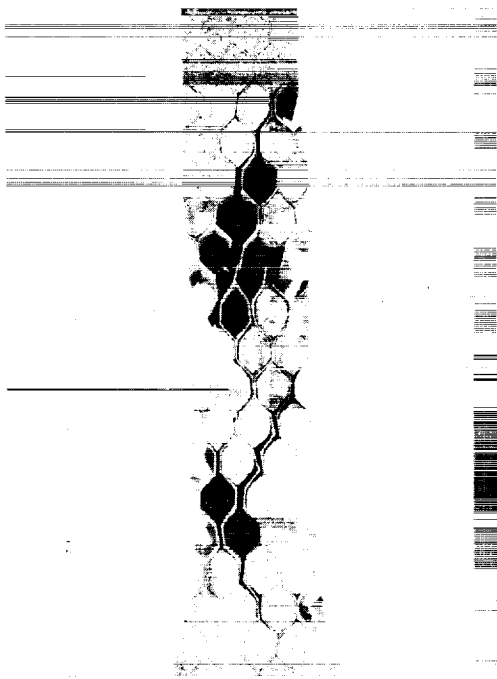
a. Specimen MG-58-5-T1a1
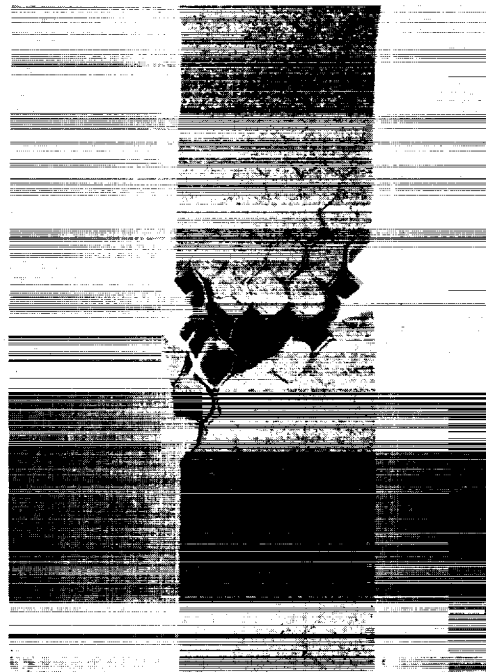
b. Specimen MG-58-2-T8a3
Note honeycomb misalignment
in failure area
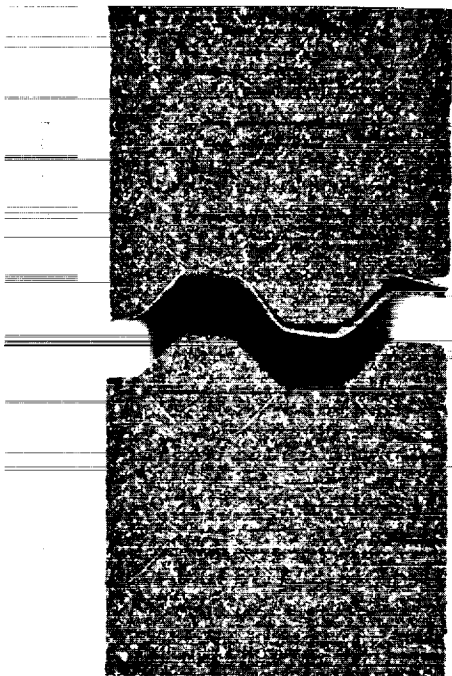
c. Specimen MG-58-3-T30b1

d. Specimen MG-58-3-T34b1

Figure 111.   Photographs of typical tensile fracture areas plane of
all pictures is ab plane (all 1X) - MG-58 material

Figure 112. Typical "a" direction tensile stress-strain curve for MG-58 material

260

The plotted figure contains the following text labels:

SRI Run No 2050-1-T-11
Material MG58
Specimen No. MG58-3-T30b1
Loading Direction: b
Stress Rate 172 N/m^2/sec

Fracture (7.4, 0.245)

$E_a = 45 \times 10^6 N/m^2$

Tensile stress in $10^6 N/m^2$

0.490

0.245

0

Unit axial strain in 10^{-3} cm/cm

20

10

0
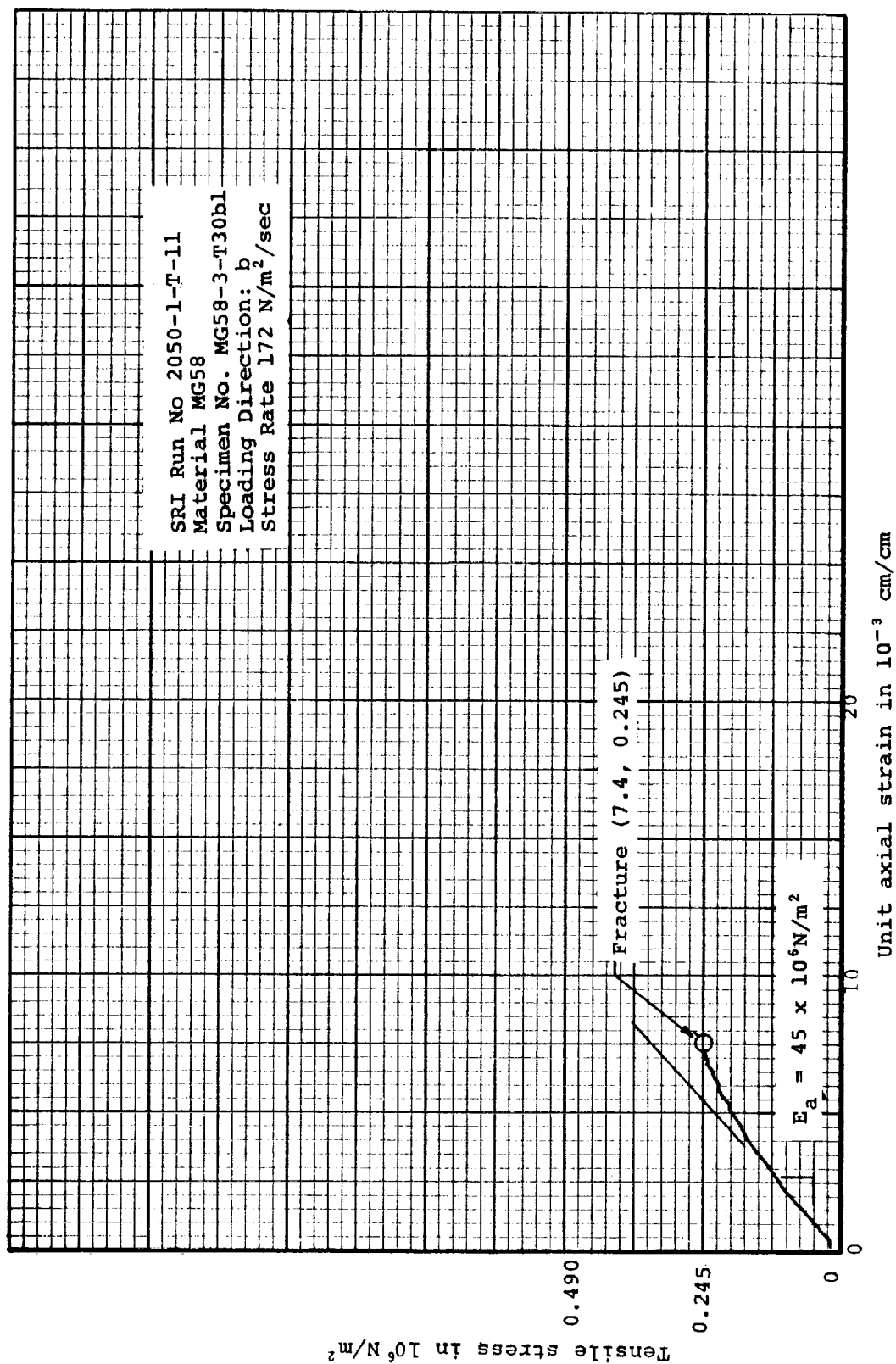
Figure 113. Typical "b" direction tensile stress-strain curve for MG-58 material

261

Figure 114. Ultimate "a" direction compressive strength versus temperature for MG-1 material

262

Figure 115. Initial compressive ("a" direction) elastic modulus versus temperature for MG-1 material
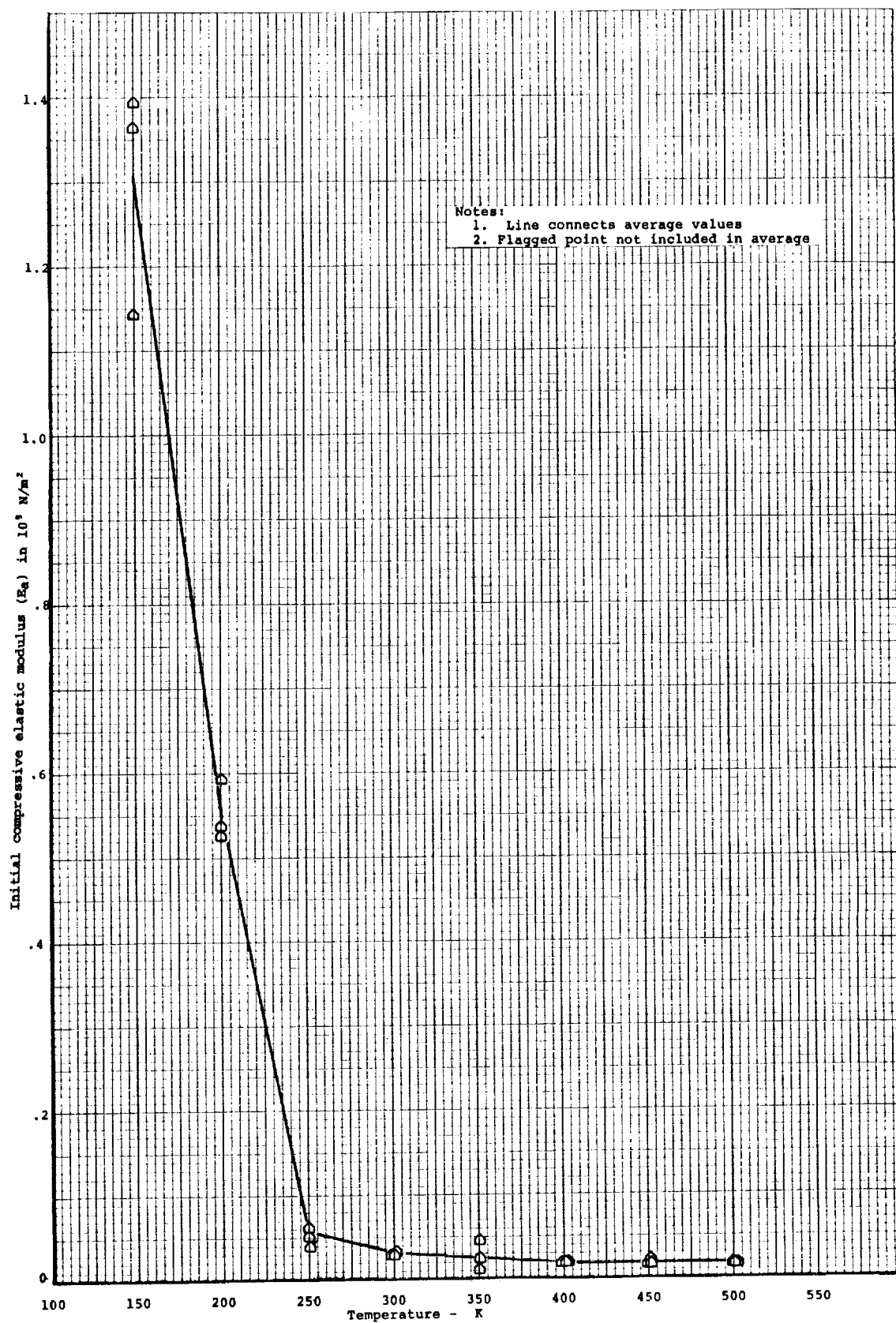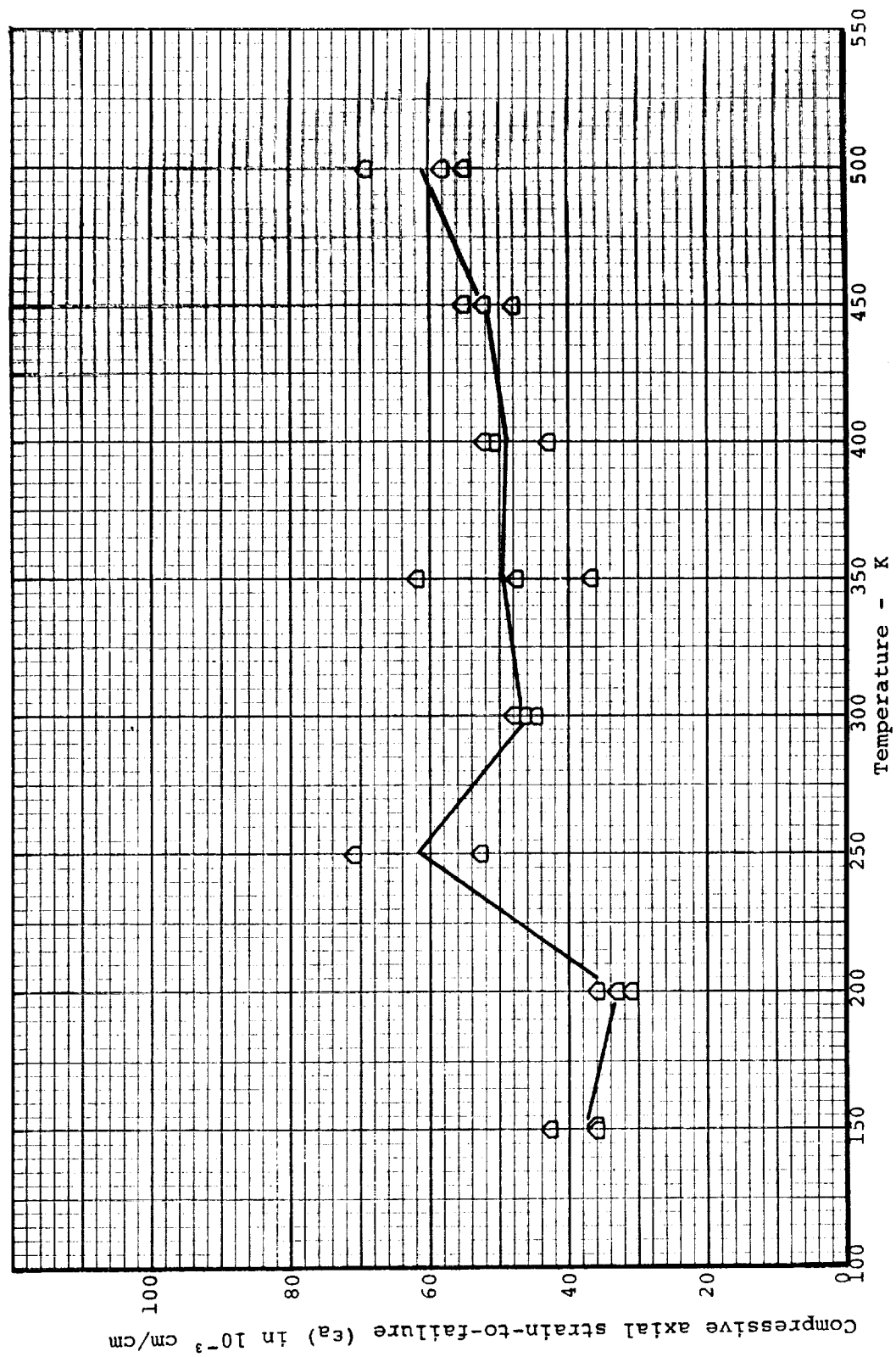
Figure 116. Compressive axial strain-to-failure ("a" direction) versus temperature for MG-1 material

264
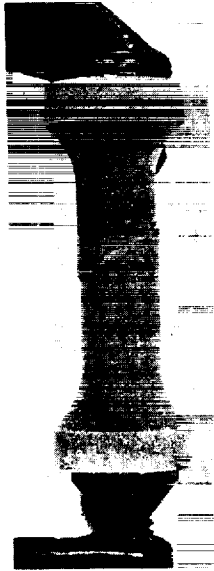
Specimen MG-1-1B-C30a4
150°K Test Temperature.
Specimen failed, however
complete separation did
not occur at fracture.
Clamp is compressing
specimen to indicate
fracture
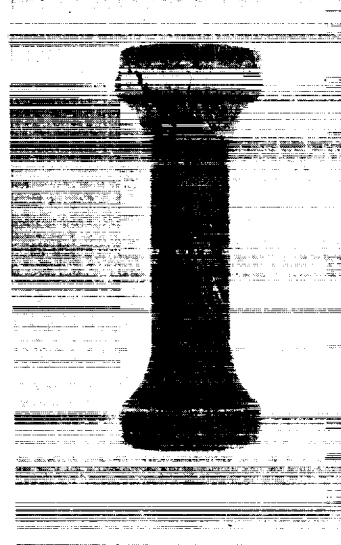
Specimen MG-1-1B-C28a4
200°K Test Temperature.
Failure at foot due to
temperature gradient
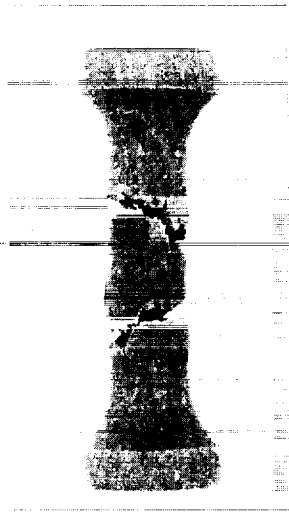
Specimen MG-1-1B-C29a4
250°K Test Temperature
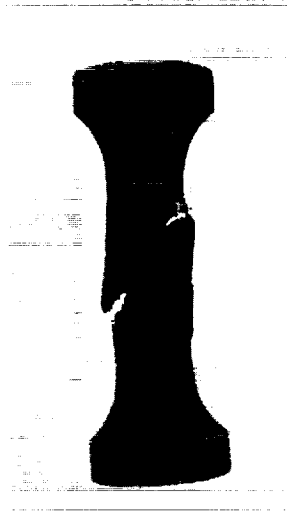
Specimen MG-1-1B-C10a4
450°K Test Temperature.
Note darkening of speci-
men resulting from heat-
ing
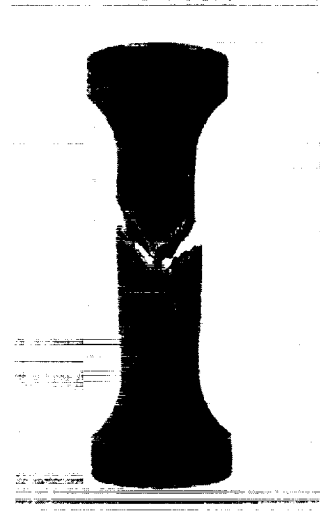
Specimen MG-1-1B-C19a4
350°K Test Temperature

Figure 117. Typical failed compressive specimens - MG-1 material
(plane of all photographs is ac plane)

265
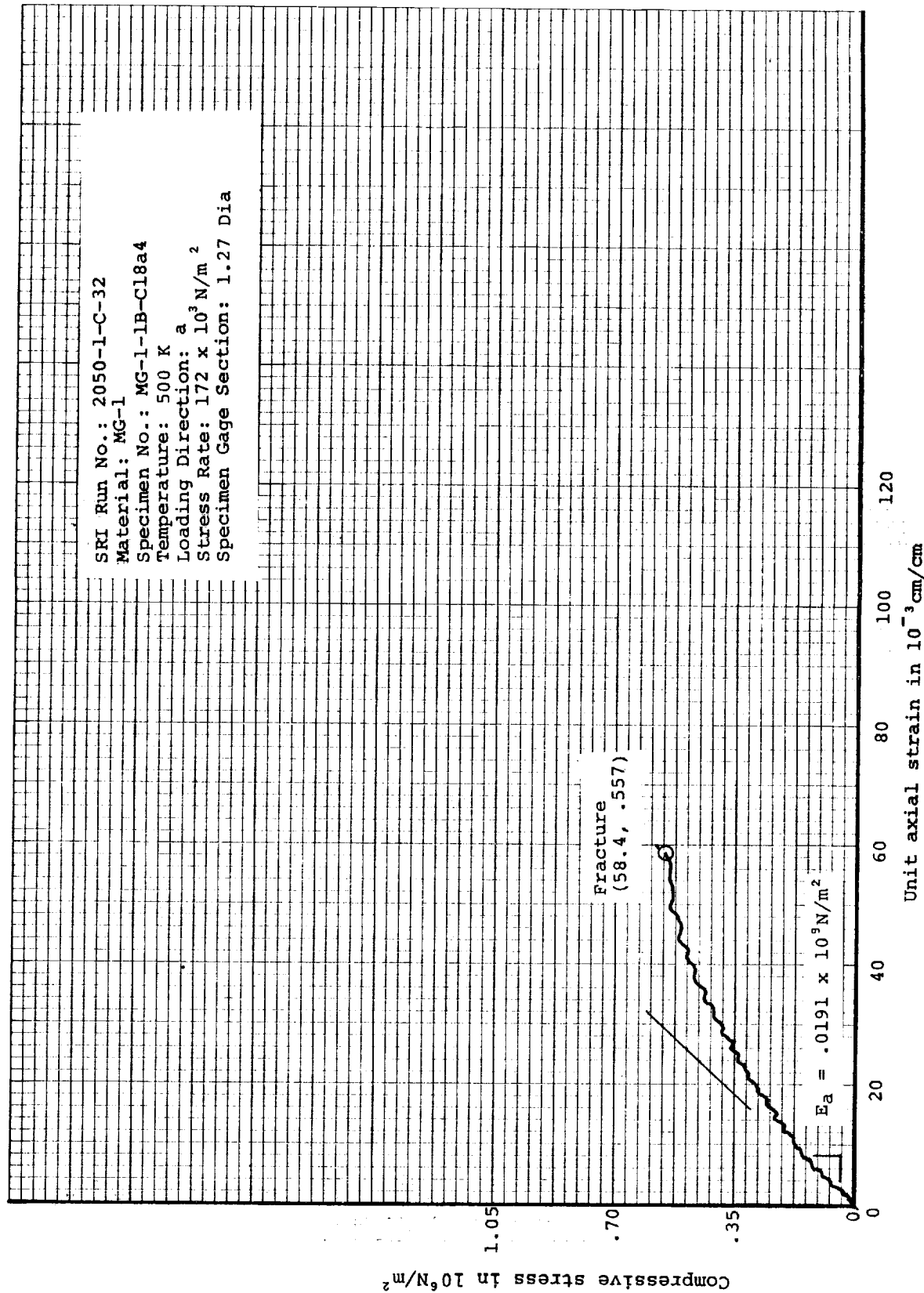
Figure 118. Typical "a" direction compressive stress-strain curve for MG-1 material at 500 K

The following information appears within the figure:

SRI Run No.: 2050-1-C-32
Material: MG-1
Specimen No.: MG-1-1B-C18a4
Temperature: 500 K
Loading Direction: a
Stress Rate: $172 \times 10^3 \, N/m^2$
Specimen Gage Section: 1.27 Dia

Fracture
(58.4, .557)

$E_a = .0191 \times 10^9 \, N/m^2$

Unit axial strain in 10^{-3} cm/cm

Compressive stress in $10^6 \, N/m^2$
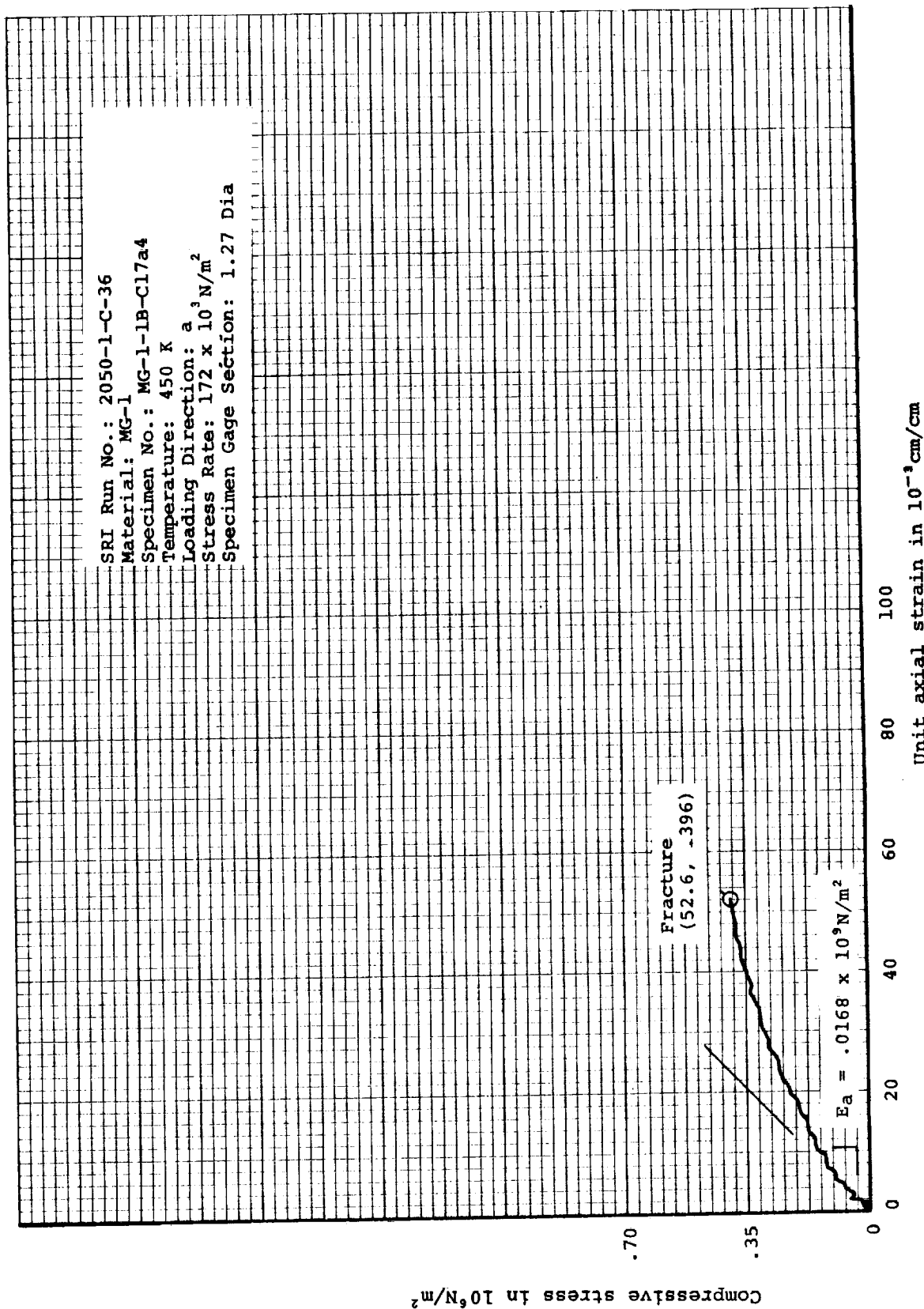
Figure 119. Typical "a" direction compressive stress-strain curve for MG-1 material at 450 K
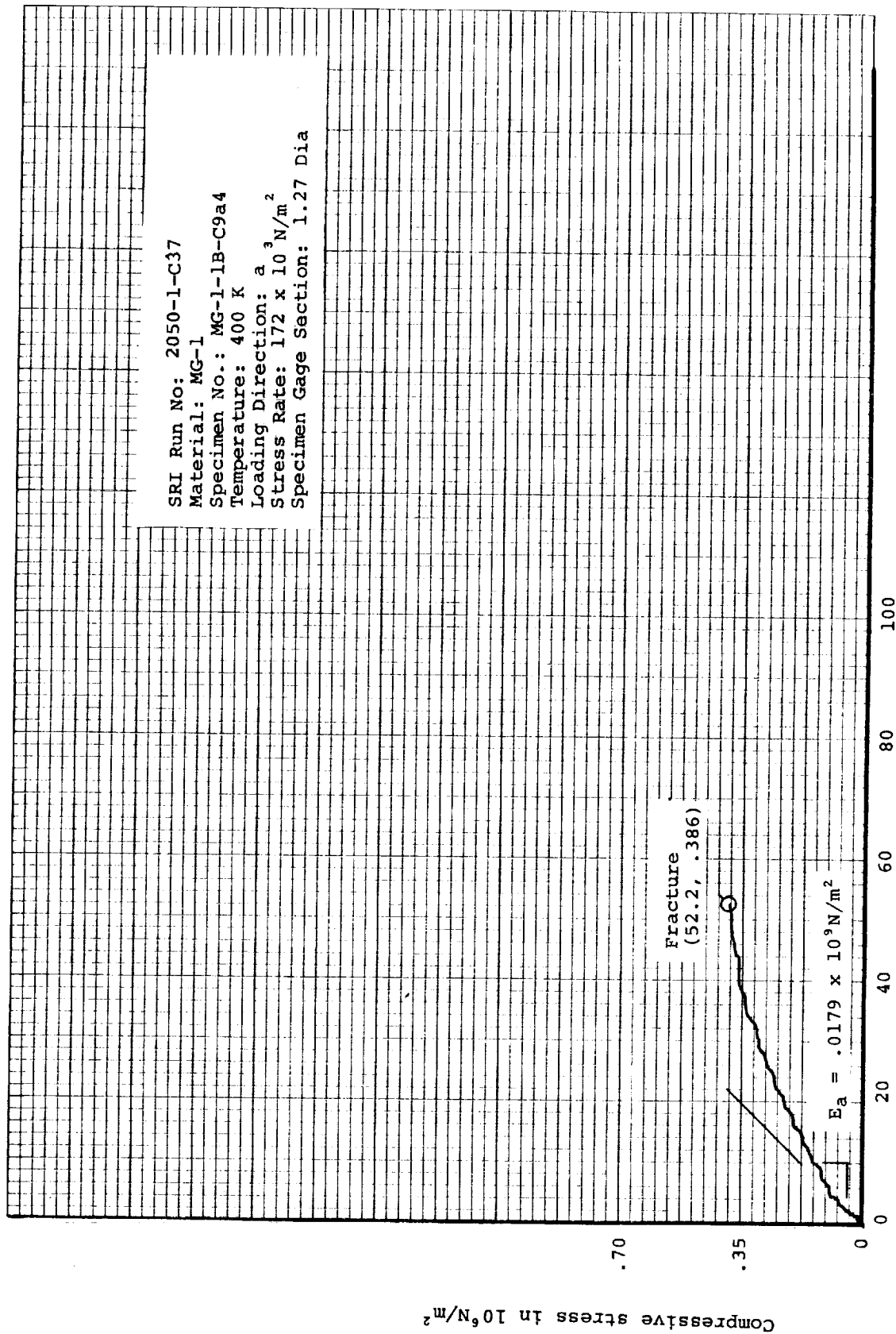
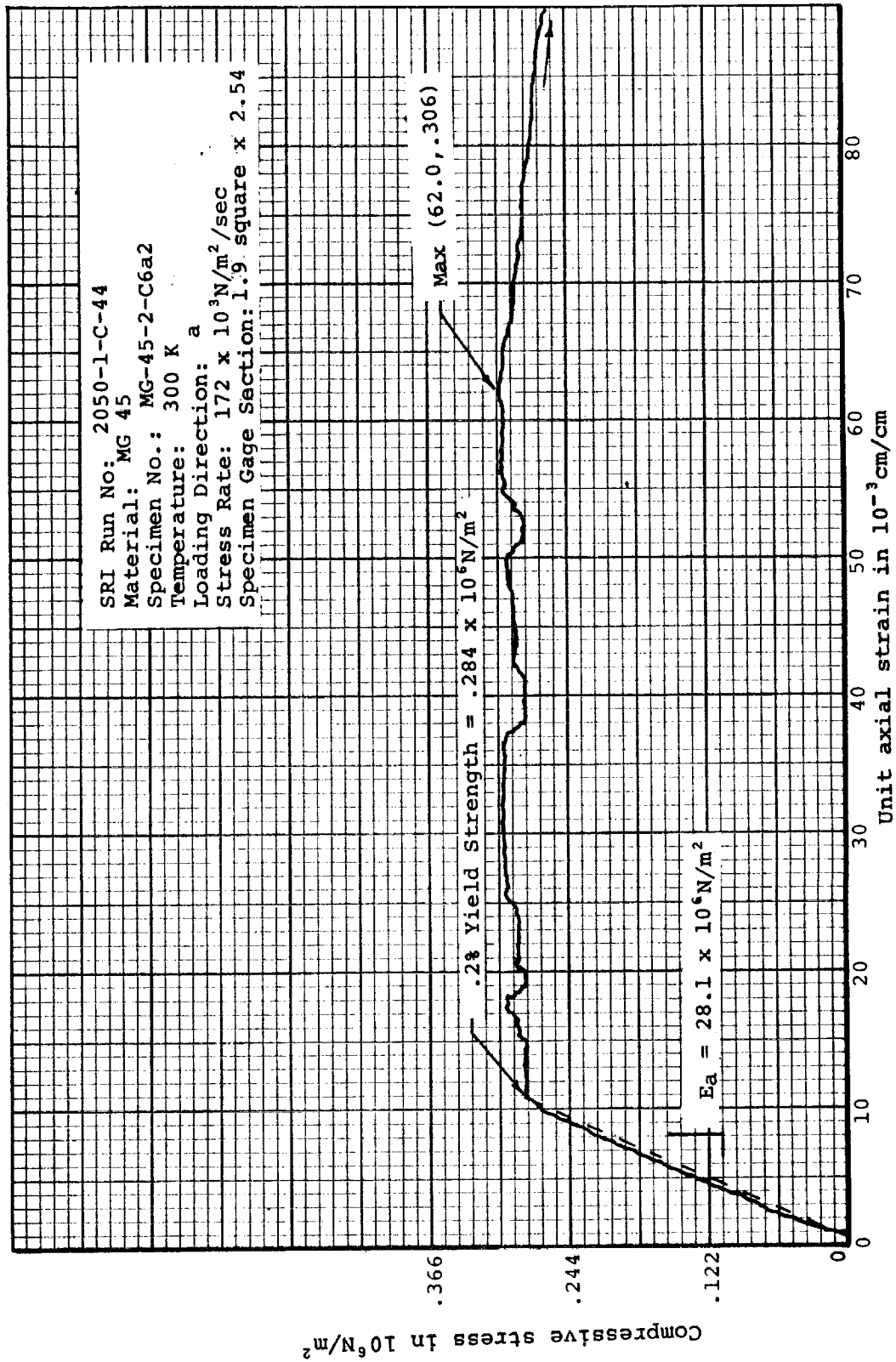Figure 120. Typical "a" direction compressive stress-strain curve for MG-1 material at 400 K

The plot contains the following annotations:

SRI Run No: 2050-1-C37
Material: MG-1
Specimen No.: MG-1-1B-C9a4
Temperature: 400 K
Loading Direction: a
Stress Rate: 172 x 10³ N/m²
Specimen Gage Section: 1.27 Dia

Fracture
(52.2, .386)

$E_a = .0179 \times 10^9 \text{ N/m}^2$

Unit axial strain in 10^{-3} cm/cm

Compressive stress in 10^6 N/m²
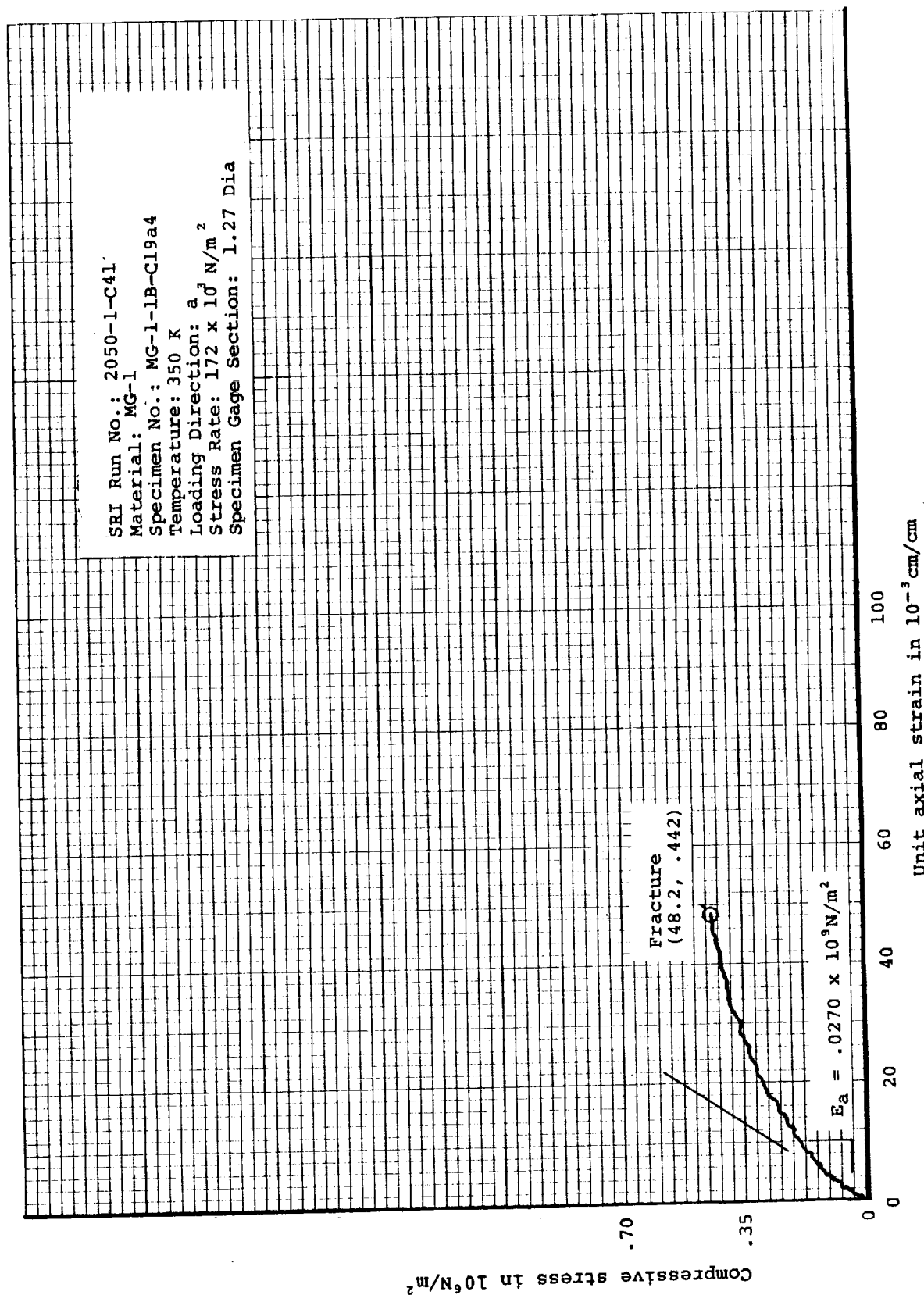
Figure 121. Typical "a" direction compressive stress-strain curve for MG-1 material at 350 K

The chart contains the following legend:

SRI Run No.: 2050-1-C41
Material: MG-1
Specimen No.: MG-1-1B-C19a4
Temperature: 350 K
Loading Direction: a
Stress Rate: 172 x 10³ N/m²
Specimen Gage Section: 1.27 Dia

Fracture (48.2, .442)

$E_a = .0270 \times 10^9 \text{ N/m}^2$

Unit axial strain in 10^{-3} cm/cm

Compressive stress in 10^6 N/m²
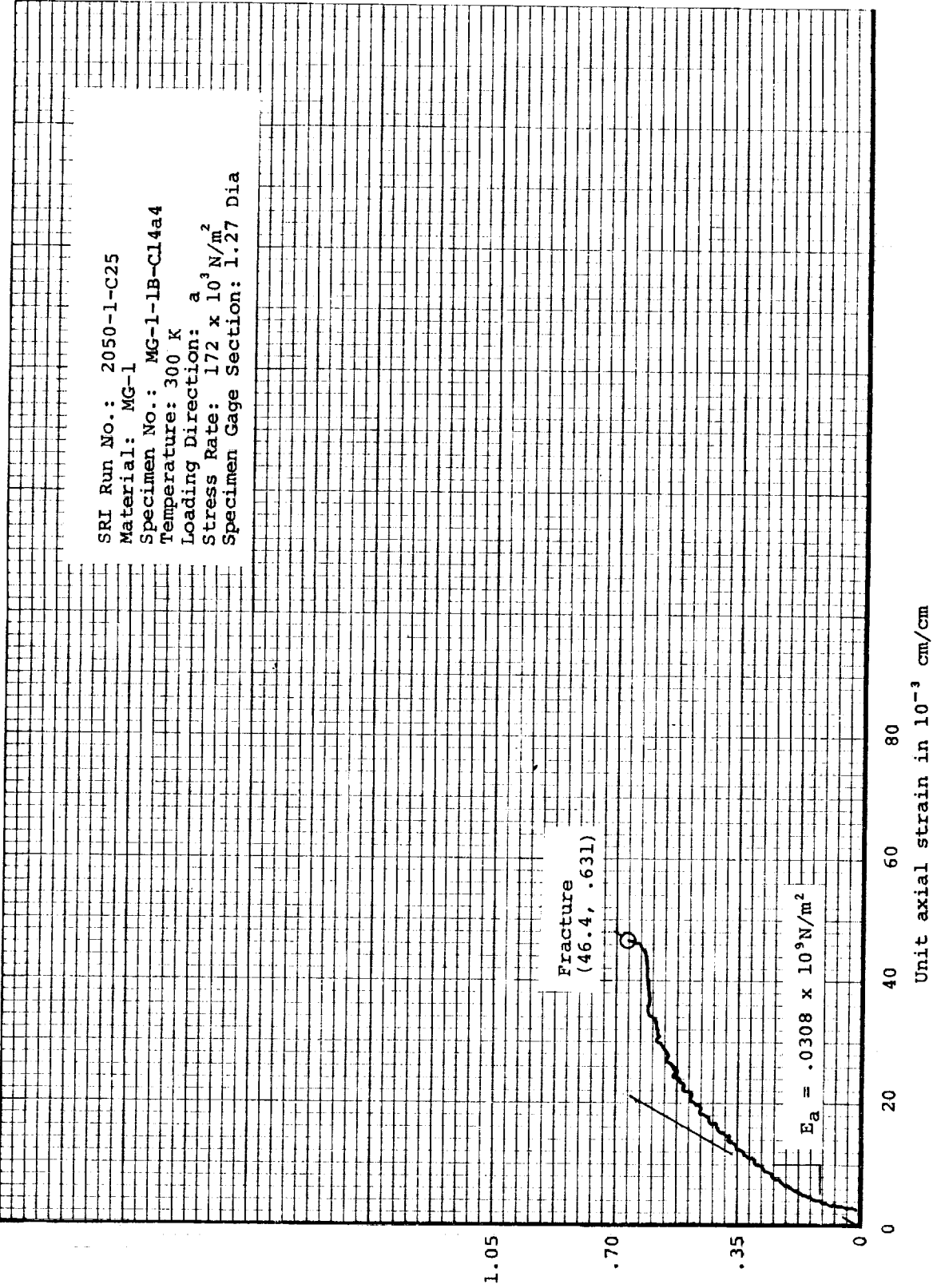
Figure 122. Typical "a" direction compressive stress-strain curve for MG-1 material at 300 K
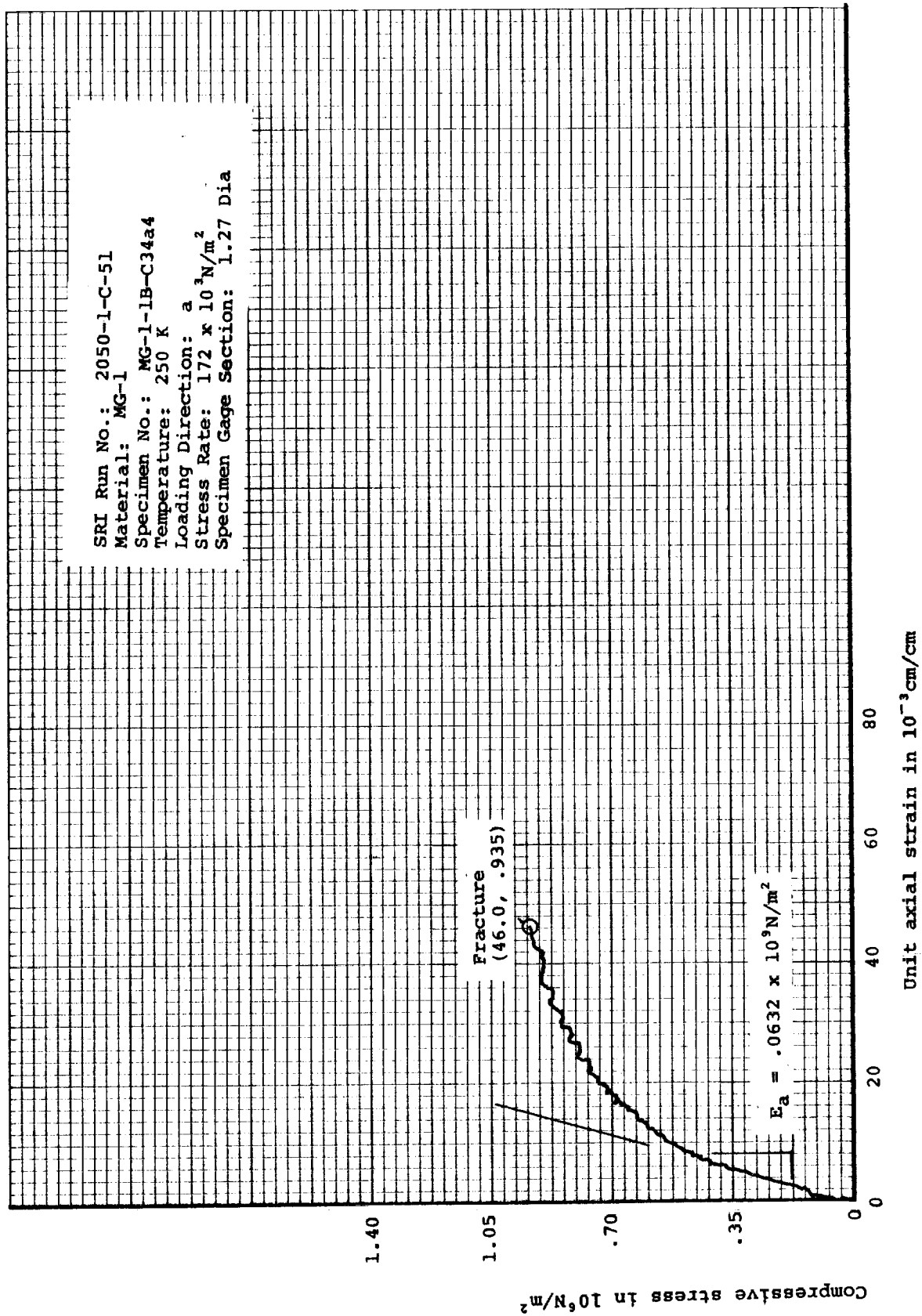
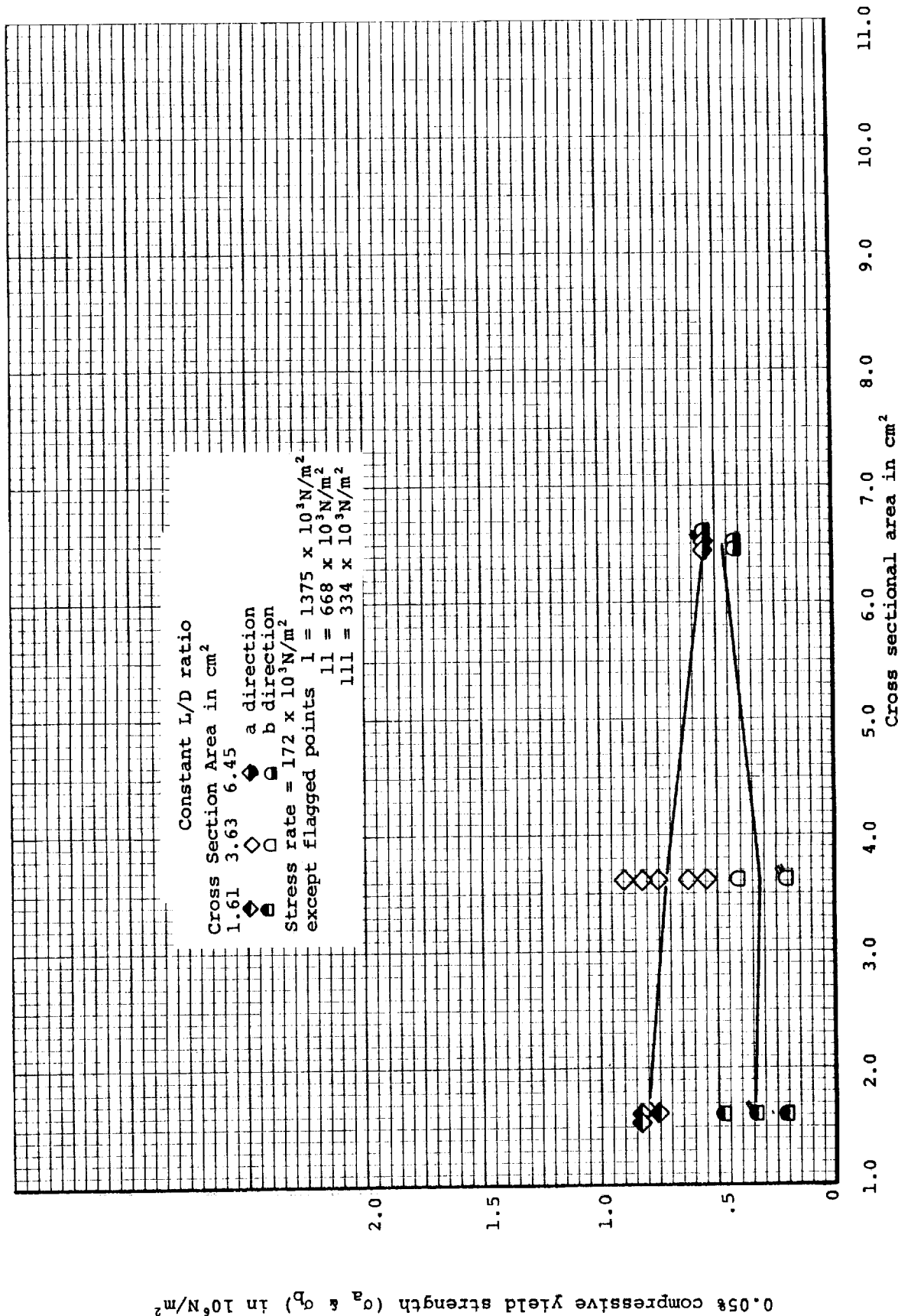Figure 123. Typical "a" direction compressive stress-strain curve for MG-1 material at 250 K

SRI Run No.: 2050-1-C-51
Material: MG-1
Specimen No.: MG-1-1B-C34a4
Temperature: 250 K
Loading Direction: a
Stress Rate: 172 x 10³N/m²
Specimen Gage Section: 1.27 Dia

Fracture
(46.0, .935)

$E_a = .0632 \times 10^9 \text{N/m}^2$

Unit axial strain in 10^{-3}cm/cm

Compressive stress in 10^6N/m²

SRI Run No.: 2050-1-C61
Material: MG-1
Specimen No.: MG-1-1B-C31a4
Temperature: 200 K
Loading Direction: a
Stress Rate: 172 x 10^3 N/m^2
Specimen Gage Section: 1.27 Dia

Fracture
(33.2, 7.66)

$E_a = .526 \times 10^9$ N/m^2

Unit axial strain in 10^{-3} cm/cm

Compressive stress in 10^6 N/m^2

Figure 124. Typical "a" direction compressive stress-strain curve for MG-1 material at 200 K
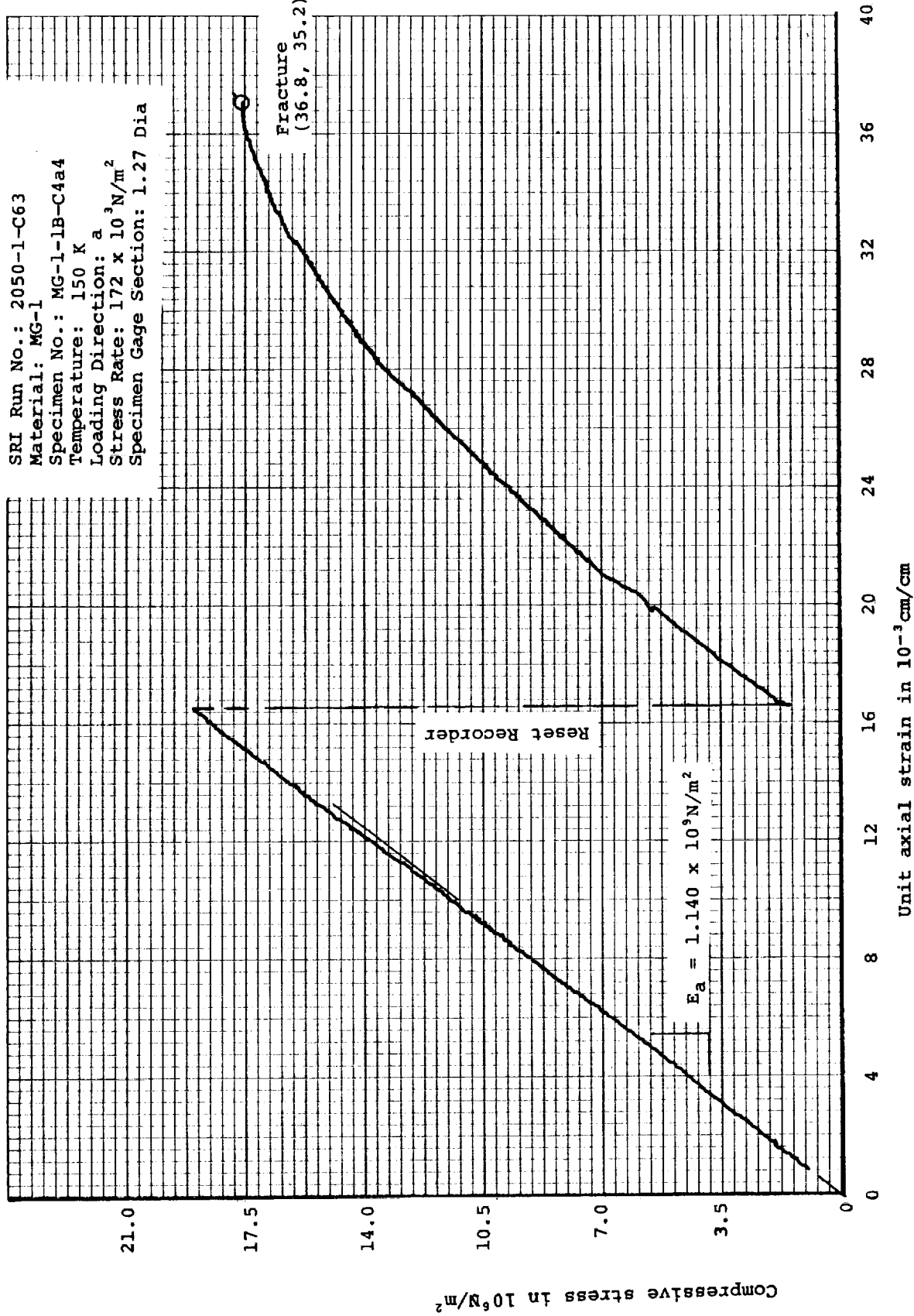
Figure 125. Typical "a" direction compressive stress-strain curve for MG-1 material at 150 K

The chart contains the following labeled information:

SRI Run No.: 2050-1-C63
Material: MG-1
Specimen No.: MG-1-1B-C4a4
Temperature: 150 K
Loading Direction: a
Stress Rate: $172 \times 10^3 \, N/m^2$
Specimen Gage Section: 1.27 Dia

Fracture (36.8, 35.2)

Reset Recorder

$E_a = 1.140 \times 10^9 \, N/m^2$

Unit axial strain in 10^{-3} cm/cm

Compressive stress in $10^6 \, N/m^2$
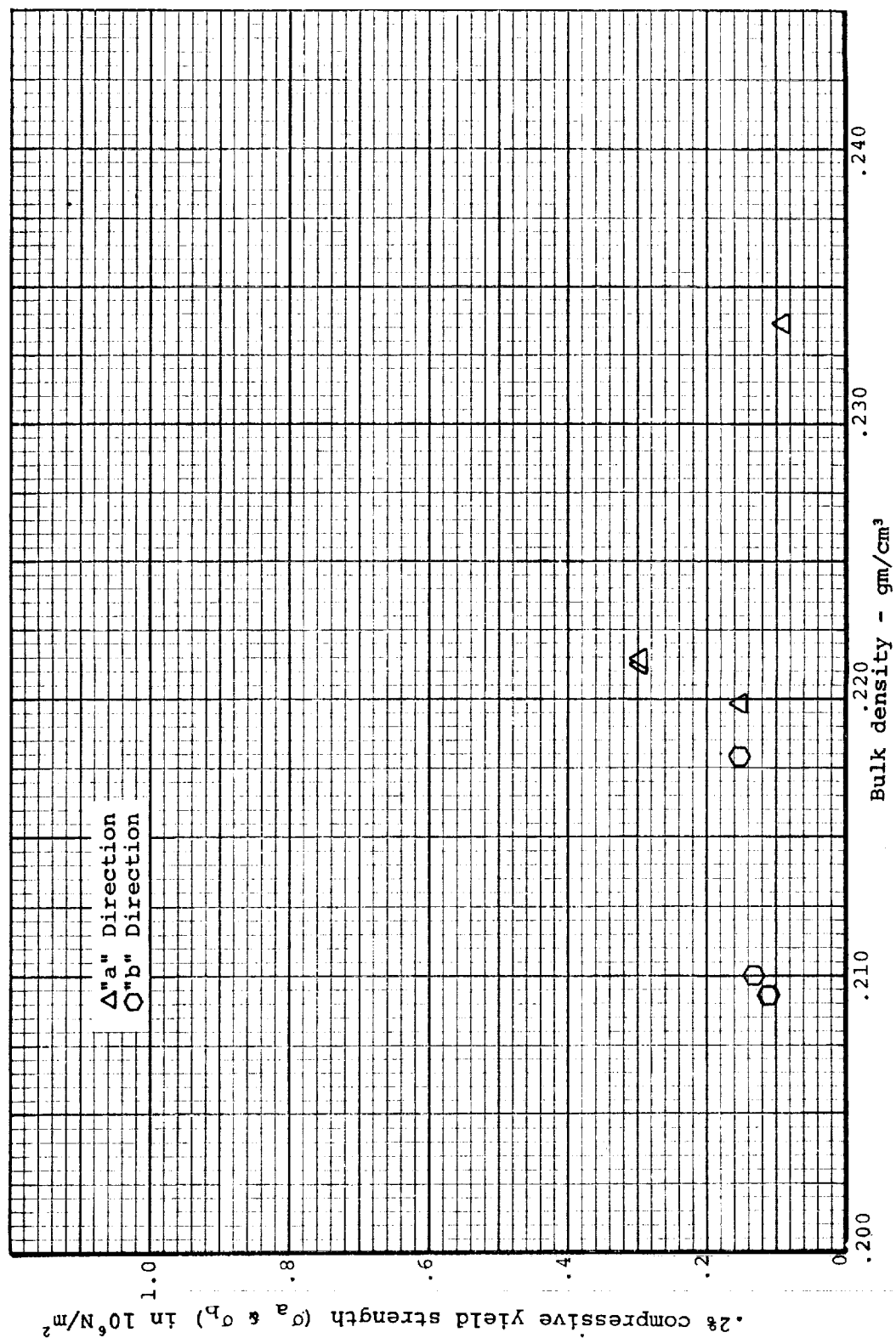
Figure 126.   0.2% compressive yield strength versus bulk density for MG-45 material

274
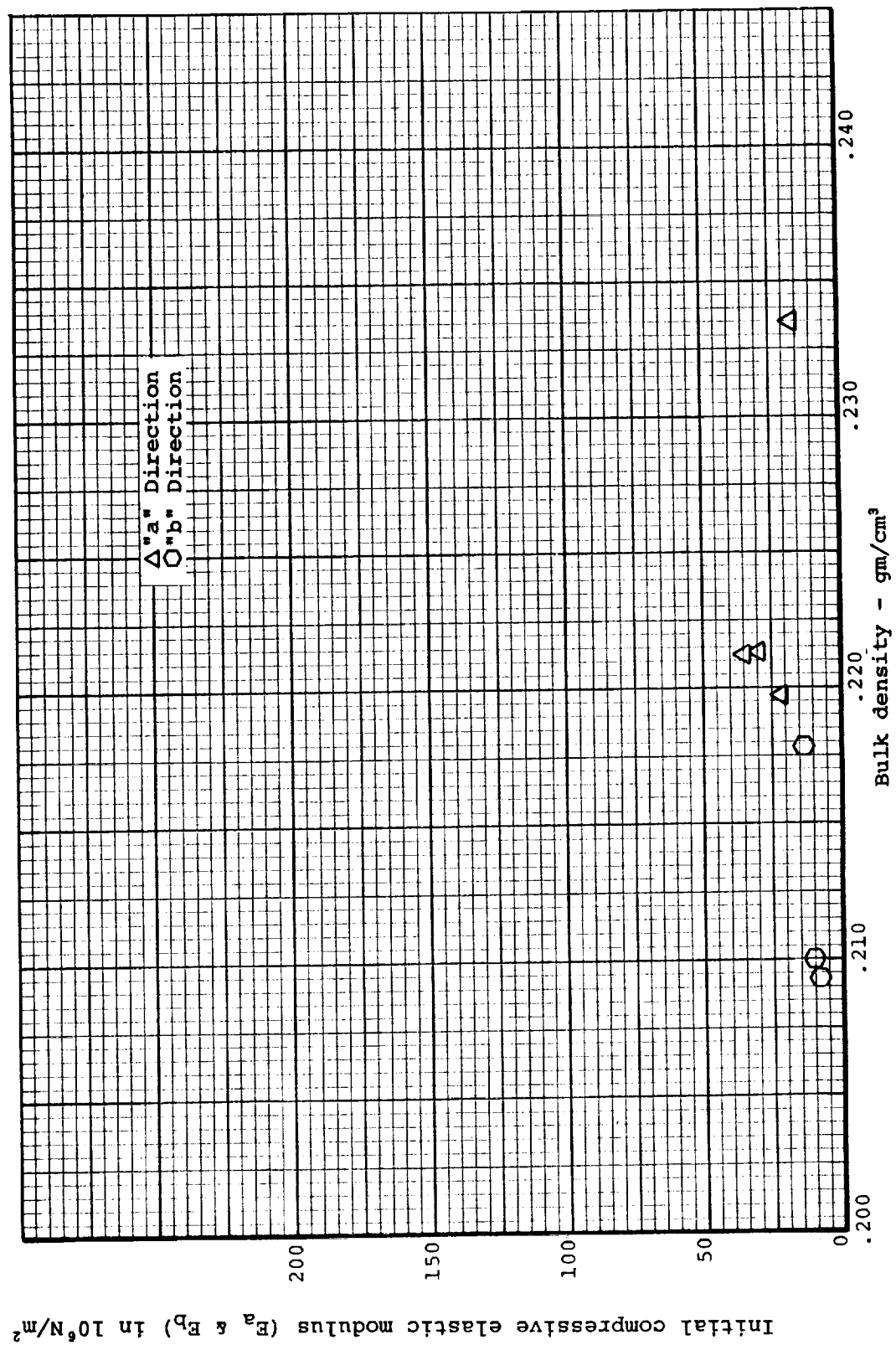
Figure 127. Initial compressive elastic modulus versus bulk density for MG-45 material

275

Figure 128. Compressive axial strain versus bulk density for MG-45 material

276
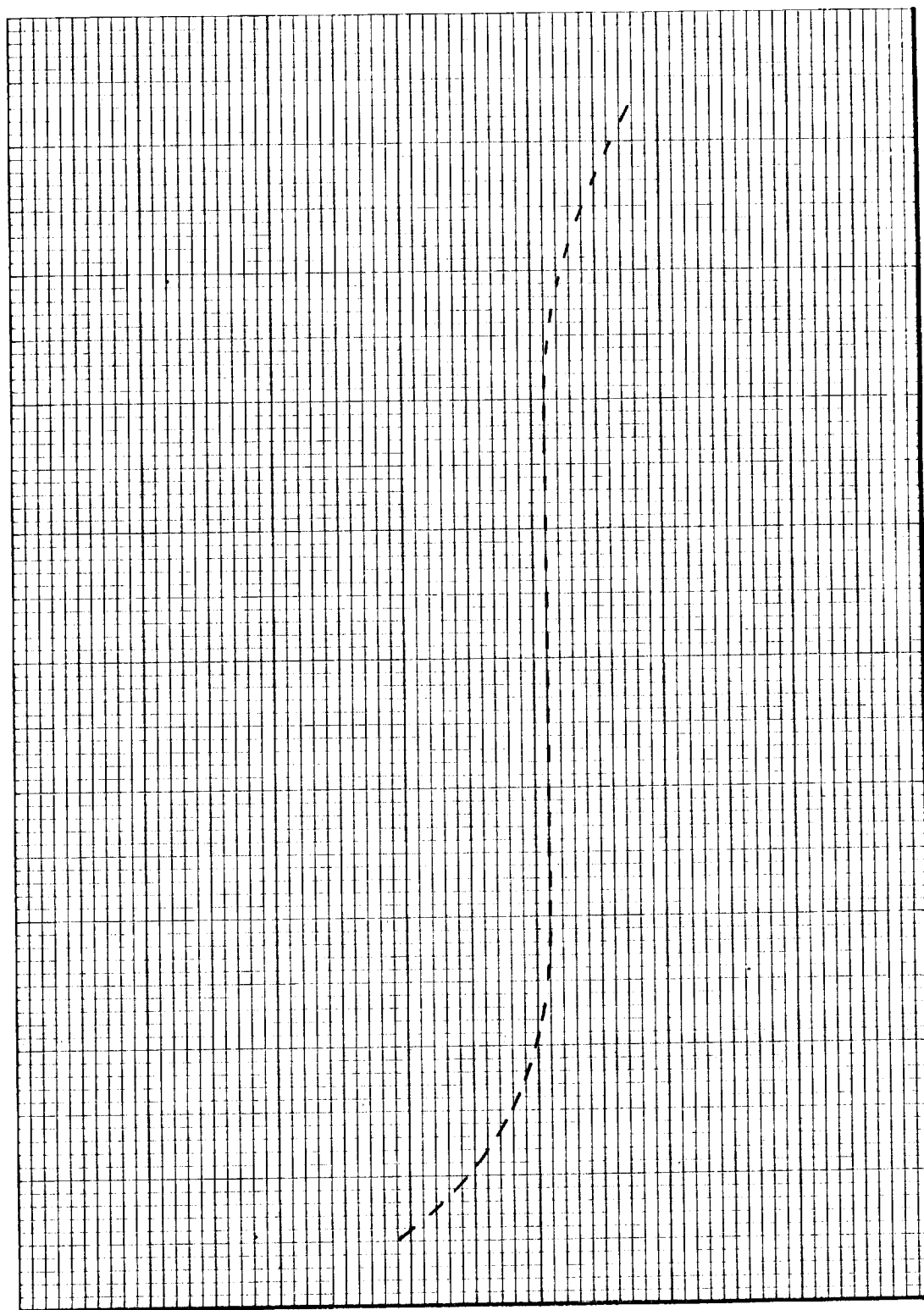
Slenderness Ratio (length/radius of gyration)

Figure 129. Relationship between initial compressive elastic modulus and slenderness ratios
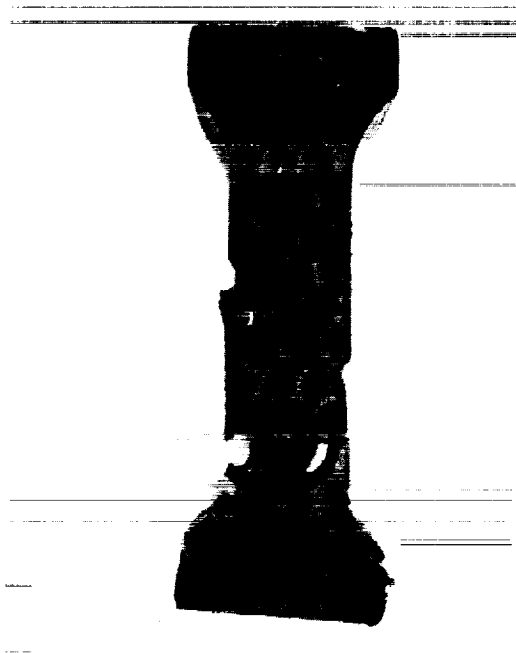
Specimen MG-45-2-C6a2
Note Honeycomb Misalign-
ment

Specimen MG-45-5-C12b2

Figure 130.   Photographs of typical failed compressive specimens -
MG-45 material

278

Figure 131. Typical "a" direction compressive stress-strain curve for MG-45 material

SRI Run No: 2050-1-C-44
Material: MG 45
Specimen No.: MG-45-2-C6a2
Temperature: 300 K
Loading Direction: a
Stress Rate: 172 x 10³N/m²/sec
Specimen Gage Section: 1.9 square x 2.54

Max (62.0,.306)

.2% Yield Strength = .284 x 10⁶ N/m²

$E_a = 28.1 \times 10^6 N/m^2$

Unit axial strain in 10⁻³ cm/cm

Compressive stress in 10⁶N/m²

279
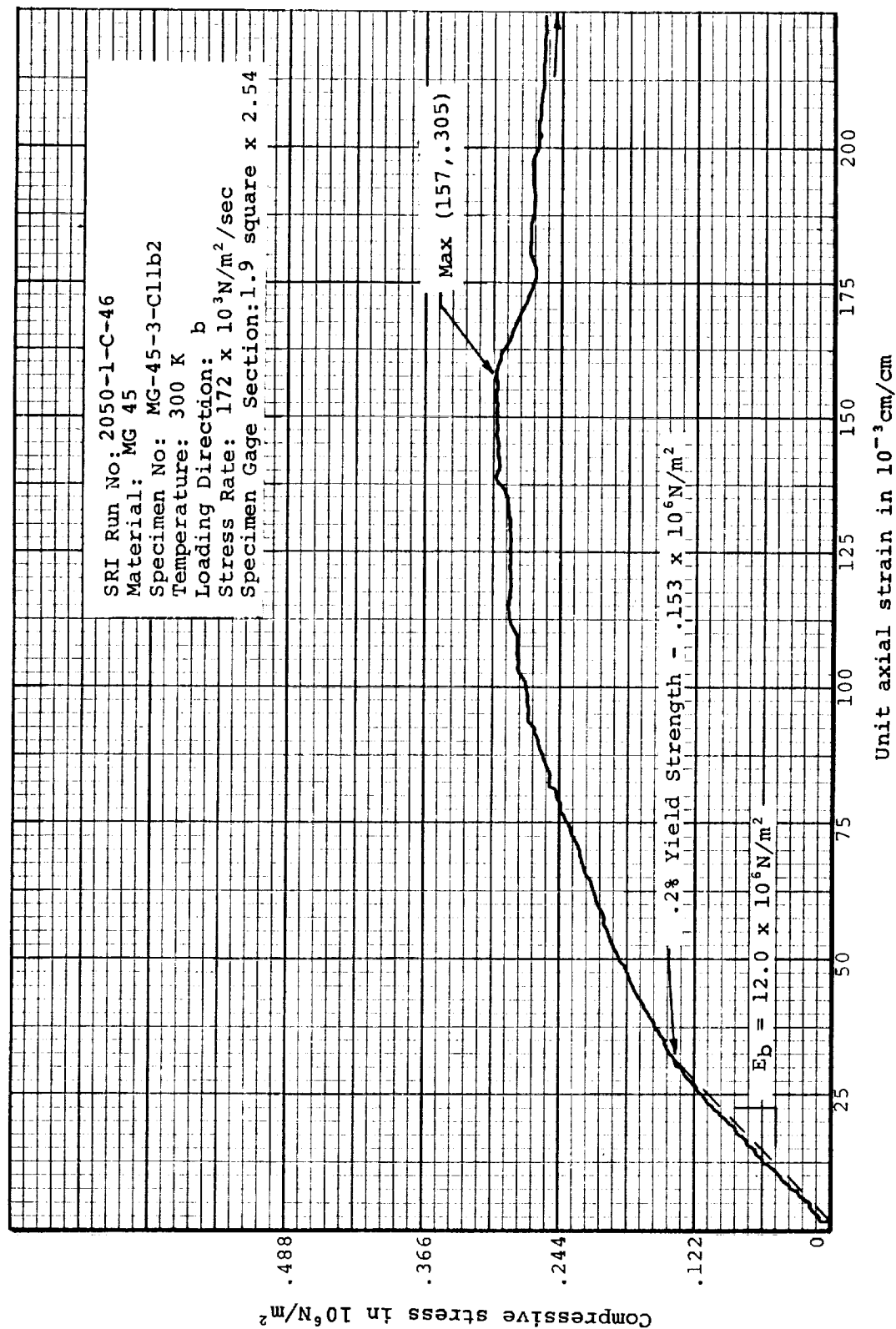
Figure 132. Typical "b" direction compressive stress-strain curve for MG-45 Material

SRI Run No: 2050-1-C-46
Material: MG 45
Specimen No: MG-45-3-C11b2
Temperature: 300 K
Loading Direction: b
Stress Rate: 172 x $10^3 N/m^2$/sec
Specimen Gage Section: 1.9 square x 2.54

Max (157,.305)

.2% Yield Strength - .153 x $10^6 N/m^2$

E_b = 12.0 x $10^6 N/m^2$

Unit axial strain in 10^{-3} cm/cm

Compressive stress in $10^6 N/m^2$

280

Figure 133. 0.05% compressive yield strength versus cross-sectional area for MG-58 Material
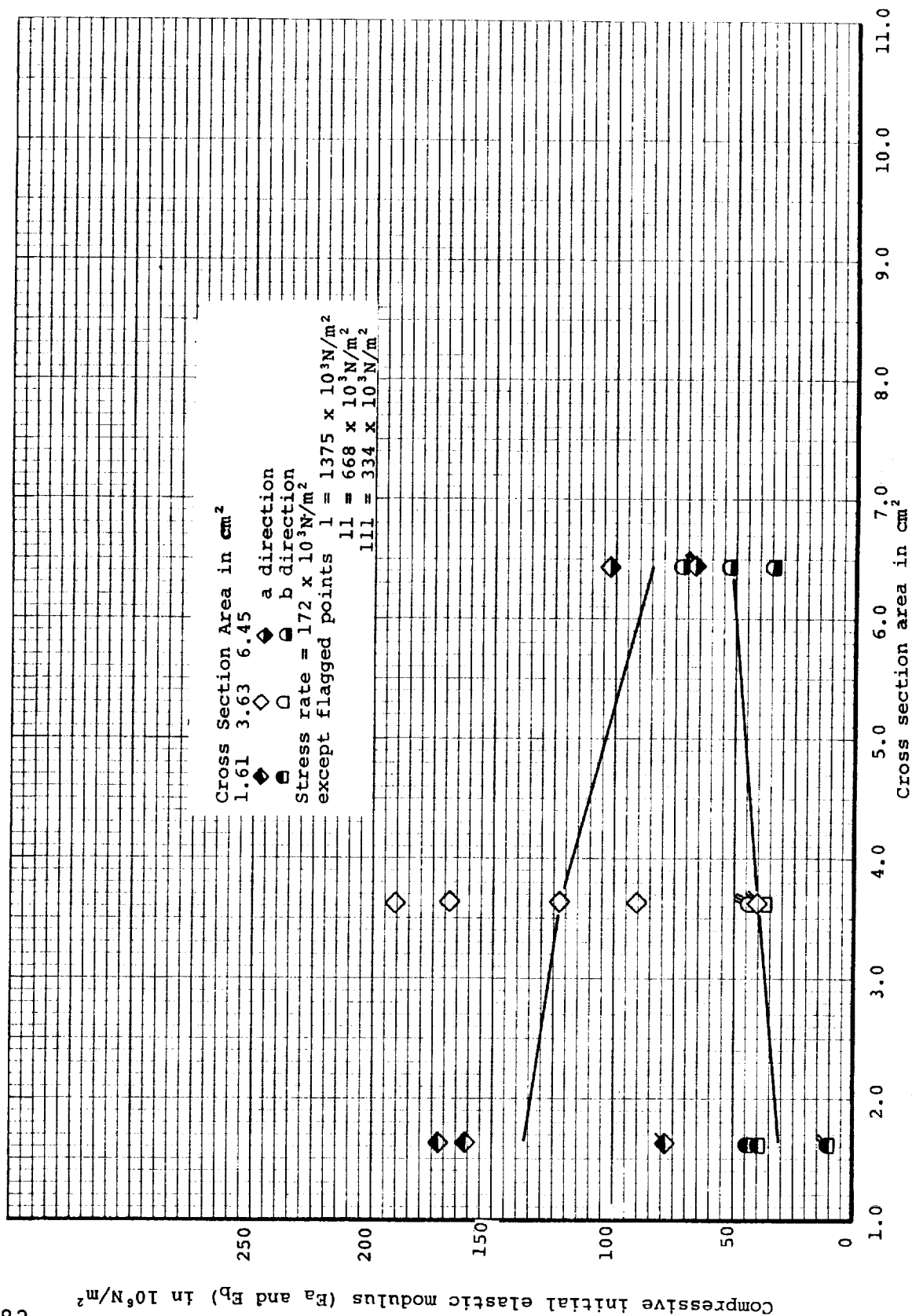
Figure 134. Compressive initial elastic modulus versus cross-sectional area for MG-58 Material
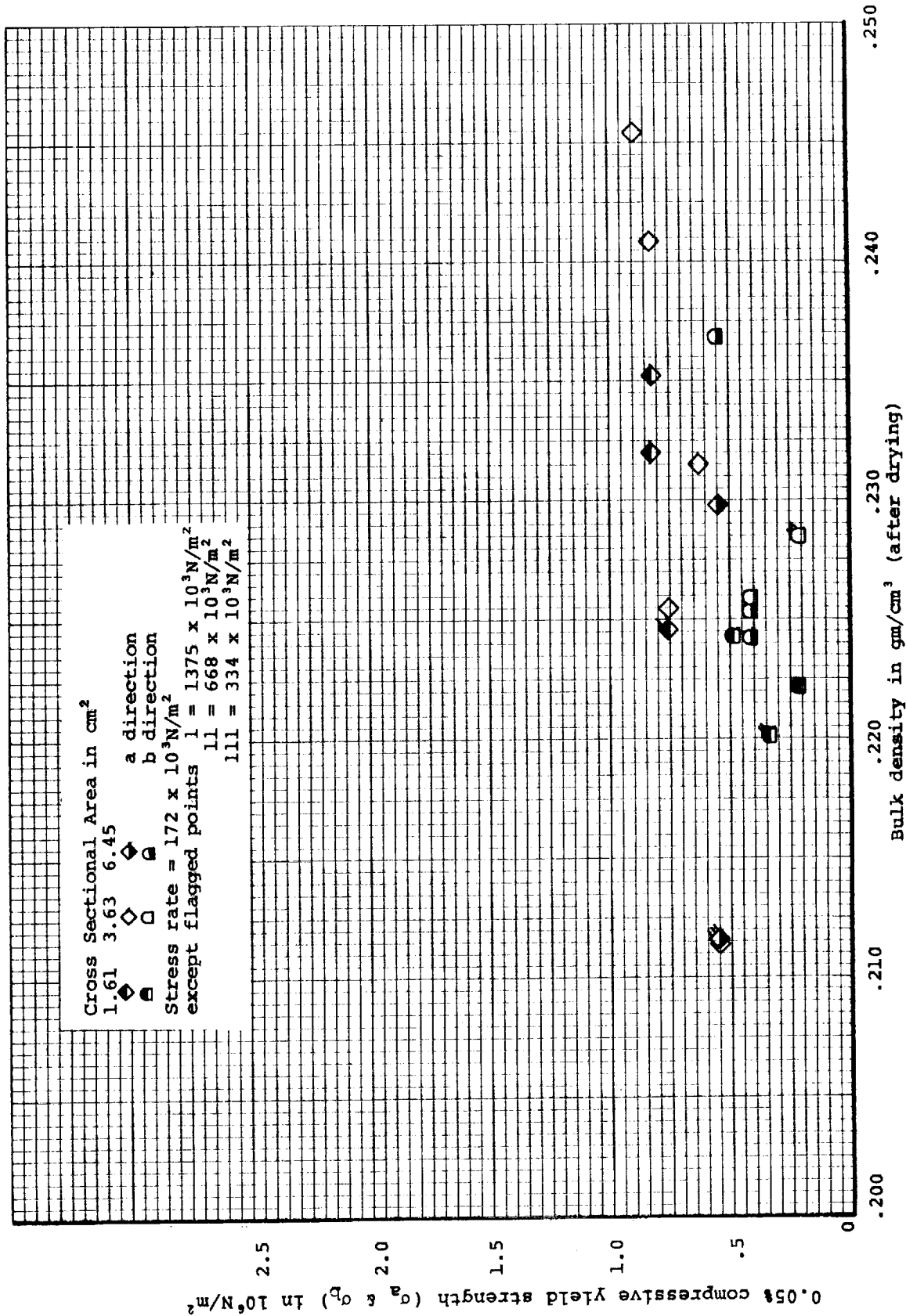
Figure 135.   0.05% compressive yield strength versus bulk density for MG-58 Material

283
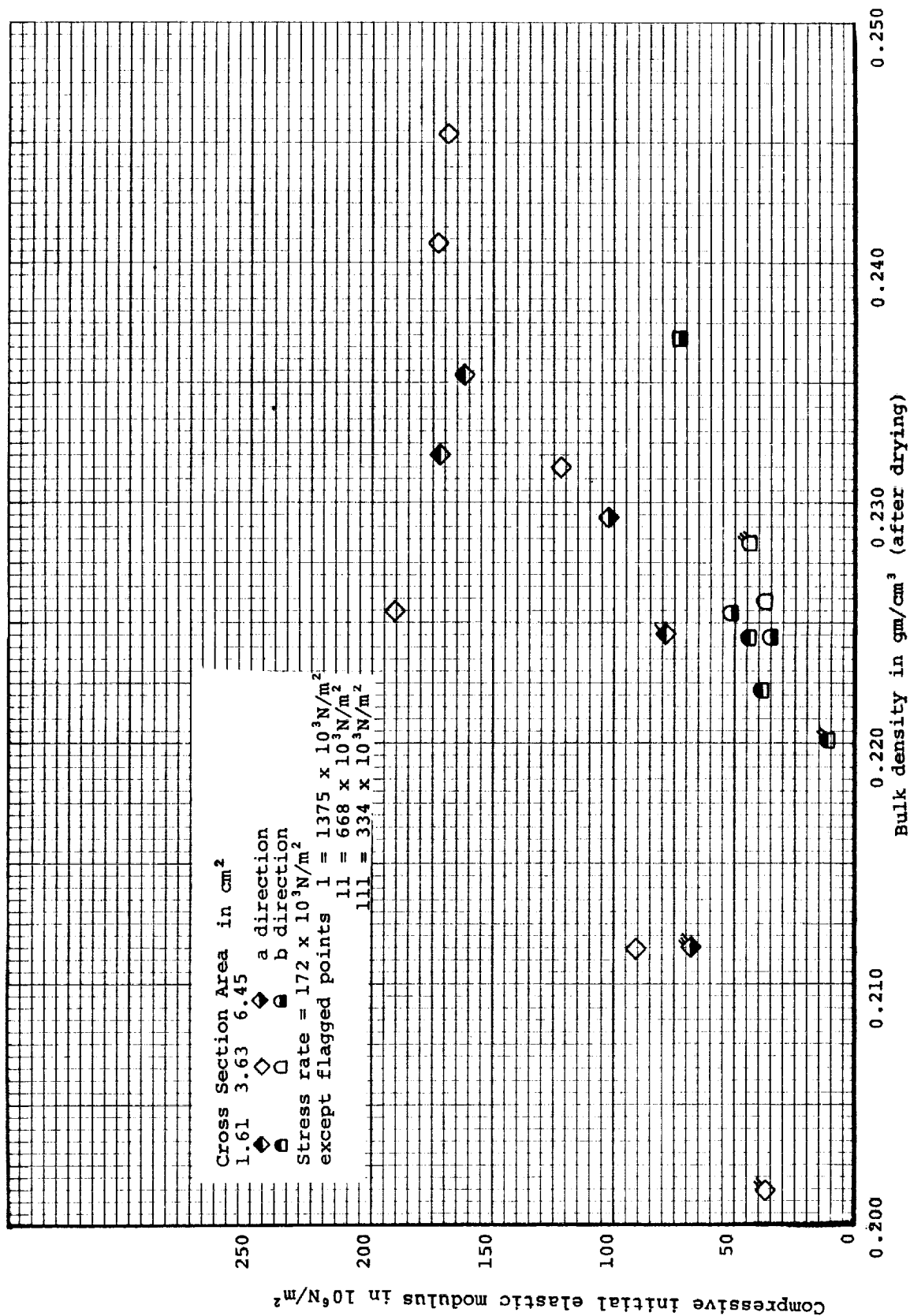
Figure 136. Compressive initial elastic modulus versus bulk density for MG-58 Material

284
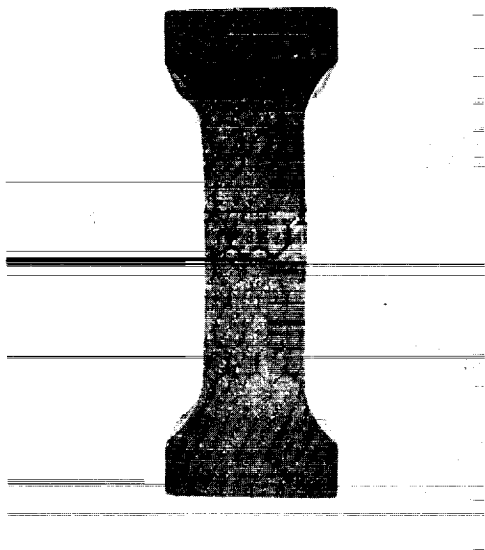
a. Specimen MG-58-5-C4a2
   Loading stopped shortly
   after reaching ultimate
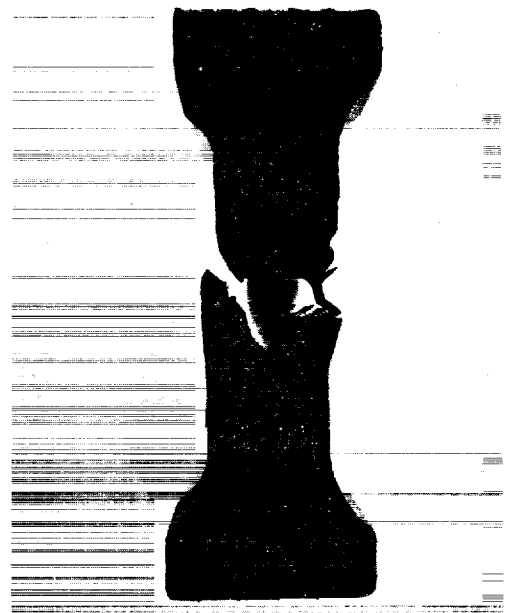
b. Specimen MG-58-5-C3a2
   Loading continued until
   failure of honeycomb. Note
   honeycomb misalignment.
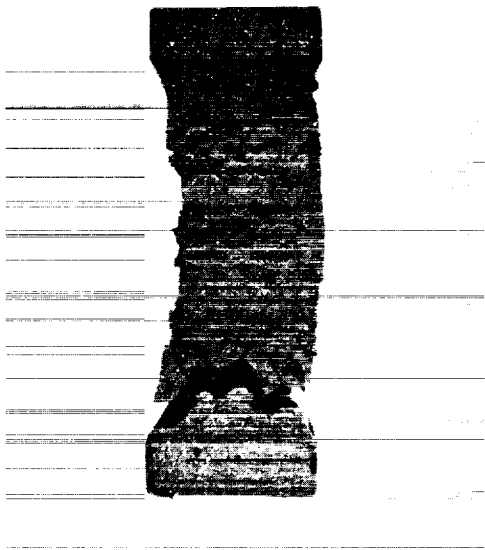
c. Specimen MG-58-3-C32b3
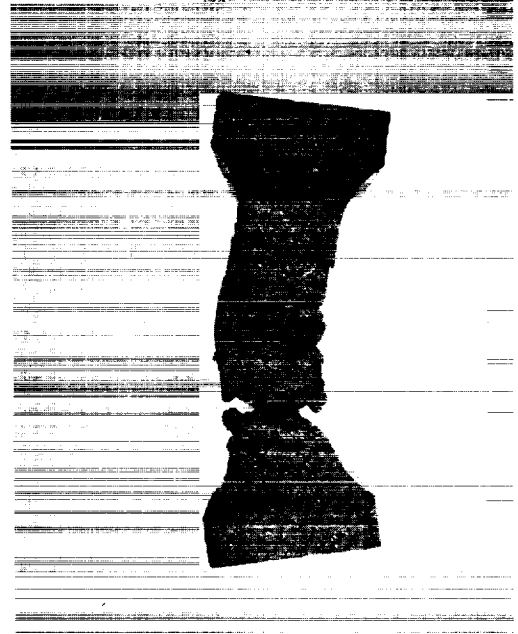
d. Specimen MG-58-3-C33b2

Figure 137. Photographs of typical failed compressive specimens,
plane of all pictures is ab plane (all 1X)
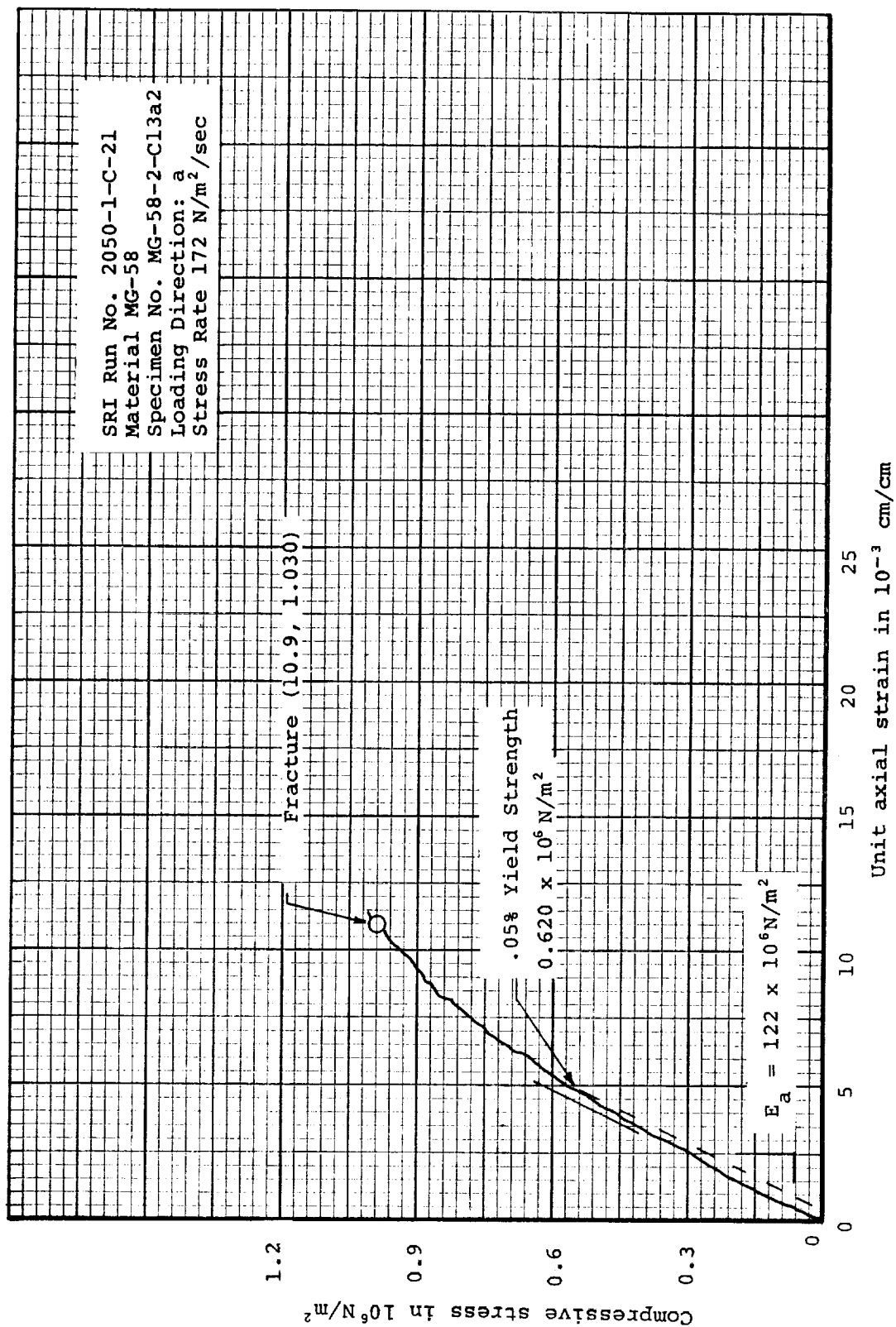
Figure 138. Typical "a" direction compressive stress-strain curve for MG-58 Material

The chart contains the following labels:

SRI Run No. 2050-1-C-21
Material MG-58
Specimen No. MG-58-2-C13a2
Loading Direction: a
Stress Rate 172 N/m²/sec

Fracture (10.9, 1.030)

.05% Yield Strength
0.620 x 10⁶ N/m²

$E_a = 122 \times 10^6 \text{N/m}^2$

Unit axial strain in 10^{-3} cm/cm

Compressive stress in 10^6N/m^2

286
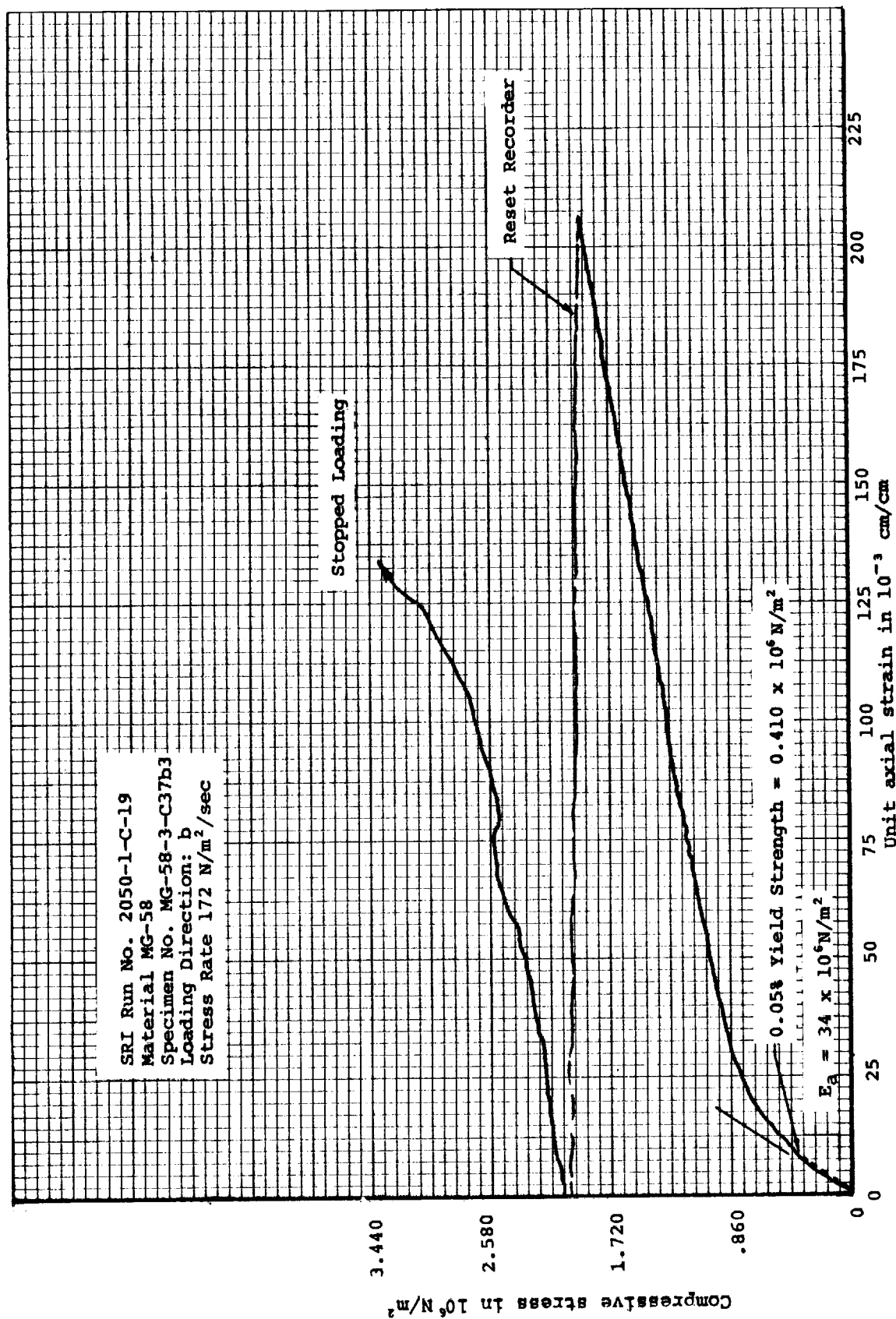
Figure 139. Typical "b" direction compressive stress-strain curve for MG-58 Material

287
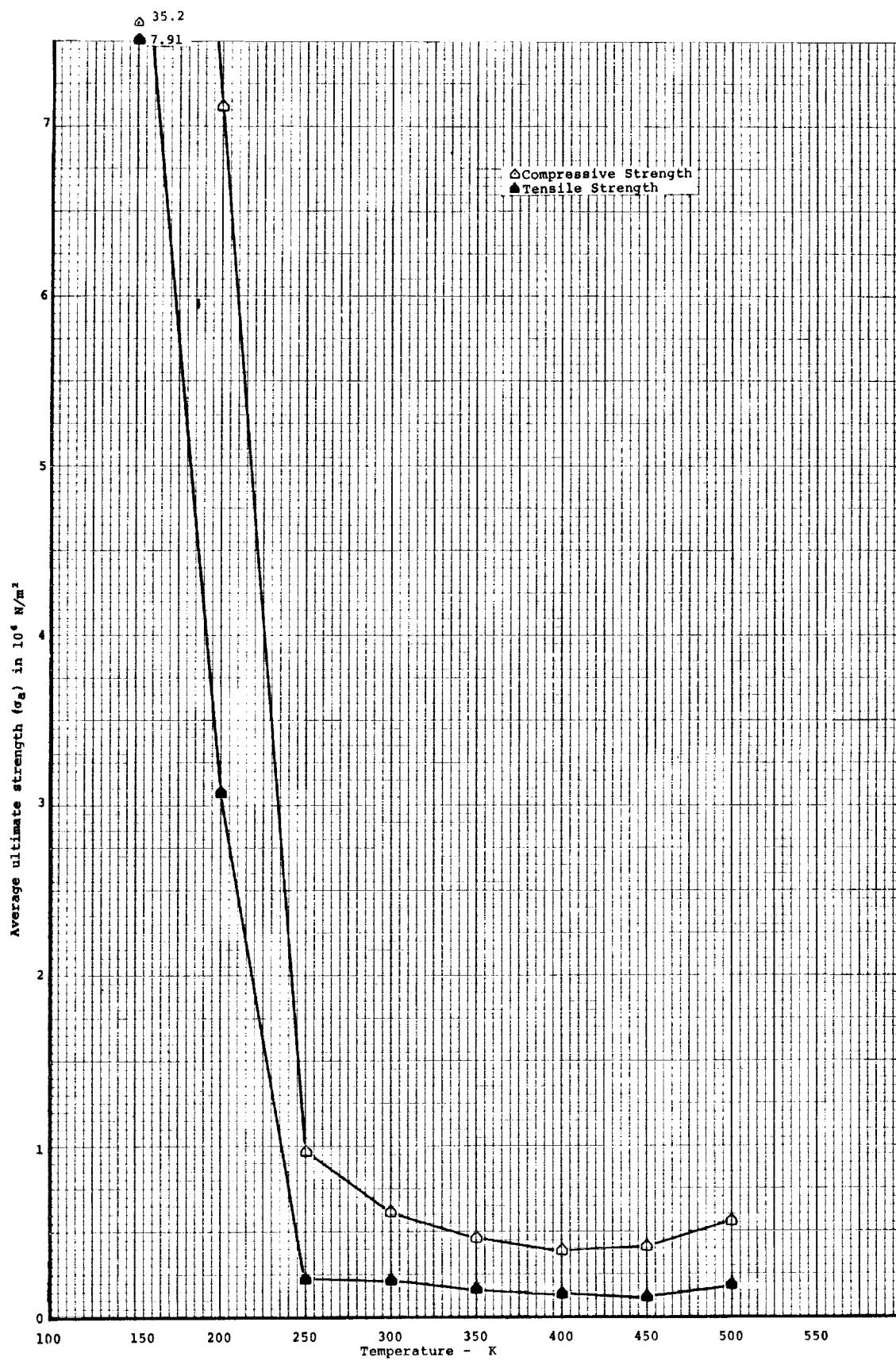
Figure 140. Average ultimate tensile and compressive strengths ("a" direction) versus temperature for MG-1 Material
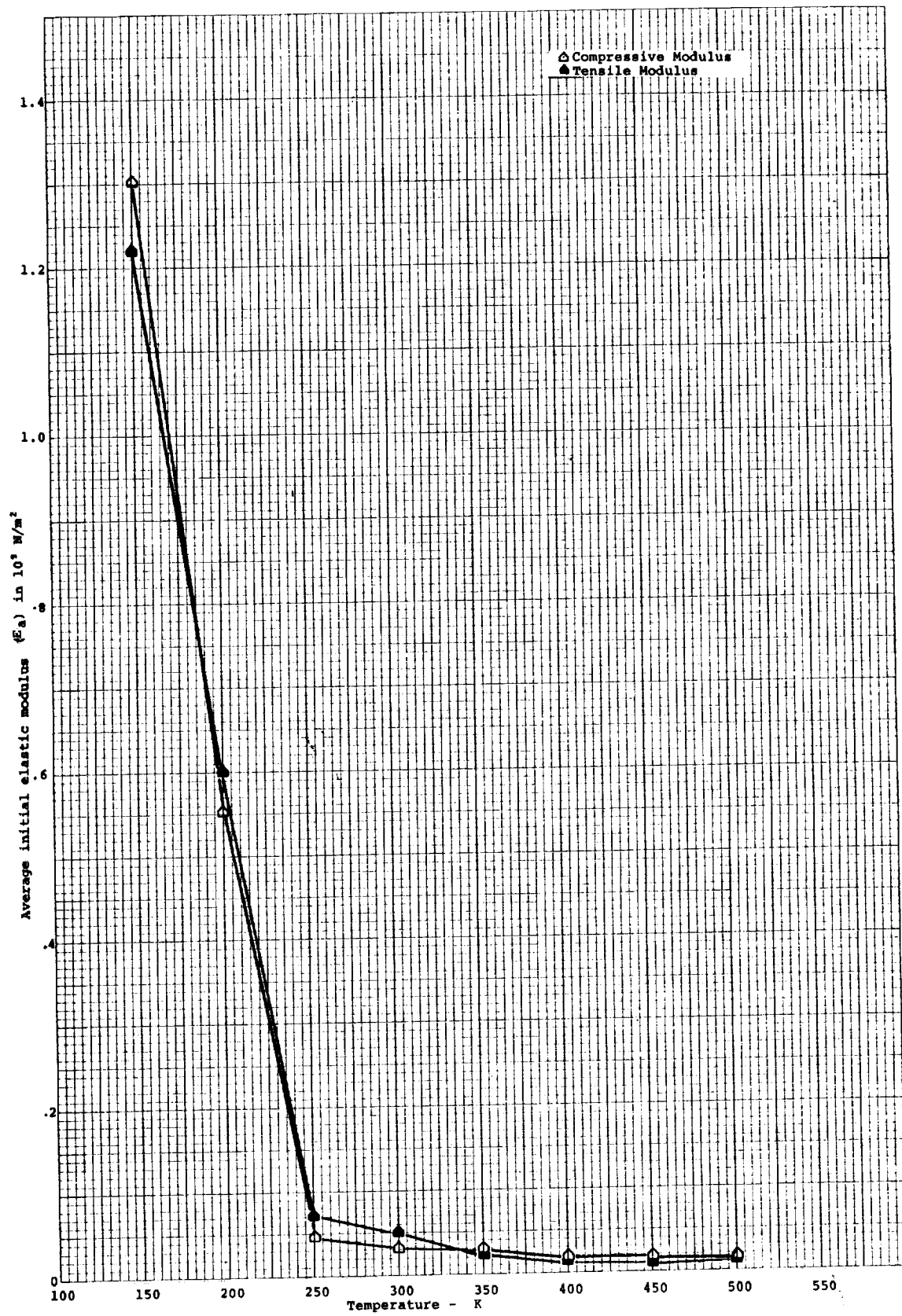
Figure 141.   Average compressive and tensile elastic modulus ("a" direction) versus temperature
for MG-1 Material

289
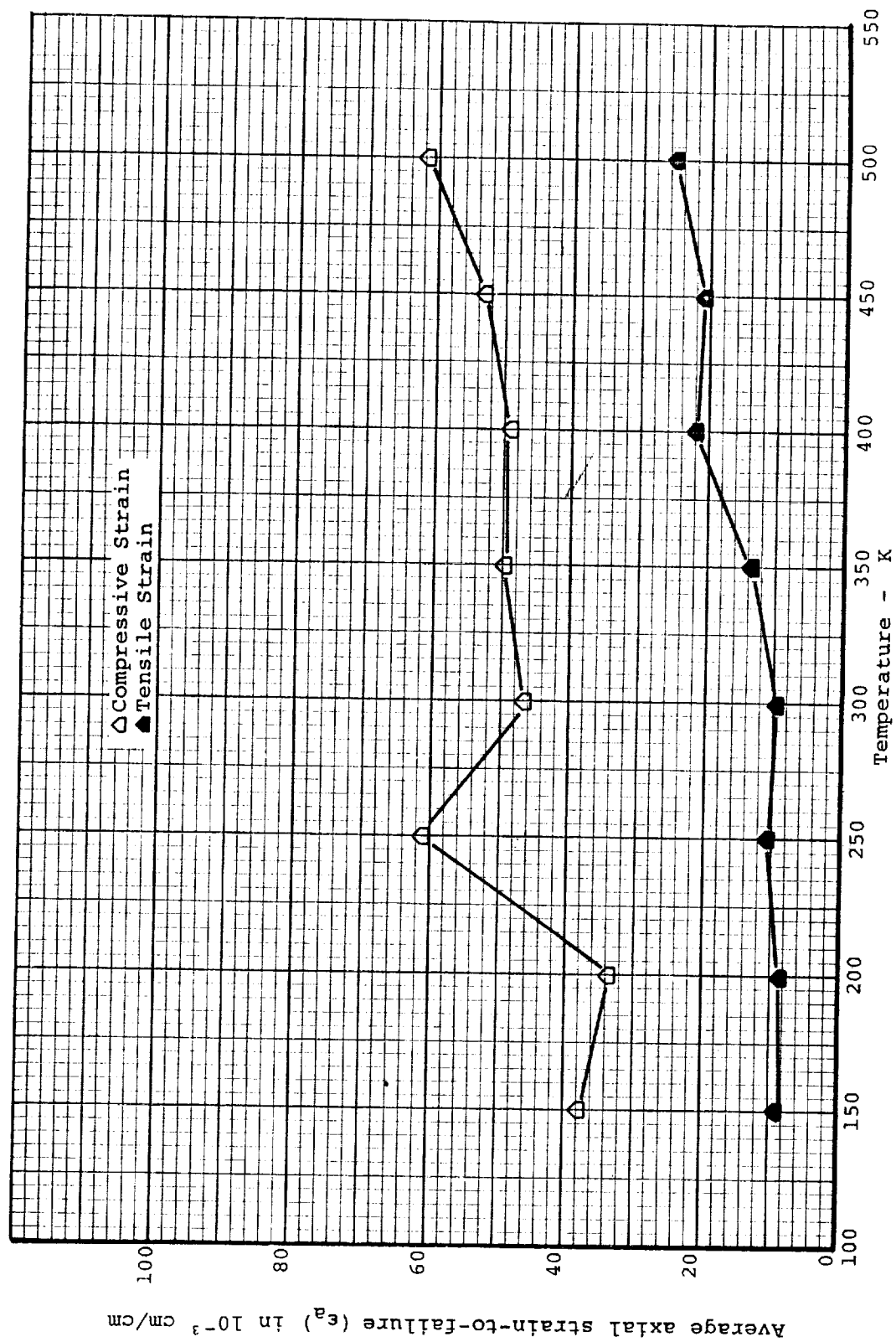
Figure 142. Average tensile and compressive axial strain-to-failure versus temperature for MG-1 Material

290
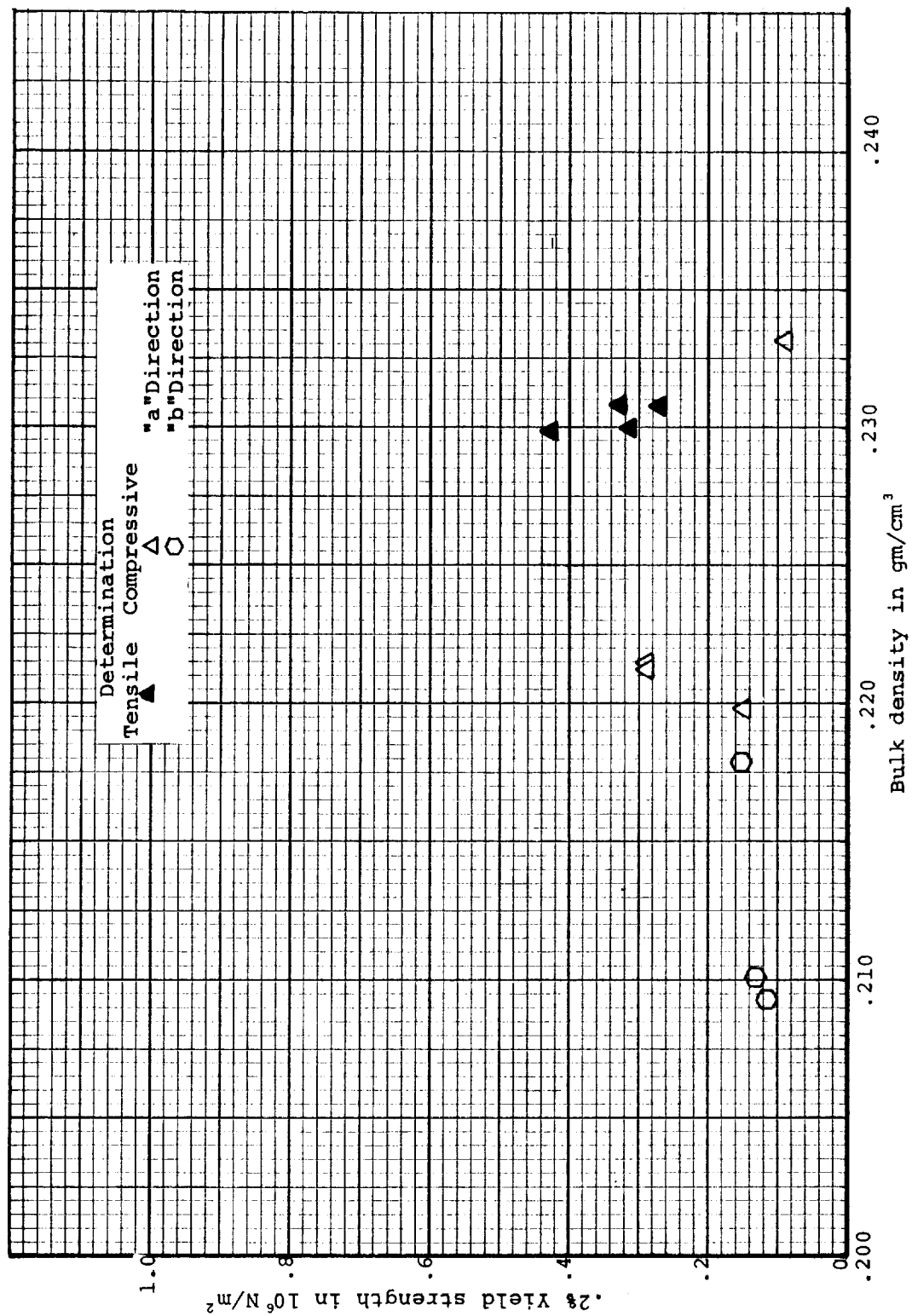
Figure 143. Composite plot of tensile and compressive .2% yield strength versus bulk density for MG-45 Material
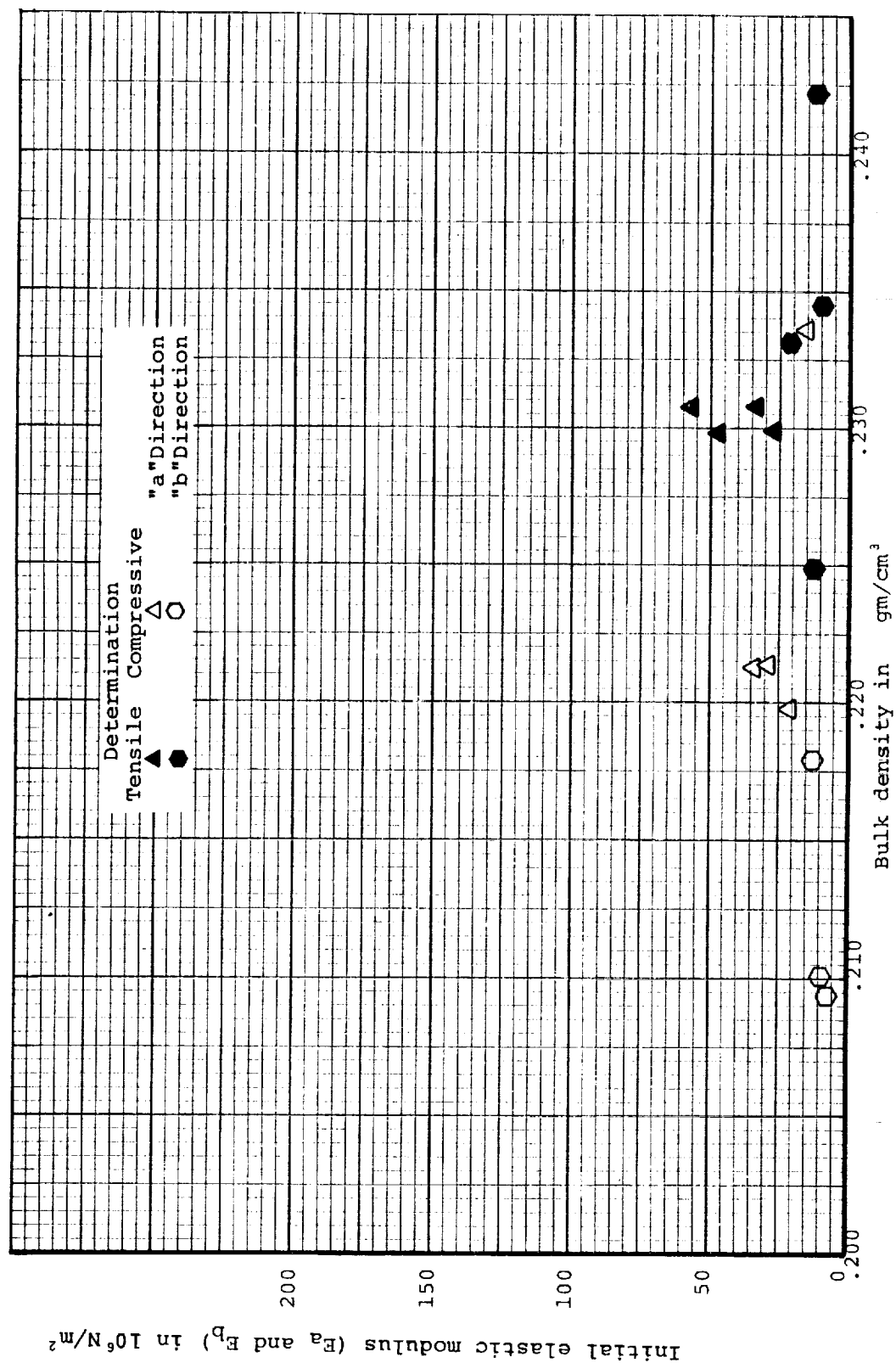
Figure 144. Composite plot of initial tensile and compressive elastic modulus versus bulk density for MG-45 Material

Figure 145. Composite plot of average ultimate tensile and compressive strengths versus bulk density for MG-58 material
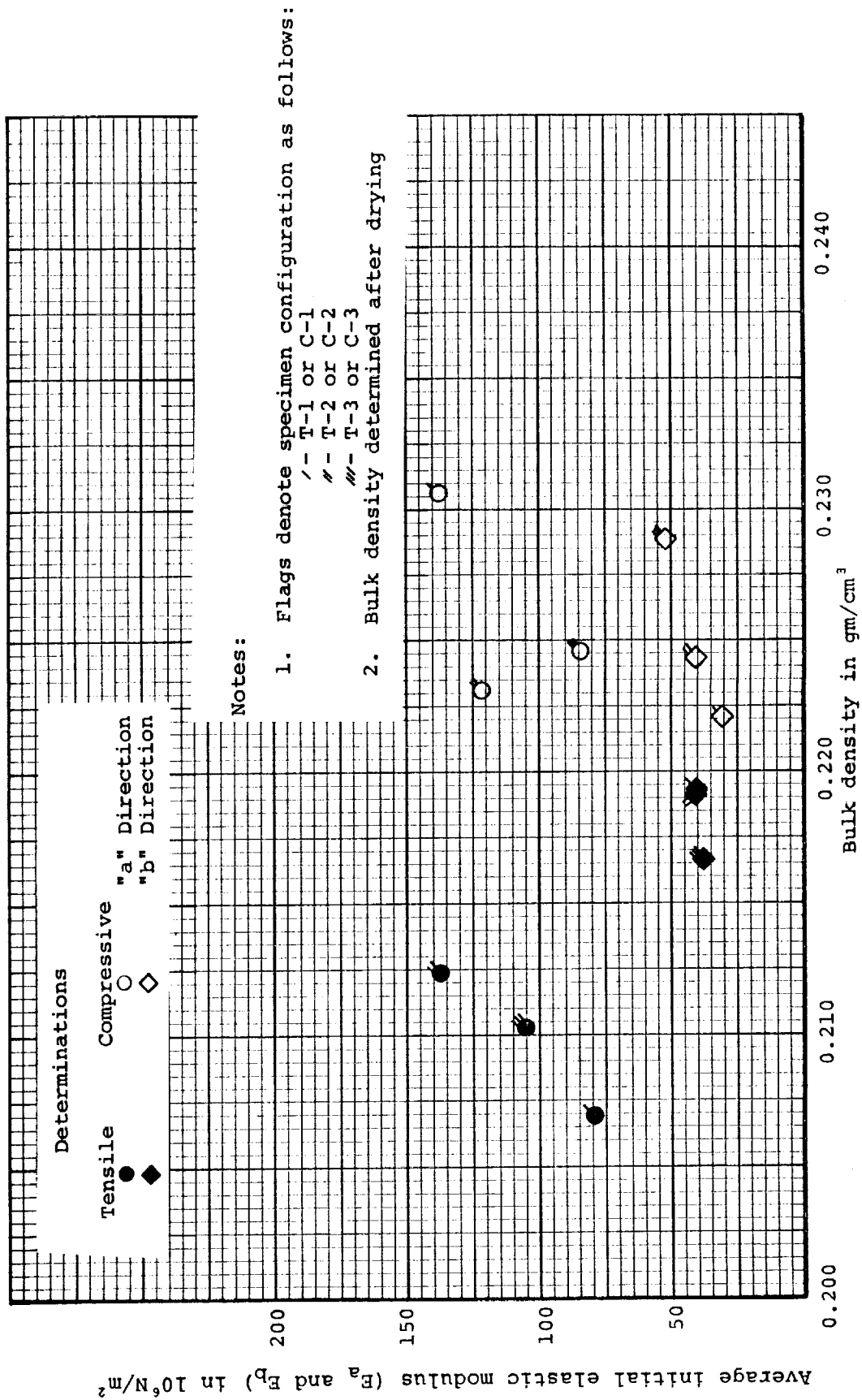
Figure 146. Composite plot of average initial tensile and compressive elastic modulus versus bulk density for MG-58 material
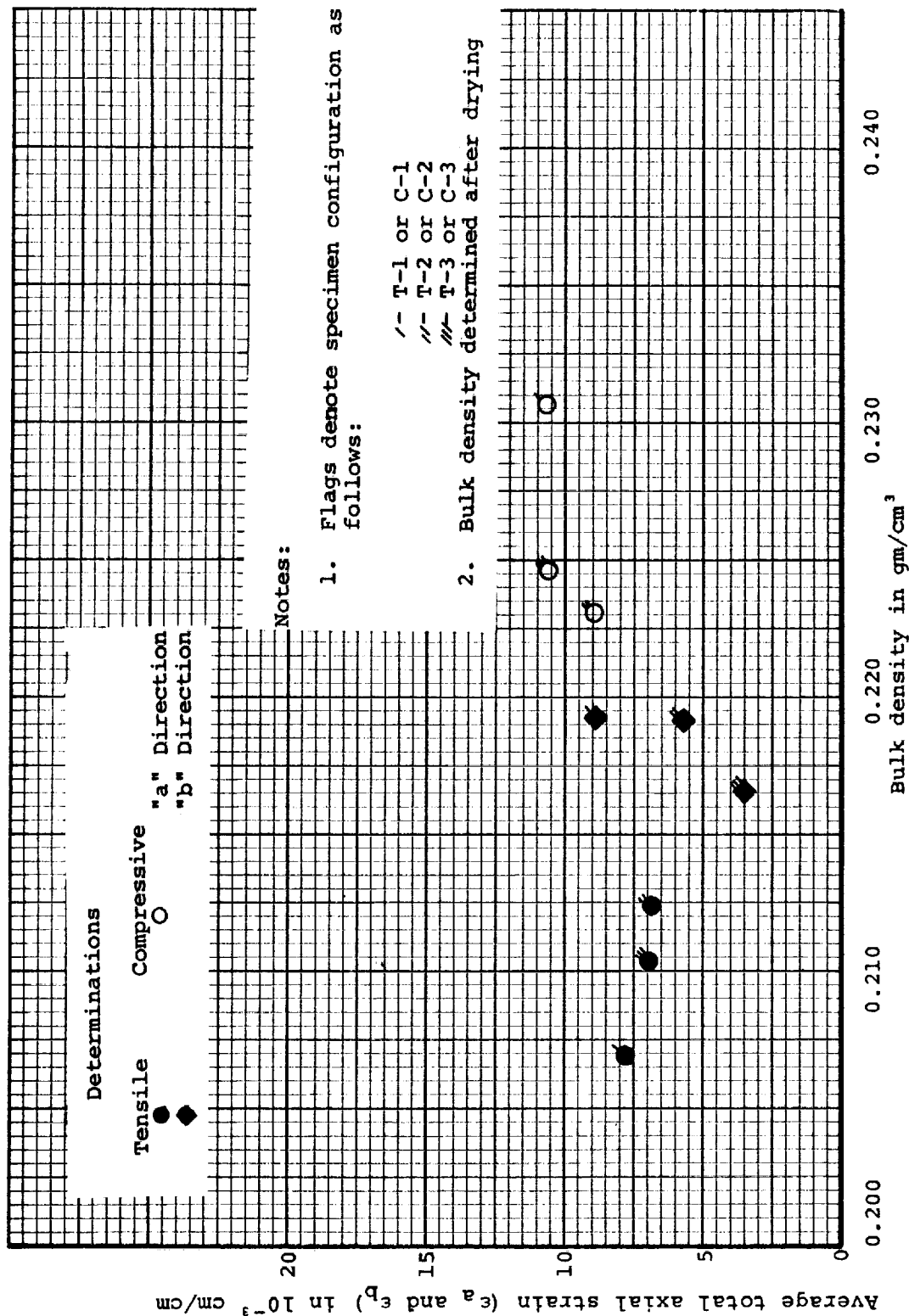
Figure 147. Composite plot of average tensile and compressive axial strain versus bulk density for MG-58 material
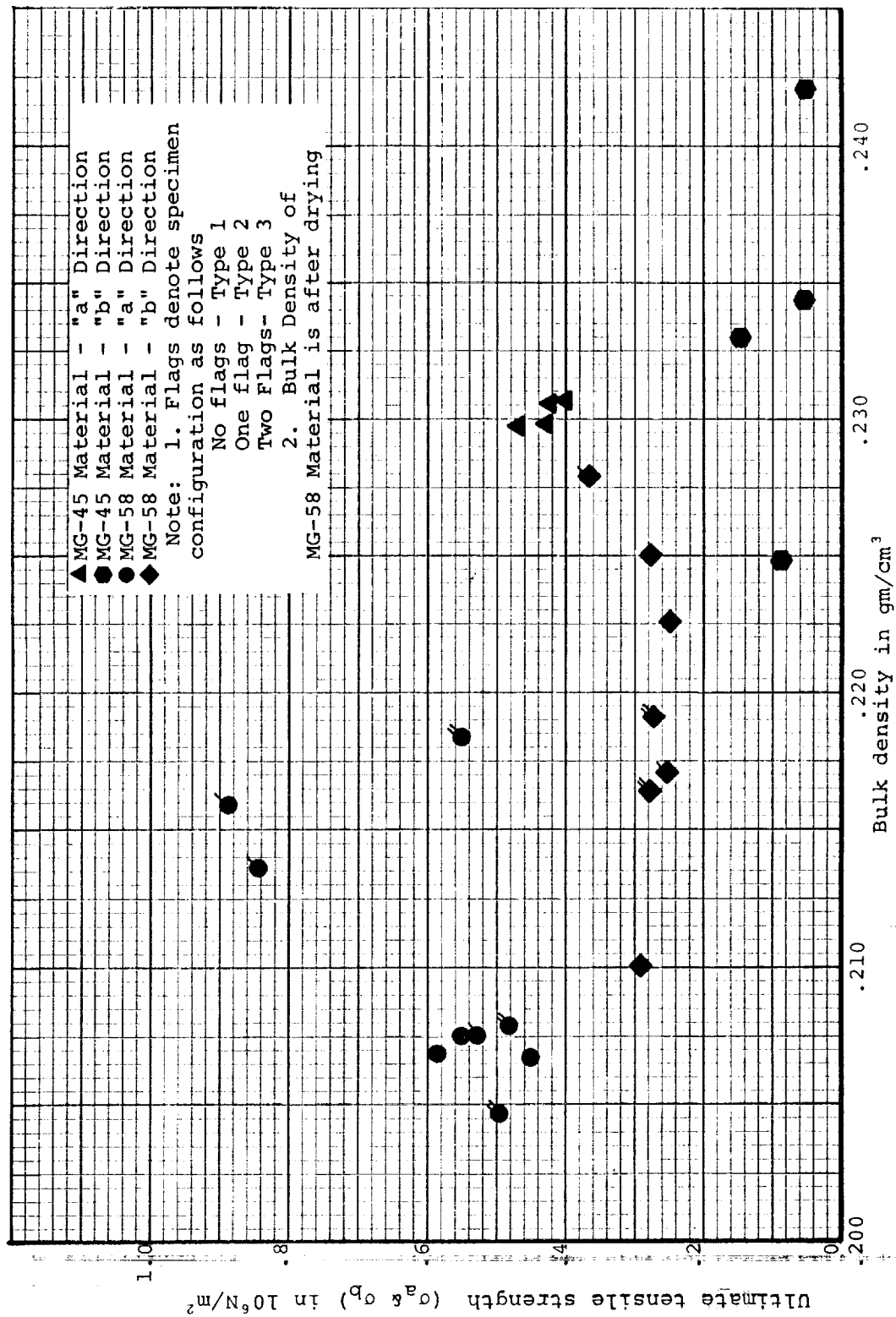
Figure 148. Ultimate tensile strength versus bulk density for MG-45 and MG-58 Materials

296
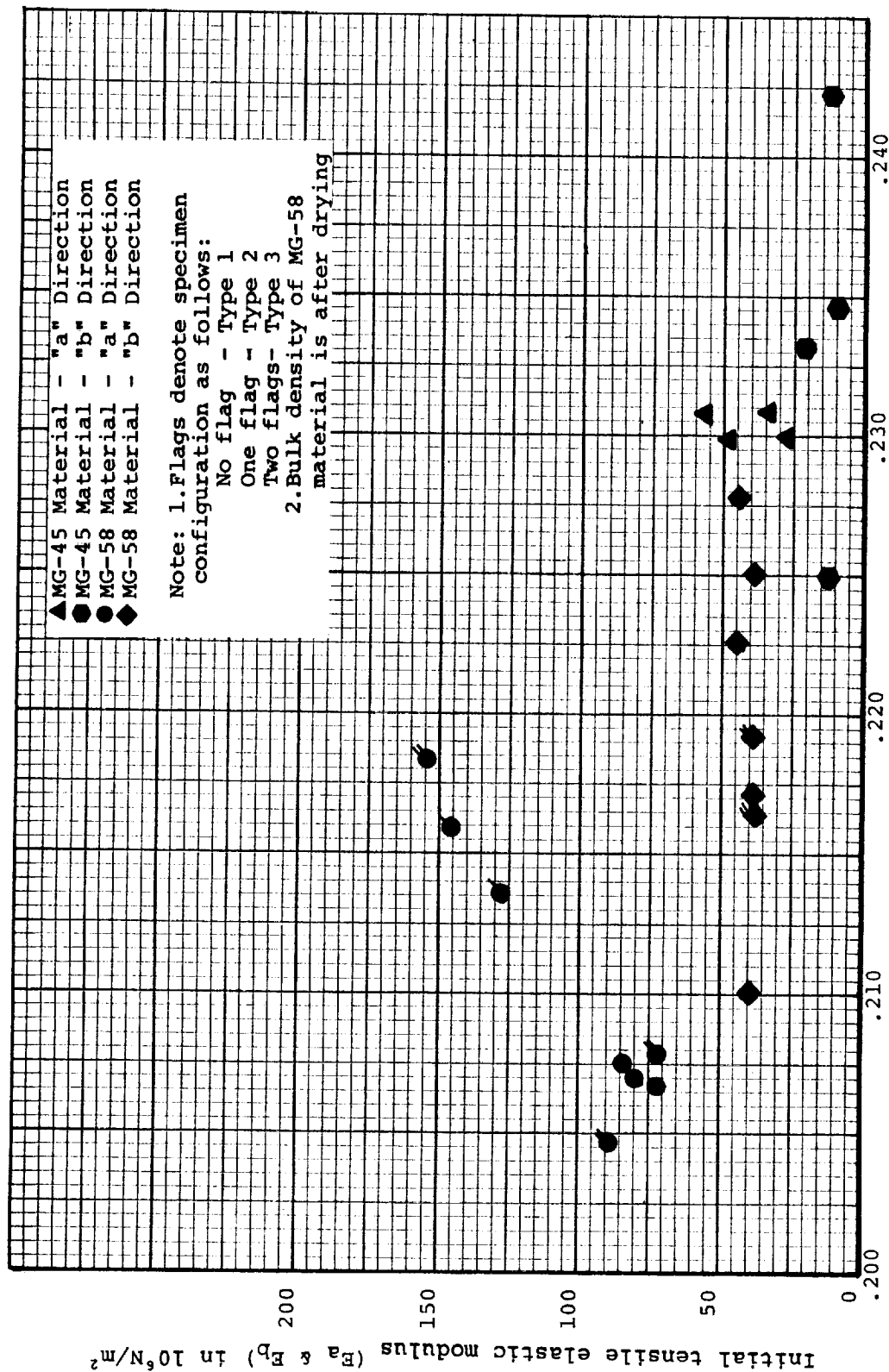
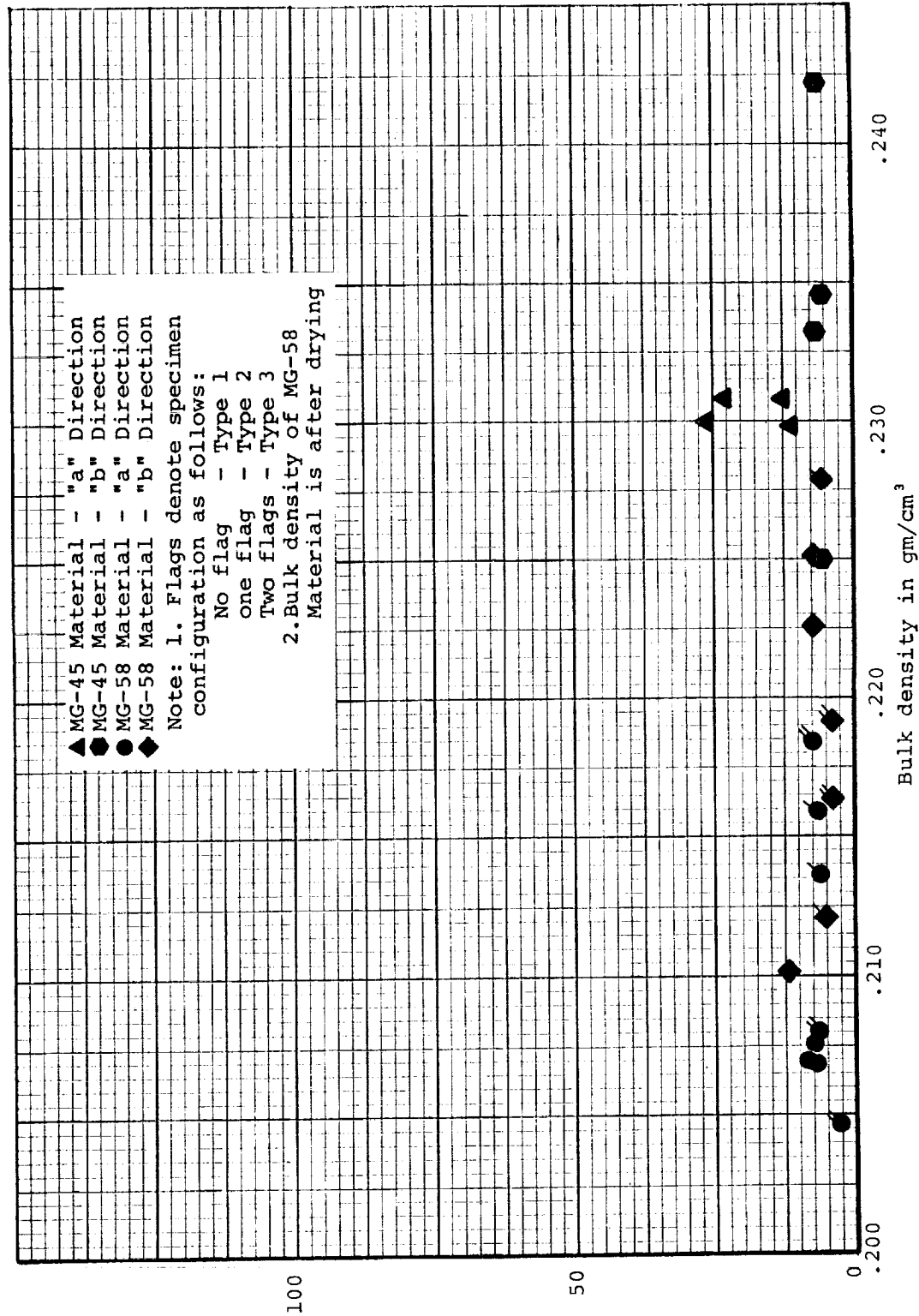Figure 149. Initial tensile elastic modulus versus bulk density for MG-45 and MG-58 Material

297

Figure 150. Total tensile unit axial strain-to-failure versus bulk density for MG-45 and MG-58 Material
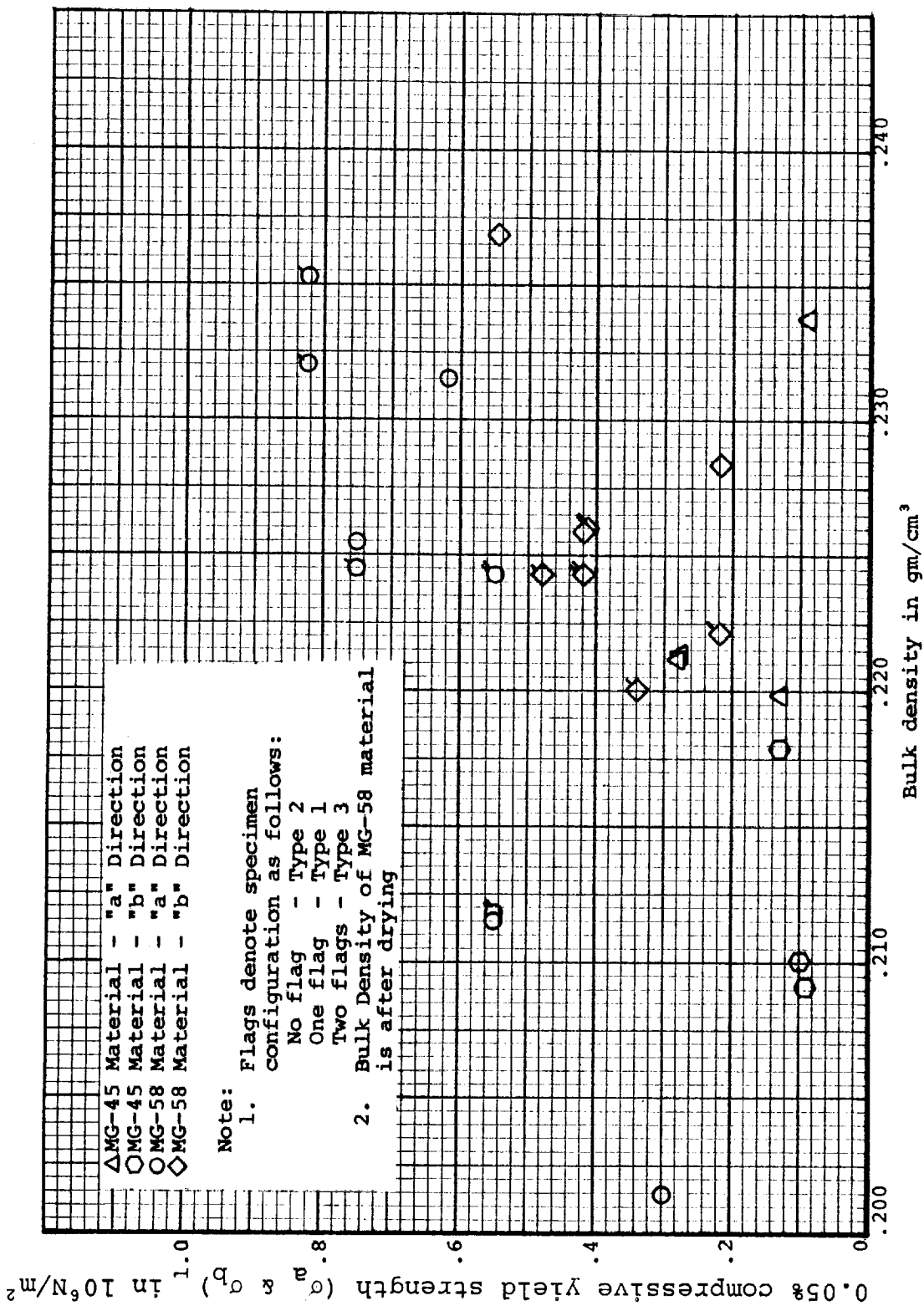
298

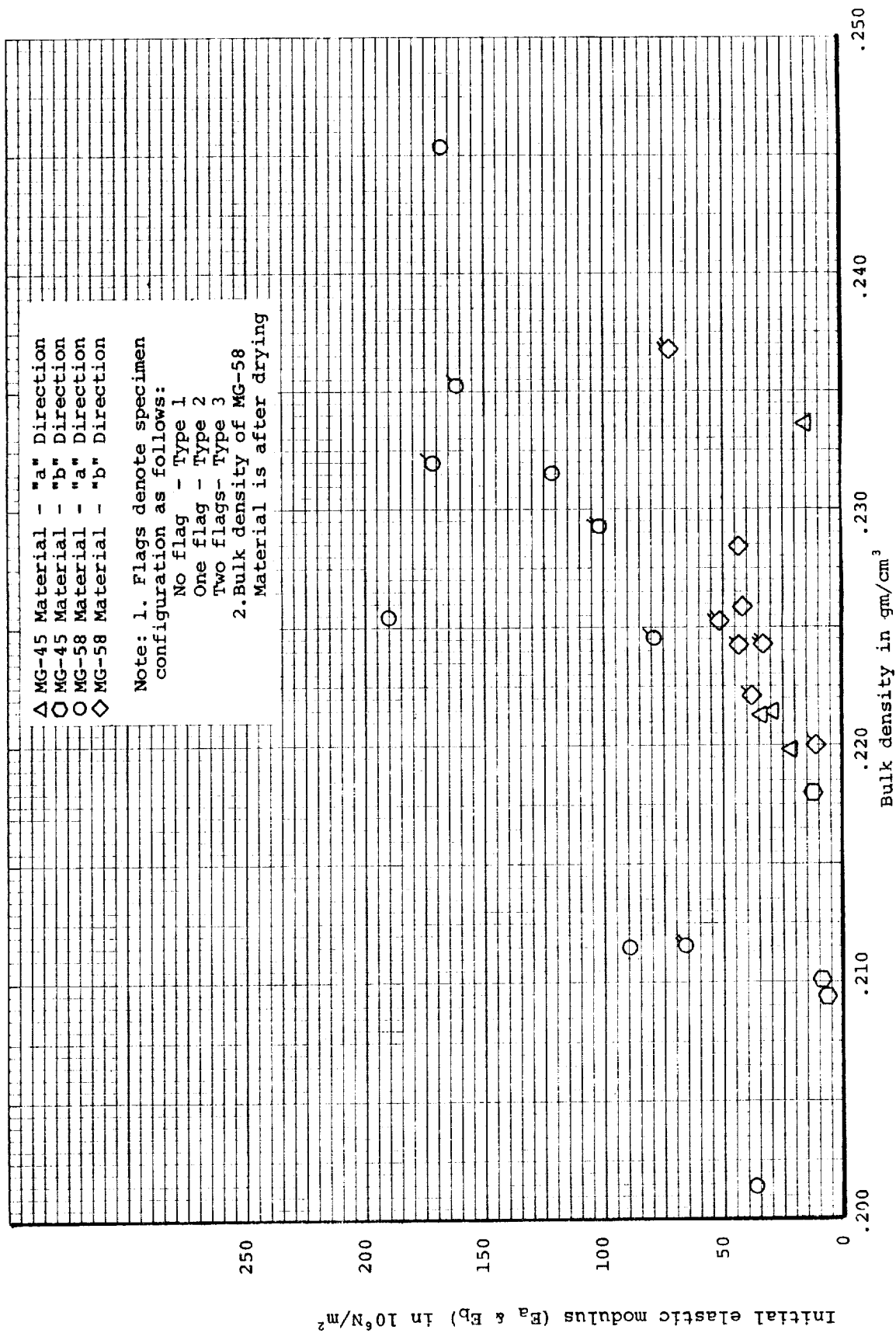Figure 151. Compressive .05% yield strength versus bulk density for MG-45 and MG-58 Material

Figure 152. Initial compressive elastic modulus versus bulk density for MG-45 and MG-58 Materials

300

REFERENCES

1. Wilson, R. Gale: Thermophysical Properties of Six Charring Ablators from 140 to 700 K and Two Chars from 800 to 3000 K. NASA TN D-2991, October, 1965.

2. Sanders, H. G.; Smyly, E. D.; and Pears, C. D.: An Investigation of Some Thermal and Mechanical Properties of a Low-Density Phenolic-Nylon Ablation Material. NASA CR-66731, February, 1969.

3. Kelley, K. K. : Contributions to the Data on Theoretical Metallurgy . XIII High-Temperature Heat Content, Heat Capacity, and Entropy Data for the Elements and Inorganic Compounds. Bureau of Mines Bulletin 584. Washington, U. S. Government Printing Office, 1960.

4. Engelke, W. T.; Pyron, C. M.; and Pears C. D. : Thermophysical Properties of a Low-Density Phenolic-Nylon Ablation Material. NASA CR-809, 1967.

5. Thermophysical Properties Research Center: Data Book, Volume 2, Nonmetallic Elements, Compounds, and Mixtures, Purdue University, Lafayette, Indiana, 1964.

6. Pears, C. D.; and Shoffner, J. E.: The Thermal Response of Ablative Materials. Presented at VIII National Symposium of the Society of Aerospace Materials and Process Engineers, San Francisco, California, May 25-28, 1965.

7. Pears, C. D.; and Pyron, C. M.: The Thermal Conductivity of Ablative Materials by the "Boxing" Analysis. Presented at the Fifth Thermal Conductivity Conference, Denver, Colorado, October, 1965.